

# **INAUGURAL - DISSERTATION**

To obtain the doctoral degree of the  
Combined Faculty of Mathematics,  
Engineering and Natural Sciences  
of the Ruprecht-Karls-University Heidelberg

presented by

M.Sc. Jonas Hädeler

Oral examination: March 27<sup>th</sup>, 2025



**Natural abiotic iron-mediated  
formation of C1 and C2 compounds  
from environmentally important  
methyl-substituted substrates  
and their implication for nature**

Reviewer:

Prof. Dr. Dr. h.c. Frank Keppler

Prof. Dr. Peter Comba



---

## Abstract

Natural processes continuously produce organic and inorganic volatile compounds with one or two carbon atoms (C1 and C2), for instance, methane, ethane, methanol, formaldehyde, methyl chloride and carbon dioxide from the whole range of organic matter. They act as greenhouse gases, control the oxidation capacity of the atmosphere, destroy tropospheric and stratospheric ozone and play an important role in atmospheric chemistry and physics, thus influencing the global carbon cycle. Their origin is typically ascribed to complex enzymatic and metabolic processes and the combustion of organic matter. Methane emissions were, in general, attributed to methanogenic archaea, which grow under anoxic conditions. High emissions of methanol into the atmosphere originate from plant growth. Lignin, as part of the plants, is degraded by fungi, which is a well-described process that leads, for instance, to the release of methanol. Also, the demethylation of lignin under elevated pressure and temperature is utilised in industrial processes to generate sustainable resources like methanol and bioaromatics.

This study presents compelling evidence for the oxic and abiotic formation of C1 and C2 compounds. These were generated from environmentally important organic substrates with sulfur-, nitrogen-, phosphorus-, and oxygen-bonded methyl groups. This was proven with the use of precursor compounds and extensive isotopically labelling studies in laboratory incubation experiments. Then, naturally occurring macro molecules like lignin were incubated, and for a direct link to nature, soil samples were incubated. The cleavage of the methyl group occurs through a highly reactive iron-oxo species which produces methyl radicals. The iron-oxo species is generated through the Fenton reaction in which iron reacts with hydrogen peroxide. Methyl radicals from methyl group-containing compounds serve as crucial intermediates in these reactions as they act as precursors of the C1 and C2 compounds. The product distribution of C1 and C2 compounds is influenced by the binding of the methyl group to different heteroatoms, ascorbic acid concentrations, and the specific iron species involved. An exchange of the iron species with other transition metals leads to identical C1 and C2 compounds with varying conversion rates. The use of isotopically labelled compounds determines the origin of carbon, hydrogen, and oxygen in the C1 and C2 compounds, identifying the methyl group, hydrogen peroxide and dioxygen as precursors depending on the heteroatom. A special case is the demethoxylation of lignin monomeric units and other aromatic methoxy compounds where the whole methoxy group is cleaved off and leads to the formation of methanol and, under the oxic conditions, additionally to formaldehyde. Extensive isotopic studies confirmed this newly described process.

With a series of sterilised soil samples with different organic carbon and methoxy contents, this process was transferred to natural environments, resulting in the observation of significant amounts of methanol and formaldehyde with the methoxy group as a precursor and, to a lesser extent, methane

and ethane formation. The incubation experiments of wet-dry cycles with soil samples have demonstrated their ability to produce methanol and formaldehyde continuously with decreasing amounts.

All environmentally significant processes described here represent a substantial abiotic source of ubiquitously distributed C1 and C2 compounds. The specific case of demethoxylation is particularly important in the pedosphere due to the high levels of lignin in organic matter; this process is expected to provide an energy source for various microorganisms. The novel demethoxylation mechanisms and the expanded demethylation mechanism demonstrate the abiotic production of C1 and C2 compounds that affect the chemical and physical properties of natural environments and the global carbon cycle, thereby highlighting the significance of these processes.

---

## Kurzfassung

Bei natürlichen Prozessen entstehen kontinuierlich organische und anorganische flüchtige Verbindungen mit einem oder zwei Kohlenstoffatomen (C1 und C2), z. B. Methan, Ethan, Methanol, Formaldehyd, Methylchlorid und Kohlendioxid aus einer Vielzahl organischer Stoffe. Sie wirken als Treibhausgase, steuern die Oxidationskapazität der Atmosphäre, zerstören troposphärisches und stratosphärisches Ozon und spielen eine wichtige Rolle in der Atmosphärenchemie und -physik, wodurch sie den globalen Kohlenstoffkreislauf beeinflussen. Ihre Entstehung wird in der Regel auf komplexe enzymatische und metabolische Prozesse und die Verbrennung organischer Stoffe zurückgeführt. Methanemissionen wurden üblicherweise methanogenen Archaeen zugeschrieben, die unter anoxischen Bedingungen wachsen. Hohe Methanolemissionen in die Atmosphäre sind auf das Pflanzenwachstum zurückzuführen. Lignin, welches ein Bestandteil von Pflanzen ist, wird durch Pilze abgebaut, welches ein gut beschriebener Prozess ist, der unter anderem zur Freisetzung von Methanol führt. Auch die Demethylierung von Lignin unter erhöhtem Druck und Temperatur wird in industriellen Prozessen genutzt, um nachhaltige Ressourcen wie Methanol und Bioaromaten zu erzeugen.

Diese Studie liefert überzeugende Beweise für die oxische und abiotische Bildung von C1- und C2-Verbindungen. Diese wurden aus umweltrelevanten organischen Substraten mit Schwefel-, Stickstoff-, Phosphor- und Sauerstoffgebundenen Methylgruppen gebildet. Dies wurde mit Vorläuferverbindungen und umfangreichen Isotopenmarkierungsstudien in Inkubationsversuchen nachgewiesen. Dann wurden natürlich vorkommende Makromoleküle wie Lignin inkubiert, und für einen direkten Übertrag zur Natur wurden Bodenproben inkubiert. Die Abspaltung der Methylgruppe erfolgt durch eine hochreaktive Eisen-Oxo-Spezies, welche Methylradikale erzeugt. Die Eisen-Oxo-Spezies wird durch die Fenton-Reaktion erzeugt, bei der Eisen mit Wasserstoffperoxid reagiert. Die Methylradikale aus methylgruppenhaltigen Verbindungen dienen als wichtige Zwischenprodukte in diesen Reaktionen, da sie als Vorläufer von C1 und C2 Verbindungen fungieren. Die Produktverteilung der C1- und C2-Verbindungen wird durch die Bindung der Methylgruppe an verschiedene Heteroatome, die Ascorbinsäurekonzentration und die beteiligten Eisenspezies beeinflusst. Ein Austausch der Eisenspezies mit anderen Übergangsmetallen führt zu identischen C1- und C2-Verbindungen mit unterschiedlichen Umwandlungsraten. Durch die Verwendung isotopisch markierter Verbindungen lässt sich die Herkunft des Kohlenstoffs, Wasserstoffs und Sauerstoffs in den C1- und C2-Verbindungen bestimmen, wobei je nach Heteroatom die Methylgruppe, Wasserstoffperoxid und Sauerstoff als Vorläufer identifiziert werden. Ein Sonderfall ist die Demethoxylierung von Ligninmonomereinheiten und anderen aromatischen Methoxyverbindungen, bei der die gesamte Methoxygruppe abgespalten wird und zur Bildung von Methanol und unter

oxischen Bedingungen zusätzlich zu Formaldehyd führt. Umfangreiche Isotopenstudien bestätigten diesen neu beschriebenen Prozess.

Mit einer Reihe von sterilisierten Bodenproben mit unterschiedlichen Gehalten an organischem Kohlenstoff und Methoxygruppen wurde dieser Prozess auf die natürliche Umgebung übertragen, was zur Beobachtung signifikanter Mengen von Methanol und Formaldehyd mit der Methoxygruppe als Vorläufer und in geringerem Maße zur Bildung von Methan und Ethan führte. Die Inkubationsexperimente von Nass-Trocken-Zyklen mit identischen Bodenproben haben gezeigt, dass diese in der Lage sind, Methanol und Formaldehyd kontinuierlich mit abnehmenden Mengen zu produzieren.

Alle beschriebenen umweltrelevanten Prozesse stellen eine wesentliche abiotische Quelle für ubiquitär verteilte C1- und C2-Verbindungen dar. Der Sonderfall der Demethoxylierung ist in der Pedosphäre besonders wichtig, da die organische Substanz im Boden große Mengen an Lignin enthält. Es wird postuliert, dass dieser Prozess eine Energiequelle für verschiedene Mikroorganismen darstellt. Der neue Demethoxylierungsmechanismus und der erweiterte Demethylierungsmechanismus führen zur abiotischen Produktion von C1- und C2-Verbindungen, die die chemischen und physikalischen Eigenschaften des Erdsystems und den globalen Kohlenstoffkreislauf beeinflussen, und unterstreichen damit die Bedeutung der Mechanismen.

---

## Acknowledgement

I want to express my sincerest gratitude to my supervisor, Prof. Dr. Dr hc Frank Keppler, for guiding me through my PhD journey and for your unwavering support, motivation, and commitment to engaging in discussions on an equal footing level. Your guidance has been instrumental in my success. I would also like to thank you for creating a friendly, collegial and supportive working atmosphere. Your passion for science truly inspires me! It encourages me to explore new and exciting paths of discovery.

I am incredibly grateful to Prof. Dr. Peter Comba, my second supervisor. He gave me invaluable insights into chemistry, inspiring me with his friendly manner. I am thankful for the excellent working relationship we have. I am also indebted to Dr Gunasekaran Velmurugan for his good cooperation and stimulating discussions on our joint project and for introducing me to chemical modelling. I would also like to thank Rejith Radhamani for synthesising the bispidine complexes used. I want to extend my gratitude to Prof. Dr Christoph Schüth and Prof. Dr Werner Aeschbach for their willingness to review my oral examination.

I would also like to thank all my students who worked with me on my project. I want to thank Kirsten Rheinberger, Rebekka Lauer, Isabel Hanstein, Jule Dörpmund and Julia Wenhuda for their support, the reliable and precise lab work, the many discussions and the consistently positive working atmosphere.

I want to extend my gratitude to the entire Orcas group, who provided an excellent working environment and were readily available to offer assistance and guidance whenever needed. I would also like to thank Bernd Knape, who was always on hand to repair the equipment and share his endless expertise. I want to thank Rebekka Lauer, Moritz Schroll, Marcus Schneider and Anna Wieland for their excellent cooperation and support. I would also like to thank Maurice Maas, Elena Zwerschke, Markus Greule, Daniela Polag, Christian Scholz, Stefan Rheinberger, Silvia Rheinberger, Ivanina Raleneikova, Martin Maier and Charlotte Stirn, as well as all Bachelor and Master students, for creating an excellent and friendly working atmosphere that always makes me look forward to starting the day at the institute. And let's not forget the exhilarating table football matches.

I'd also like to thank my family, especially my parents, Gundel Hädeler and Rolf Bourgeois, for their unwavering support. I'd also like to thank my grandparents for supporting me, who unfortunately passed away before seeing the end of this chapter.

I want to express my sincerest gratitude to my partner, Lisa Dönges, for her unwavering support over the past five years. Thank you for listening to my endless stories about the fascinating connections between chemistry and nature.

## Abbreviations

This list contains frequently used abbreviations throughout this study. Parameters and elements are described within the text.

BID	<i>Barrier ion discharge detector</i>	PFPH	<i>Pentafluorophenylhydrazine</i>
BVOCs	<i>Biogenic volatile organic compounds</i>	ppb <sub>v</sub>	<i>parts per billion by volume</i>
DMS	<i>Dimethylsulfide</i>	ppm <sub>v</sub>	<i>parts per million by volume</i>
DMSO	<i>Dimethylsulfoxide</i>	ppm <sub>w</sub>	<i>part per million by weight</i>
FID	<i>Flame ionisation detector</i>	ppt <sub>v</sub>	<i>parts per trillion by volume</i>
Game	<i>Galacturonic acid methyl ester</i>	ROS	<i>Reactive oxygen species</i>
GC	<i>Gas chromatography</i>	SAM	<i>S-adenosyl-L-methionine</i>
HAA	<i>Hydrogen atom abstraction</i>	TMA	<i>Trimethylamine</i>
MS	<i>Mass spectrometer</i>	VOC	<i>Volatile organic compounds</i>
OAT	<i>Oxygen atom transfer</i>		

---

## Table of contents

<b>1</b>	<b>Introduction .....</b>	<b>1</b>
1.1	State of knowledge .....	2
1.1.1	Abiotic formation of C1 and C2 compounds from hetero-bonded CH <sub>3</sub> groups.....	2
1.1.2	Formation of CH <sub>3</sub> OH from methoxy group containing compounds .....	5
1.2	Properties of C1 and C2 compounds and their role in the natural environments .....	5
1.2.1	Methane.....	7
1.2.2	Ethane .....	8
1.2.3	Carbon monoxide.....	9
1.2.4	Carbon dioxide .....	9
1.2.5	Methanol.....	10
1.2.6	Formaldehyde .....	11
1.2.7	Formic acid and acetic acid .....	12
1.2.8	Chloromethane .....	12
1.3	Precursor compounds and their function in natural systems.....	13
1.3.1	S-, N- and P- bonded CH <sub>3</sub> group containing compounds .....	14
1.3.1.1	DMSO .....	14
1.3.1.2	Methionine.....	15
1.3.1.3	Trimethylamine.....	15
1.3.1.4	Choline .....	16
1.3.1.5	Methylphosphonate.....	16
1.3.2	OCH <sub>3</sub> aromatic compounds.....	17
1.3.3	Galacturonic acid methyl ester .....	17
1.4	Transition metal species and their occurrence in soils.....	18
1.4.1	Tetradentate Bispidine Ligand .....	18
1.4.2	Hematite .....	19
1.4.3	Transition metals .....	19
1.5	Ascorbic acid as an OH radical scavenger .....	20
1.6	ROS and the formation of C1 and C2 in soils .....	21
1.7	DFT modelling .....	22
1.8	Motivation and research aim of this study .....	22
<b>2</b>	<b>Materials and Methods.....</b>	<b>23</b>
2.1	Experimental setup and details for the incubation experiments .....	23
2.1.1	Experiments with hetero-bonded CH <sub>3</sub> groups.....	24
2.1.2	Sampling of the experiments .....	24
2.1.3	Experiments with labelled substrates and other setups .....	25
2.1.4	Experiments with soils .....	25
2.1.4.1	Sampling and Preparation of the samples .....	25
2.1.4.2	Location and Sample Description .....	26

---

2.2	Laboratory analysis of CH <sub>4</sub> , C <sub>2</sub> H <sub>6</sub> , CH <sub>3</sub> OH, CH <sub>2</sub> O, CH <sub>3</sub> Cl, CO, CO <sub>2</sub> , HCOOH and CH <sub>3</sub> COOH ...	30
2.2.1	Principles of Gas Chromatography.....	30
2.2.2	Principles of an FID and BID .....	31
2.2.2.1	Analysis of low CH <sub>4</sub> and C <sub>2</sub> H <sub>6</sub> concentrations with a GC-FID .....	31
2.2.2.2	Analysis of CH <sub>4</sub> and CO <sub>2</sub> with a GC-BID .....	31
2.2.2.3	Analysis of CH <sub>3</sub> OH with a GC-FID .....	32
2.2.2.4	Analysis of OCH <sub>3</sub> with a GC-FID.....	32
2.2.3	Principles of Mass Spectrometry .....	32
2.2.3.1	Analysis of CH <sub>2</sub> O with a GC-TOF-MS .....	33
2.2.3.2	Analysis of CH <sub>3</sub> Cl and labelled CH <sub>3</sub> OH with a GC-MS.....	34
2.2.3.3	Analysis of HCOOH and CH <sub>3</sub> COOH with a GC-MS .....	34
2.2.4	Analysis of δ <sup>13</sup> C and δ <sup>18</sup> O of CO <sub>2</sub> with a GC-IRMS .....	35
2.2.5	Analysis of TOC with a SSM-5000A .....	36
2.3	Calculations of the conversion rates and concentrations.....	36
2.3.1	Calculations of the conversion ratio of CH <sub>3</sub> OH and CH <sub>2</sub> O.....	36
2.3.2	Calculation for gases .....	37
2.3.3	Calculation of the mass fraction of CH <sub>3</sub> OH and CH <sub>2</sub> O in soil .....	37
2.3.4	Calculation of the mass fraction .....	38
2.4	Statistics of the measurements .....	38
<b>3</b>	<b>Results and Discussion.....</b>	<b>39</b>
3.1	Conversion rates and mechanistic details of d <sub>6</sub> -DMSO to C1 and C2 compounds.....	40
3.1.1	Determination of the general experimental setup.....	40
3.1.2	Conversion rates of d <sub>6</sub> -DMSO to CD <sub>3</sub> H, C <sub>2</sub> D <sub>6</sub> , CD <sub>3</sub> OH, and CD <sub>2</sub> O and the impact of different Asc concentrations.....	42
3.1.3	Impact of O <sub>2</sub> in the headspace and H <sub>2</sub> O phase on the conversion rates of CD <sub>3</sub> H, C <sub>2</sub> D <sub>6</sub> , CD <sub>3</sub> OH, and CD <sub>2</sub> O derived from d <sub>6</sub> -DMSO .....	44
3.1.4	Investigation of the intermediate dimethyl sulfone and the conversion rates to CH <sub>4</sub> , C <sub>2</sub> H <sub>6</sub> , CH <sub>3</sub> OH, and CH <sub>2</sub> O .....	46
3.1.5	Investigation of the mechanism of the reaction of d <sub>6</sub> -DMSO to C1 and C2 compounds with isotopically labelled compounds.....	47
3.1.5.1	Identification of the origin of the CH <sub>3</sub> group in C1 and C2 compounds with fully deuterated DMSO .....	47
3.1.5.2	Oxidation of CD <sub>3</sub> OH to CD <sub>2</sub> O .....	50
3.1.5.3	Identification of the origin of the carbon in CO <sub>2</sub> with <sup>13</sup> C-labelled DMSO.....	51
3.1.5.4	Identification of the origin of the oxygen atom in CH <sub>3</sub> OH, CH <sub>2</sub> O and CO <sub>2</sub> with <sup>18</sup> O-labelled H <sub>2</sub> O, H <sub>2</sub> O <sub>2</sub> and O <sub>2</sub> .....	51
3.1.6	Trapping CH <sub>3</sub> radicals with CH <sub>2</sub> Br <sub>2</sub> and CCl <sub>3</sub> Br .....	53
3.1.7	Discussion of DMSO as a case study to characterise the reaction to C1 and C2 compounds . .....	55
3.2	Conversion of S-, N- and P- bonded CH <sub>3</sub> group containing compounds to C1 and C2 compounds.....	60
3.2.1	Conversion rates of S-, N- and P- bonded CH <sub>3</sub> group containing compounds to CD <sub>3</sub> H, C <sub>2</sub> D <sub>6</sub> , CD <sub>3</sub> OH, and CD <sub>2</sub> O .....	61

---

3.2.2	Investigation of the reaction mechanism with deuterium-labelled compounds .....	62
3.2.3	Discussion of the formation of C1 and C2 compounds originated in S-, N- and P- bonded CH <sub>3</sub> group containing compounds .....	64
3.3	Conversion rates and mechanistic details of methoxy compounds to C1 and C2 compounds .....	66
3.3.1	Conversion rates of OCH <sub>3</sub> compounds to CD <sub>3</sub> H, C <sub>2</sub> D <sub>6</sub> , CD <sub>3</sub> OH, and CD <sub>2</sub> O .....	66
3.3.2	Trapping CH <sub>3</sub> radicals with CH <sub>2</sub> Br <sub>2</sub> and CCl <sub>3</sub> Br .....	67
3.3.3	Investigation of the reaction mechanism with deuterium and <sup>18</sup> O-labelled compounds ...	68
3.3.4	Discussion and mechanistic details of the conversion of methoxy group containing compounds to CH <sub>3</sub> OH and CH <sub>2</sub> O .....	69
3.4	Results of the studies with different Mn, Fe, Co, Ni and Cu species instead of LFe <sup>II</sup> Cl <sub>2</sub> and Fe <sub>2</sub> O <sub>3</sub> .....	71
3.4.1	Conversion of d <sub>6</sub> -DMSO, d <sub>3</sub> -methionine and 2-methoxyphenol to CD <sub>3</sub> H, C <sub>2</sub> D <sub>6</sub> , CD <sub>3</sub> OH, CD <sub>2</sub> O and CH <sub>3</sub> Cl mediated by transition metals .....	71
3.4.1.1	d <sub>6</sub> -DMSO.....	72
3.4.1.2	d <sub>3</sub> -Methionine .....	74
3.4.1.3	2-Methoxyphenol.....	75
3.4.1.4	CH <sub>3</sub> Cl.....	77
3.4.2	Discussion and implications of the different transition metal species in reaction with d <sub>6</sub> -DMSO, d <sub>3</sub> -methionine and 2-methoxyphenol and the formation of CH <sub>4</sub> , C <sub>2</sub> H <sub>6</sub> , CH <sub>3</sub> OH, CH <sub>2</sub> O and CH <sub>3</sub> Cl.....	78
3.4.2.1	d <sub>6</sub> -DMSO.....	78
3.4.2.2	d <sub>3</sub> -methionine .....	81
3.4.2.3	2-Methoxyphenol.....	81
3.4.2.4	Methyl chloride .....	82
3.5	Lignin and pectin as precursors of CH <sub>4</sub> , C <sub>2</sub> H <sub>6</sub> , CH <sub>3</sub> OH and CH <sub>2</sub> O .....	83
3.5.1	Formation of CH <sub>4</sub> , C <sub>2</sub> H <sub>6</sub> , CH <sub>3</sub> OH and CH <sub>2</sub> O from lignin and pectin under abiotic and oxic conditions.....	83
3.5.2	Discussion of the production CH <sub>4</sub> , C <sub>2</sub> H <sub>6</sub> , CH <sub>3</sub> OH and CH <sub>2</sub> O and the influence of Fe <sub>2</sub> O <sub>3</sub> , H <sub>2</sub> O <sub>2</sub> and Asc .....	84
3.6	Abiotic and oxic production of CH <sub>3</sub> OH, CH <sub>2</sub> O, CH <sub>4</sub> and C <sub>2</sub> H <sub>6</sub> from sterile soils and their controlling factors .....	86
3.6.1	Production of CH <sub>3</sub> OH, CH <sub>2</sub> O, CH <sub>4</sub> and C <sub>2</sub> H <sub>6</sub> from sterile soils under abiotic and atmospheric conditions.....	86
3.6.2	Methoxy groups in soils as a precursor of CH <sub>3</sub> OH, CH <sub>2</sub> O, CH <sub>4</sub> and C <sub>2</sub> H <sub>6</sub> .....	87
3.6.3	Identification of the origin of CH <sub>3</sub> OH in soils with deuterated or <sup>18</sup> O-OCH <sub>3</sub> labelled 2-methoxyphenol .....	89
3.6.4	Determination of the ability of soils to degrade d <sub>6</sub> -DMSO .....	90
3.6.5	Wet-dry cycles with soils and their effect on CH <sub>3</sub> OH and CH <sub>2</sub> O formation .....	92
3.6.6	Influence of pH variations on soil and the impact on CH <sub>3</sub> OH, CH <sub>2</sub> O, CH <sub>4</sub> and C <sub>2</sub> H <sub>6</sub> production.....	94
3.6.7	Variation of incubation temperature in soil and the influence on CH <sub>3</sub> OH, CH <sub>2</sub> O, CH <sub>4</sub> and C <sub>2</sub> H <sub>6</sub> production.....	94
3.6.8	Addition of CH <sub>3</sub> OH to non-sterile soils for demonstration of soil degradation potential ...	95

3.6.9	Correlation of TOC and methoxy content as a basis for a first extrapolation of the production of CH <sub>3</sub> OH and CH <sub>2</sub> O from soils on a global scale.....	96
3.6.10	TOC and CH <sub>3</sub> OH + CH <sub>2</sub> O correlation for initial global predictions of CH <sub>3</sub> OH and CH <sub>2</sub> O production.....	97
3.6.11	Discussion and implications of the abiotic production of CH <sub>3</sub> OH, CH <sub>2</sub> O, CH <sub>4</sub> and C <sub>2</sub> H <sub>6</sub> in natural environments, especially the pedosphere .....	98
3.7	Global implications of the abiotic and oxic formation of CH <sub>3</sub> OH, CH <sub>2</sub> O, CH <sub>4</sub> and C <sub>2</sub> H <sub>6</sub> in soils .....	102
<b>4</b>	<b>Summary and Outlook.....</b>	<b>104</b>
<b>5</b>	<b>Related scientific work.....</b>	<b>110</b>
<b>6</b>	<b>Appendix.....</b>	<b>110</b>
<b>7</b>	<b>References.....</b>	<b>111</b>

## List of Figures

- Figure 1: A postulated mechanism for the production of CH<sub>4</sub> from methionine by [Fe=O<sup>IV</sup>]<sup>2+</sup> species in the presence of Asc. Taken from Althoff et al. (2014)<sup>14</sup> ..... 4
- Figure 2: Complex interactions of gas phase reactions and heterogeneous reactions of VOCs in the atmosphere. Taken from Shen et al. (2013).<sup>3</sup> ..... 6
- Figure 3: Mechanism for CH<sub>4</sub> formation in living organisms due to the oxidative demethylation of DMSO. Taken from Ernst et al. (2022).<sup>72</sup> ..... 8
- Figure 4: Structures of the Tetradentate Bispidine Ligand **a**) L ([Fe(N<sub>2</sub>Py<sub>2</sub>)Cl<sub>2</sub>]•CH<sub>3</sub>CN) and its **b**) Iron(IV)-Oxido complex in aqueous solution. Taken from Hädeler et al. (2023).<sup>205</sup> ..... 18
- Figure 5: Sources and pathways of ROS in soils. The Fenton reaction, which forms part of the present investigation, represents a significant component of ROS production in soil. Taken from Yu et al. (2021).<sup>229</sup> ..... 22
- Figure 6: Locations of the soil samples near Heidelberg A-M.<sup>239</sup> ..... 28
- Figure 7: Derivatisation of CH<sub>2</sub>O with PFPH and the formation of a hydrazone due to a condensation reaction..... 34
- Figure 8: Differences in the conversion rate between DMSO and d<sub>6</sub>-DMSO relative to the added d<sub>6</sub>-DMSO (25 μmol) with LFe<sup>II</sup>Cl<sub>2</sub> (bars B) or Fe<sub>2</sub>O<sub>3</sub> (bars H) (10 μmol), Asc (100 μmol) and H<sub>2</sub>O<sub>2</sub> (200 μmol) converted to one CH<sub>3</sub> group. Error bars refer to the SD of the total conversion of all major C1 and C2 compounds for n = 9, except for C<sub>2</sub>D<sub>6</sub>, n = 3. Taken from Hädeler et al. (2023).<sup>205</sup> ..... 41
- Figure 9: Formation of CD<sub>3</sub>H over time from the deuterium-labelled CH<sub>3</sub> groups of DMSO, mediated by LFe<sup>II</sup>Cl<sub>2</sub> (red symbols) compared to Fe<sub>2</sub>O<sub>3</sub> (blue symbols) (10 μmol) with Asc (100 μmol) and H<sub>2</sub>O<sub>2</sub> (200 μmol) converted to one CH<sub>3</sub> group. The reaction with LFe<sup>II</sup>Cl<sub>2</sub> is nearly completed after 0.5 h, and the reaction with Fe<sub>2</sub>O<sub>3</sub> is completed after more than 24 h. Error bars refer to mean values of CD<sub>3</sub>H (n = 9). Taken from Hädeler et al. (2023).<sup>205</sup> 42
- Figure 10: Formation of C1 and C2 compounds from d<sub>6</sub>-DMSO mediated by LFe<sup>II</sup>Cl<sub>2</sub> (bars B) compared to Fe<sub>2</sub>O<sub>3</sub> (bars H). Experiments show the dependence of the rates of the formed products (CD<sub>3</sub>H, C<sub>2</sub>D<sub>6</sub>, CD<sub>3</sub>OH, and CD<sub>2</sub>O) on the Asc concentrations (10 ml H<sub>2</sub>O, 48 h reaction time, ambient conditions) with added d<sub>6</sub>-DMSO (25 μmol), with LFe<sup>II</sup>Cl<sub>2</sub> or Fe<sub>2</sub>O<sub>3</sub> (10 μmol), H<sub>2</sub>O<sub>2</sub> (200 μmol); error bars refer to the SD of the total conversion of all major C1 and C2 compounds for n = 9, except for C<sub>2</sub>D<sub>6</sub>, n = 3. Taken from Hädeler et al. (2023).<sup>205</sup> ..... 44

- Figure 11: Impact of O<sub>2</sub> and Asc on forming C<sub>1</sub> and C<sub>2</sub> compounds with LFe<sup>II</sup>Cl<sub>2</sub>. Experiments with 25 μmol d<sub>6</sub>-DMSO, 100 μmol Asc (or none: -Asc), 200 μmol H<sub>2</sub>O<sub>2</sub> and 10 μmol LFe<sup>II</sup>Cl<sub>2</sub> in 10 ml ultra-pure H<sub>2</sub>O without O<sub>2</sub> (-O<sub>2</sub>) or in ambient atmosphere with a reaction time 48 h. Error bars refer to the SD of the total conversion of all major C1 and C2 compounds for n = 9, except for C<sub>2</sub>D<sub>6</sub>, n = 3. Taken from Hädeler et al. (2023).<sup>205</sup> ..... 46
- Figure 12: Chromatogram of the formation of CH<sub>4</sub> in the experiment with 25 μmol dimethyl sulfone (black line), 100 μmol ascorbic acid, 200 μmol H<sub>2</sub>O<sub>2</sub>, 10 μmol LFe<sup>II</sup>Cl<sub>2</sub>, compared with the blank experiment (100 μmol ascorbic acid, 200 μmol H<sub>2</sub>O<sub>2</sub>, 10 μmol LFe<sup>II</sup>Cl<sub>2</sub> and no substrate added) under ambient atmosphere with a reaction time 48 h. Taken from Hädeler et al. (2023).<sup>205</sup> ..... 47
- Figure 13: Mass fragmentation patterns of CH<sub>4</sub>, C<sub>2</sub>H<sub>6</sub>, CH<sub>3</sub>OH and CH<sub>2</sub>O of experiments with d<sub>6</sub>-DMSO (25 μmol) with LFe<sup>II</sup>Cl<sub>2</sub> (10 μmol), Asc (100 μmol) and H<sub>2</sub>O<sub>2</sub> (200 μmol) under ambient atmospheric conditions with a reaction time of 48 h. **a)** Mass shift of 3 from 16 to 19 for CD<sub>3</sub>H from d<sub>6</sub>-DMSO; **b)** mass shift of 6 from 30 to 36 for C<sub>2</sub>D<sub>6</sub> from d<sub>6</sub>-DMSO; **c)** mass shift of 3 from 32 to 35 for CD<sub>3</sub>OH from d<sub>6</sub>-DMSO; **d)** mass shift of 2 from 210 to 212 for deuterated and derivatised CD<sub>2</sub>O from d<sub>6</sub>-DMSO. Taken from Hädeler et al. (2023).<sup>205</sup> 48
- Figure 14: Mass fragmentation of an experiment with 25 μmol d<sub>6</sub>-DMSO, 100 μmol ascorbic acid, 200 μmol H<sub>2</sub>O<sub>2</sub> and 10 μmol LFe<sup>II</sup>Cl<sub>2</sub> under ambient atmospheric conditions with a reaction time of 48 h. Chromatogram and the corresponding mass track from **a)** HCOOH with a mass shift of 1 AMU from 103 to 104 and **b)** CH<sub>3</sub>COOH with a mass shift of 3 AMU from 117 to 120. Taken from Hädeler et al. (2023).<sup>205</sup> ..... 49
- Figure 15: Chromatogram of deuterium labelled CD<sub>3</sub>Cl in the experiment with 25 μmol d<sub>6</sub>-DMSO, 100 μmol ascorbic acid, 200 μmol H<sub>2</sub>O<sub>2</sub> and 10 μmol LFe<sup>II</sup>Cl<sub>2</sub> under ambient atmospheric conditions with a reaction time of 48 h. The chromatogram illustrates the masses 53 (black) and 55 (pink). These represent a mass shift of 3 AMU to the CD<sub>3</sub>Cl, with the stable isotopes 35 and 37 (mass of 50 or 52 for CH<sub>3</sub>Cl). Taken from Hädeler et al. (2023).<sup>205</sup> .... 49
- Figure 16: Mass fragmentation of deuterium-labelled CH<sub>2</sub>O to track the oxidation from CH<sub>3</sub>OH to CH<sub>2</sub>O. Mass track of CH<sub>2</sub>O with a mass shift of 2 AMU from 210 to 212 **a)** without DMSO and added CD<sub>3</sub>OH and **b)** with DMSO and added CD<sub>3</sub>OH. Experiment with or without 25 μmol DMSO, 100 μmol Asc, 200 μmol H<sub>2</sub>O<sub>2</sub> and 10 μmol LFe<sup>II</sup>Cl<sub>2</sub> under ambient atmospheric conditions with a reaction time of 48 h. Taken from Hädeler et al. (2023).<sup>205</sup> 50
- Figure 17: Chromatogram of isotopic labelled CH<sub>3</sub>OH. Experiment with 2.5 μmol d<sub>6</sub>-DMSO, 10 μmol Asc, 20 μmol H<sub>2</sub><sup>18</sup>O<sub>2</sub> and 1 μmol LFe<sup>II</sup>Cl<sub>2</sub> in 1 ml ultra-pure H<sub>2</sub>O under ambient

- atmospheric conditions with a reaction time of 48 h. Chromatogram of  $C^2H_3^{18}OH$  at  $m/z = 37$ . Taken from Hädel et al. (2023).<sup>205</sup> ..... 52
- Figure 18: Chromatogram of isotopically labelled  $CH_3OH$ . Experiment with 25  $\mu mol$   $d_6$ -DMSO, 100  $\mu mol$  Asc, 200  $\mu mol$   $H_2O_2$  and 10  $\mu mol$   $LFe^{II}Cl_2$  under 79 %  $N_2$  and 21 %  $^{18}O_2$  atmosphere with a reaction time of 48 h. Chromatogram of  $CD_3^{18}OH$  at  $m/z$ -ratio at 37. Taken from Hädel et al. (2023).<sup>205</sup> ..... 52
- Figure 19: Formation of  $CD_3H$ ,  $C_2D_6$ ,  $CD_3OH$  and  $CD_2O$  from  $d_6$ -DMSO with the 10  $\mu mol$   $LFe^{II}Cl_2$  (bars B) or  $Fe_2O_3$  (bars H) 100  $\mu mol$  Asc and 200  $\mu mol$   $H_2O_2$  in the presence of 1.25 mmol  $CH_2Br_2$  or  $CCl_3Br$ , respectively, compared to the conversion rates observed in Chapter 3.1.2, without alkyl radical scavengers. Experiments were conducted under ambient atmospheric conditions with a reaction time of 48 h. Error bars refer to the SD of the total conversion of all major C1 and C2 compounds for  $n = 9$ , except for  $C_2D_6$ ,  $n = 3$ . Taken from Hädel et al. (2023).<sup>205</sup> ..... 54
- Figure 20: The chromatograms of isotopically labelled  $CH_3Br$  in the experiments with **a)**  $LFe^{II}Cl_2$  and  $CH_2Br_2$  (1.25 mmol), **b)**  $LFe^{II}Cl_2$  and 1.25 mmol of  $CCl_3Br$  and as well **c)**  $Fe_2O_3$  and 1.25 mmol of  $CCl_3Br$  and 25  $\mu mol$   $d_6$ -DMSO, 100  $\mu mol$  Asc and 200  $\mu mol$   $H_2O_2$  under ambient atmospheric conditions with a reaction time of 48 h. The presented chromatograms refer to the masses 97 (black) and 99 (pink), representing the  $CD_3Br$  with the stable isotopes of Br (79, 81). This represents a mass shift of 3 concerning  $CH_3Br$  (the mass of  $CH_3Br$  is 94 and 96). Taken from Hädel et al. (2023).<sup>205</sup> ..... 55
- Figure 21: The portfolio of C1 and C2 components arises from the  $CH_3$  radical, which is formed abiotically by the  $LFe^{II}Cl_2/H_2O_2$  system from DMSO. Deuterated and  $^{13}C$ -labelled DMSO and  $^{18}O$ -labelled  $H_2O_2$  and  $O_2$  were utilised to investigate the different pathways. The observed  $^{13}C$  and  $^2H$  labels are presented in bold red and green, respectively. Oxygenated C1 compounds with  $^{18}O$  isotopes are highlighted in bold orange or blue, originating from  $^{18}O$ -labeled  $H_2O_2$  or  $O_2$ , respectively. Oxygen atoms in orange and blue indicate that the product derived oxygen from  $H_2O_2$  and  $O_2$ . The oxidation states of carbon are shown in Roman numbers. Taken from Hädel et al. (2023).<sup>205</sup> ..... 58
- Figure 22: Postulated mechanism for forming  $CH_4$ ,  $C_2H_6$ ,  $CH_3OH$  and  $CH_2O$  by reaction of DMSO with a Fe species ( $LFe^{II}Cl_2$  or  $Fe_2O_3$ ),  $H_2O_2$  and Asc. (Postulated intermediates are highlighted in red; reactants are shown in green; products are shown in blue; for simplicity, the stoichiometry of some of the reactions has not been adjusted). Taken from Hädel et al. (2023).<sup>205</sup> ..... 59

- Figure 23: The formation of C1 and C2 compounds in experiments with 10  $\mu\text{mol}$   $\text{LFe}^{\text{II}}\text{Cl}_2$  (bar B) or  $\text{Fe}_2\text{O}_3$  (bar H), 200  $\mu\text{mol}$   $\text{H}_2\text{O}_2$  and 100  $\mu\text{mol}$  Asc with 25  $\mu\text{mol}$   $\text{d}_3$ -methionine ( $\text{d}_3$ -Met), methylphosphonate (MPA; unlabelled C1 and C2 compounds),  $\text{d}_9$ -choline ( $\text{d}_9$ -Cho) or  $\text{d}_9$ -trimethylamine ( $\text{d}_9$ -TMA) as precursor compounds under ambient atmospheric conditions with a reaction time of 48 h. Error bars refer to the SD of the total conversion of all major C1 and C2 compounds for  $n = 9$ , except for  $\text{CH}_4$  and  $\text{C}_2\text{D}_6$ ,  $n = 3$ ..... 62
- Figure 24: Chromatograms and mass tracks of  $\text{CD}_3\text{OH}$  with a shift to 35 in experiments with 25  $\mu\text{mol}$  **a)**  $\text{d}_3$ -methionine, **b)**  $\text{d}_9$ -choline and **c)**  $\text{d}_9$ -trimethylamine and 10  $\mu\text{mol}$   $\text{LFe}^{\text{II}}\text{Cl}_2$ , 100  $\mu\text{mol}$  Asc and 200  $\mu\text{mol}$   $\text{H}_2\text{O}_2$  as an oxidant under ambient atmospheric conditions with a reaction time of 48 h. .... 63
- Figure 25: Mass tracks of  $\text{CD}_2\text{O}$  with a shift of 2 AMU from 210 to 212 in experiments with 25  $\mu\text{mol}$  **a)**  $\text{d}_3$ -methionine, **b)**  $\text{d}_9$ -choline and **c)**  $\text{d}_9$ -trimethylamine and 10  $\mu\text{mol}$   $\text{LFe}^{\text{II}}\text{Cl}_2$ , 100  $\mu\text{mol}$  Asc and 200  $\mu\text{mol}$   $\text{H}_2\text{O}_2$  as an oxidant under ambient atmospheric conditions with a reaction time of 48 h. .... 64
- Figure 26: Investigations of  $\text{OCH}_3$  group-containing compounds (25  $\mu\text{mol}$  of Sinapyl alcohol (Sin); Galacturonic acid methyl ester (Game); 2-, 3- and 4-Methoxyphenol (2-, 3- and 4-Methph); Anisole; Syringic acid (Syr acid) and Syringaldehyde (Syr ald)), without Asc replaced by 0.05  $\mu\text{mol}$  triflic acid (with 100  $\mu\text{mol}$  Asc is marked as +Asc), 10  $\mu\text{mol}$   $\text{LFe}^{\text{II}}\text{Cl}_2$  (bar B) or  $\text{Fe}_2\text{O}_3$  (bar H) and 200  $\mu\text{mol}$   $\text{H}_2\text{O}_2$  as an oxidant under ambient atmospheric conditions with a reaction time of 48 h. Error bars refer to the SD of the total conversion of all major C1 and C2 compounds for  $n = 9$ ..... 67
- Figure 27: Comparison of  $\text{CH}_3\text{Br}$  in experiments with 10  $\mu\text{mol}$   $\text{LFe}^{\text{II}}\text{Cl}_2$ , 100  $\mu\text{mol}$  Asc and 200  $\mu\text{mol}$   $\text{H}_2\text{O}_2$ , 25  $\mu\text{mol}$  sinapyl alcohol, 2-Methoxyphenol or Game and 1,25 mmol  $\text{CCl}_3\text{Br}$  (alkyl radical trapping agent) compared to the blank experiment with the same setup but only without substrate ( $n = 3$ ) under ambient atmospheric conditions with a reaction time of 48 h. **a)** Mass 94 (stable isotope 79 of bromine) and **b)** 96 (stable isotope 81 of bromine) of  $\text{CH}_3\text{Br}$ . .... 68
- Figure 28: Chromatograms and mass track of  $\text{CH}_3\text{OH}$  from different isotopic labelling experiments with 10  $\mu\text{mol}$   $\text{LFe}^{\text{II}}\text{Cl}_2$ , 100  $\mu\text{mol}$  Asc and 200  $\mu\text{mol}$   $\text{H}_2\text{O}_2$  and 25  $\mu\text{mol}$  sinapyl alcohol, coniferyl alcohol or 2-methoxyphenol under ambient atmospheric conditions with a reaction time of 48 h: **a)** with  $\text{H}_2^{18}\text{O}_2$  instead of  $\text{H}_2\text{O}_2$  ( $n = 3$ ) and **b)**  $\text{O}_2$  replaced in  $\text{H}_2\text{O}$  and headspace by  $^{18}\text{O}_2$  ( $n = 3$  measurement). **c)** Experiment with 1/10 of all compounds and with  $^{18}\text{OCH}_3$  2-methoxyphenol instead of unlabelled 2-methoxyphenol ( $n = 3$  measurement). Pink, blue and brown chromatograms are the measured mass of 29, 30 and 31 of the produced  $\text{CH}_3\text{OH}$ . The black line is the blank without substrate, and green,

dark blue, and olive are the masses 33 and 34 of  $\text{CH}_3^{18}\text{OH}$  measured in the experiments.

**d)** Mass track of  $\text{CH}_3\text{OH}$  in a standard experiment with d3-2-methoxyphenol with a mass shift of 3 AMU from 32 to 35 representing the  $\text{CD}_3\text{OH}$ ..... 69

Figure 29: The experiments investigated the formation of C1 and C2 compounds from  $\text{d}_6$ -DMSO using 10  $\mu\text{mol}$  different transition metal species in conjunction with 200  $\mu\text{mol}$   $\text{H}_2\text{O}_2$  and 100  $\mu\text{mol}$  Asc under ambient atmospheric conditions with a reaction time of 48 h. All C1 and C2 compounds could be measured for all transition metal species. Except for  $\text{CuCl}_2$ ,  $\text{CH}_2\text{O}$  concentrations could not be determined; hence, no conversion rate was calculated.  $\text{CuOx}$  is a mixture of copper oxides ( $\text{CuO}$  and  $\text{Cu}_2\text{O}$ ), whereas  $\text{Cu}(\text{OAc})_2$  refers to copper(II) acetate. Error bars refer to the SD of the total conversion of all major C1 and C2 compounds for  $n = 9$ , except for  $\text{C}_2\text{D}_6$ ,  $n = 3$ . ..... 73

Figure 30: The experiments investigated the formation of C1 and C2 compounds from 25  $\mu\text{mol}$   $\text{d}_3$ -methionine using 10  $\mu\text{mol}$  of different transition metal species in conjunction with 200  $\mu\text{mol}$   $\text{H}_2\text{O}_2$  and 100  $\mu\text{mol}$  Asc under ambient atmospheric conditions with a reaction time of 48 h. For  $\text{CuCl}_2$ ,  $\text{CH}_2\text{O}$  concentrations could not be determined; hence, no conversion rate was calculated.  $\text{CuOx}$  is a mixture of copper oxides ( $\text{CuO}$  and  $\text{Cu}_2\text{O}$ ), whereas  $\text{Cu}(\text{OAc})_2$  refers to copper(II) acetate. Error bars refer to the SD of the total conversion of all major C1 and C2 compounds for  $n = 9$ , except for  $\text{C}_2\text{D}_6$ ,  $n = 3$ . ..... 75

Figure 31: The formation of  $\text{CH}_3\text{OH}$  and  $\text{CH}_2\text{O}$  compounds from 25  $\mu\text{mol}$  2-methoxyphenol was investigated using 10  $\mu\text{mol}$  of different transition metal species, 200  $\mu\text{mol}$   $\text{H}_2\text{O}_2$  and 0.05  $\mu\text{mol}$  triflic acid under ambient atmospheric conditions with a reaction time of 48 h. No  $\text{CH}_4$  and  $\text{C}_2\text{H}_6$  formation was observed. For  $\text{CuCl}_2$ ,  $\text{CH}_2\text{O}$  concentrations could not be determined due to analytical issues. Hence, no conversion rate was calculated.  $\text{CuOx}$  is a mixture of copper oxides ( $\text{CuO}$  and  $\text{Cu}_2\text{O}$ ), whereas  $\text{Cu}(\text{OAc})_2$  refers to copper(II) acetate. Error bars refer to the SD of the total conversion of all major C1 and C2 compounds for  $n = 9$ . ..... 77

Figure 32: The formation of  $\text{CH}_3\text{Cl}$  from 25  $\mu\text{mol}$   $\text{d}_6$ -DMSO,  $\text{d}_3$ -methionine, or 2-methylphenol with 100  $\mu\text{mol}$  Asc or 0.05  $\mu\text{mol}$  triflic acid in case of 2-methoxyphenol and 200  $\mu\text{mol}$   $\text{H}_2\text{O}_2$  was investigated using 10  $\mu\text{mol}$  different transition metal species with chlorine counter ions in the experiments described above. Error bars refer to the SD of the conversion of  $\text{CH}_3\text{Cl}$  for  $n = 3$ . ..... 78

Figure 33: Formation of **a)**  $\text{CH}_3\text{OH}$  and  $\text{CH}_2\text{O}$  and **b)**  $\text{CH}_4$  and  $\text{C}_2\text{H}_6$  were detected in experiments involving 50 mg (dry weight) of either lignin or pectin. These experiments were carried out with either 10  $\mu\text{mol}$   $\text{Fe}_2\text{O}_3$  and 100  $\mu\text{mol}$  Asc or without Asc and 10  $\mu\text{mol}$   $\text{Fe}_2\text{O}_3$ , and the third experiment with 0.05  $\mu\text{mol}$  triflic acid and no  $\text{Fe}_2\text{O}_3$  and with 200  $\mu\text{mol}$   $\text{H}_2\text{O}_2$  in

- each experiment under ambient atmospheric conditions with a reaction time of 48 h. Error bars refer to the SD of the total conversion of all major C1 and C2 compounds for  $n = 9$ , except for  $\text{CH}_4$  and  $\text{C}_2\text{D}_6$ ,  $n = 3$ . ..... 84
- Figure 34: abiotic formation of  $\text{CH}_3\text{OH}$ ,  $\text{CH}_2\text{O}$ ,  $\text{CH}_4$ , and  $\text{C}_2\text{H}_6$  from 24 sterilised soils at  $105^\circ\text{C}$  (5 g each, with indicated depths in cm) using ultra-pure  $\text{H}_2\text{O}$  (10 ml), incubated for 48 h under ambient conditions ( $22^\circ\text{C}$  and 1013 mbar). **a)**  $\text{CH}_3\text{OH}$  and  $\text{CH}_2\text{O}$  were displayed in  $\mu\text{g}/\text{g}_{\text{soil,dw}}$ , with three orders of magnitude lower concentrations for **b)**  $\text{CH}_4$  and  $\text{C}_2\text{H}_6$  displayed in  $\text{ng}/\text{g}_{\text{soil,dw}}$ . Error bars refer to the SD of the total conversion of all major C1 and C2 compounds for  $n = 9$ , except for  $\text{CH}_4$  and  $\text{C}_2\text{D}_6$ ,  $n = 3$ . Parts of the data are taken from Hädeler et al. (2023).<sup>205</sup> ..... 87
- Figure 35: **a)**  $\text{OCH}_3$  content in soil samples AL 20, PT 0-10 and WA2 0-10 before and after  $\text{OCH}_3$  removal due to HI treatment. **b)** Comparison of the concentrations of  $\text{CH}_3\text{OH}$  and  $\text{CH}_2\text{O}$  and **c)**  $\text{CH}_4$  and  $\text{C}_2\text{H}_6$  from soil experiments with and without  $\text{OCH}_3$  group removal. Error bars refer to the SD of the total conversion of all major C1 and C2 compounds for  $n = 9$ , except for  $\text{CH}_4$  and  $\text{C}_2\text{D}_6$ ,  $n = 3$ . ..... 88
- Figure 36: Chromatogram of labelled  $\text{CH}_3\text{OH}$  in soil experiments with added deuterated or  $^{18}\text{O}$ - $\text{OCH}_3$  labelled 2-Methoxyphenol. The  $m/z$  33, 34 and 35 of  $\text{CD}_3\text{OH}$  **a)** or  $m/z$  33 and 34 of  $\text{CH}_3^{18}\text{OH}$  **b)** in experiments where the  $\text{OCH}_3$  groups were removed from the soil samples GL1, PO and GL2 using the Zeisel method. 1 g soil and 2 ml ultra-pure  $\text{H}_2\text{O}$  with added 5  $\mu\text{mol}$  **a)** deuterated  $\text{OCH}_3$ -2-Methoxyphenol and **b)** 5  $\mu\text{mol}$   $^{18}\text{O}$ - $\text{OCH}_3$ -2-Methoxyphenol. Blue, brown and pink are the experiments with labelled 2-methoxyphenol; light green, dark green and purple are the non-spiked soils, and black is pure  $\text{H}_2\text{O}$ . ..... 90
- Figure 37: Chromatogram and mass track 33 and 35 of deuterated  $\text{CH}_3\text{OH}$  in an experiment with 5 g sterile soil (WF 0-5) in 10 ml ultra-pure  $\text{H}_2\text{O}$  and 25  $\mu\text{mol}$   $\text{d}_6$ -DMSO. Taken from Hädeler et al. (2023).<sup>205</sup> ..... 91
- Figure 38: Chromatogram and mass track 210 and 212 of deuterated and derivatised  $\text{CH}_2\text{O}$  in an experiment with 5 g sterile soil (WF 0-5) in 10 ml ultra-pure  $\text{H}_2\text{O}$  and  $\text{d}_6$ -DMSO. Taken from Hädeler et al. (2023).<sup>205</sup> ..... 92
- Figure 39:  $\text{CH}_3\text{OH}$  **a)** and  $\text{CH}_2\text{O}$  **b)** concentrations in 10 wet-dry-cycle experiments (5 g soil with 10 ml  $\text{H}_2\text{O}$ ; 2-day wetting phase and then sterilisation at  $105^\circ\text{C}$ ) of soil UH 0-10 and AL 20 (also with added  $\text{H}_2\text{O}_2$ ) and the sum of  $\text{CH}_3\text{OH}$  and  $\text{CH}_2\text{O}$  concentrations **c)**. Error bars refer to the SD of the total conversion of  $\text{CH}_3\text{OH}$  and  $\text{CH}_2\text{O}$  for  $n = 9$ . ..... 93
- Figure 40: Measurement of  $\text{CH}_3\text{OH}$ ,  $\text{CH}_2\text{O}$  **a)** and  $\text{CH}_4$  and  $\text{C}_2\text{H}_6$  **b)** in soil sample PT 0-10 (5 g and 10 ml  $\text{H}_2\text{O}$ ) with the adjustment of the pH-value with NaOH. Error bars refer to the SD of

- the total conversion of all major C1 and C2 compounds for n = 9, except for CH<sub>4</sub> and C<sub>2</sub>D<sub>6</sub>, n = 3. .... 94
- Figure 41: Measurement of CH<sub>3</sub>OH, CH<sub>2</sub>O **a)** and CH<sub>4</sub> and C<sub>2</sub>H<sub>6</sub> **b)** in soil WA2 0-10 at different incubation temperatures (-26, 6, 12, 22, 30, 40 and 50°C). Error bars refer to the SD of the total conversion of all major C1 and C2 compounds for n = 9, except for CH<sub>4</sub> and C<sub>2</sub>D<sub>6</sub>, n = 3. .... 95
- Figure 42: **a)** Degradation of added CH<sub>3</sub>OH in untreated soil samples AL 20 0-20, WA2 0-10, and UH 0-10 (n = 3). **b)** Measurement of CH<sub>3</sub>OH and CH<sub>2</sub>O in soil AL 20 with added methylotrophic bacteria (*Methylobacterium extorquens*) before and after the incubation compared with the experiment of AL 20 from Figure 34. Error bars refer to the SD of the total conversion of CH<sub>3</sub>OH and CH<sub>2</sub>O for n = 9. .... 96
- Figure 43: Correlation of the TOC (n = 1) with OCH<sub>3</sub> content (n = 3) of the 24 investigated soil samples with an R<sup>2</sup> = 0.88. .... 97
- Figure 44: The TOC was correlated with the sum of CH<sub>3</sub>OH and CH<sub>2</sub>O concentrations of all 24 soils investigated. The experiments involved a two-day incubation period, during which 5 g of soil was incubated in 10 ml ultra-pure H<sub>2</sub>O. .... 98
- Figure 45: Overview of the cycle of iron-mediated demethylation from lignin-derived substrates and the production of CH<sub>3</sub>OH and CH<sub>2</sub>O. Subsequently, the degradation by microbes or emission into the atmosphere and, finally, the mineralisation to CO<sub>2</sub>, which is taken up by plants. .... 103
- Figure 46: Summary of the CH<sub>3</sub> radical-based (left) and OCH<sub>3</sub>-based cycles (right) that form C1 and C2 compounds. Fenton Chemistry generates the [Fe<sup>IV</sup>=O]<sup>2+</sup> species that initiates the demethylation (left) or the demethoxylation (right) of the substrates with hetero-bonded CH<sub>3</sub> groups. The observed <sup>13</sup>C and <sup>2</sup>H labels in the CH<sub>3</sub> radical-based mechanism are presented in bold red and green, respectively. Oxygenated C1 compounds with <sup>18</sup>O isotopes are highlighted in bold orange or blue, originating from <sup>18</sup>O-labeled H<sub>2</sub>O<sub>2</sub> or O<sub>2</sub>, respectively. The deuterated and <sup>18</sup>O labels from the OCH<sub>3</sub> group of 2-methoxyphenol are shown in red and pink, respectively. .... 108

## List of Tables

Table 1: A comprehensive overview of all chemical components utilised, including their respective chemical structures. ....	14
Table 2: Overview of transition metal species used instead of the $\text{LFe}^{\text{II}}\text{Cl}_2$ or $\text{Fe}_2\text{O}_3$ . ....	19
Table 3: Used amounts of substrates in the standard experiments dissolved in 10 ml $\text{H}_2\text{O}$ . ....	24
Table 4: Sample name, location and a short description of the sampled soils according to the “Leitboden-assoziationen” of the Soil Atlas of Germany of the Federal Institute for Geosciences and Natural Resources. ....	27
Table 5: Experimental setups to determine the differences between DMSO and $\text{d}_6$ -DMSO. ....	40
Table 6: Composition of the experiments to determine the conversion rates with different Asc concentrations. ....	42
Table 7: Composition of the experiments with (+) and without (-) $\text{O}_2$ to determine the conversion rates and possible differences. ....	45
Table 8: Composition of the experiments with the alkyl radical scavenger $\text{CH}_2\text{Br}_2$ and $\text{CCl}_3\text{Br}$ to determine the conversion rates and possible differences. ....	53
Table 9: Composition of the experiments with $\text{d}_3$ -methionine, methylphosphonate, $\text{d}_9$ -choline and $\text{d}_9$ -trimethylamine to determine the conversion rates and possible differences. ....	60
Table 10: Composition of the experiments on different transition metal species with $\text{d}_6$ -DMSO, $\text{d}_3$ -methionine and 2-methoxyphenol as precursor compounds to determine the conversion rates and possible differences. ....	72
Table 11: Composition of the experiments with lignin or pectin and with or without $\text{Fe}_2\text{O}_3$ and Asc to determine the conversion rates and possible differences. ....	83

## 1 Introduction

Many different types of volatile carbon compounds (VOCs) are released into the atmosphere from various natural and anthropogenic processes and play a prominent role in all parts of the environment.<sup>1,2</sup> Crucial compounds with one or two carbon atoms (C1 and C2) are methane (CH<sub>4</sub>), ethane (C<sub>2</sub>H<sub>6</sub>), methanol (CH<sub>3</sub>OH), formaldehyde (CH<sub>2</sub>O), methyl chloride (CH<sub>3</sub>Cl), carbon dioxide (CO<sub>2</sub>), carbon monoxide (CO), formic acid (HCOOH) and acetic acid (CH<sub>3</sub>COOH) with oxidation states for carbon between -IV to +IV. These strongly influence the chemical and physical properties of the atmosphere due to the reaction with oxidants such as hydroxyl radicals, nitrogen oxides and ozone to form new radicals/VOCs. They also influence the radiation budget, act as a greenhouse gas, and influence cloud formation.<sup>1,3,4</sup>

The C1 and C2 compounds are typically attributed to the thermal degradation of organic matter or complex metabolic processes occurring in plants and microorganisms. Through the C1 and C2 components, these compounds can regulate essential ecological functions, such as the growth of plants and microbes, and act as stress resistance or signalling substances in communication reproduction.<sup>5,6</sup> Methanogenic archaea produce the majority of atmospheric CH<sub>4</sub>, thriving under anoxic conditions and utilising CO<sub>2</sub>, H<sub>2</sub>, and acetate as substrates for a series of enzymatic reactions.<sup>7</sup> Further sources of CH<sub>4</sub> include industrial coal, gas, and oil processing; incomplete combustion of hydrocarbons; and geological activities at elevated temperatures and/or pressures.<sup>8</sup> These processes are also sources of many different VOCs.<sup>9,10</sup> The primary identified sources of CH<sub>3</sub>OH are vegetation,<sup>11</sup> soils,<sup>12</sup> and the ocean.<sup>13</sup>

A hitherto unexplained phenomenon has been reported where CH<sub>4</sub> and other C1 compounds formed abiotically, primarily by compounds with a sulphur-bonded CH<sub>3</sub> group, in oxic environments and under ambient atmospheric pressure and temperature. CH<sub>4</sub> is generated via iron mediation, with hydrogen peroxide (H<sub>2</sub>O<sub>2</sub>) acting as an exogenous agent oxidant.<sup>14-16</sup> Consequently, the formation of those above-mentioned C1 and C2 compounds is investigated under abiotic, oxic, and atmospheric conditions. Intensive isotopic labelling studies were conducted to understand the reaction mechanism leading to the formation of C1 and C2 components. Various precursor compounds are investigated involving hetero-bonded CH<sub>3</sub> group-containing compounds sulphur, nitrogen, phosphorus and oxygen (S, N, P, and O) with Fe, H<sub>2</sub>O<sub>2</sub>, and ascorbic acid (Asc). The occurrence of these components in nature in substantial quantities underscores the importance of this reaction. A comprehensive understanding of the production of these C1 and C2 compounds is essential for grasping their impact on natural processes, particularly those that influence the climate, and for evaluating the subsequent consequences of the current climate change.

The current state of research concerning these reactions is presented, followed by an examination of the individual C1 and C2 components and their influence on the atmosphere and other compartments of the Earth's system. The precursor compounds, Fe or transition metal species and Asc, are then discussed, along with soils in the context of C1 and C2 compounds and the reactive oxygen species (ROS) in soils. Finally, the objectives of the study are outlined.

## 1.1 State of knowledge

The discovery by Keppler et al. (2006)<sup>17</sup> and subsequent research that plants<sup>18</sup>, fungi<sup>19,20</sup> and animals<sup>21-23</sup> can produce CH<sub>4</sub> under atmospheric conditions, leading to a new field of research. These investigations, along with all subsequent research in this field, are presented here. Also, research investigating the formation of CH<sub>3</sub>OH from OCH<sub>3</sub> groups is discussed separately due to the new mechanism described here of the formation of CH<sub>3</sub>OH directly from OCH<sub>3</sub> groups.

### 1.1.1 Abiotic formation of C1 and C2 compounds from hetero-bonded CH<sub>3</sub> groups

Keppler et al. (2006) used stable carbon isotopes to identify the hitherto unknown oxic production from plants of CH<sub>4</sub>. High global emissions were observed from intact plants (62-236 Tg yr<sup>-1</sup>) and detached leaves (1-7 Tg yr<sup>-1</sup>), suggesting an important source of CH<sub>4</sub>.<sup>17</sup> This discovery subsequently became the subject of considerable controversy.<sup>24-26</sup> However, a growing scientific literature emerged on oxic CH<sub>4</sub> formation in the following years. The previously mentioned formation of CH<sub>4</sub> from plants<sup>18</sup>, fungi<sup>19,20</sup> and animals<sup>21-23</sup> extended this knowledge by providing more CH<sub>4</sub> sources. Research has shown that with deuterated OCH<sub>3</sub>-pectin, the OCH<sub>3</sub> group serves as a precursor of CH<sub>4</sub>.<sup>27</sup> Another precursor compound was found due to the addition of <sup>13</sup>CH<sub>3</sub>-methionine to plants and the subsequent detection of deuterium-labelling in CH<sub>4</sub>.<sup>28</sup> Another approach involved H<sub>2</sub>O<sub>2</sub>, Asc, FeCl<sub>2</sub>, or FeCl<sub>3</sub>, resulting in the production of choline, CH<sub>4</sub>, CO, and CO<sub>2</sub>, with choline identified as the source. This system was investigated in rat liver mitochondria, which was postulated to serve as a protective function against reductive stress. The aim of these experiments was to ascertain how CH<sub>4</sub> is generated in living organisms.<sup>21,29</sup> However, these investigations do not provide a detailed mechanism of CH<sub>4</sub> production. Leaf wax was employed to examine the underlying mechanism, and a Norrish I reaction was proposed to generate CH<sub>3</sub> radicals via UV light in oxic conditions and, subsequently, CH<sub>4</sub>.<sup>30</sup> However, this CH<sub>4</sub> is not produced directly by the plant, as previously postulated by Keppler et al. (2006).

The H<sub>2</sub>O<sub>2</sub>, Asc, Fe system was taken up by Althoff et al. (2010) and investigated further. Other Fe species (hematite, ferrihydrite, goethite and lepidocrocite) with H<sub>2</sub>O<sub>2</sub> and Asc as a precursor compound were varied in concentration. It turned out that H<sub>2</sub>O<sub>2</sub> and Asc in a ratio of 2:1 gave the highest yields

of CH<sub>4</sub> at a pH value of approx. 3. Furthermore, nine other substances (e.g. 2-methoxyphenol, vanillin and methionine) instead of Asc were analysed for CH<sub>4</sub> production, but none could be detected.<sup>31</sup> These studies were further advanced by Althoff et al. (2014), who conducted experiments with Asc, H<sub>2</sub>O<sub>2</sub>, Fe minerals, and precursor compounds containing sulfur-bonded CH<sub>3</sub> groups. In these experiments, Asc acted as an OH radical scavenger rather than as a precursor compound. Up to 83% CH<sub>4</sub> is produced from DMSO, and all other compounds also yield CH<sub>4</sub>. Further compounds with N-, O-, and C-bonded CH<sub>3</sub> groups do not produce CH<sub>4</sub>, except for choline chloride, which produces 0.6 % CH<sub>4</sub>. In experiments utilising dissolved Fe (e.g. Fe salts), however, the generation of CH<sub>4</sub> was observed to be negligible. This leads to the conclusion that OH radicals, which are generated by the Fenton reaction there, must play a very minor role in the experiments with Fe minerals, given that a considerable amount of CH<sub>4</sub> is produced in the former and a minimal amount in the latter. This leads to the assumption that another oxidising agent is present in the experiment. The reaction of Asc with the Fe mineral undergoes reductive dissolution, and together with H<sub>2</sub>O<sub>2</sub>, a [Fe<sup>IV</sup>=O]<sup>2+</sup> species and OH radicals are generated, with the latter being scavenged by the ascorbate. This was confirmed using an artificial bispidine complex, which exclusively forms the [Fe<sup>IV</sup>=O]<sup>2+</sup> species and leads to similar results. In this reaction, CH<sub>3</sub> radicals were formed, which were detected using electron paramagnetic resonance (EPR) spectroscopy and subsequently produced CH<sub>4</sub>. Additionally, CH<sub>3</sub>OH was also detected (Figure 1). To identify the precursor atom of CH<sub>4</sub>, <sup>13</sup>CH<sub>3</sub> labelled methionine was used. The δ<sup>13</sup>C of CH<sub>4</sub> rises drastically because the <sup>13</sup>C labelled CH<sub>3</sub> group of methionine is the precursor of CH<sub>4</sub>.<sup>14</sup> This attack of the [Fe<sup>IV</sup>=O]<sup>2+</sup> species at the sulphur atom of methionine and the subsequent transfer of the oxygen to the sulphur atom is named oxygen atom transfer (OAT). An electrophile (e.g. Fe<sup>2+</sup>, Fe<sup>3+</sup>) may react with the CH<sub>3</sub> group to produce CH<sub>3</sub> radicals, which react further to CH<sub>4</sub> and other compounds.

This mechanism was further investigated in laboratory experiments and extended with various bispidine complexes. The created [Fe<sup>IV</sup>=O]<sup>2+</sup> species was observed to oxidise the sulphur atom, resulting in the formation of methionine sulphoxide. Subsequently, the compound oxidised further to a sulphone or a CH<sub>3</sub> radical and was split off homolytically<sup>16</sup>, as previously reported by Althoff et al. (2014). This mechanism was supported by computational modelling (Figure 1).

Taking up this system, a mechanism for CH<sub>4</sub> production from methylated sulfur and nitrogen compounds via Fenton reactions, which utilise iron (Fe<sup>2+</sup>) and ROS generated by light and heat in aqueous environments, has been postulated. OH radicals and [Fe<sup>IV</sup>=O]<sup>2+</sup> species oxidatively demethylate these compounds, forming CH<sub>3</sub> radicals that subsequently lead to the generation of CH<sub>4</sub>. This non-enzymatic process is supposed to have contributed to CH<sub>4</sub> levels before the emergence of life and may have played a significant role in the early atmospheric evolution of Earth.<sup>32</sup>



those observed in the thioether mechanism, with conversion rates below 1 %.<sup>37</sup> Further CH<sub>4</sub>-emitting organisms have been identified, including fungi<sup>19</sup>, marine algae<sup>38</sup>, animals<sup>21,23</sup> and humans.<sup>39,40</sup>

### 1.1.2 Formation of CH<sub>3</sub>OH from methoxy group containing compounds

Due to the ubiquitous distribution of pectin and lignin and the monomeric units, they are of interest and could be possible precursors of C1 and C2 compounds. The OCH<sub>3</sub> groups of pectin were identified as the source of CH<sub>4</sub>.<sup>27,30</sup> CH<sub>4</sub> production from leave wax could also be measured.<sup>41</sup> Previously, the OCH<sub>3</sub> group had also been identified as a precursor of CH<sub>3</sub>Cl at temperatures above 200°C.<sup>42</sup> No detailed reaction mechanism was postulated in either case.

Many different catalytic reactions for the demethoxylation of 2-methoxyphenol and other methoxybenzenes have been described in the literature. However, these are always carried out at high temperatures (>285°C), high pressure (>0.5 MPa) and often in a hydrogen atmosphere.<sup>43-45</sup> Consequently, these conditions do not arise in natural environments and are irrelevant for naturally occurring processes.

Other research has demonstrated that wood treated with Fe can release CH<sub>2</sub>O. The addition of H<sub>2</sub>O<sub>2</sub> has been shown to significantly enhance the release of CH<sub>2</sub>O, while the incorporation of lignin into the experimental setup has been observed to increase CH<sub>2</sub>O production further. The hypothesis that the OCH<sub>3</sub> group is cleaved and CH<sub>3</sub>OH is produced, which is then attacked by OH radicals to yield CH<sub>2</sub>O, has been postulated.<sup>46</sup> Further studies indicate that cellobiose dehydrogenase may be involved in the degradation of OCH<sub>3</sub> groups in lignin. This process generates hydroxyl radicals via the Fenton reaction, which attacks the aromatic ring and splits off an OCH<sub>3</sub> group, reacting further to form CH<sub>3</sub>OH.<sup>47,48</sup> The proposed enzymatic mechanisms have not been verified by chemical modelling or isotopic labelling experiments, so the precise mechanisms remain unclear.

The findings outlined above contribute to the conceptualisation of this study and represent the fundamental elements upon which this work is conceptualised.

## 1.2 Properties of C1 and C2 compounds and their role in the natural environments

C1 and C2 compounds significantly influence the atmosphere, affecting its chemical and physical composition, human health, and climate conditions. Of these compounds, CO<sub>2</sub> as a non-VOC and CH<sub>4</sub> are of particular importance in the atmosphere, with concentrations of 425 parts per million by volume (ppm<sub>v</sub>) and 1936 parts per billion by volume (ppb<sub>v</sub>), respectively.<sup>49</sup> Other VOCs include CH<sub>3</sub>OH, C<sub>2</sub>H<sub>6</sub>, and halogenated compounds such as CH<sub>3</sub>Cl, which can react with hydroxyl radicals (OH<sup>•</sup>), nitrogen

oxides ( $\text{NO}_x$ ), and ozone ( $\text{O}_3$ ), leading to the formation of new VOCs, peroxides, or radicals, such as hydroperoxyl ( $\text{HO}_2\bullet$ ), peroxy ( $\text{RO}_2\bullet$ ), or organic radicals ( $\text{RO}\bullet$ ). Other secondary organic aerosols are also formed by isoprene, terpenes, and aromatics, among other compounds (Figure 2).<sup>3,50–52</sup>

## Gas phase reactions of VOCs

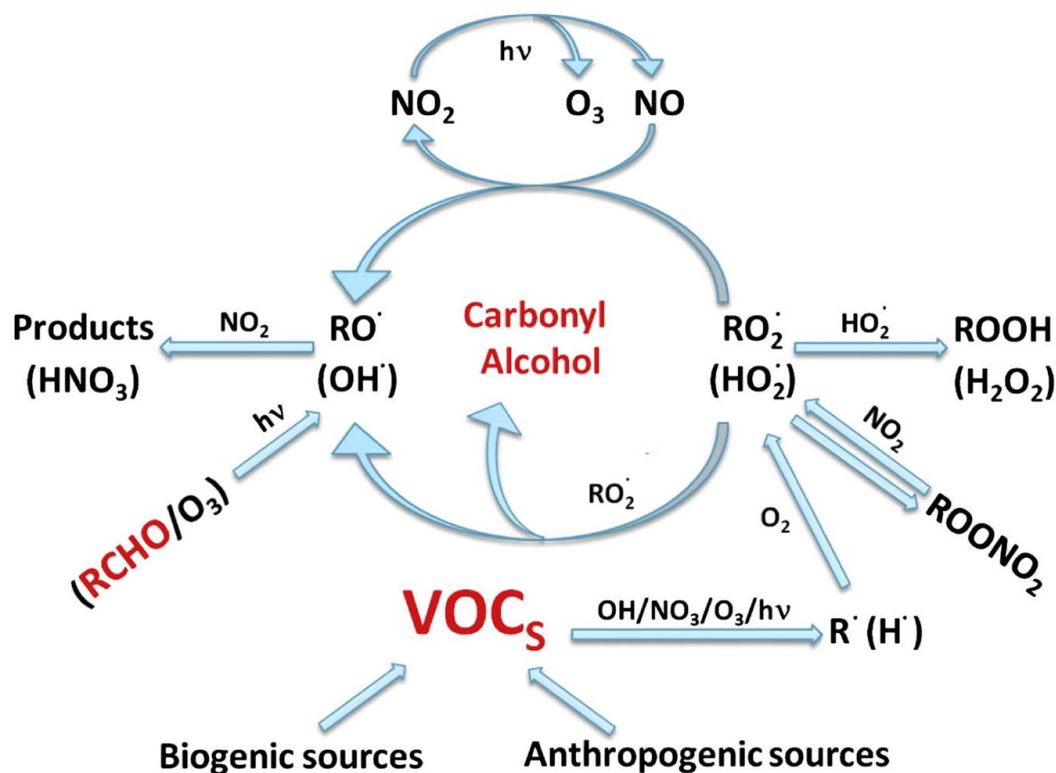


Figure 2: Complex interactions of gas phase reactions and heterogeneous reactions of VOCs in the atmosphere. Taken from Shen et al. (2013).<sup>3</sup>

A subcategory of the VOCs are the biogenic volatile organic compounds (BVOCs) which primarily originated from terrestrial and marine ecosystems. In terrestrial ecosystems, BVOCs are emitted predominantly by plants or through the decomposition of organic matter by microorganisms.<sup>50,53,54</sup> In the ocean, plankton represents the primary source of BVOCs.<sup>55</sup> In these ecosystems they have crucial ecological functions, including promoting plant and microbial growth, enhancing resilience to environmental stress, and releasing signalling compounds that facilitate communication and reproduction.<sup>5,6</sup> Other sources of BVOCs include the combustion of biomass and fossil fuels. An increase in BVOCs is postulated due to climate change, as the temperature and, thus, the vapour pressure is rising. Another factor is the longer growing season, as plants can produce more BVOCs.<sup>56</sup> Many of these C1 and C2 compounds are investigated here and are known to be produced from a mechanism different from the oxic and abiotic formations involving Fe, H<sub>2</sub>O<sub>2</sub>, and Asc investigated here.

### 1.2.1 Methane

Since 1750, CH<sub>4</sub> has contributed 23 % to the greenhouse effect, the most abundant reduced compound in the atmosphere.<sup>57</sup> The ratio of CH<sub>4</sub> in the atmosphere has increased from 715 (ppb<sub>v</sub>) in 1750 to 1936 ppb<sub>v</sub> in 2024<sup>49</sup>. This increase is predominantly attributable to anthropogenic emissions. There is a considerable degree of uncertainty surrounding anthropogenic and natural CH<sub>4</sub> emissions estimates, with numbers ranging from 538 to 884 Tg yr<sup>-1</sup>.<sup>8,58</sup> Additionally, discrepancies exist between bottom-up and top-down approaches due to the incomplete understanding of global CH<sub>4</sub> fluxes.<sup>8,58</sup> It has been proposed that a significant aquatic source of CH<sub>4</sub> remains unidentified due to the considerable uncertainty surrounding the budget for aquatic CH<sub>4</sub> emissions.<sup>59</sup> The numerous emission sources are effectively offset by tropospheric oxidation via OH radicals, which serve as a sink, accounting for approximately 90 % of the total removal.<sup>60</sup> Other sinks include the degradation of methanotrophic bacteria in soils<sup>61,62</sup> (4 %), the reaction with chlorine and atomic oxygen radicals in the stratosphere<sup>63</sup> (3 %), and the reaction of chlorine radicals derived from sea salt in the marine boundary layer<sup>64</sup> (3 %).

A fundamental differentiation can be made between pyrogenic, thermogenic and biogenic CH<sub>4</sub> sources<sup>65</sup>, with the latter representing the predominant contributor to atmospheric emissions, estimated at approximately 70 %. Until 2006, biogenic CH<sub>4</sub> was mainly attributed to methanogenesis by microorganisms of the archaea domain under anoxic conditions. These utilise CO<sub>2</sub>, hydrogen (H<sub>2</sub>) and acetate (CH<sub>3</sub>COO<sup>-</sup>) as an energy source, which is enzymatically catalysed to CH<sub>4</sub>.<sup>7</sup> In 2006, oxic CH<sub>4</sub> formation was demonstrated for the first time by Keppler et al.<sup>17</sup> Subsequent studies were conducted to investigate the formation of oxic CH<sub>4</sub> in a range of organisms, including saprotrophic fungi<sup>66</sup>, animals<sup>67</sup>, humans<sup>68</sup>, marine<sup>69</sup> and freshwater<sup>70</sup> algae, and cyanobacteria<sup>71</sup>. The mechanisms underlying the CH<sub>4</sub> production remain inadequately understood. A recent study has demonstrated that the combination of Fe<sup>2+</sup> and H<sub>2</sub>O<sub>2</sub>, produced by ROS, generates a highly reactive [Fe<sup>IV</sup>=O]<sup>2+</sup> species in living organisms. This species can effectively oxidative demethylate DMSO, forming a CH<sub>3</sub> radical and subsequently forming CH<sub>4</sub> (Figure 3).<sup>72</sup>

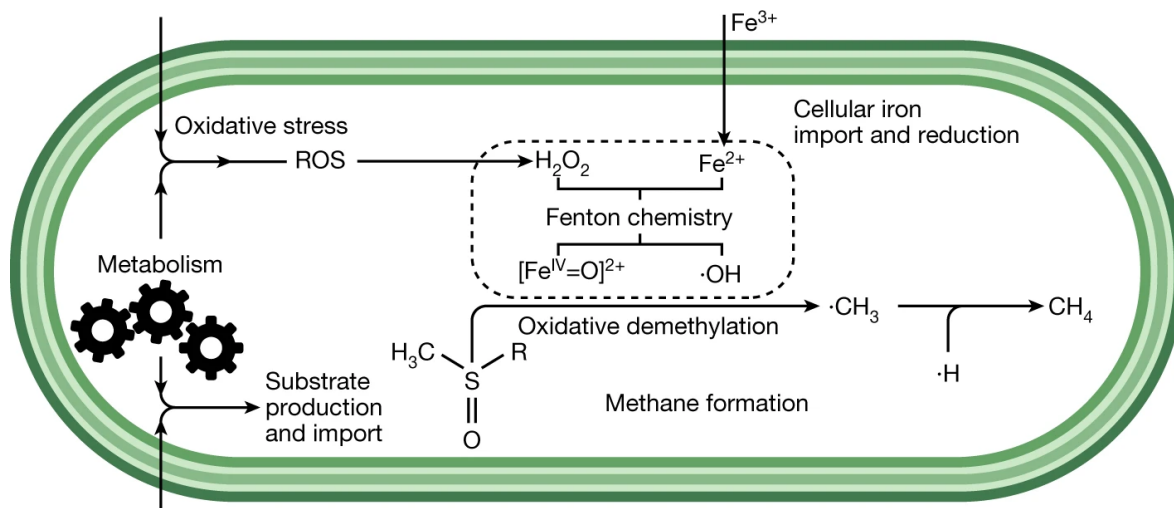


Figure 3: Mechanism for  $\text{CH}_4$  formation in living organisms due to the oxidative demethylation of DMSO. Taken from Ernst et al. (2022).<sup>72</sup>

An intriguing phenomenon is the  $\text{CH}_4$  paradox, predominantly observed in oxygen-saturated marine environments but also occurs in other water surfaces.<sup>70,73</sup> In this instance, the concentration of  $\text{CH}_4$  is greater than its solubility, resulting in supersaturation. Several potential explanations have been proposed for this phenomenon, including the upwelling of anaerobically produced  $\text{CH}_4$ ,<sup>74–76</sup> the production of  $\text{CH}_4$  by algae<sup>69,77</sup> or phytoplankton.<sup>78,79</sup> Other sources that have been discussed are the bacterial degradation of organic matter<sup>80</sup> and DMSO in the ocean, which could be another possible source of  $\text{CH}_4$  in the ocean and thus contribute to the  $\text{CH}_4$  paradox. A positive correlation between DMSO or dimethylsulfoniopropionate and  $\text{CH}_4$  content was measured in a north-south transect in the Western Pacific Ocean. The study's authors conclude that DMSO or a degradation product thereof may be substrates for  $\text{CH}_4$  formation.<sup>81</sup> A further study was also able to observe this correlation. However, no mechanism for  $\text{CH}_4$  production was proposed.<sup>82</sup>

The substances in the aforementioned studies are highly analogous to those under investigation here, except that the reaction in the present study is purely abiotic, in contrast to the living organisms that were previously investigated and could contribute to explaining this phenomenon.

### 1.2.2 Ethane

$\text{C}_2\text{H}_6$  is the second most abundant hydrocarbon in the atmosphere, with a mean concentration of 0.5–2 ppb<sub>v</sub><sup>83</sup> and can reach a maximum of 1000 ppb<sub>v</sub> near gas production facilities<sup>84</sup>. There are pronounced seasonal and latitudinal fluctuations in concentrations, with a peak in winter and a minimum in summer. These fluctuations can be attributed to the degradation of  $\text{C}_2\text{H}_6$  by OH radicals.<sup>84</sup> The higher concentrations observed in the northern hemisphere can be ascribed to the concentration of anthropogenic sources in that region and the relatively short lifetime of  $\text{C}_2\text{H}_6$ , which is only three months. This

is insufficient time for interhemispheric mixing to occur. The most significant sources of atmospheric  $C_2H_6$  are the use of fossil fuels and leakage from oil and gas extraction. Other sources include biomass combustion and the use of biofuels.<sup>84,85</sup> It is also acknowledged that lower emissions are derived from the ocean, terrestrial vegetation and soils.<sup>86</sup> Furthermore, the potential for volcanic sources to contribute to these emissions is also being discussed.<sup>87</sup> Like  $CH_4$ , the hydroxyl radicals represent the primary sink for  $C_2H_6$ . This affects the oxidation potential of the atmosphere, resulting in the production of acetaldehyde ( $CH_3CHO$ ), a precursor of peroxyacetyl nitrile. This pollutant functions as a reservoir for  $NO_x$ , contributing to tropospheric ozone formation.<sup>85,88,89</sup>

### 1.2.3 Carbon monoxide

Carbon monoxide (CO) is a colourless, odourless, and tasteless gas that can cause significant harm to the health of living creatures.<sup>90</sup> The most significant primary source of CO is the incomplete combustion of hydrocarbons<sup>91,92</sup> and other sources, such as vegetation<sup>93</sup> and the ocean.<sup>94</sup> The most prevalent secondary sources are the photochemical oxidation of  $CH_4$  and other VOCs, including isoprene and monoterpenes, with  $CH_2O$  serving as an intermediate product.<sup>95</sup> The primary sink for CO is the reaction with OH radicals, which contributes 40 % to removing OH radicals from the troposphere.<sup>96</sup> Consequently, CO plays an important role in ozone formation and acts as a precursor to preventing the radical degradation of other components in the troposphere, such as  $CH_4$ , which significantly influences the radiation budget and the chemical composition of the troposphere.<sup>97</sup> Soils act as carbon sinks, exhibiting a net flux between -163 and -145 Tg per year, with tropical evergreen forests, savannas, and deciduous forests being the most important sinks with 123 Tg  $CO\ yr^{-1}$ .<sup>98</sup> As with the alkanes, there is a strong gradient for CO from the northern hemisphere to the southern hemisphere since, as previously stated, most emissions are anthropogenic, and the mixing ratio is between 100-150 ppb<sub>v</sub>.<sup>99</sup> In the southern hemisphere, the sources of CO are characterised by biogenic sources and biomass combustion. Given the atmospheric lifetime of approximately two months, a complete atmosphere mixing cannot occur. In conjunction with the highly variable sources, the aforementioned factors result in a highly complex seasonal cycle.<sup>100,101</sup>

### 1.2.4 Carbon dioxide

$CO_2$  is the second most significant natural greenhouse gas after  $H_2O$  vapour and the most important anthropogenic greenhouse gas. The current atmospheric concentration of carbon dioxide is 425 ppm<sub>v</sub>, while the pre-industrial concentration is approximately 277 ppm<sub>v</sub>.<sup>49</sup> This represents an annual increase between 1 and 2.2 ppm<sub>v</sub> over the past 60 years.<sup>102</sup> The primary cause of this increase is the anthropogenic emission of  $CO_2$  resulting from the combustion of fossil fuels and alterations in land use.<sup>103</sup> The

faster degradation of organic matter in soils due to surface alteration could also influence the described reaction because more OCH<sub>3</sub> groups could be available. Also, more energy is in the system due to increasing temperatures. The rising CO<sub>2</sub> levels have resulted in significant alterations to the Earth's climate system, including the acidification of the oceans, which has disrupted the calcium carbonate balance and has had a detrimental impact on marine calcifiers.<sup>104</sup> The combustion of biomass, volcanic activity and respiration (autotrophic and heterotrophic) by organisms represent the most substantial natural sources of atmospheric CO<sub>2</sub>. Gas exchange between the ocean and the atmosphere also influences its levels, which is a sink for atmospheric CO<sub>2</sub>. Other natural processes that contribute to removing CO<sub>2</sub> from the atmosphere include rock weathering and photosynthesis.<sup>105–107</sup>

### 1.2.5 Methanol

CH<sub>3</sub>OH is the most abundant oxygenated and reactive VOC in the atmosphere and plays an important role in atmospheric physics and chemistry. The atmospheric concentration of CH<sub>3</sub>OH exhibits considerable seasonal and regional variability due to the short lifetime, with a mixing ratio of 0.2–195 ppbv.<sup>108</sup> The primary sources are plant growth and reactions in the atmosphere. Other sources include biomass burning, urban areas, and plant decay. These add up to an emission rate of 75–490 Tg yr<sup>-1</sup>.<sup>109–111</sup> Another CH<sub>3</sub>OH source are root exudates in soils<sup>112</sup> and the physical-chemical decomposition of organic matter in the soil.<sup>113</sup> These studies mainly focus on interactions between the biosphere, pedosphere and the atmosphere. The source of CH<sub>3</sub>OH is primarily ascribed to biotic sources. Little is known about the abiotic sources of CH<sub>3</sub>OH in soils and other related carbon pools<sup>114</sup> and nothing about the reaction mechanism.<sup>115</sup>

Several investigations have highlighted the exchange of CH<sub>3</sub>OH between soil and the atmosphere. The highest air concentrations of CH<sub>3</sub>OH among all measured 19 VOCs were measured in a Mediterranean shrubland.<sup>116</sup> In Amazonian soils, CH<sub>3</sub>OH release occurs during dry periods and is weakly absorbed during wet periods.<sup>117</sup> High CH<sub>3</sub>OH levels of up to 25 nmol mol<sup>-1</sup> were reported near an agricultural soil surface, leading to approximately a flux of 0.05 mgC m<sup>-2</sup> h<sup>-1</sup>. The flux correlated to sensible heat flux, suggesting CH<sub>3</sub>OH production near the surface. Measurements were taken during the hot and dry 2003 heatwave in Germany.<sup>113</sup> However, the precise origin of all these emissions remains unclear.<sup>116</sup> Rewetted and dried leaves were the subjects by Warnecke et al. (1999), and it was discovered that CH<sub>3</sub>OH emissions were produced abiotically. The authors report high emission rates for CH<sub>3</sub>OH (18–40 Tg per year) from dead leaf material, and no mechanism for production has been postulated.<sup>118</sup> CH<sub>3</sub>OH emissions from 12 different litters were investigated, and abiotic CH<sub>3</sub>OH production ranges from 26–140 μmol g<sub>litter</sub><sup>-1</sup>, and higher biotic production ranges from 54–3340 μmol g<sub>litter</sub><sup>-1</sup>.<sup>119</sup>

Other sources include the reaction of methylperoxy ( $\text{CH}_3\text{O}_2$ ) radicals with themselves or higher organic peroxy radicals present in the atmosphere and other anthropogenic sources, such as solvents or bio-fuels.<sup>111</sup> The reaction with OH radicals represents the largest sink, accounting for 63 % of the total removal, followed by dry deposition on land (26 %), wet deposition (6 %), ocean uptake (5 %) and aqueous-phase oxidation in clouds (<1 %).<sup>111</sup> The chemical reaction occurring in the clouds can result in the formation of HCOOH, which subsequently affects the acidity of the precipitation.<sup>110</sup> Most biotic  $\text{CH}_3\text{OH}$  production is attributable to the demethylation of pectin in the plant cell wall, catalysed by the enzyme pectin methyl esterase. Demethylation occurs throughout the plant's life cycle, including during pollination, fruit ripening and the response of plant cells to stress factors.<sup>120</sup>

These surfaces of leaves, in turn, serve as a habitat for microorganisms that utilise  $\text{CH}_3\text{OH}$  as an energy source, so-called pink-pigmented facultative methylotrophs. These microorganisms directly utilise the  $\text{CH}_3\text{OH}$  produced and ultimately metabolise it to  $\text{CO}_2$ , which the plants then take up.<sup>121</sup> However, how these bacteria survive when the plant dies and metabolism stops remains unresolved. The abiotic formation of  $\text{CH}_3\text{OH}$  may play a role, that these bacteria can survive during winter.

### 1.2.6 Formaldehyde

$\text{CH}_2\text{O}$  has a mixing ratio of 0.03-176 ppbv in the atmosphere, making it the most prevalent carbonyl compound in the atmosphere. Its atmospheric lifetime is relatively brief, estimated to be a few hours. However, due to its high reactivity and associated carcinogenic and mutagenic properties, the significance of  $\text{CH}_2\text{O}$  is considerable.<sup>108</sup> The primary sources of  $\text{CH}_2\text{O}$  are vegetation, soil<sup>122</sup>, seawater<sup>123</sup>, industrial processes, combustion exhaust gases<sup>124-126</sup> and the burning of biomass.<sup>127</sup> Secondary sources of  $\text{CH}_2\text{O}$  include the oxidation of  $\text{CH}_4$  and other long-lived VOCs, which represent a global background.<sup>128</sup> In continental regions, the oxidation of  $\text{CH}_3\text{OH}$  and isoprene dominates.<sup>129</sup> The heterogeneous sources yield a complex picture of the global atmospheric distribution of  $\text{CH}_2\text{O}$ , with high concentrations observed in urban areas<sup>127</sup> and tropical rainforests.<sup>108</sup> The sinks of  $\text{CH}_2\text{O}$  are the reaction with OH radicals, photolysis, and the formation of peroxyacetyl nitrate and  $\text{O}_3$ .<sup>95</sup> Other sinks include wet and dry deposition.<sup>128</sup> Additionally,  $\text{CH}_2\text{O}$  is absorbed by plants and subsequently converted to  $\text{CO}_2$  through enzymatic processes, which then enters the Calvin cycle.<sup>86,130,131</sup>

Different studies show that the production of  $\text{CH}_2\text{O}$  from wood/lignin is mostly at elevated temperatures, with either the  $\text{OCH}_3$  group or a  $\text{C}_2\text{OH}$  group bonded to an alkyl chain as a precursor.<sup>132-134</sup> Fu et al. (2022) proposed a lignin-mediated Fenton reaction where Fe and  $\text{H}_2\text{O}_2$  promote the  $\text{CH}_2\text{O}$  and  $\text{CH}_3\text{OH}$  production from Lignin. Due to the generation of OH radicals, demethylation of lignin occurs, and the aforementioned products are generated, but no reaction mechanism is postulated.<sup>132</sup> Also, no abiotic production mechanism is currently known in soils.

### 1.2.7 Formic acid and acetic acid

The atmospheric mixing ratio of HCOOH is 0.02-40 ppb<sub>v</sub>, while that of CH<sub>3</sub>COOH is 0.05-17.8 ppb<sub>v</sub>.<sup>108</sup> The modelling, based on air and ground measurements, suggests the presence of an unknown source or an incorrect interpretation of sources and sinks.<sup>135</sup> These are the two most emitted organic acids from vegetation. HCOOH is predominantly produced as formate, while CH<sub>3</sub>COOH is primarily formed as acetyl-coenzyme A (acetyl-CoA). It is evident that the two acids have a similar source. The most significant contribution to their formation is derived from emissions originating from terrestrial vegetation. With regard to the synthesis of HCOOH in plants, there are numerous potential pathways, including those associated with C1 metabolism, C<sub>2</sub>H<sub>4</sub> biosynthesis, the oxidation of CH<sub>2</sub>O, and photorespiration. The formation of CH<sub>3</sub>COOH is a consequence of the hydrolysis of acetyl-CoA, the principal product of the catabolism of carbohydrates and fats.<sup>86</sup>

Another important source is the photochemical oxidation of various VOCs (especially isoprene, acetaldehyde and alkenes).<sup>136</sup> Additionally, biogenic sources include the formation by soil bacteria<sup>137</sup> and the combustion of biomass.<sup>138</sup> In contrast, anthropogenic sources encompass fossil fuels, exhaust gases from the combustion of fossil fuels, biofuels and agriculture.<sup>108</sup> The residence time in the atmosphere for both acids are more than one week, given that they are the final product of photooxidation. The largest sink is the wet deposition due to the high H<sub>2</sub>O solubility of the acids, which also strongly influences the residence time in the atmosphere.<sup>139</sup> The acids can account for up to 60 % of the acid content of precipitation.<sup>140</sup> Another sink is the adsorption of dust particles, which can be highly significant on a regional scale.<sup>141</sup>

### 1.2.8 Chloromethane

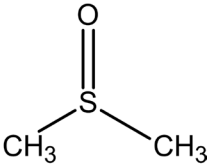
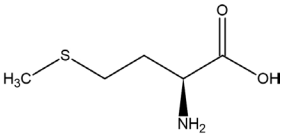
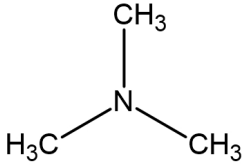
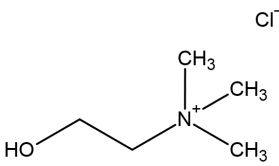
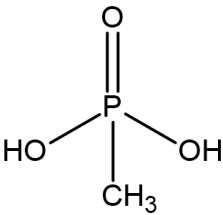
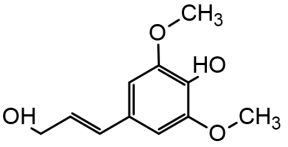
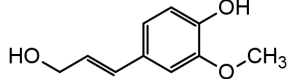
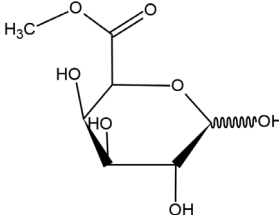
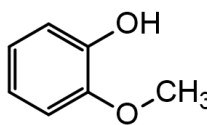
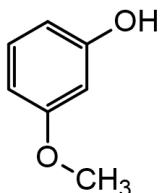
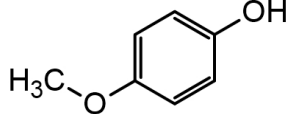
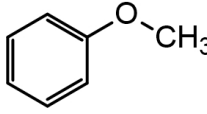
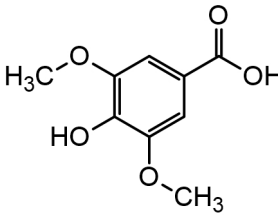
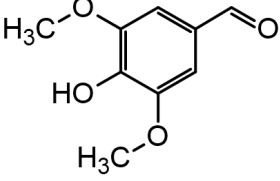
CH<sub>3</sub>Cl is the most prevalent halogenated hydrocarbon in the atmosphere, with a mixing ratio of 550 ppt<sub>v</sub>. Global emissions are estimated to range from 4,000 to 5,000 Gg. It is assumed that the tropical rainforest produces approximately half of the emissions.<sup>142</sup> Overall, the global CH<sub>3</sub>Cl budget is not balanced, with sinks outweighing sources. However, it is unclear whether there are unknown sources or whether emission estimates are inaccurate.<sup>143</sup> Recent experiments and calculations of the kinetic isotope effect, on which the emission in the calculations for the rain forest are based, suggest the presence of a significant unidentified source in the tropical rain forest, estimated to be approximately 1,500 Gg.<sup>144</sup> The abiotic conversion of chloride and pectin, a CH<sub>3</sub> donor ubiquitous in plants, has been observed to produce CH<sub>3</sub>Cl in dead leaves under ambient conditions. Emissions exhibited a marked increase at elevated temperatures, indicating a significant contribution of terrestrial ecosystems and biomass burning to global chloromethane cycling.<sup>145</sup> Other sources include the ocean<sup>146</sup>, grassland<sup>147</sup>, oxidative turnover of organic matter<sup>148</sup>, salt marshes<sup>149</sup>, wetlands<sup>150</sup>, biomass burning<sup>151</sup>, and fungi.<sup>152</sup>

The main anthropogenic source is coal combustion. Degradation occurs mainly by OH radicals in the atmosphere.<sup>153</sup> Methylophilic bacteria in the soil and ocean can degrade CH<sub>3</sub>Cl and extract energy from it.<sup>154</sup> In addition, CH<sub>3</sub>Cl is degraded by chlorine radicals in the marine boundary layer.<sup>153</sup> Given a typical lifetime of approximately one year, the substance is incorporated into the stratospheric environment, where it is known to release chlorine radicals due to photolytic cleavage. It is estimated that approximately 16 % of the observed depletion of stratospheric ozone can be ascribed to this chemical reaction, which makes it the most significant source of reactive chlorine within the stratosphere.<sup>144</sup>

### 1.3 Precursor compounds and their function in natural systems

Various precursor compounds with hetero-bonded CH<sub>3</sub> groups were analysed to ascertain their potential for forming C1 and C2 components (Table 1). Environmentally relevant compounds with CH<sub>3</sub> groups bound to sulphur, nitrogen, phosphorus, or oxygen were analysed. The primary focus is on the sulphur- and oxygen-bound CH<sub>3</sub> groups. Given that work is being conducted in aquatic systems and that a substantial number of soils have been analysed, the role of the substances in these compartments is being given particular attention. To trace the reaction pathway, <sup>2</sup>H, <sup>13</sup>C and <sup>18</sup>O labelled substances were applied. Subsequently, the aforementioned stable isotopes were analysed in the C1 and C2 components. A detailed discussion of the formation of CH<sub>3</sub> radicals from these substances is presented in a separate section (1.1).

Table 1: A comprehensive overview of all chemical components utilised, including their respective chemical structures.

DMSO	Methionine	Trimethylamine	Choline chloride
			
Methylphosphonic acid	Sinaply alcohol	Coniferyl alcohol	Galacturonic acid methyl ester
			
2-Methoxyphenole	3-Methoxyphenole	4-Methoxyphenole	Anisole
			
Syringic acid	Syringic aldehyde		
			

### 1.3.1 S-, N- and P- bonded CH<sub>3</sub> group containing compounds

#### 1.3.1.1 DMSO

Dimethylsulfoxide (DMSO) is a product of the photochemical and biological oxidation of dimethylsulfide (DMS) and has two S-bound CH<sub>3</sub> groups. DMS is produced by bacteria from dimethylsulfoniopropionate in the ocean and also serves as a metabolite in phytoplankton. DMS represents the largest natural source of sulphur in the atmosphere. DMS, DMSO and dimethylsulfoniopropionate are, therefore, the most important components of the global sulphur cycle.<sup>155</sup> DMS is oxidised at the ocean/atmosphere boundary layer to form sulphuric and methanesulfonic acids, which act as cloud

nuclei. These influence the radiation budget of the atmosphere, thus exerting a feedback effect on biogenic DMS emissions (CLAW hypothesis).<sup>156,157</sup> The atmospheric oxidation of DMS produces DMSO as an intermediate product, with mixing ratios of up to 30 parts per trillion by volume (ppt<sub>v</sub>) modelled.<sup>158</sup> Sediments, soils, and freshwater compartments are also sources of DMS.<sup>159,160</sup> Given the production of ROS in soils, as outlined in section 1.6, it is plausible that the DMS undergoes oxidation to form DMSO. Furthermore, it is suggested that DMSO has an anti-oxidative effect in the cell.<sup>161,162</sup>

### 1.3.1.2 Methionine

Methionine is an essential amino acid not synthesised by the body and, thus, must be obtained from dietary sources. Two isomers of methionine have been identified: D-methionine and L-methionine, which contain one sulfur-bound CH<sub>3</sub> group. L-methionine is the naturally occurring form and, in conjunction with cysteine, is the sole sulphur-containing amino acid.<sup>163</sup> Succinyl-CoA, cysteine, creatine, homocysteine and carnitine all require methionine as a precursor compound during synthesis and thus represent an essential component in protein biosynthesis and metabolism.<sup>164</sup> Moreover, methionine directly influences immune system function, increasing the production of taurine, glutathione and other metabolites through methionine catabolism.<sup>165</sup> Furthermore, methionine reacts with adenosine triphosphate to form S-adenosyl-L-methionine (SAM), which is a principal CH<sub>3</sub> donor in organisms.<sup>166</sup>

### 1.3.1.3 Trimethylamine

Trimethylamine (TMA) is a volatile tertiary aliphatic amine consumed through food. The precursor compounds carnitine, choline (described in Chapter 1.3.1.4) and lecithin, found in large quantities in meat and eggs, are absorbed and then converted to TMA by gut microbiota.<sup>167–169</sup> Subsequently, TMA is converted to trimethyl-N-oxide by flavone monooxygenase.<sup>170</sup> Marine organisms utilise the substance for several purposes, including the equalisation of hydrostatic pressure and the function of an osmolyte. It is also employed to reduce the freezing point of body fluids and provide protection against elevated urea concentrations.<sup>171,172</sup> Trimethyl-N-oxide can be metabolised by bacteria to tri-, di-, and monomethylamine, which are responsible for the characteristic fishy odour.<sup>171</sup> Moreover, trimethyl-N-oxide can be metabolised to dimethylamine and CH<sub>2</sub>O with the assistance of trimethylamine monooxygenase and trimethylamine-oxide aldolase. Another enzymatic pathway is the direct demethylation of TMA by trimethylamine dehydrogenase, which is energetically preferred.<sup>173</sup> Additionally, plants possess intrinsic levels of trimethyl-N-oxide, which are elevated during abiotic stress. This phenomenon enhances the plant's tolerance to abiotic stressors, including frost, drought, and high salinity.<sup>174</sup>

TMA is released into the atmosphere from various sources, including pig faeces, fish processing, vehicle exhaust, marine organisms and anaerobic fermentation of food waste.<sup>175–178</sup> The primary reaction pathways of aliphatic amines in the gas phase are postulated to occur via interaction with atmospheric oxidants, such as hydroxyl radicals and ozone. The formation of non-salt organic aerosols results from the TMA oxidation, which has been demonstrated to exhibit enhanced stability relative to nitrate salts.<sup>179</sup>

#### 1.3.1.4 Choline

Choline has three CH<sub>3</sub> groups attached to the nitrogen of ethanolamine, making it a quaternary amine; as earlier mentioned, it is a precursor for TMA. It is a vitamin-like substance for humans and animals, but it is also produced by the body in small amounts.<sup>180</sup> Choline fulfils a multitude of biological functions within the human body. One such function is that choline can be oxidised by an enzyme to betaine, whereby the CH<sub>3</sub> group of betaines can be utilised to synthesise methionine from homocysteine. Additionally, choline is a precursor to phosphatidylcholine and sphingomyelin, which are integral components of biological membranes. It also serves as a precursor to diacylglycerol and ceramide, which are intracellular messengers. The neurotransmitter acetylcholine is also dependent on choline as a precursor compound.<sup>180–182</sup> Choline is synthesised within the body through the methylation of phosphatidylethanolamine by SAM.<sup>183</sup> The synthesis of choline has also been observed in plants and yeast cells.<sup>184,185</sup>

#### 1.3.1.5 Methylphosphonate

Methylphosphonate is an organic phosphonate, a category of reduced phosphorus compounds distinguished by their chemically stable C-P bond. These compounds constitute a substantial portion of the dissolved organic matter in marine environments.<sup>186</sup> This observation underscores the significance of phosphonates as an important source of phosphorus, particularly in oligotrophic (phosphorus-limited) areas of the ocean. Specialised enzymatic pathways (C-P lyase pathways) have evolved in microorganisms to facilitate the cleavage of the C-P bond in phosphates, thereby enabling the utilisation of phosphorus by these organisms. Inorganic phosphorus, which is typically more readily available, is the preferred source of phosphorus.<sup>187</sup> A multi-enzyme complex splits the phosphonate into phosphate and a corresponding hydrocarbon, thereby enabling the degradation of methylphosphonate to produce CH<sub>4</sub>.<sup>188,189</sup> This process may offer a potential explanation for the CH<sub>4</sub> paradox, as it results in CH<sub>4</sub> supersaturation in the upper layers of the ocean, where this process occurs.<sup>80,190</sup>

### 1.3.2 OCH<sub>3</sub> aromatic compounds

The two most significant lignin monomers, namely sinapyl alcohol and coniferyl alcohol, which are endowed with OCH<sub>3</sub> groups, were subjected to analysis. These monomers, in conjunction with p-coumaryl alcohol (S-, G- and H-units), serve as the fundamental building blocks of lignin. It represents an essential wood component comprising between 18 and 35 % of the total composition. The remaining essential components are cellulose (40-45 %), hemicellulose (25-35 %), and a range of other components, including polysaccharides and minerals, which collectively account for up to 10 % of the total composition.<sup>191-194</sup> Lignin is a vital component of the cell wall, providing structural integrity and hindering the decomposition of polysaccharides. Additionally, it serves as a barrier against pathogens, insects, and other herbivores.<sup>195</sup> Most softwoods are composed of coniferyl units, while hardwoods primarily comprise coniferyl and sinapyl alcohol units. In contrast, grasses are known to contain all three lignin monomers.<sup>193</sup> Decomposition of the aromatic compound lignin is principally facilitated by the action of white-rot and brown-rot fungi, in addition to certain bacteria. These organisms synthesise a range of heme peroxidases, which enable the direct degradation of lignin and the demethylation processes. Furthermore, the by-product of this process is the formation of humic substances, which are integral components of soil humus.<sup>196-198</sup> Lignin is an essential component of wood, which is ultimately deposited in the soil following the decay process and is found in nearly all terrestrial ecosystems. Given the substantial quantities of lignin available and the hetero-bonded CH<sub>3</sub> groups present, it is a potential source of VOCs in this study. Furthermore, wood is utilised as an energy source through combustion, producing numerous VOCs, including 2-methoxyphenol (guaiacol).<sup>199</sup> This also occurs as a monomer in lignin and is employed as an example substance due to its favourable availability and is also isotopically labelled available. Furthermore, analysis was conducted on 3- and 4-methoxyphenol due to their structural similarities. Other components selected for their structural similarity and relevance to the environment are anisole, syringic acid and syringic aldehyde.

### 1.3.3 Galacturonic acid methyl ester

Galacturonic acid methyl ester (Game) represents the esterified galacturonic acid that constitutes the fundamental building block for pectin. It is linked alpha-1,4-glycosidically and exhibits varying degrees of esterification depending on the plant species.<sup>200,201</sup> Also, numerous side chains containing up to 17 different monosaccharides and more than 20 linkages are possible.<sup>202</sup> The cell walls of plants and fruits contain pectin, which constitutes between 10 and 35 % of their composition. This pectin plays a crucial role in maintaining the stability and development of the cell wall.<sup>203</sup> The pectin methyl esterase catalyses the hydrolysis of pectin methyl esters, releasing CH<sub>3</sub>OH through the stomata.<sup>121,203</sup> The ester/OCH<sub>3</sub>

group is of interest for this study as it plays an integral role in Game and pectin and is worthy of further investigation.

## 1.4 Transition metal species and their occurrence in soils

### 1.4.1 Tetradentate Bispidine Ligand

An iron-bispidine complex was employed in a multitude of experiments. Its selection was predicated on its high reactivity and the necessity for modelling using DFT (density functional theory). These properties were used in previous studies described in Chapter 1.1.1. Additionally, it has been the subject of extensive research and has been utilised for over half a century.<sup>204</sup>

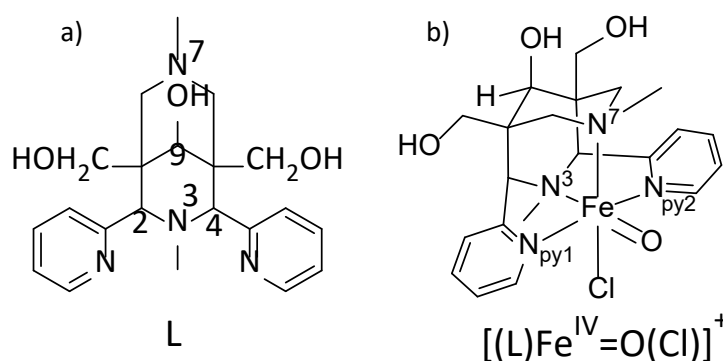


Figure 4: Structures of the Tetradentate Bispidine Ligand **a)** L ( $[\text{Fe}(\text{N}_2\text{Py}_2)\text{Cl}_2] \cdot \text{CH}_3\text{CN}$ ) and its **b)** Iron(IV)-Oxido complex in aqueous solution. Taken from Hädel et al. (2023).<sup>205</sup>

The non-haem iron complex is displayed in Figure 4a, in which a tetradentate bispidine-based ligand ( $\text{LFe}^{\text{II}}\text{Cl}_2$ ) coordinates  $\text{Fe}^{2+}$  via two tertiary amines and two pyridine donor groups.<sup>16,205</sup> The synthesis of this complex is achieved through a two-step process involving consecutive double Mannich reactions, followed by the addition of  $\text{Fe}^{2+}$ .<sup>206</sup> Subsequently, the compound is oxidised by adding an oxidising agent, in this case,  $\text{H}_2\text{O}_2$ , which forms an iron-oxo complex (Figure 4b).<sup>16</sup>

These bispidine-based iron-oxo complexes are regarded as highly effective catalysts for the epoxidation of alkenes, hydroxylation and halogenation of alkanes, as well as the oxidation of alkanes, alcohols and sulphur compounds, including thioethers.<sup>22,207–211</sup> Due to the high oxidising power of iron-oxo complexes, organic substances can also be converted with great efficiency, which is why highly valent iron-oxo complexes play a significant role in natural processes.<sup>15</sup> The processes of oxygen atom transfer (OAT) and hydrogen atom abstraction (HAA) are of significant importance in this context (Chapter 1.1.1) and could be performed by the iron-oxo complex (Figure 4b).

### 1.4.2 Hematite

Hematite ( $\text{Fe}_2\text{O}_3$ ) is a trivalent reddish-coloured Fe oxide very common in rocks and as a pedogenic mineral in soils. There,  $\text{Fe}_2\text{O}_3$  can be regarded as the end product of the transformation of other Fe oxides and hydroxides. The weathering of primary minerals results in the release of  $\text{Fe}^{2+}$ , which is then oxidised to  $\text{Fe}^{3+}$ , which is then hydrolysed at a pH >3, e.g. to ferrihydrite ( $5 \times \text{Fe}_2\text{O}_3 \cdot 9 \times \text{H}_2\text{O}$ ).<sup>212</sup> The primary mechanism of  $\text{Fe}_2\text{O}_3$  formation in soil is the dehydration and rearrangement of ferrihydrite.<sup>213</sup> The metastable ferrihydrite can be transformed into  $\text{Fe}_2\text{O}_3$  and/or goethite ( $\alpha\text{-FeOOH}$ ) in soils, which is particularly influenced by temperature, moisture and pH:  $\text{Fe}_2\text{O}_3$  forms at higher temperatures, low moisture and neutral pH, while lower temperatures and higher pH favour the formation of goethite.<sup>214</sup> Accordingly,  $\text{Fe}_2\text{O}_3$  is particularly common in soils of the tropics and subtropics, while goethite dominates in soils of temperate latitudes.

$\text{Fe}_2\text{O}_3$  can react with many inorganic and organic colloids to form even more complex aggregates. The solubility is highly dependent on Eh-pH conditions and is generally very low. Due to that, a major problem is that plants may not be able to absorb enough Fe at pH values above 7, which can lead to growth problems. Microorganisms may have similar problems<sup>215</sup> as Fe is a micronutrient for them.<sup>216</sup>

### 1.4.3 Transition metals

Different transition metal species are investigated to investigate whether other transition metals than iron can mediate the reaction described in Chapter 1.1.1 (Table 2). Selected minerals and salts are analysed, and each transition metal is investigated in isolation. The formation of  $\text{CH}_3\text{Cl}$  was investigated by selecting transition metal chlorides. Distinct oxidation states of the transition metal cation were also selected, allowing the investigation of different oxidation states of the transition metals.

Table 2: Overview of transition metal species used instead of the  $\text{LFe}^{\text{II}}\text{Cl}_2$  or  $\text{Fe}_2\text{O}_3$ .

transition metal	halogenated species	other species
manganese	$\text{MnCl}_2 \cdot 4\text{H}_2\text{O}$	$\text{MnO}_2$ , $\text{MnSO}_4 \cdot 4\text{H}_2\text{O}$
iron	$\text{FeCl}_2 \cdot 4\text{H}_2\text{O}$	$\text{FeSO}_4$
cobalt	$\text{CoCl}_2 \cdot 6\text{H}_2\text{O}$	-
nickel	$\text{NiCl}_2 \cdot 6\text{H}_2\text{O}$	$\text{NiSO}_4 \cdot 6\text{H}_2\text{O}$
copper	$\text{CuCl}_2$	$\text{CuO}/\text{Cu}_2\text{O}$ , $\text{Cu}(\text{CH}_3\text{COO})_2$

Here, a brief description of the transition metals used focuses on the occurrence in soils. Manganese (Mn) is naturally present in three oxidation states (+II, +III, and +IV), influenced by soil redox conditions. Manganese is often found as Mn(IV) oxides in well-aerated soils, while Mn(II) is present in waterlogged

or anaerobic conditions.<sup>217</sup> The manganese content of the soil is principally derived from the weathering of manganese-bearing minerals present within rock formations.<sup>218</sup>

Cobalt (Co) is an inherent constituent of the earth's natural environment, originating from the weathering of parent rocks such as cobaltite and erythrite. It is predominantly observed in two valence states: Co(II) and Co(III). Volcanic ash has been shown to enhance cobalt levels in soil samples.<sup>219</sup> Furthermore, using fertilisers and additives in agricultural practices has been demonstrated to contribute to elevated levels of cobalt in soil.<sup>220</sup> Cobalt is an indispensable trace element for the functioning of plant and animal life, and thus humans. The key physiological role of cobalt is as the central metal ion in vitamin B12 (cyanocobalamin), ensuring its catalytic activity in CH<sub>3</sub> group transfer reactions.<sup>221</sup>

Nickel (Ni) concentrations in soils range from 5 to 500 mg kg<sup>-1</sup>, with the primary source of nickel being the geological weathering of (ultra)mafic rocks enriched in Ni-bearing minerals, such as limonite and garnierite.<sup>222,223</sup> Nickel is a biologically essential micronutrient found in enzymes across all domains of life. It is crucial for diverse biogeochemical processes, including the fixation of nitrogen and its uptake and the fixation of carbon and methanogenesis.<sup>222</sup>

The concentration of copper (Cu) in soil is contingent on many interacting factors, including the characteristics of the parent material, the physico-chemical properties of the soil, and potential exogenous inputs from agricultural or industrial activities. For instance, the availability of copper is known to decrease in soils with elevated pH levels, high concentrations of soil organic carbon, and substantial clay content.<sup>224</sup> An analysis of agricultural soils, focusing on those associated with vineyards and orchards, revealed an elevated presence of copper. This phenomenon can be attributed to using copper-based fungicides in agricultural practices.<sup>225,226</sup>

## 1.5 Ascorbic acid as an OH radical scavenger

Vitamin C (Asc) is an antioxidant and a vital human nutrient which must be consumed with food. The highest concentrations of the substance in food are found in vegetables, fruit, and other plant materials, which accumulate in the soil in the end.<sup>227</sup> Asc is easily oxidised and functions as an effective scavenger of ROS. Other compounds, such as glutathione peroxidase, catalase and other forms of Asc, also possess these properties. This is important for all living organisms, protecting them from cell damage and other adverse effects.<sup>227,228</sup> This property is of crucial importance in the experiments carried out.

## 1.6 ROS and the formation of C1 and C2 in soils

As outlined in Chapters 1.4 and 1.5, transition metals have been detected in the soil, and Asc and its derivatives have also been identified in the same environment. The precursor compounds described in Chapter 1.3 are commonly present in the soil. Specifically, lignin and pectin, as representatives of the oxygen-bonded CH<sub>3</sub> group, occur extensively in the soil due to their essential role in plant composition.

The need for ROS, especially H<sub>2</sub>O<sub>2</sub>, in the investigated reaction is ubiquitous in soil (Figure 5). Most of these are O<sub>2</sub><sup>-</sup> radical, H<sub>2</sub>O<sub>2</sub>, and OH radicals formed during photochemical reactions, atmospheric precipitation, plant and microbial exudation and heterogeneous catalysis mediated by biochar or quinone-like substances (Figure 5).<sup>229</sup> The photochemical process can occur within the soil, whereby mineral oxides act as catalysts to produce ROS, including O<sub>2</sub><sup>\*-</sup> and H<sub>2</sub>O<sub>2</sub>.<sup>230</sup> Additionally, this process can take place on hydrated mineral surfaces<sup>231</sup> or during the reaction with transition metals, such as Fe.<sup>232</sup> Another source is the precipitation, which contains up to 78 μmol L<sup>-1</sup> H<sub>2</sub>O<sub>2</sub>, which contributes significantly to the ROS in the soil.<sup>233</sup> Moreover, a considerable number of microorganisms are involved in the production of ROS. These generate H<sub>2</sub>O<sub>2</sub> in conjunction with enzymes such as oxidase enzymes.<sup>234</sup> A further source is the alteration of redox conditions resulting from alternating aerobic and anaerobic conditions in soils. The conversion of Fe<sup>III</sup> into Fe<sup>II</sup> causes desorption and/or the production of ROS.<sup>235</sup> Quinones are pervasive in soil environments, formed through the decomposition of leaves and lignin and synthesised by microorganisms.<sup>236,237</sup> They are redox active, exhibiting three distinct oxidation states, and thus capable of reacting with O<sub>2</sub>, transition metals or catalysts to produce ROS.<sup>237</sup> These processes, particularly the abiotic ones, significantly influence the formation of C1 and C2 components in soil, functioning as a primary driving force behind these chemical reactions.

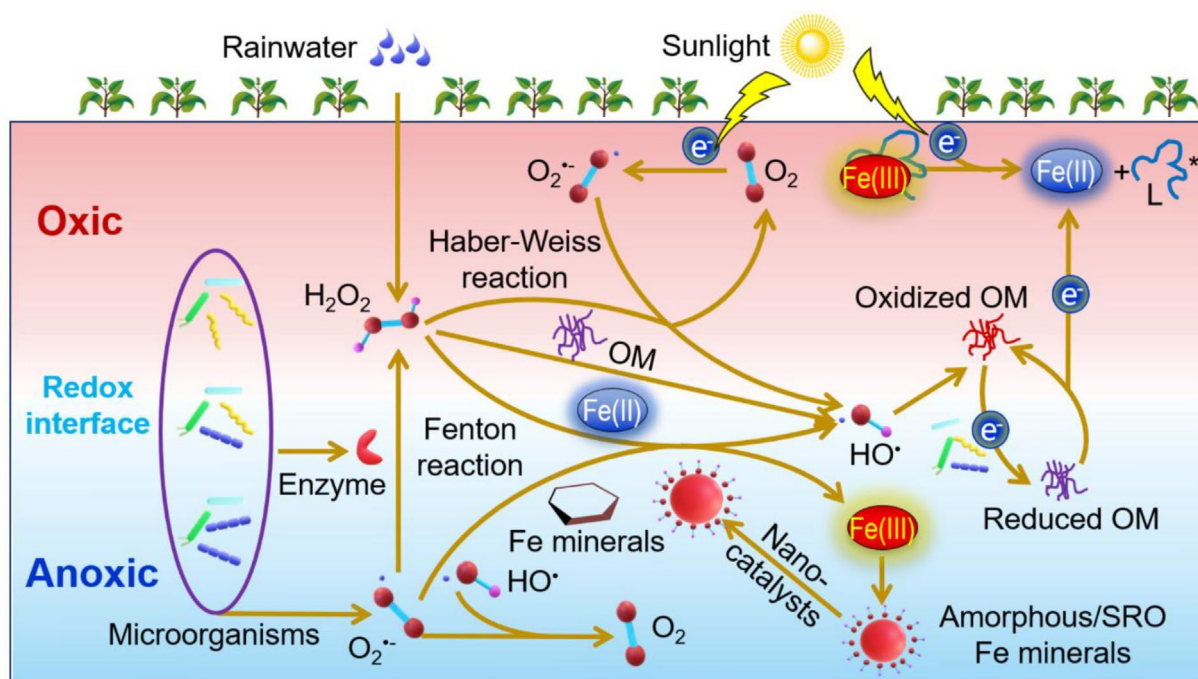


Figure 5: Sources and pathways of ROS in soils. The Fenton reaction, which forms part of the present investigation, represents a significant component of ROS production in soil. Taken from Yu et al. (2021).<sup>229</sup>

## 1.7 DFT modelling

The computer-aided chemical modelling conducted by Gunasekaran Velmurugan and Peter Comba to accompany the experiments is outlined in Hädel et al. (2023).<sup>205</sup> It constitutes an indispensable element of the reaction mechanisms but was not conducted in the present study and, therefore, not described here.

## 1.8 Motivation and research aim of this study

Based on the previously described research,  $CH_3$  radicals are precursors of C1 and C2 compounds in the environment.<sup>14,31,37,238</sup> These reactions occur under oxic, abiotic and atmospheric conditions with mostly  $H_2O_2$  as an oxidant that activates Fe to a  $[Fe^{IV}=O]^{2+}$  species, naturally occurring substrates with a hetero-bonded  $CH_3$  group (S, N, P and O) and Asc as an OH radical scavenger. These processes are only less described for  $CH_4$  formation in natural environments<sup>33</sup> and poorly for other C1 and C2 compounds. Thus, a comprehensive understanding of all processes is crucial to fully understanding the interactions between all these C1 and C2 compounds and how they influence the natural environments.

Thus, the primary objective of this study was to gain a thorough understanding of the processes and conversion rates involved in both the oxic and abiotic production of C1 and C2 compounds. Moreover, a comprehensive understanding of these processes within the pedosphere is imperative, particularly with regard to methoxy compounds as a precursor.

The fundamental objective is further subdivided into the following more precise aims:

1. Studying several potential precursor compounds with S-, O-, N- and P-bonded CH<sub>3</sub> groups in the laboratory, using different Fe species, Asc and H<sub>2</sub>O<sub>2</sub>. Quantitative and qualitative analysis of C1 and C2 compounds in all oxidation states of carbon, ranging from -IV to +IV.
2. Identification of novel pathways that contribute to forming environmentally relevant C1 and C2 compounds with isotopic <sup>2</sup>H-, <sup>13</sup>C and <sup>18</sup>O-labelled substances.
3. Replacement of Fe species by various transition metal species and studying the qualitative and quantitative amount of C1 and C2 compounds produced.
4. Quantifying and determining the potential of soils to release C1 and C2 compounds and identifying the underlying reaction mechanism.
5. Varying the conditions in the soil experiments (pH, temperature, wet-dry cycles, and the removal of reactive groups) to gain further insight into the controlling factors of C1 and C2 production.
6. Estimating initial global emission rates of the produced C1 and C2 compounds.

## 2 Materials and Methods

The various experimental setups and the preparation and collection of the soil samples are described below. Furthermore, the individual methods for analysing CH<sub>4</sub>, C<sub>2</sub>H<sub>6</sub>, CH<sub>3</sub>OH, CH<sub>2</sub>O, CH<sub>3</sub>Cl, CO<sub>2</sub>, HCOOH and CH<sub>3</sub>COOH and all calculations are described.

### 2.1 Experimental setup and details for the incubation experiments

All chemicals were of reagent grade or higher and purchased from Fischer Scientific GmbH, Merck KGaA, Cayman Chemicals, Carl Roth GmbH + Co. KG, Linde GmbH, AIR LIQUIDE Deutschland GmbH and Campro Scientific GmbH.

### 2.1.1 Experiments with hetero-bonded CH<sub>3</sub> groups

All experiments with hetero-bonded CH<sub>3</sub> groups containing a transition metal species, a substrate, an acid and H<sub>2</sub>O<sub>2</sub> in the following ratios: 10:25:100:200 (Table 3). Deviations from this are always described.

Table 3: Used amounts of substrates in the standard experiments dissolved in 10 ml H<sub>2</sub>O.

Reactant	Amount [μmol]
Transition metal species	10
Substrate	25
Asc /Triflic acid	100/0.05
H <sub>2</sub> O <sub>2</sub>	200

The standard experiments were conducted in 50 ml glass vials (IVA Analysetechnik GmbH & Co. KG, Germany) that were sealed with an aluminium crimp cap with a Pharma-Fix-Septum, Butyl/PTFE septum (3.0 mm thickness, 20 mm diameter, IVA Analysetechnik GmbH & Co. KG, Germany). The vials contain 10 μmol of tetradentate bispidine ligand (see Figure 2; LFe<sup>II</sup>Cl<sub>2</sub>) or Fe<sub>2</sub>O<sub>3</sub> as a catalyst. Subsequently, 25 μmol of different hetero-bonded CH<sub>3</sub> group-containing substrates are dissolved in 5 ml ultra-pure H<sub>2</sub>O. Additionally, 100 μmol Asc is dissolved in 2.5 ml H<sub>2</sub>O and introduced to the experiments as an OH radical scavenger, maintaining a consistent pH across all experiments. In the absence of Asc, 0.05 μmol trifluoromethanesulfonic acid (triflic acid) is dissolved in 2.5 ml H<sub>2</sub>O, and the vials are then sealed with an aluminium crimp cap. A solution of 200 μmol H<sub>2</sub>O<sub>2</sub> (dissolved in 2.5 ml) was added through the septum with a 2.5 ml syringe (SETonic GmbH, Germany) to initiate the reaction. This was done to prevent the produced gas from being degassed. The total volume of the liquid phase is 10 ml, resulting in a headspace volume of 40 ml. Afterwards, the experiments were stored in a climate chamber in the absence of light for 48 h. All individual experiments were performed in triplicate with the same composition and under the same environmental conditions to obtain comparable and statistically reliable results. Control samples ("blanks") were also prepared to account for the background values of the investigated components in the liquid and gas phases and were subtracted from the measured values. These also contained the specified amounts of Fe species, Asc, and H<sub>2</sub>O<sub>2</sub>; however, the solution with the initial substance was replaced by 5 mL of ultra-pure H<sub>2</sub>O.

### 2.1.2 Sampling of the experiments

Following a period of 48 h, the samples were collected. All gas samples were collected using a 30 ml gas-tight plastic syringe (BD Plastipak™, BD, Switzerland). A volume of 6 ml was transferred to a 3 ml

glass container (Exetainer®, Labco Limited, UK) for subsequent analysis with the GC-BID (Chapter 2.2.2.2). The remaining headspace (ca. 30 ml) was stored in a 12 ml glass container (Exetainer®, Labco Limited, UK) for subsequent analysis of the hydrocarbons (Chapter 2.1) and any additional measurements deemed necessary. Subsequently, the experiments were opened, and the liquid phase was sampled. The liquid was initially filtered through a sterile filter with a mesh size of 0.2 µm (Whatman™, GE Healthcare Life Sciences, USA). A 1.5 ml sample was mixed with 10 µl of catalase (1 mg ml<sup>-1</sup>) to terminate the reaction. The sample was then stored in crimp-top vials (IVA Analysentechnik GmbH & Co.) and sealed with an aluminium crimp cap with a natural rubber/butyl/PTFE septum (1.0 mm thickness, 11 mm diameter, IVA Analysentechnik GmbH & Co. KG, Germany) for the CH<sub>3</sub>OH analysis. For the CH<sub>2</sub>O analysis, a solution of 1 ml of sample, 1 ml of pH 7 buffer solution, 1 ml of Pentafluorophenylhydrazine (PFPH; 1 mg ml<sup>-1</sup>) and 10 µl of catalase (1 mg ml<sup>-1</sup>) was prepared in a glass flask and subsequently transferred to a 1.5 ml crimp-top vial. The remaining samples were stored in 20 ml crimp-top vials (IVA Analysentechnik GmbH & Co. KG, Germany), and the pH value was measured at least once in each experiment (WTW-SenTix® 81, Xylem Analytics Germany Sales GmbH & Co. KG, Germany). All quantitative data shown represents triplicates, measured three times for CH<sub>4</sub>, CH<sub>3</sub>OH and CH<sub>2</sub>O and one time for C<sub>2</sub>H<sub>6</sub> (n = 9/3), with the total error of all experiments displayed and the total error calculated after equation 10. Any deviations in procedure or measurements are explicitly noted.

### 2.1.3 Experiments with labelled substrates and other setups

To trace the origin and reaction path of the individual components, <sup>2</sup>H, <sup>13</sup>C and <sup>18</sup>O-labelled starting materials were employed, as well as H<sub>2</sub><sup>18</sup>O, H<sub>2</sub><sup>18</sup>O<sub>2</sub> and <sup>18</sup>O<sub>2</sub>; however, due to the high cost of some of the labelled substances and the subsequent limited availability, reduced quantities were often utilised. Furthermore, the concentrations of the several components were varied. All deviations from the standard experiments are indicated.

### 2.1.4 Experiments with soils

#### 2.1.4.1 Sampling and Preparation of the samples

A total of 24 soil samples were examined to ascertain their potential for forming C1 and C2 compounds. The samples were collected in the Rhein-Neckar-Kreis and the Rhein-Pfalz-Kreis, Germany. A diverse range of soil samples was collected concerning the genesis and the composition of the organic material to facilitate a comprehensive and representative study. Furthermore, the sampling sites were selected to minimise the potential for human influence. The initial step involved the collection of a 1-metre-deep profile using the Pürckhauer method to determine the soil horizons. Subsequently, a hole of an equivalent depth was excavated using a stainless-steel spade, and the requisite mixing samples were

obtained from the respective horizons with a stainless-steel spatula to conduct experiments investigating the formation of C1 and C2 components. If the deepest horizon is less than one metre in depth or rock is present below, only the overlying horizons were sampled.

The samples were subsequently subjected to sterilisation by drying at 105°C for three days, after which they were ground using a planetary mill (PULVERISETTE 5, Fritsch GmbH, Germany) at a rate of 400 rotations per minute for five minutes to achieve complete homogenisation. A total of 5 g of soil was incubated in a 50 ml glass vial, which was sterilised once more for a minimum of one hour. Subsequently, 10 ml of ultra-pure H<sub>2</sub>O was added, and the experiment was sealed (see Chapter 2.1.1 for a description of the materials used). All quantitative data shown represents triplicates, measured three times for CH<sub>4</sub>, CH<sub>3</sub>OH and CH<sub>2</sub>O and one time for C<sub>2</sub>H<sub>6</sub>, with the total error of all experiments displayed and the total error calculated after equation 10. Any deviations in procedure or measurements are explicitly noted.

#### 2.1.4.2 Location and Sample Description

The soil samples are briefly described below in accordance with DIN standard 18196. Figure 6 and Table 4 show the sampling locations, the abbreviations used, and the classification according to the "leading soil associations". The overlying dead plant material was removed before sampling.

Table 4: Sample name, location and a short description of the sampled soils according to the “Leitboden-assoziationen” of the Soil Atlas of Germany of the Federal Institute for Geosciences and Natural Resources.

<b>Name</b>	<b>Location</b>	<b>Description</b>
MX	Maxdorf (A)	Chernozem from loess and loess-like silt deposits
BI	Birkenheide (B)	Pararendzina from loess alternating with Rendzina from marl and limestone
AL1	Altlußheim (C)	Fenland soil
AL2	Altlußheim (D)	Alluvial soil / gley from loamy to clayey alluvial sediments
HO	Hockenheim (E)	Fenland soil - podzolic brown earth from sandy terrace deposits
WA1	Walldorf (F)	Podzolic brown earth from sandy terrace deposits
WA2	Walldorf (G)	Alluvial soil / gley from loamy to clayey alluvial sediments
MA	Malschenberg (H)	Pelosol brown earth / Pelosol pseudogley from weathering products of marl and clay rocks
SH1	Schriesheim (I)	Brown earth from acidic igneous and metamorphic rocks
SH2	Schriesheim (J)	Chernozem-parabrown earth / parabrown earth-chernozem from loess or loess loam
LR	St. Leon-Rot (K)	Pelosol brown earth / Pelosol pseudogley from weathering products of marl and clay rocks
UH	Unterhof (L)	Chernozem-parabrown earth / parabrown earth-chernozem from loess or loess loam
PT	Peterstal (M)	Podzolic brown earth from base-poor quartzitic sandstones and conglomerates

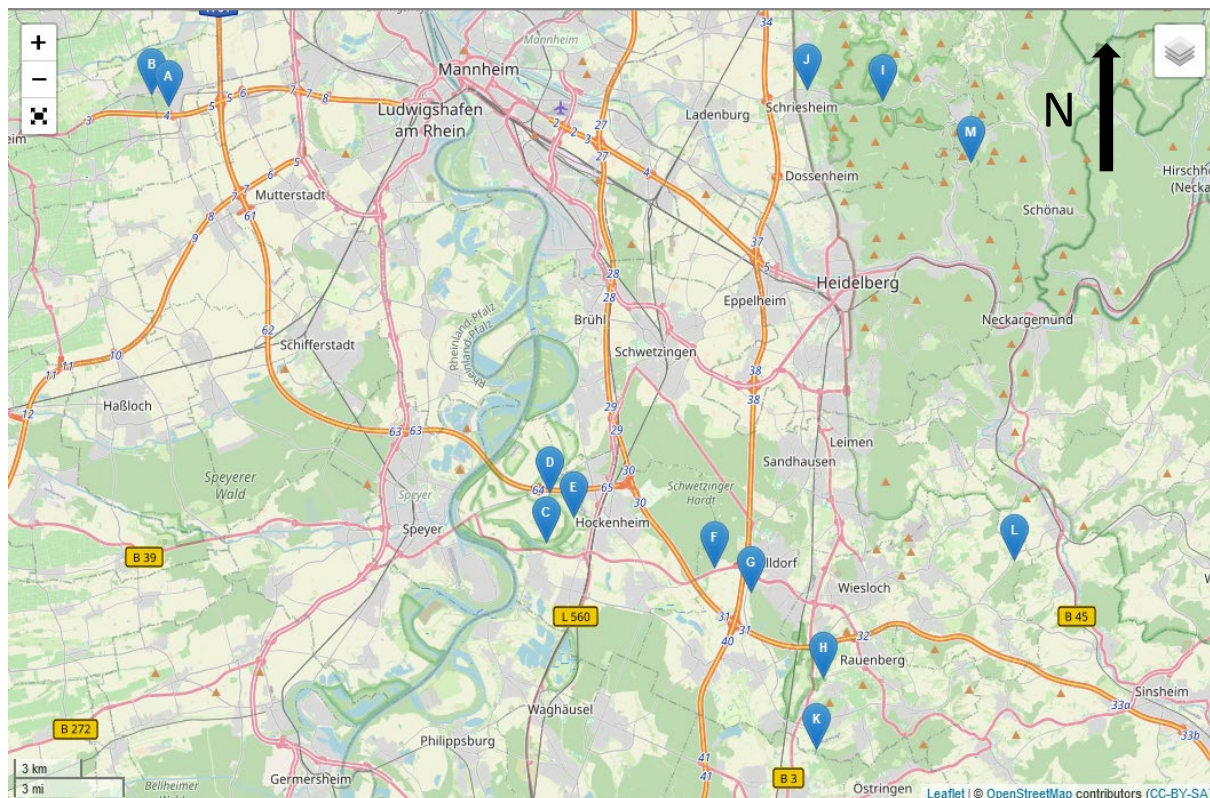


Figure 6: Locations of the soil samples near Heidelberg A-M.<sup>239</sup>

Three soil samples were obtained from a soil profile in a mixed forest near Maxdorf (A) at depths of 0-5 cm, 5-15 cm and 15-30 cm, respectively. The topsoil is characterised by a slightly medium sandy and slightly silty fine sand with a dark brown colour and a high humus content. The humus content decreases in the 5-15 cm depth layer, and the colour shifts from dark brown to brown. From 15 cm depth onwards, the soil is characterised by a homogeneous, light brown, medium sandy fine sand with a significantly higher silt and humus content.

Two samples were obtained from the area of Birkenheide (B) at depths of 10-25 cm and 25-35 cm. The soil type is also characterised by a high proportion of medium-sized sand particles, as observed in the soil samples from Maxdorf. The colouration of the topsoil transitions from dark brown to brown with depth, whereas in the subsoil, it becomes increasingly light brown. The samples were obtained from a meadow comprising grass and heather vegetation.

The Altlußheim (C) soil sample is distinguished by a dark colouration and markedly elevated humus content. The soil type is classified as slightly fine sandy and very slightly clayey silt. The sample originates from the "Hockenheimer Rheinbogen", a nature and landscape conservation area comprising a silted-up oxbow of the Rhine where a fen has developed.<sup>240</sup> The landscape is characterised by grass and moorland, partly influenced by agricultural practices. The soil sample was taken from a depth of 20 cm.

Another soil sample was collected at a depth of 0-10 cm in the area of Altlußheim (D) in the "Hockenheimer Rheinbogen" area, which has a black colour and a high humus content. The predominant soil component is silt, which exhibits slight fine sandy and medium sandy properties.

The soil profile in the Hockenheim (E) area was developed in the eastern section of the "Hockenheimer Rheinbogen" region. Two soil samples were obtained from depths of 10–20 cm and 20-30 cm. The soil is characterised by a dark brown, soft silt with slightly clayey and humic properties and a very slight sand content in the upper area. The lower area consists of strongly humic (peaty) silt, which is slightly clayey and slightly sandy with a high H<sub>2</sub>O content. The parent rock is a flood sediment that lies on river gravel.<sup>240</sup>

Three additional soil samples were obtained in a mixed forest near Walldorf (F) at 0-5 cm, 5-15 cm, and 20-35 cm. The topsoil is characterised by a dark brown, silty medium sand to fine sand texture and a high humus content. Towards the base of the profile, the colour transitions to a lighter brown. The humus content declines and the soil is predominantly medium sand with fine sand content. At a second site near Walldorf (G), soil samples were obtained from a mixed forest at depths of 0-10 cm, 10-40 cm, and 40-100 cm. The initial 10 cm of soil is characterised by dark brown pigmentation, a high humus content, and a fine to medium sand and silt composition. At a depth of 10-40 cm, the soil transitions to a silty and fine to medium sand texture with a brown to light brown colouration. At a 40-100 cm depth, the soil exhibits slight silty characteristics, fine and slightly medium sand, a light brown hue, and a low humus content.

A soil sample was obtained from a depth of 5-20 cm at Malschenberg (H) in an area that comprises a variety of habitats, including grassland and shrubland, which are utilised by humans. A dark brown colour characterises the soil sample, clayey silt with a high humus content. The soil formation below this layer consists of marl and claystone.

Two distinct locations were identified for sampling in the area surrounding Schriesheim. The initial site (I) is situated on a mixed forest slope comprising slightly weathered rhyolite as the parent rock, where only a shallow soil profile has developed. The sample was obtained from a 0-5 cm depth and comprises a heterogeneous mixture of gravel with strong silty and sandy components. A dark brown colour and a high humus content characterise the soil. In contrast, a soil profile (J) at the foot of the slope in a grassland was sampled with loess and loess loam as parent materials. The top 5 cm of soil is a brown, humic, slightly fine sandy silt. Below 5 cm, the colour changes to light brown with a low humus content. Additionally, lime concretions can be observed in the lower area. One sample was taken from the top 5 cm and one from 45-55 cm.

Two soil samples were obtained from the surface to a depth of 10 cm and 100 cm at the St. Leon-Rot location (K). The samples were taken in a mixed forest. The soil exhibited a medium humus content in the upper area and a dark brown colour. The soil was identified as silty and very slightly medium sand. The deeper soil sample was characterised by a brown colour with a low humus content and, like the upper part, was also very slightly medium sandy and silty.

Two further soil samples were taken at Unterhof (L) in a mixed forest at 0-10 cm and 10-100 cm depths. The soil consists of loess and is dark brown at 0-10 cm level, transitioning to brown at 10-100 cm level. It is primarily silt, with a medium humus content in the upper part, which decreases sharply from 10 cm.

Soil samples were taken from a coniferous forest near Peterstal (M) at two depth intervals: 0–10 cm and 10–40 cm. The entire profile is characterised by a fine sand composition, with a minor proportion of medium sand and silt. A dark brown hue and a high humus content characterise the soil. The soil exhibits a reddish-brown colouration from a depth of 10 cm to 40 cm due to the underlying sandstone and a relatively low humus content.

## 2.2 Laboratory analysis of $\text{CH}_4$ , $\text{C}_2\text{H}_6$ , $\text{CH}_3\text{OH}$ , $\text{CH}_2\text{O}$ , $\text{CH}_3\text{Cl}$ , $\text{CO}$ , $\text{CO}_2$ , $\text{HCOOH}$ and $\text{CH}_3\text{COOH}$

### 2.2.1 Principles of Gas Chromatography

Gas chromatography (GC) is a technique employed for the separation of volatile compounds present in a mixture. The fundamental principle of this technique is that a mobile phase (the analyte) interacts with a stationary phase within the column, resulting in the separation of the components due to the differing adsorption capabilities between the two phases. This enables the qualitative and quantitative determination of the individual components present in a given sample. The gas chromatographic system consists of three main components: an injector, a column, and a detector. The injector is kept at a high temperature to facilitate the sample's vaporisation. Additionally, a split may be used to dilute the sample and improve chromatographic performance. Subsequently, the sample is transferred to the column using an inert carrier gas (e.g., helium or nitrogen). This is the point where the stationary phase separates the analytes. The necessary time depends on the specific components being analysed and is referred to as the retention time. This is a characteristic property of each substance, enabling its identification. Following this, the detector generates an electric signal. A quantitative determination can be made based on the peak area and a linear calibration with a known concentration.<sup>241</sup>

### 2.2.2 Principles of an FID and BID

The carrier gas with the sample is introduced to the bottom of the **flame ionisation detector (FID)**, where it is mixed with hydrogen gas and a make-up gas ( $N_2$ ). This mixture is combined with synthetic air and burned above the jet tip. The carbon samples are first reduced to  $CH_4$ , then pyrolysed to CH radicals, and subsequently react with  $O_2$  to produce  $CHO^+$  and electrons in stoichiometric amounts. These electrons are then detected by a plate collector and displayed as a chromatogram.<sup>242,243</sup>

The **barrier ionisation-discharge-detector (BID)** operates with helium, whereby the helium atoms are excited by a high voltage to generate a plasma. Upon relaxation into their ground state, the atoms emit photons with high energies (17.7 eV), which ionise the analyte molecules. The resulting ions generate an electric signal at the collector electrode.<sup>243,244</sup>

#### 2.2.2.1 Analysis of low $CH_4$ and $C_2H_6$ concentrations with a GC-FID

$CH_4$  and  $C_2H_6$  were measured (low  $CH_4$  concentrations < 200 ppm<sub>v</sub>) with a GC-FID (Nexis GC-2030 with FID-2030; Shimadzu, Japan) or with a CARLO ERBA STRUMENTAZIONE with a coupled FID (GC6000 Vega Series 2). The Nexis is equipped with a 50 m aluminium oxide coated column (SH-Alumina BOND/KCl; Shimadzu, Japan; 50 m x 0.53 mm x 15  $\mu$ m) connected to a second aluminium oxide coated column (30 m x 0.53 mm x 10  $\mu$ m, Agilent Technologies Inc., USA). The temperature program of the oven started at 30°C and was held for 6,5 min. Then, it was heated up to 170°C at a rate of 50°C and held for 2.2 min. Helium was used as a carrier gas (30.2 ml min<sup>-1</sup>). The FID (200°C) runs with hydrogen gas (32 ml min<sup>-1</sup>), synthetic air (200 ml min<sup>-1</sup>) and nitrogen gas (24 ml min<sup>-1</sup>) as a makeup gas.

The CARLO ERBA is equipped with an aluminium oxide coated column (30 m x 0.53 mm x 10  $\mu$ m, Agilent Technologies Inc., USA), and the oven program starts at 50°C for 1 min, is heated with 5°C min<sup>-1</sup> to 70°C and then heated up to 190°C with a rate of 20°C min<sup>-1</sup> and is held for 5 min. In both systems, a 7 ml sample was injected with a gas-tight syringe (BD Luer-Lok Becton Dickinson, Switzerland) equipped with a side-port needle (7751-13/00/2, Hamilton Co., USA) into a 2 ml sample loop with a pre-connected trap filled with Drierite® (calcium sulphate) to remove  $H_2O$  from the sample and then transferred to the column. Calibration was done with an internal standard with 16.28 ppm<sub>v</sub>  $CH_4$  and 10.38 ppm<sub>v</sub>  $C_2H_6$ . Calibration was done down to 0.01 ppm<sub>v</sub> with a minimum  $R^2 = 0.99$ . A daily factor (standard and/or 1/50 of the standard) was measured within any measurement sequence.

#### 2.2.2.2 Analysis of $CH_4$ and $CO_2$ with a GC-BID

High  $CH_4$  concentrations (>200ppm<sub>v</sub> – 100 %) were measured with a GC-BID (GC-2010 Plus; Shimadzu, Japan) equipped with a packed column (ShinCarbon ST 80/100, 2m,  $\varnothing=0.53$  mm; SilcoSmooth Tubing). 50  $\mu$ l were injected with an autosampler (AOC 20i; Shimadzu, Japan) in the injector (150°C) with a split

of 5. Helium ( $5.72 \text{ ml min}^{-1}$ ) was used as a carrier gas. The chromatographic conditions were  $30^\circ\text{C}$  for 7.5 min,  $10^\circ\text{C min}^{-1}$  until  $100^\circ\text{C}$  for 4 min and  $30^\circ\text{C min}^{-1}$  until  $200^\circ\text{C}$  for 2 min. For  $\text{CH}_4$ , a 1000 ppm<sub>v</sub> and a 60 % standard (CRYSTAL-Standard; Air Liquide GmbH, Germany) were diluted and used for the calibration ( $R^2 \geq 0,99$ ). The 1000 ppm<sub>v</sub>  $\text{CH}_4$  was always measured as a daily factor and quality control each day after every 9-12 measurements.

#### 2.2.2.3 Analysis of $\text{CH}_3\text{OH}$ with a GC-FID

All  $\text{CH}_3\text{OH}$  concentrations were measured with a GC-FID (GC-2010 Plus; Shimadzu, Japan) and an autosampler (AOC 20i; Shimadzu, Japan). The GC is equipped with an SH 200 column (30 m x 0.25 mm x 1.00  $\mu\text{m}$ ). 1  $\mu\text{l}$  aqueous sample was injected ( $250^\circ\text{C}$ ) with a split of 10. The carrier gas is helium ( $1.5 \text{ ml min}^{-1}$ ). The FID ran with hydrogen gas ( $40 \text{ ml min}^{-1}$ ), synthetic air ( $400 \text{ ml min}^{-1}$ ) and nitrogen as a makeup gas ( $30 \text{ ml min}^{-1}$ ). The starting temperature of the oven is  $50^\circ\text{C}$  and is constantly increased from  $3^\circ\text{C min}^{-1}$  to  $65^\circ\text{C}$ . The oven is then heated to  $250^\circ\text{C}$  at a rate of  $50^\circ\text{C}$  and held for 3 min. Standards were prepared using 99.9 %  $\text{CH}_3\text{OH}$  and diluting between 0.1 and 50 ppm<sub>w</sub> ( $R^2 \geq 0.99$ ). Also, a daily factor of 10 ppm<sub>w</sub> was measured for quality control and daily variations of the measurements.

#### 2.2.2.4 Analysis of $\text{OCH}_3$ with a GC-FID

Quantification of the  $\text{OCH}_3$  was done with a GC-FID (HP 6890 GC and an HP 6890 autosampler; Hewlett Packard, USA). The injector temperature was  $200^\circ\text{C}$ , a split of 10 was applied, and 50  $\mu\text{l}$  of sample was injected with the autosampler. A DB-5 (25 m x 0.32 mm x 0.52  $\mu\text{m}$ ) column with a nitrogen gas flow of  $1.1 \text{ ml min}^{-1}$  was used. The column temperature was held constant at  $150^\circ\text{C}$  for 6 min. The FID ran with hydrogen ( $40 \text{ ml min}^{-1}$ ), synthetic air ( $400 \text{ ml min}^{-1}$ ), and nitrogen as a makeup gas ( $45 \text{ mL min}^{-1}$ ). Calibration was done with an internal beech wood (HUBG4<sup>245</sup>) or vanillin standard with a calibration between 6  $\mu\text{g}$  and 200  $\mu\text{g}$  ( $R^2 \geq 0.99$ ). A daily factor (HUBG4) was measured as quality control.

Before the measurement, the samples had to be treated with hydroiodic acid (HI).<sup>246</sup> 40 mg of the soil sample was mixed with 250 ml HI (57 %) in a 1.5 ml glass bottle. The vials were sealed with aluminium crimp caps with a natural rubber/butyl/TEF septum (1.0 mm thickness, 11 mm diameter, IVA Analyse-technik GmbH & Co. KG, Germany) and incubated at  $130^\circ\text{C}$  for 30 min and afterwards left to cool down and then the samples are measured.

### 2.2.3 Principles of Mass Spectrometry

Many measurements were conducted on mass spectrometers (MS) coupled with gas chromatographs. Three fundamental principles underlying the operation of a mass spectrometer are the generation of

ions from both inorganic and organic substances, followed by their separation based on their mass-to-charge ratio ( $m/z$ ). This process is achieved by irradiating the molecules with high-energy ions.

The essential configuration of a mass spectrometer comprises an ion source, an analyser, and a detector. Following this, ionisation occurs after chromatographic separation. Ions are generated by a rhenium (or other metals, e.g. tungsten or wolfram) filament, which is subjected to a defined current; the electrons then impact the analytes, resulting in ion generation. The separation of ions into specific mass fragments depends on the ionisation energy. The aforementioned fragments are accelerated in an electric field, bundled with focusing lenses, and transferred to the analyser. The analyser's function is to separate ions based on their  $m/z$  ratio. Various analytical instruments are available for this purpose, differing in their operational characteristics. Employed were a quadrupole analyser, a time-of-flight (TOF) analyser, and an ion trap analyser. The quadrupole analyser consists of four rod electrodes arranged in the  $xy$ -direction, with the ion flow occurring in the  $z$ -direction. By applying a defined direct current (DC) voltage and a high-frequency alternating voltage, only ions with a specific mass-to-charge ratio ( $m/z$ ) will pass through the quadrupole. The TOF analyser utilises a method of separation based on the ions' flight time. The ions are subjected to a constant voltage, resulting in differing velocities due to their varying  $m/z$  ratios, which in turn produce distinct flight paths and arrival times. In the ion trap, ions are collected in a potential well formed by a ring electrode, and two end cap electrodes to which direct current and radio frequency potentials are applied. The quadrupole ion trap can then release the ions from the trap in a targeted manner by altering the potential and/or resonance excitation based on their differing  $m/z$  ratios. These mass fragments from all different detectors subsequently collide with a collector equipped with a secondary electron multiplier, generating an amplified electrical signal that is detected and used to create a mass spectrum.

#### 2.2.3.1 Analysis of $\text{CH}_2\text{O}$ with a GC-TOF-MS

The quantification and isotopic measurements of  $\text{CH}_2\text{O}$  were conducted using a GC-TOF-MS (GC 6890N, Agilent Technologies Inc., USA, coupled with a GCT Premier™ Mass Spectrometer, Waters Co., USA). It was equipped with a DB-5 column (60 m x 0.32 mm x 1  $\mu\text{m}$ ), and helium was used as a carrier gas at a flow rate of 1.5 ml  $\text{min}^{-1}$ . An autosampler (COMBIPAL, CTC Analytics AG, Schweiz) injected 1.5  $\mu\text{l}$  of the aqueous sample into the injector at 280°C with a split ratio of 2. The oven's starting temperature was set to 30°C, increasing at a rate of 10°C  $\text{min}^{-1}$  to 200°C, then further heated to 250°C at a rate of 40°C  $\text{min}^{-1}$  and held for 5 minutes. For samples containing 2-methoxyphenol, a distinct temperature programme was utilised. The initial temperature was again set to 30°C, with a heating rate of 4°C  $\text{min}^{-1}$  until 160°C was reached. Subsequently, the heating rate increased to 40°C  $\text{min}^{-1}$ . The final

temperature of 250°C was maintained for 5 minutes. The mass spectrometer selectively detected masses ranging from 100 to 250 atomic mass units (AMU).

To analyse the CH<sub>2</sub>O, a derivatisation step is needed to make the CH<sub>2</sub>O more suitable for the GC-MS analysis. 1 ml PFPH (1 mg ml<sup>-1</sup>) and 1 ml pH-phosphate buffer (from buffer tablets) were added to the sample to prevent decomposition at low pH. A hydrazone is formed with a mass of 210 g mol<sup>-1</sup> and is analysed after a reaction time of half an hour (Figure 7). Standards in the range of 0.1 – 25 ppm<sub>w</sub> (R<sup>2</sup> ≥ 0.99) were prepared using 30 % CH<sub>2</sub>O without CH<sub>3</sub>OH.

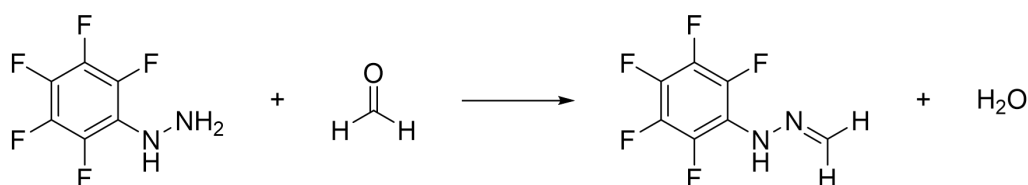


Figure 7: Derivatization of CH<sub>2</sub>O with PFPH and the formation of a hydrazone due to a condensation reaction.

#### 2.2.3.2 Analysis of CH<sub>3</sub>Cl and labelled CH<sub>3</sub>OH with a GC-MS

Concentrations of CH<sub>3</sub>Cl and isotopic labels of CH<sub>3</sub>Cl and CH<sub>3</sub>OH were measured using a GC-MS (GC-2010 Plus; GCMS-QP2020; Shimadzu, Japan). A ZB-624 column (60 m x 0.32 mm x 1.8 μm; Phenomenex, USA) was employed with helium as the carrier gas (1.51 ml min<sup>-1</sup>) and a split ratio of 5 in the injector (200°C). For the measurement of CH<sub>3</sub>Cl, 50 μl of gas was injected with a 250 μl gas-tight Pressure-Lok glass syringe (VICI, USA). The MS operates in two simultaneous modes: Total Ion Current (TIC) with a mass range of 46 – 200, and Selected Ion Monitoring (SIM) with the m/z ratios CH<sub>3</sub><sup>35</sup>Cl: 50, CH<sub>3</sub><sup>37</sup>Cl: 52, CD<sub>3</sub><sup>35</sup>Cl: 53, and CD<sub>3</sub><sup>37</sup>Cl: 55. The initial temperature was set to 30°C for 5.5 minutes, followed by a heating phase at a constant rate of 30°C min<sup>-1</sup> up to 180°C for 1 minute. Calibration was achieved by diluting a 99.8 % gas (Air Liquide, France) between 300 ppb<sub>v</sub> and 25 ppm<sub>v</sub> (R<sup>2</sup> = 1.00), and a daily factor of 6 ppm<sub>v</sub> was measured for each sequence as part of quality control. For the labelled CH<sub>3</sub>OH, the same column, injector temperature, column flow, and split ratio were employed but with a different oven program. It commenced at 40°C for 2 minutes, then increased at 50°C min<sup>-1</sup> to 150°C, where it was held for 3 minutes. The TIC mode was consistently used at 29 – 150 m/z, and the SIM mode was employed with m/z ratios of 33 and 34 for CH<sub>3</sub><sup>18</sup>OH and for CD<sub>3</sub>OH, 33, 34, and 35 m/z. Prior to injection, the samples were equilibrated at 85°C for 30 minutes. A volume of 200 μL of headspace was manually injected (n = 3) using a heated gas-tight glass syringe (VICI, USA) at 85°C.

#### 2.2.3.3 Analysis of HCOOH and CH<sub>3</sub>COOH with a GC-MS

The labelled HCOOH and CH<sub>3</sub>COOH in the samples were analysed using a 450-GC gas chromatograph coupled with a 240-MS IT mass spectrometer (both manufactured by Varian Inc. and Agilent

Technologies Inc., USA). A DB-5 column (60 m x 0.32 mm x 1.0  $\mu\text{m}$ ; Agilent Technologies Inc., USA) was utilised with a helium flow of 1.5 ml  $\text{min}^{-1}$  and a split of 10. A volume of 1  $\mu\text{l}$  was transferred to the injector at a temperature of 220°C using an autosampler (Varian PAL, CTC Analytics AG, Switzerland). The temperature programme commences at 40°C and is maintained for one minute. Thereafter, the temperature is increased to 60°C at a rate of 15°C  $\text{min}^{-1}$  and subsequently to 110°C at a rate of 5°C  $\text{min}^{-1}$ . The temperature is then increased with a rate of 70°C  $\text{min}^{-1}$  to 250°C, which is maintained for a further five minutes.

Derivatisation is a prerequisite for analysing HCOOH and CH<sub>3</sub>COOH in GC-MS, as these compounds decompose at the elevated temperatures typically encountered in the injector. The methodology presented here is based on the approach developed initially by Moreau et al. (2003).<sup>247</sup> Silylation is carried out, but the HCOOH and CH<sub>3</sub>COOH must first be extracted twice using diethyl ether, as the derivatising agent N-tert-butyltrimethylsilyl-N-methyltrifluoroacetamide is highly susceptible to H<sub>2</sub>O contamination.<sup>248</sup> To this end, 25  $\mu\text{L}$  of 25 % hydrochloric acid is added to each 1 mL sample in the polypropylene tubes. Subsequently, the tubes are filled to the 3 mL mark with diethyl ether, sealed, and mixed for 30 minutes at 1000 rpm using a vortexer (IKA MTS, IKA GmbH & Co. KG, Germany). The HCOOH and CH<sub>3</sub>COOH are then transferred into the diethyl ether. Subsequently, the samples are centrifugated for five minutes at 1200 rpm. The organic phase is aspirated and transferred to a 5 mL rolled rim vessel (IVA Analysentechnik GmbH & Co. KG, Germany). The extraction process is repeated with the remaining sample. Subsequently, Drierite<sup>®</sup> is added to the extract to remove residual H<sub>2</sub>O. The samples are then subjected to a second centrifugation for three minutes and then transferred to 1.5 mL rolling rim tubes (IVA Analysentechnik GmbH & Co. KG, Deutschland). In the final step, 20  $\mu\text{L}$  of N-tert-butyltrimethylsilyl-N-methyltrifluoroacetamide is added to each sample, and the samples are stored in the dark for five days before measurement for the derivatisation.

An ion trap is employed as an MS, operating within the range of 80-250 AMU. Derivatisation results in masses of 103 g  $\text{mol}^{-1}$  (HCOOH) and 117 g  $\text{mol}^{-1}$  (CH<sub>3</sub>COOH), or 104 g  $\text{mol}^{-1}$  and 120 g  $\text{mol}^{-1}$ , should deuterium-labelled HCOOH and CH<sub>3</sub>COOH have been formed in the experiments.

#### 2.2.4 Analysis of $\delta^{13}\text{C}$ and $\delta^{18}\text{O}$ of CO<sub>2</sub> with a GC-IRMS

The  $\delta^{13}\text{C}$  and  $\delta^{18}\text{O}$  stable isotope values of CO<sub>2</sub> were measured utilising an HP 6890N gas chromatograph (Agilent, Santa Clara, USA) equipped with an autosampler A200S (CTC Analytics, Zwingen, Switzerland). The GC system was coupled to a DeltaPLUSXL isotope ratio mass spectrometer (IRMS) (Thermo Fisher Scientific, Bremen, Germany) via a GC Combustion III Interface (ThermoQuest Finnigan, Bremen, Germany). To circumvent the conventional procedure of combustion IRMS analysis, the

combustion reactor was bypassed through a capillary. The resulting transfer of the CO<sub>2</sub> analyte eluting from the GC column was conducted directly from the column to the interface and then to the IRMS.

The gas chromatograph was equipped with a GS-GasPro capillary column (60 m x 0.32 mm; Agilent J&W, USA). The following conditions were employed: a split of 20 and an isothermal oven temperature of 30°C. Helium was used as the carrier gas, with a constant flow rate of 1.4 ml min<sup>-1</sup>. A tank of high-purity CO<sub>2</sub> (CO<sub>2</sub> 4.5, Air Liquide, Düsseldorf, Germany) with a known isotopic composition was utilised as the monitoring gas. All <sup>13</sup>C/<sup>12</sup>C and <sup>18</sup>O/<sup>16</sup>O isotope ratios are expressed in the conventional δ notation per mil or mUr versus Vienna Pee Dee Belemnite (VPDB).

### 2.2.5 Analysis of TOC with a SSM-5000A

The total organic carbon (TOC) in soils was quantified using a TOC-V<sub>CPH</sub> coupled with a solid module, specifically the SSM-5000A. The procedure involved the combustion of a dried soil sample at 900°C in an oven with oxygen and vanadium(V) oxide as a catalyst. The total carbon (TC) is oxidised to CO<sub>2</sub> and transferred with oxygen to a non-dispersive infrared detector. Additionally, the total inorganic carbon (TIC) was quantified by acidifying the sample with phosphoric acid, which produced CO<sub>2</sub> that was then transferred to the detector. The TOC is not directly measured but is calculated as the difference between the TC and TIC. Calibration was conducted using sodium bicarbonate (1-200 mg; R<sup>2</sup> = 1.00), with a daily factor of 80 mg measured for quality control purposes.

## 2.3 Calculations of the conversion rates and concentrations

The conversion of precursor compounds to various C1-C2 components is represented by yields calculated from the mixing ratios. These mixing ratios are determined through the calibration of the measured values. For each starting material, it is assumed that a complete conversion of a single CH<sub>3</sub> group occurs.

### 2.3.1 Calculations of the conversion ratio of CH<sub>3</sub>OH and CH<sub>2</sub>O

For CH<sub>3</sub>OH and CH<sub>2</sub>O, which are analysed in aqueous solution, the conversion rate is determined by the ratio of the amount of substance in the sample vessel to the maximum possible amount of substance (Eq. 1). The maximum possible amount corresponds to the amount of starting material added (25 μmol unless otherwise indicated). The calculation of the amount of substance in the samples is carried out according to Eq. 2.

$$Y_i = \frac{n_i}{n_{max}} \cdot 10^2 \quad (1)$$

$Y_i$  = conversion rate of the component  $i$  [%]

$n_i$  = amount of substance of component  $i$  per vial [ $\mu\text{mol}$ ]

$n_{max}$  = maximum amount of substance per vial [ $\mu\text{mol}$ ]

$$n_i = \frac{w_i}{M_i} \cdot m_L \quad (2)$$

$w_i$  = mass fraction of component  $i$  per vial [ $\text{ppm}_w$ ]

$M_i$  = molar mass of component  $i$  [ $\text{g}\cdot\text{mol}^{-1}$ ]

$m_L$  = mass of solution per vial [g]

### 2.3.2 Calculation for gases

For the gases, the conversion rate is determined by the measured ratio to the maximum achievable volume fractions in the sample vessel (Eq. 3).

$$Y_i = \frac{\varphi_i}{\varphi_{max}} \cdot 10^2 \quad (3)$$

$Y_i$  = Conversion rate of component  $i$  [%]

$\varphi_i$  = Volume fraction of component  $i$  per vial [ $\text{ppm}_v$ ]

$\varphi_{max,i}$  = Maximum volume fraction of component  $i$  per vessel [ $\text{ppm}_v$ ]

The volume fractions are calculated according to Eqs. 4 and 5.

$$\varphi_{max,i} = \frac{V_{max,i}}{V_{HS}} \quad (4)$$

$$V_{max,i} = \frac{n_{max} \cdot V_m}{n_{CH_3}} \quad (5)$$

$V_{max,i}$  = Maximum gas volume of component  $i$  [ $\mu\text{l}$ ]

$V_{HS}$  = Headspace volume in the vial [L].

$n_{max}$  = Maximum amount of substance per vessel [mol]

$V_m$  = Molar volume [ $\text{mol}\cdot\text{L}^{-1}$ ]

$n_{CH_3}$  = Number of  $\text{CH}_3$  groups required to form the gas

### 2.3.3 Calculation of the mass fraction of $\text{CH}_3\text{OH}$ and $\text{CH}_2\text{O}$ in soil

$$w_{Boden, TG} = \frac{w_i}{m_{dw}} \cdot 10^3 \quad (6)$$

$w_{soil, dw}$  = Mass fraction of component  $i$  in dried soil [ $\text{ng}/\text{g}_{soil, dw}$ ]

$w_i$  = Mass fraction of component  $i$  per vial [ $\text{ppm}_w$ ]

$m_{dw}$  = Dry weight of the soil in the vial [g]

Calculation of the amount of substance according to the ideal gas law:

$$n_i = \frac{p \cdot V}{R \cdot T} \cdot \varphi_i \cdot 10^3 \quad (7)$$

$n_i$  = Amount of substance of component  $i$  per vial [nmol]

$p$  = Pressure = 101.3 kPa

$V$  = Vial Volume =  $46.9 \cdot 10^{-3}$  L

$R$  = Universal gas constant = 8.314 (kPa•L)/(mol•K)

$T$  = Temperature = 295 K

$\varphi_i$  = Volume fraction of component  $i$  per vial [ppm<sub>v</sub>]

### 2.3.4 Calculation of the mass fraction

$$m_i = n_i \cdot M_i \quad (8)$$

$$w_{soil, dw} = \frac{m_i}{m_{dw}} \quad (9)$$

$m_i$  = Mass of component  $i$  per vial [ng]

$M_i$  = Molar mass of component  $i$  [g/mol]

## 2.4 Statistics of the measurements

Standard deviations were calculated using Equation 10. They are based on three replicates and three CH<sub>4</sub>, CH<sub>3</sub>OH and CH<sub>2</sub>O measurements. C<sub>2</sub>H<sub>6</sub> is only measured once per experiment due to the measurement setup. The number of experiments and measurements is listed in the corresponding section. The total error is calculated from the error propagation according to Eq. 10.

$$\sigma_{ges} = \sqrt{\sigma_1^2 + \sigma_2^2 + \dots + \sigma_n^2} \quad (10)$$

$\sigma_{tot}$  = Total conversion rate error [%]

$\sigma_n$  = Error of the individual conversion rate [%]

Linear regression analysis was conducted with Microsoft Excel (Microsoft Office 2019), where the R square value (R<sup>2</sup>) shows how well the linear regression model fits the analysed data.

### 3 Results and Discussion

Throughout the present study, the C1 and C2 components CH<sub>4</sub>, C<sub>2</sub>H<sub>6</sub>, CH<sub>3</sub>OH and CH<sub>2</sub>O were measured in all investigations. The additional C1 and C2 compounds (CH<sub>3</sub>Cl, CO<sub>2</sub>, CO, HCOOH and CH<sub>3</sub>COOH) measured in the studies are described in each case. The first set of results focuses on the reaction of DMSO as an example substrate with a sulphur-bonded CH<sub>3</sub> group and to dive deep into the reaction mechanism. The general experimental setup contains 25 μmol DMSO, 10 μmol LFe<sup>II</sup>Cl<sub>2</sub>/Fe<sub>2</sub>O<sub>3</sub>, 200 μmol H<sub>2</sub>O<sub>2</sub> and 100 μmol Asc, and every time the concentrations in the experiments are measured, a blank experiment is conducted to get the background concentrations of all analysed components. Additionally, the following isotopically labelled substances, d<sub>6</sub>-DMSO, H<sub>2</sub><sup>18</sup>O, H<sub>2</sub><sup>18</sup>O<sub>2</sub>, and <sup>18</sup>O<sub>2</sub>, were used to investigate the reaction mechanism and the precursor atoms of all formed C1 and C2 compounds (Chapter 3.1). Subsequently, experiments with compounds containing S-, N-, and P-bonded CH<sub>3</sub> groups are presented to determine the individual conversion rates mainly. The same setup contains 25 μmol S-, N-, and P-bonded CH<sub>3</sub> groups compounds, 10 μmol LFe<sup>II</sup>Cl<sub>2</sub>/Fe<sub>2</sub>O<sub>3</sub>, 200 μmol H<sub>2</sub>O<sub>2</sub> and 100 μmol Asc (Chapter 3.2). The next chapter investigates compounds containing OCH<sub>3</sub> groups with the setting containing 25 μmol OCH<sub>3</sub> compound, 10 μmol LFe<sup>II</sup>Cl<sub>2</sub>/Fe<sub>2</sub>O<sub>3</sub>, 200 μmol H<sub>2</sub>O<sub>2</sub> and 0.05 μmol trifluoromethanesulfonic acid instead of Asc. The investigations of the reaction mechanism and precursor atom with isotopically labelled compounds (<sup>2</sup>H- or <sup>13</sup>C-CH<sub>3</sub>-2-methoxyphenol, H<sub>2</sub><sup>18</sup>O<sub>2</sub>, and <sup>18</sup>O<sub>2</sub>) are described in detail (Chapter 3.3).

Moreover, a series of studies are outlined in which LFe<sup>II</sup>Cl<sub>2</sub>/Fe<sub>2</sub>O<sub>3</sub> is substituted for a range of different transition metals (Mn, Fe, Co, Ni and Cu) species to investigate the potential to produce CH<sub>4</sub>, C<sub>2</sub>H<sub>6</sub>, CH<sub>3</sub>OH, CH<sub>2</sub>O and CH<sub>3</sub>Cl. The precursor compounds are 25 μmol d<sub>6</sub>-DMSO, d<sub>3</sub>-methionine or 2-methoxyphenol along with 10 μmol transition metal species, 200 μmol H<sub>2</sub>O<sub>2</sub> and 100 μmol Asc (Chapter 3.4).

The next phase of the study involves transferring the results to natural conditions. This is achieved through a series of experiments with 50 mg lignin or pectin (essential parts of plants), 200 μmol H<sub>2</sub>O<sub>2</sub>, with or without 10 μmol Fe<sub>2</sub>O<sub>3</sub>, and with or without 100 μmol Asc (Chapter 3.5). A range of sterile soils (5g) with 10 ml ultra-pure H<sub>2</sub>O were incubated and analysed for CH<sub>4</sub>, C<sub>2</sub>H<sub>6</sub>, CH<sub>3</sub>OH and CH<sub>2</sub>O production. To get deeper insights into their formation, labelled precursor compounds were added, and also the physical and chemical parameters of the incubation were varied. Also, the TOC and the OCH<sub>3</sub> content of all soil samples were measured to conduct initial global extrapolations (Chapter 3.6).

### 3.1 Conversion rates and mechanistic details of d<sub>6</sub>-DMSO to C1 and C2 compounds<sup>1</sup>

Given the substantial environmental distribution of DMSO<sup>249</sup>, particularly within the marine ecosystem<sup>81</sup>, detailed studies were conducted to enhance the knowledge about the conversion rate to different C1 and C2 compounds and their formation processes.

#### 3.1.1 Determination of the general experimental setup

Initial experiments with DMSO or d<sub>6</sub>-DMSO were conducted to detect differences in conversion rates and produced C1 and C2 compounds (Table 5). d<sub>6</sub>-DMSO provides the advantage that deuterium from d<sub>6</sub>-DMSO can be tracked through the reaction chain, offering more profound insights into the reaction pathway.

Table 5: Experimental setups to determine the differences between DMSO and d<sub>6</sub>-DMSO.

No.	Precursor compound	Fe species	Oxidant	acid
1	25 μmol DMSO	10 μmol LFe <sup>II</sup> Cl <sub>2</sub>	200 μmol H <sub>2</sub> O <sub>2</sub>	100 μmol Asc
2	25 μmol d <sub>6</sub> -DMSO	10 μmol LFe <sup>II</sup> Cl <sub>2</sub>	200 μmol H <sub>2</sub> O <sub>2</sub>	100 μmol Asc
3	25 μmol DMSO	10 μmol Fe <sub>2</sub> O <sub>3</sub>	200 μmol H <sub>2</sub> O <sub>2</sub>	100 μmol Asc
4	25 μmol d <sub>6</sub> -DMSO	10 μmol Fe <sub>2</sub> O <sub>3</sub>	200 μmol H <sub>2</sub> O <sub>2</sub>	100 μmol Asc

Only minor differences between DMSO and d<sub>6</sub>-DMSO with LFe<sup>II</sup>Cl<sub>2</sub> or Fe<sub>2</sub>O<sub>3</sub>, H<sub>2</sub>O<sub>2</sub> and Asc were observed in the conversion rate, and CH<sub>4</sub>, C<sub>2</sub>H<sub>6</sub>, CH<sub>3</sub>OH and CH<sub>2</sub>O were identified for all reactions. Total conversion rates of 39.0 ± 1.50 % vs 49.7 ± 1.13 % for LFe<sup>II</sup>Cl<sub>2</sub> and 73.0 ± 1.00 % vs 85.7 ± 1.41 % for Fe<sub>2</sub>O<sub>3</sub> were detected for DMSO and d<sub>6</sub>-DMSO, respectively (Figure 8). Due to the minor differences, only d<sub>6</sub>-DMSO was used for further investigations. The 48-hour reaction time was selected based on the findings of time-dependent measurements of the conversion rate of d<sub>6</sub>-DMSO to CH<sub>4</sub> (Figure 9), conducted with setups 2 and 4 (Table 5). CH<sub>4</sub> was selected because it does not undergo further reactions, is easy to sample, and separates from the compounds in the H<sub>2</sub>O phase during the experiment due to degassing in the headspace. The reaction with the LFe<sup>II</sup>Cl<sub>2</sub> complex is completed after 0.5 h, but the reaction with Fe<sub>2</sub>O<sub>3</sub> is completed after more than 24 h. A reaction time of 48 h is appropriate to finish the reaction. The ratio between H<sub>2</sub>O<sub>2</sub> and Asc was previously tested, and the amount of Fe species was slightly adapted<sup>14</sup> (For details of the setup, see Chapter 2.1.1).

<sup>1</sup> Please note that parts of this section are taken from Hädel et al (2023)<sup>205</sup>.

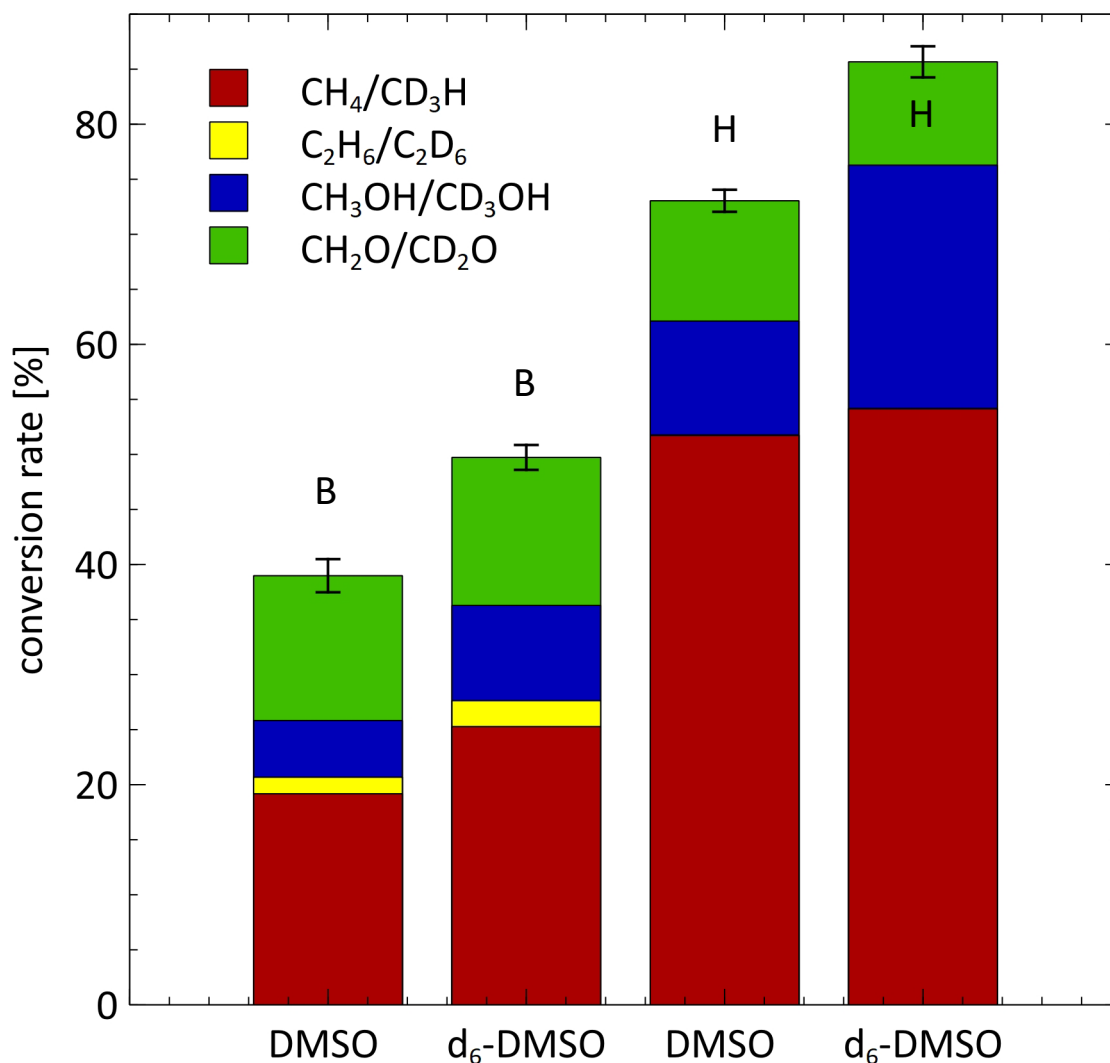


Figure 8: Differences in the conversion rate between DMSO and d<sub>6</sub>-DMSO relative to the added d<sub>6</sub>-DMSO (25 μmol) with LFe<sup>II</sup>Cl<sub>2</sub> (bars B) or Fe<sub>2</sub>O<sub>3</sub> (bars H) (10 μmol), Asc (100 μmol) and H<sub>2</sub>O<sub>2</sub> (200 μmol) converted to one CH<sub>3</sub> group. Error bars refer to the SD of the total conversion of all major C1 and C2 compounds for n = 9, except for C<sub>2</sub>D<sub>6</sub>, n = 3. Taken from Hädel et al. (2023).<sup>205</sup>

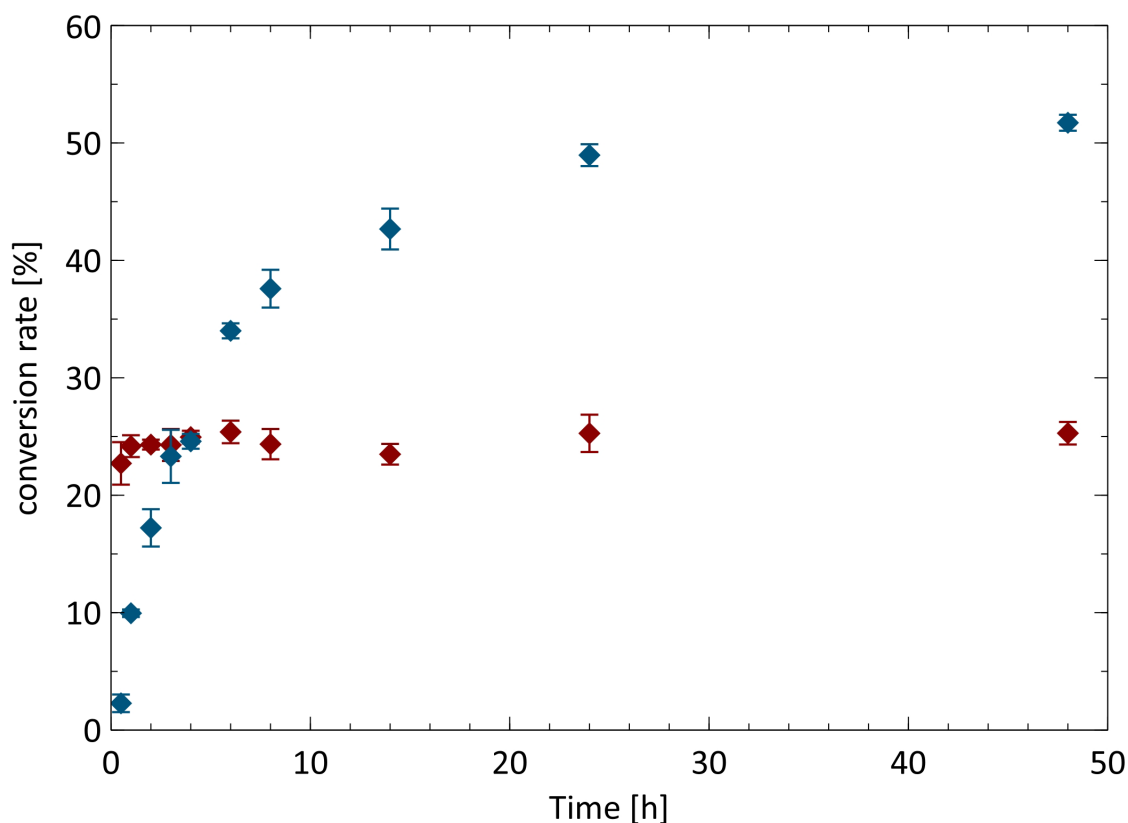


Figure 9: Formation of CD<sub>3</sub>H over time from the deuterium-labelled CH<sub>3</sub> groups of DMSO, mediated by LFe<sup>II</sup>Cl<sub>2</sub> (red symbols) compared to Fe<sub>2</sub>O<sub>3</sub> (blue symbols) (10 μmol) with Asc (100 μmol) and H<sub>2</sub>O<sub>2</sub> (200 μmol) converted to one CH<sub>3</sub> group. The reaction with LFe<sup>II</sup>Cl<sub>2</sub> is nearly completed after 0.5 h, and the reaction with Fe<sub>2</sub>O<sub>3</sub> is completed after more than 24 h. Error bars refer to mean values of CD<sub>3</sub>H (n = 9). Taken from Hädeler et al. (2023).<sup>205</sup>

### 3.1.2 Conversion rates of d<sub>6</sub>-DMSO to CD<sub>3</sub>H, C<sub>2</sub>D<sub>6</sub>, CD<sub>3</sub>OH, and CD<sub>2</sub>O and the impact of different Asc concentrations

Figure 10 illustrates the conversion rate of d<sub>6</sub>-DMSO to CD<sub>3</sub>H, C<sub>2</sub>D<sub>6</sub>, CD<sub>3</sub>OH, and CD<sub>2</sub>O mediated by LFe<sup>II</sup>Cl<sub>2</sub> or Fe<sub>2</sub>O<sub>3</sub> with H<sub>2</sub>O<sub>2</sub> under standard conditions but with varying Asc concentrations (Table 6).

Table 6: Composition of the experiments to determine the conversion rates with different Asc concentrations.

No.	Precursor compound	Fe species	Oxidant	acid
1, 3, 5 and 7	25 μmol d <sub>6</sub> -DMSO	10 μmol LFe <sup>II</sup> Cl <sub>2</sub>	200 μmol H <sub>2</sub> O <sub>2</sub>	0, 10, 100, 1000 μmol Asc
2, 4, 6 and 8	25 μmol d <sub>6</sub> -DMSO	10 μmol Fe <sub>2</sub> O <sub>3</sub>	200 μmol H <sub>2</sub> O <sub>2</sub>	0, 10, 100, 1000 μmol Asc

In the absence of Asc (No. 1 and 2), the only products are CD<sub>3</sub>OH (B: 23.8 ± 2.55 % and H: 23.6 ± 1.75 %) and CD<sub>2</sub>O (B: 17.4 ± 1.47 % and H: 12.9 ± 2.14 %). The addition of 10 μmol Asc (No. 3 and 4) results in the formation of CD<sub>3</sub>OH (B: 16.6 ± 6.44 % and H: 12.6 ± 0.77 %) and CD<sub>2</sub>O (B: 12.3 ± 2.46 % and H: 4.06 ± 0.94 %) and along with CD<sub>3</sub>H (B: 6.47 ± 0.25 % and H: 10.9 ± 0.42 %) and C<sub>2</sub>D<sub>6</sub> (B: 1.35 n = 1 due to measurement issues and H: zero %). The conversion rates from d<sub>6</sub>-DMSO to the C1 and C2 components are highest with 100 μmol Asc with a total conversion of 49.7 ± 1.13 % for LFe<sup>II</sup>Cl<sub>2</sub> (No. 5). This was comprised of 25.3 ± 0.85 % CD<sub>3</sub>H, 2.35 ± 0.01 % C<sub>2</sub>D<sub>6</sub>, 8.65 ± 0.27 % CD<sub>3</sub>OH, and CD<sub>2</sub>O 13.5 ± 0.69 % and with Fe<sub>2</sub>O<sub>3</sub> (No. 6) a total conversion rate of 85.7 ± 1.41 % and individual rates of 54.1 ± 1.1 % CD<sub>3</sub>H, 0.039 ± 0.002 % C<sub>2</sub>D<sub>6</sub>, 22.1 ± 0.7 % CD<sub>3</sub>OH and 9.4 ± 0.6 % CD<sub>2</sub>O are observed. When the concentration of Asc is 1000 μmol (No. 7 and 8), the conversion rate declines substantially, with CD<sub>3</sub>H (B: 13.0 ± 0.3 % and H: 22.2 ± 0.6 %) as the primary product, along with small amounts of CD<sub>3</sub>OH (B: 2.94 ± 2.19 % and H: 2.52 ± 0.46 %) and C<sub>2</sub>D<sub>6</sub> (B: 0.012 %; n = 1 due to measurement issues and H: zero %).

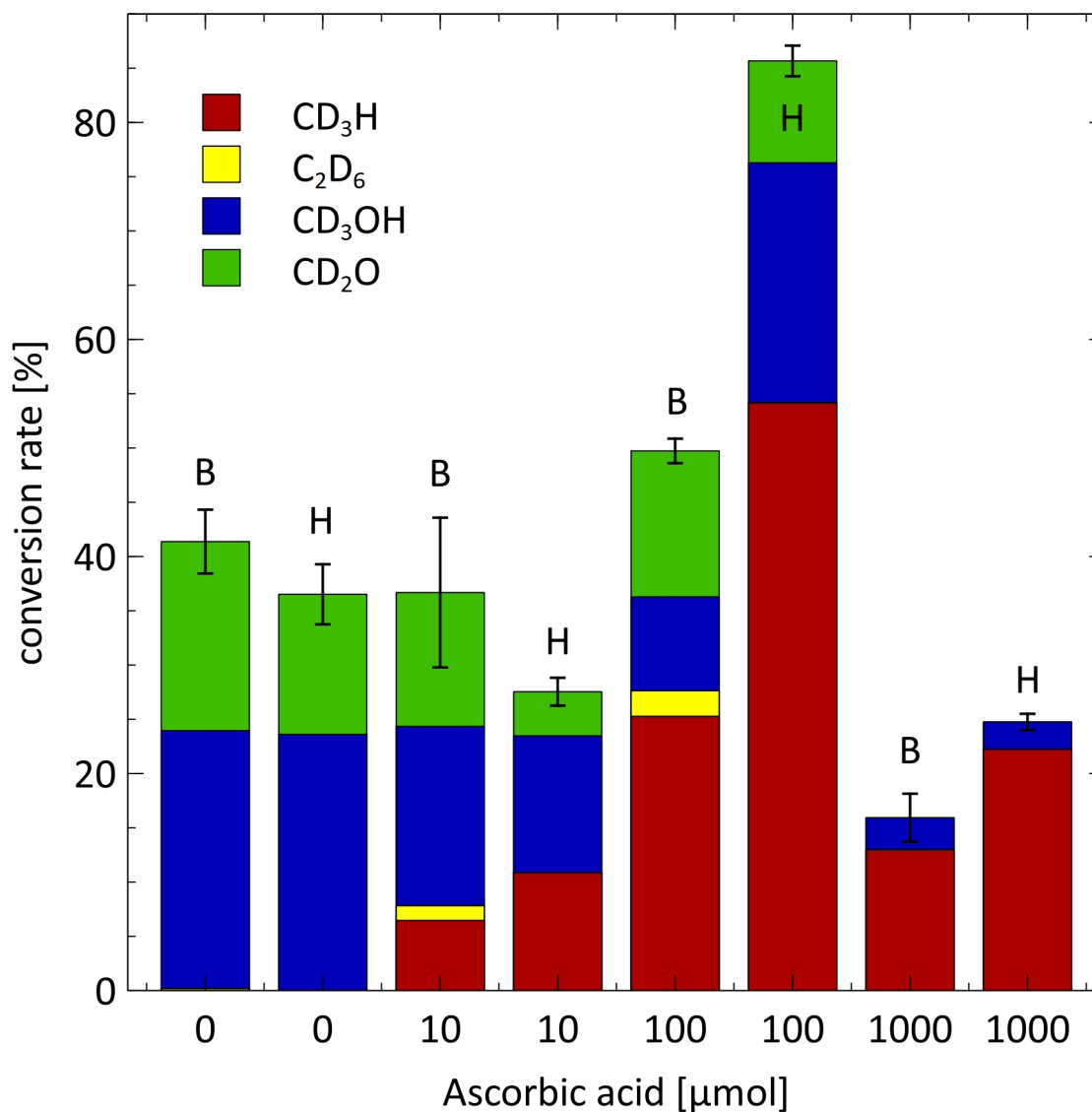


Figure 10: Formation of C1 and C2 compounds from  $d_6$ -DMSO mediated by  $LFe^{II}Cl_2$  (bars B) compared to  $Fe_2O_3$  (bars H). Experiments show the dependence of the rates of the formed products ( $CD_3H$ ,  $C_2D_6$ ,  $CD_3OH$ , and  $CD_2O$ ) on the Asc concentrations (10 ml  $H_2O$ , 48 h reaction time, ambient conditions) with added  $d_6$ -DMSO (25  $\mu mol$ ), with  $LFe^{II}Cl_2$  or  $Fe_2O_3$  (10  $\mu mol$ ),  $H_2O_2$  (200  $\mu mol$ ); error bars refer to the SD of the total conversion of all major C1 and C2 compounds for  $n = 9$ , except for  $C_2D_6$ ,  $n = 3$ . Taken from Hädeler et al. (2023).<sup>205</sup>

### 3.1.3 Impact of $O_2$ in the headspace and $H_2O$ phase on the conversion rates of $CD_3H$ , $C_2D_6$ , $CD_3OH$ , and $CD_2O$ derived from $d_6$ -DMSO

These experiments (Table 7) were done to investigate the role of  $O_2$  in the experiments and whether it influences the conversion rates.

Table 7: Composition of the experiments with (+) and without (-) O<sub>2</sub> to determine the conversion rates and possible differences.

No.	O <sub>2</sub>	Precursor compound	Fe species	Oxidant	acid
1	-	25 μmol d <sub>6</sub> -DMSO	10 μmol LFe <sup>II</sup> Cl <sub>2</sub>	200 μmol H <sub>2</sub> O <sub>2</sub>	100 μmol Asc
2	+	25 μmol d <sub>6</sub> -DMSO	10 μmol LFe <sup>II</sup> Cl <sub>2</sub>	200 μmol H <sub>2</sub> O <sub>2</sub>	100 μmol Asc
3	-	25 μmol d <sub>6</sub> -DMSO	10 μmol LFe <sup>II</sup> Cl <sub>2</sub>	200 μmol H <sub>2</sub> O <sub>2</sub>	0 μmol Asc
4	+	25 μmol d <sub>6</sub> -DMSO	10 μmol LFe <sup>II</sup> Cl <sub>2</sub>	200 μmol H <sub>2</sub> O <sub>2</sub>	0 μmol Asc

The results of experiments conducted without O<sub>2</sub> and with or without Asc and LFe<sup>II</sup>Cl<sub>2</sub> are illustrated in Figure 11. In the absence of O<sub>2</sub> and with or without Asc, the same C1 and C2 compounds are produced. In the absence of O<sub>2</sub> (No. 1), CD<sub>3</sub>H, C<sub>2</sub>D<sub>6</sub>, CD<sub>3</sub>OH and CD<sub>2</sub>O are produced with a total conversion rate of 59.1 ± 9.3 % (21.7 ± 4.1 % CD<sub>3</sub>H, 2.4 ± 0.5 % C<sub>2</sub>D<sub>6</sub>, 17.2 ± 8.2 % CD<sub>3</sub>OH, 17.8 ± 1.6 % CD<sub>2</sub>O). The total conversion rates are identical within the error margin of the experiment No. 2 with O<sub>2</sub>. In the absence of Asc and O<sub>2</sub> (No. 3), the total conversion rate is identical within the error bar of the experiment with O<sub>2</sub> (No. 4). Only CD<sub>3</sub>OH and CD<sub>2</sub>O in experiment No. 3 with a total conversion rate of 45.4 ± 7.0 % (15.6 ± 0.9 % CD<sub>3</sub>OH, 29.8 ± 6.9 % CD<sub>2</sub>O, 0.00 % CD<sub>3</sub>H, 0.00 % C<sub>2</sub>D<sub>6</sub>) is produced.

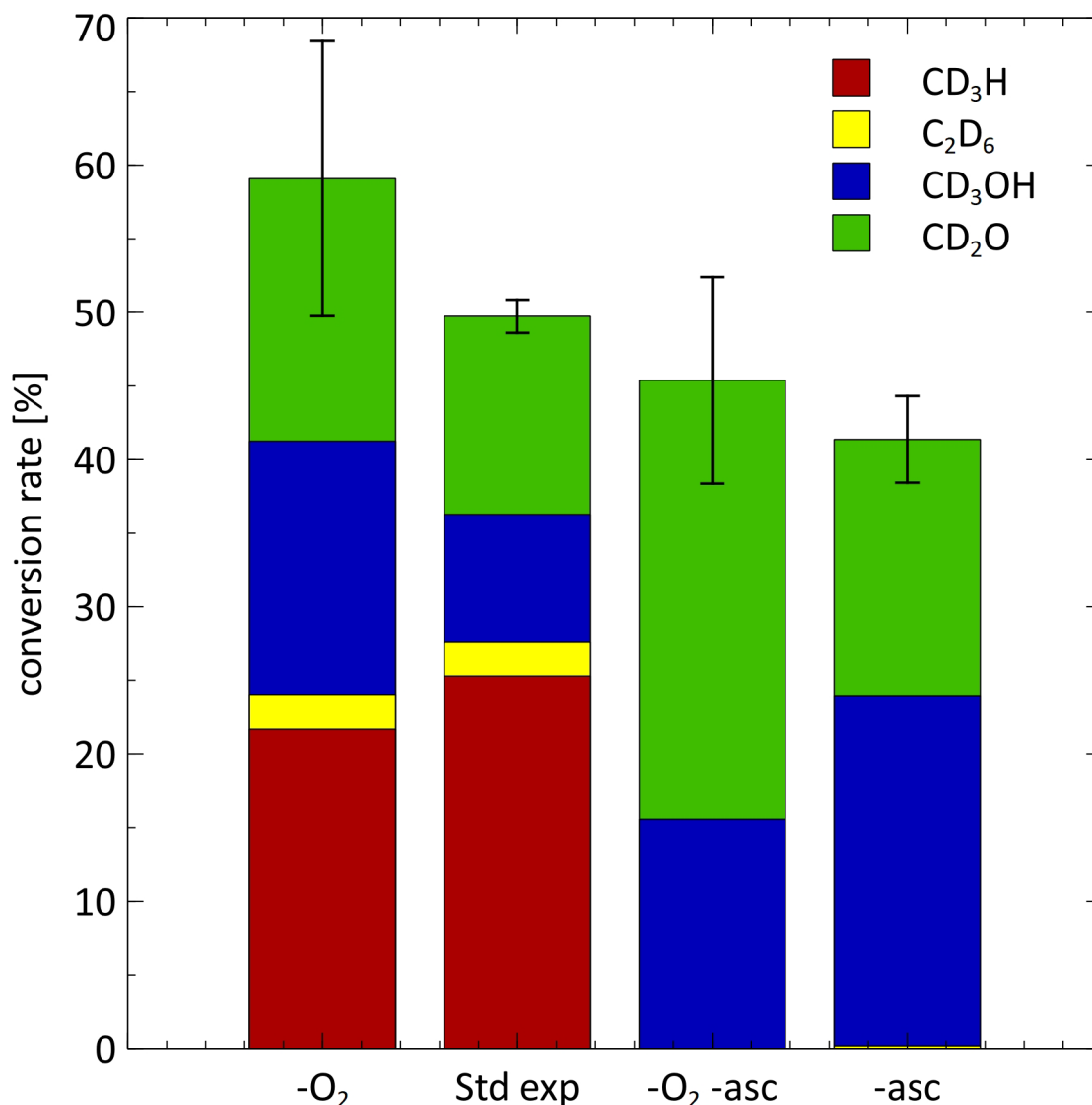


Figure 11: Impact of O<sub>2</sub> and Asc on forming C<sub>1</sub> and C<sub>2</sub> compounds with LFe<sup>II</sup>Cl<sub>2</sub>. Experiments with 25 μmol d<sub>6</sub>-DMSO, 100 μmol Asc (or none: -Asc), 200 μmol H<sub>2</sub>O<sub>2</sub> and 10 μmol LFe<sup>II</sup>Cl<sub>2</sub> in 10 ml ultra-pure H<sub>2</sub>O without O<sub>2</sub> (-O<sub>2</sub>) or in ambient atmosphere with a reaction time 48 h. Error bars refer to the SD of the total conversion of all major C<sub>1</sub> and C<sub>2</sub> compounds for n = 9, except for C<sub>2</sub>D<sub>6</sub>, n = 3. Taken from Hädeler et al. (2023).<sup>205</sup>

#### 3.1.4 Investigation of the intermediate dimethyl sulfone and the conversion rates to CH<sub>4</sub>, C<sub>2</sub>H<sub>6</sub>, CH<sub>3</sub>OH, and CH<sub>2</sub>O

To investigate whether the oxidised form of DMSO, dimethyl sulfone, acts as a precursor for C<sub>1</sub> and C<sub>2</sub> compounds, taking into account the possibility of their production in the experiment due to the highly oxidative conditions, experiments with 25 μmol dimethyl sulfone, 100 μmol Asc, 200 μmol H<sub>2</sub>O<sub>2</sub> and 10 μmol LFe<sup>II</sup>Cl<sub>2</sub> were conducted. Only low conversion rates of CH<sub>4</sub> (0.03 %) were observed, and no other C<sub>1</sub> and C<sub>2</sub> compounds were produced. Figure 12 shows the chromatogram of CH<sub>4</sub> formation with dimethyl sulfone compared with a blank experiment.

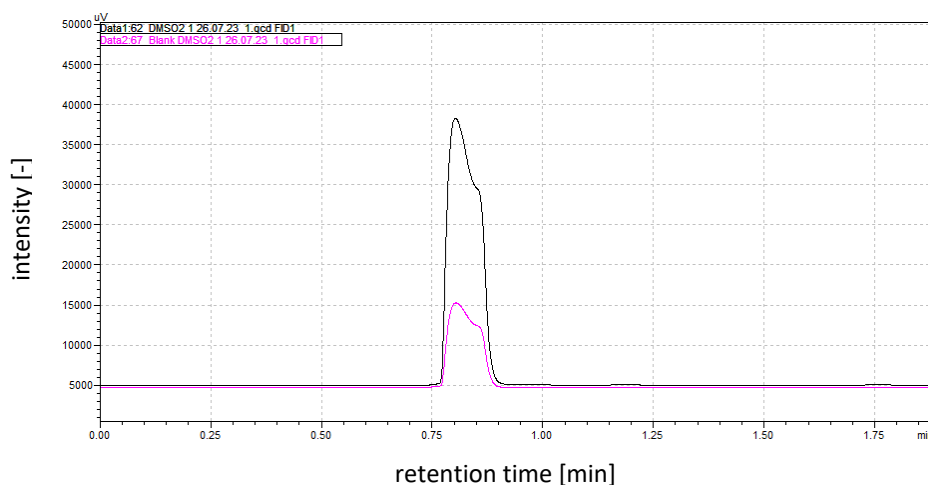


Figure 12: Chromatogram of the formation of CH<sub>4</sub> in the experiment with 25 μmol dimethyl sulfone (black line), 100 μmol ascorbic acid, 200 μmol H<sub>2</sub>O<sub>2</sub>, 10 μmol LFe<sup>II</sup>Cl<sub>2</sub>, compared with the blank experiment (100 μmol ascorbic acid, 200 μmol H<sub>2</sub>O<sub>2</sub>, 10 μmol LFe<sup>II</sup>Cl<sub>2</sub> and no substrate added) under ambient atmosphere with a reaction time 48 h. Taken from Hädeler et al. (2023).<sup>205</sup>

### 3.1.5 Investigation of the mechanism of the reaction of d<sub>6</sub>-DMSO to C1 and C2 compounds with isotopically labelled compounds

A broad set of isotopically labelled experiments were conducted to gain deeper insights into the precursor atoms and reaction mechanism. These involved <sup>2</sup>H and <sup>13</sup>C labelled DMSO and <sup>18</sup>O labelled H<sub>2</sub>O, H<sub>2</sub>O<sub>2</sub>, and O<sub>2</sub>.

#### 3.1.5.1 Identification of the origin of the CH<sub>3</sub> group in C1 and C2 compounds with fully deuterated DMSO

Fully deuterated DMSO enables tracking of the CH<sub>3</sub> group throughout the reaction, with the mass shifts detectable through various MS analyses. The MS pattern of the C1 and C2 compounds measured in Chapter 3.1.2 for experiment No. 5 (25 μmol d<sub>6</sub>-DMSO, 100 μmol ascorbic acid, 200 μmol H<sub>2</sub>O<sub>2</sub>, 10 μmol LFe<sup>II</sup>Cl<sub>2</sub>) shows a clear mass shift of 3 AMU for CH<sub>4</sub> vs CD<sub>3</sub>H, 6 for C<sub>2</sub>H<sub>6</sub> vs C<sub>2</sub>D<sub>6</sub>, 3 for CH<sub>3</sub>OH vs CD<sub>3</sub>OH and 2 for CH<sub>2</sub>O vs CD<sub>2</sub>O (Figure 13a, b, c and d, respectively). Also, traces of HCOOH and CH<sub>3</sub>COOH could be detected, but no quantification could be made because of the low concentrations and the large variability of the conversion rate during the analysis. However, a mass shift of 1 for HCOOH and 3 for CH<sub>3</sub>COOH to DCOOH and CD<sub>3</sub>COOH could be measured (Figure 14a and b). The presence of chlorine in LFe<sup>II</sup>Cl<sub>2</sub> also resulted in the detection of labelled CH<sub>3</sub>Cl in setup No. 5 from Chapter 3.1.2, which showed a mass shift of 3 from CH<sub>3</sub>Cl to CD<sub>3</sub>Cl (Figure 15).

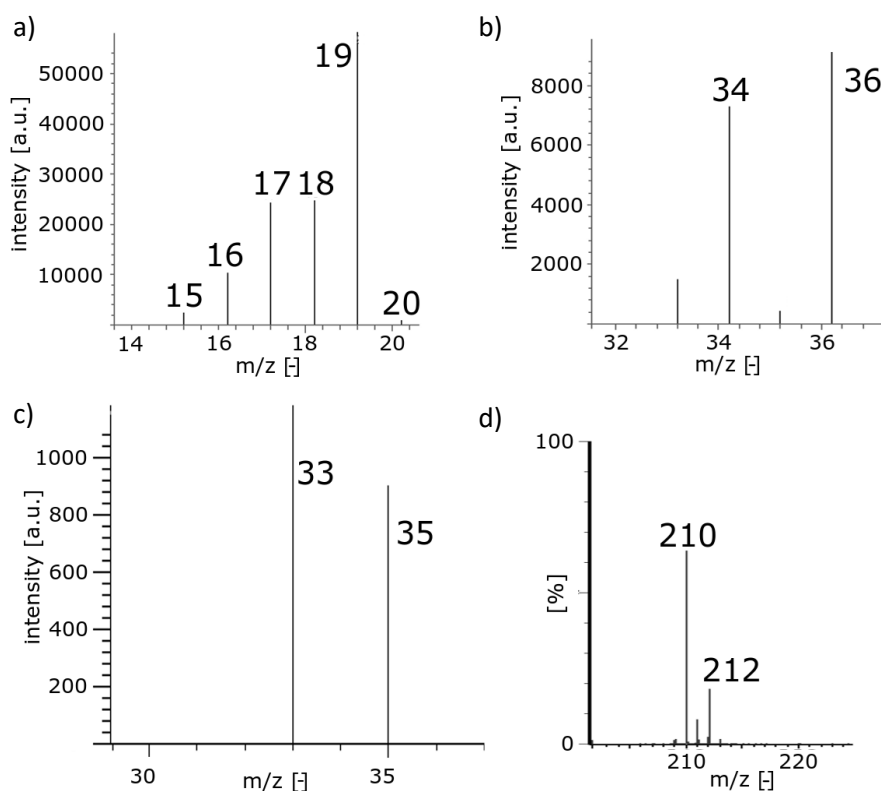


Figure 13: Mass fragmentation patterns of  $\text{CH}_4$ ,  $\text{C}_2\text{H}_6$ ,  $\text{CH}_3\text{OH}$  and  $\text{CH}_2\text{O}$  of experiments with  $\text{d}_6$ -DMSO ( $25 \mu\text{mol}$ ) with  $\text{LFe}^{\text{II}}\text{Cl}_2$  ( $10 \mu\text{mol}$ ), Asc ( $100 \mu\text{mol}$ ) and  $\text{H}_2\text{O}_2$  ( $200 \mu\text{mol}$ ) under ambient atmospheric conditions with a reaction time of 48 h. **a)** Mass shift of 3 from 16 to 19 for  $\text{CD}_3\text{H}$  from  $\text{d}_6$ -DMSO; **b)** mass shift of 6 from 30 to 36 for  $\text{C}_2\text{D}_6$  from  $\text{d}_6$ -DMSO; **c)** mass shift of 3 from 32 to 35 for  $\text{CD}_3\text{OH}$  from  $\text{d}_6$ -DMSO; **d)** mass shift of 2 from 210 to 212 for deuterated and derivatised  $\text{CD}_2\text{O}$  from  $\text{d}_6$ -DMSO. Taken from Hädel et al. (2023).<sup>205</sup>

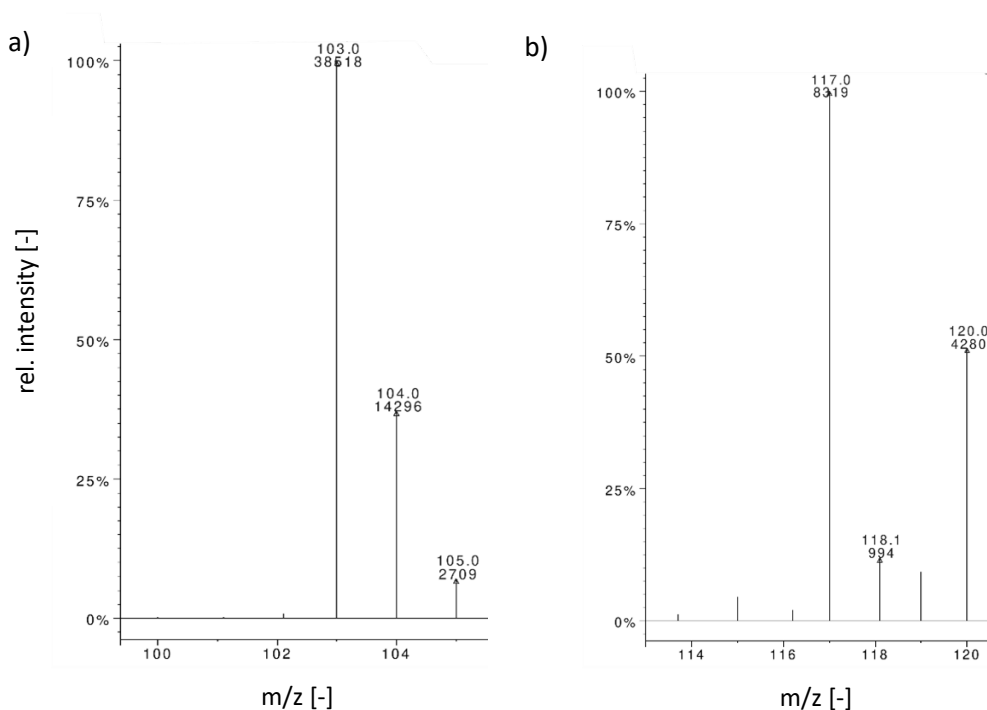


Figure 14: Mass fragmentation of an experiment with 25  $\mu\text{mol}$   $\text{d}_6$ -DMSO, 100  $\mu\text{mol}$  ascorbic acid, 200  $\mu\text{mol}$   $\text{H}_2\text{O}_2$  and 10  $\mu\text{mol}$   $\text{LFe}^{\text{II}}\text{Cl}_2$  under ambient atmospheric conditions with a reaction time of 48 h. Chromatogram and the corresponding mass track from a) HCOOH with a mass shift of 1 AMU from 103 to 104 and b)  $\text{CH}_3\text{COOH}$  with a mass shift of 3 AMU from 117 to 120. Taken from Hädel et al. (2023).<sup>205</sup>

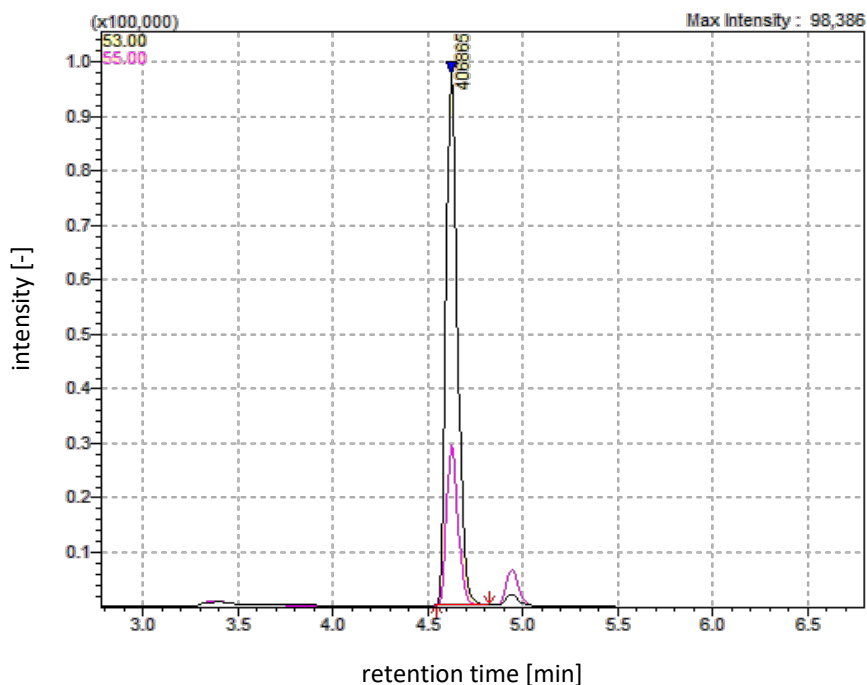


Figure 15: Chromatogram of deuterium labelled  $\text{CD}_3\text{Cl}$  in the experiment with 25  $\mu\text{mol}$   $\text{d}_6$ -DMSO, 100  $\mu\text{mol}$  ascorbic acid, 200  $\mu\text{mol}$   $\text{H}_2\text{O}_2$  and 10  $\mu\text{mol}$   $\text{LFe}^{\text{II}}\text{Cl}_2$  under ambient atmospheric conditions with a reaction time of 48 h. The chromatogram illustrates the masses 53 (black) and 55 (pink). These represent a mass shift of 3 AMU to the  $\text{CD}_3\text{Cl}$ , with the stable isotopes 35 and 37 (mass of 50 or 52 for  $\text{CH}_3\text{Cl}$ ). Taken from Hädel et al. (2023).<sup>205</sup>

### 3.1.5.2 Oxidation of CD<sub>3</sub>OH to CD<sub>2</sub>O

To ascertain whether CH<sub>2</sub>O is an oxidation product of CH<sub>3</sub>OH and not directly produced in all investigations conducted, an experiment was performed without DMSO, with CD<sub>3</sub>OH, and another with DMSO and CD<sub>3</sub>OH. Both with the addition of 10 μmol LFe<sup>II</sup>Cl<sub>2</sub>, 100 μmol Asc and 200 μmol H<sub>2</sub>O<sub>2</sub>. In both experimental setups, the deuterium-labelling in CD<sub>2</sub>O could be clearly detected by the mass shift of 2 AMU from 210 to 212 in the derivatised CD<sub>2</sub>O (Figure 16a and b).

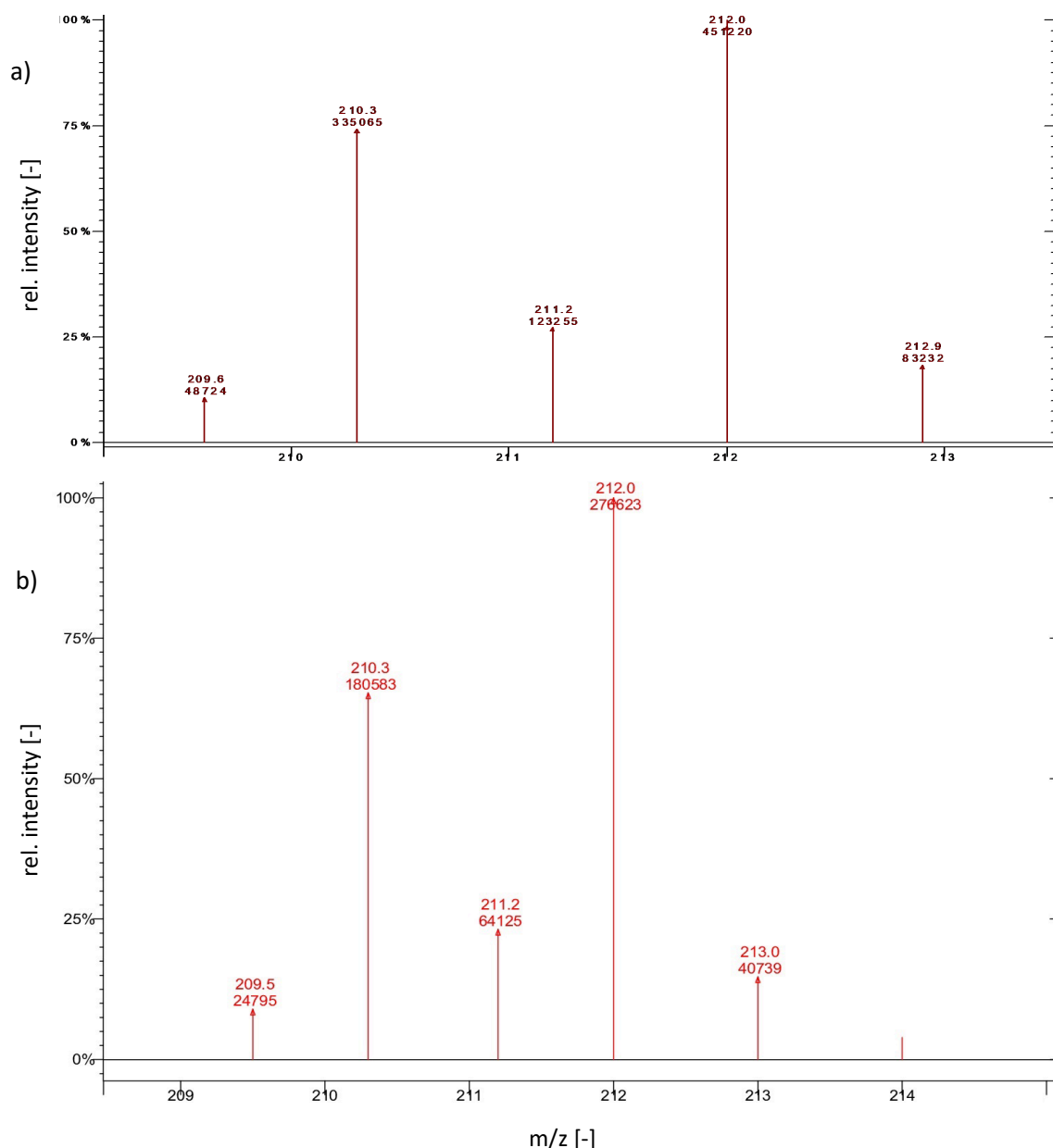


Figure 16: Mass fragmentation of deuterium-labelled CH<sub>2</sub>O to track the oxidation from CH<sub>3</sub>OH to CH<sub>2</sub>O. Mass track of CH<sub>2</sub>O with a mass shift of 2 AMU from 210 to 212 **a)** without DMSO and added CD<sub>3</sub>OH and **b)** with DMSO and added CD<sub>3</sub>OH. Experiment with or without 25 μmol DMSO, 100 μmol Asc, 200 μmol H<sub>2</sub>O<sub>2</sub> and 10 μmol LFe<sup>II</sup>Cl<sub>2</sub> under ambient atmospheric conditions with a reaction time of 48 h. Taken from Hädeler et al. (2023).<sup>205</sup>

### 3.1.5.3 Identification of the origin of the carbon in CO<sub>2</sub> with <sup>13</sup>C-labelled DMSO

To trace the carbon atom from the CH<sub>3</sub> group of DMSO during the oxidation reaction up to CO<sub>2</sub> due to the presence of H<sub>2</sub>O<sub>2</sub>, 25 μmol <sup>13</sup>C-labelled DMSO was employed with the following substances: 100 μmol Asc, 200 μmol H<sub>2</sub>O<sub>2</sub> and 10 μmol LFe<sup>II</sup>Cl<sub>2</sub>. The CO<sub>2</sub> formed in traces was then subjected to analysis using GC-C-IRMS. The δ<sup>13</sup>C-CO<sub>2</sub> vs VPDB (Vienna Pee Dee Belemnite) is markedly elevated (196 ± 2.2 mUr) in comparison to laboratory air (-16.8 ± 0.9 mUr). This allows us to rule out that a natural isotope effect is responsible for the marked elevation. Additional standard experiments with 25 μmol <sup>13</sup>C-DMSO, 100 μmol Asc, 200 μmol H<sub>2</sub>O<sub>2</sub> and 10 μmol Fe<sub>2</sub>O<sub>3</sub> also demonstrated an elevated δ<sup>13</sup>C-CO<sub>2</sub> value (267 ± 0.2 mUr). The utilisation of 25 μmol <sup>13</sup>CH<sub>3</sub>OH without added <sup>13</sup>C-labelled DMSO and 100 μmol Asc, 200 μmol H<sub>2</sub>O<sub>2</sub> and 10 μmol LFe<sup>II</sup>Cl<sub>2</sub> exhibited an even higher δ<sup>13</sup>C-CO<sub>2</sub> value of 1206 ± 0.2 mUr.

### 3.1.5.4 Identification of the origin of the oxygen atom in CH<sub>3</sub>OH, CH<sub>2</sub>O and CO<sub>2</sub> with <sup>18</sup>O-labelled H<sub>2</sub>O, H<sub>2</sub>O<sub>2</sub> and O<sub>2</sub>

To ascertain the oxygen atoms' origin in the oxygenated reaction compounds, experiments were conducted utilising H<sub>2</sub>O, H<sub>2</sub>O<sub>2</sub> and O<sub>2</sub> labelled with <sup>18</sup>O. To investigate the behaviour of the OH radicals generated by the Fenton reaction, 5 μmol d<sub>6</sub>-DMSO, 10 μmol Asc, 20 μmol H<sub>2</sub><sup>18</sup>O<sub>2</sub> and 1 μmol LFe<sup>II</sup>Cl<sub>2</sub> were utilised due to limitations in the availability of H<sub>2</sub><sup>18</sup>O<sub>2</sub>, smaller quantities were employed. A mass shift of 5 AMU from 37 in CD<sub>3</sub><sup>18</sup>OH compared to 32 in CH<sub>3</sub>OH was observed, which is caused by the CD<sub>3</sub> in d<sub>6</sub>-DMSO and the <sup>18</sup>O in H<sub>2</sub><sup>18</sup>O<sub>2</sub> (Figure 17). Moreover, to investigate the role of O<sub>2</sub> in the reaction, 25 μmol DMSO, 100 μmol Asc, 200 μmol H<sub>2</sub>O<sub>2</sub> and 10 μmol LFe<sup>II</sup>Cl<sub>2</sub> were utilised, and the O<sub>2</sub> present in the headspace and the H<sub>2</sub>O-phase was replaced by <sup>18</sup>O<sub>2</sub>. This enabled the determination of whether O<sub>2</sub> was also involved in the reaction. Also, as previously observed, a mass shift of 5 AMU in CD<sub>3</sub><sup>18</sup>OH compared to 32 in CH<sub>3</sub>OH, was detected in this instance and proves that the CD<sub>3</sub> in d<sub>6</sub>-DMSO and the <sup>18</sup>O in O<sub>2</sub> is the precursor of CD<sub>3</sub><sup>18</sup>OH (Figure 18). The setup with 2.5 μmol d<sub>6</sub>-DMSO, 10 μmol Asc, 20 μmol H<sub>2</sub>O<sub>2</sub> and 1 μmol LFe<sup>II</sup>Cl<sub>2</sub> with 1 ml H<sub>2</sub><sup>18</sup>O demonstrated no transfer of <sup>18</sup>O to CD<sub>3</sub>OH and proved that the oxygen in H<sub>2</sub>O is not involved in the reaction. CO<sub>2</sub> was also analysed for δ<sup>18</sup>O values versus VPDB in all previously described <sup>18</sup>O-labelling experiments. A markedly elevated δ<sup>18</sup>O value of 1316 ± 14 mUr was observed for H<sub>2</sub><sup>18</sup>O<sub>2</sub>, while for <sup>18</sup>O<sub>2</sub>, an elevated value of 55-93 mUr was recorded. That proves that the oxygen in CO<sub>2</sub> originates from the H<sub>2</sub>O<sub>2</sub> and the O<sub>2</sub> present.

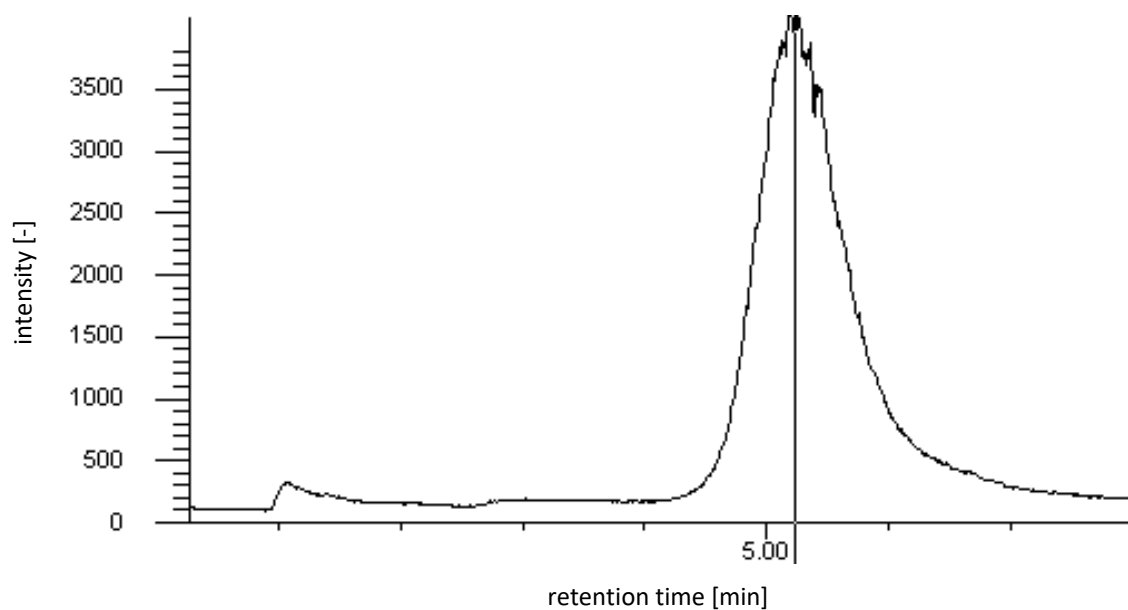


Figure 17: Chromatogram of isotopic labelled  $\text{CH}_3\text{OH}$ . Experiment with 2.5  $\mu\text{mol}$   $\text{d}_6$ -DMSO, 10  $\mu\text{mol}$  Asc, 20  $\mu\text{mol}$   $\text{H}_2^{18}\text{O}_2$  and 1  $\mu\text{mol}$   $\text{LFe}^{\text{II}}\text{Cl}_2$  in 1 ml ultra-pure  $\text{H}_2\text{O}$  under ambient atmospheric conditions with a reaction time of 48 h. Chromatogram of  $\text{C}^2\text{H}_3^{18}\text{OH}$  at  $m/z = 37$ . Taken from Hädeler et al. (2023).<sup>205</sup>

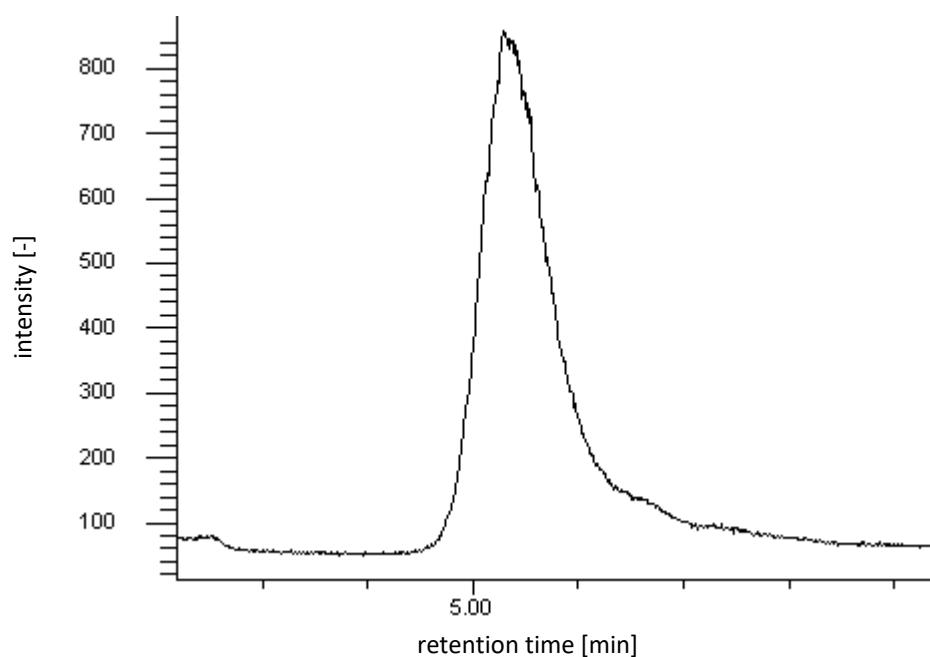


Figure 18: Chromatogram of isotopically labelled  $\text{CH}_3\text{OH}$ . Experiment with 25  $\mu\text{mol}$   $\text{d}_6$ -DMSO, 100  $\mu\text{mol}$  Asc, 200  $\mu\text{mol}$   $\text{H}_2\text{O}_2$  and 10  $\mu\text{mol}$   $\text{LFe}^{\text{II}}\text{Cl}_2$  under 79 %  $\text{N}_2$  and 21 %  $^{18}\text{O}_2$  atmosphere with a reaction time of 48 h. Chromatogram of  $\text{CD}_3^{18}\text{OH}$  at  $m/z$ -ratio at 37. Taken from Hädeler et al. (2023).<sup>205</sup>

### 3.1.6 Trapping $\text{CH}_3$ radicals with $\text{CH}_2\text{Br}_2$ and $\text{CCl}_3\text{Br}$

To provide further evidence for the formation of  $\text{CH}_3$  radicals, alkyl radical scavengers  $\text{CH}_2\text{Br}_2$  and  $\text{CCl}_3\text{Br}$  were applied (1.25 mmol). Both were incorporated into separate experiments with 25  $\mu\text{mol}$  d6-DMSO, 100  $\mu\text{mol}$  Asc, 200  $\mu\text{mol}$   $\text{H}_2\text{O}_2$  and 10  $\mu\text{mol}$   $\text{LFe}^{\text{II}}\text{Cl}_2$  and the conversion rates to  $\text{CD}_3\text{H}$ ,  $\text{C}_2\text{D}_6$ ,  $\text{CD}_3\text{OH}$  and  $\text{CD}_2\text{O}$  were quantified (Table 8).

Table 8: Composition of the experiments with the alkyl radical scavenger  $\text{CH}_2\text{Br}_2$  and  $\text{CCl}_3\text{Br}$  to determine the conversion rates and possible differences.

No.	Precursor compound	Fe species	Oxidant	acid
1	25 $\mu\text{mol}$ d6-DMSO	10 $\mu\text{mol}$ $\text{LFe}^{\text{II}}\text{Cl}_2$	200 $\mu\text{mol}$ $\text{H}_2\text{O}_2$	100 $\mu\text{mol}$ Asc
2 with $\text{CH}_2\text{Br}_2$	25 $\mu\text{mol}$ d6-DMSO	10 $\mu\text{mol}$ $\text{LFe}^{\text{II}}\text{Cl}_2$	200 $\mu\text{mol}$ $\text{H}_2\text{O}_2$	100 $\mu\text{mol}$ Asc
3 with $\text{CCl}_3\text{Br}$	25 $\mu\text{mol}$ d6-DMSO	10 $\mu\text{mol}$ $\text{LFe}^{\text{II}}\text{Cl}_2$	200 $\mu\text{mol}$ $\text{H}_2\text{O}_2$	100 $\mu\text{mol}$ Asc
4	25 $\mu\text{mol}$ d6-DMSO	10 $\mu\text{mol}$ $\text{Fe}_2\text{O}_3$	200 $\mu\text{mol}$ $\text{H}_2\text{O}_2$	100 $\mu\text{mol}$ Asc
5 with $\text{CCl}_3\text{Br}$	25 $\mu\text{mol}$ d6-DMSO	10 $\mu\text{mol}$ $\text{Fe}_2\text{O}_3$	200 $\mu\text{mol}$ $\text{H}_2\text{O}_2$	100 $\mu\text{mol}$ Asc

In the case of  $\text{CH}_2\text{Br}_2$  in No. 2, only a minor decline in the conversion rates of all C1 and C2 compounds was recorded compared to No. 1 (Figure 19). Conversely, a pronounced reduction in the conversion rates was observed when  $\text{CCl}_3\text{Br}$  was used in No. 3 and No. 5 (Figure 19). No. 2 yielded a total conversion rate of  $44.0 \pm 3.3$  ( $\text{CD}_3\text{H}$  ( $22.0 \pm 2.5$  %),  $\text{C}_2\text{D}_6$  ( $2.14 \pm 0.28$  %),  $\text{CD}_3\text{OH}$  ( $12.6 \pm 2.0$  %),  $\text{CD}_2\text{O}$  ( $5.89 \pm 0.64$  %)) The total conversion rate in No. 3 is  $12.8 \pm 1.4$  ( $\text{CD}_3\text{H}$  ( $6.73 \pm 0.39$  %),  $\text{C}_2\text{D}_6$  ( $0.75 \pm 0.07$  %),  $\text{CD}_3\text{OH}$  ( $5.36 \pm 1.31$  %) and zero for  $\text{CD}_2\text{O}$  and for No. 5 is  $9.23 \pm 1.25$  % ( $\text{CD}_3\text{H}$  ( $0.36 \pm 0.01$  %),  $\text{C}_2\text{D}_6$  (zero %),  $\text{CD}_3\text{OH}$  ( $4.76 \pm 0.60$  %),  $\text{CD}_2\text{O}$  ( $4.11 \pm 1.09$  %)).

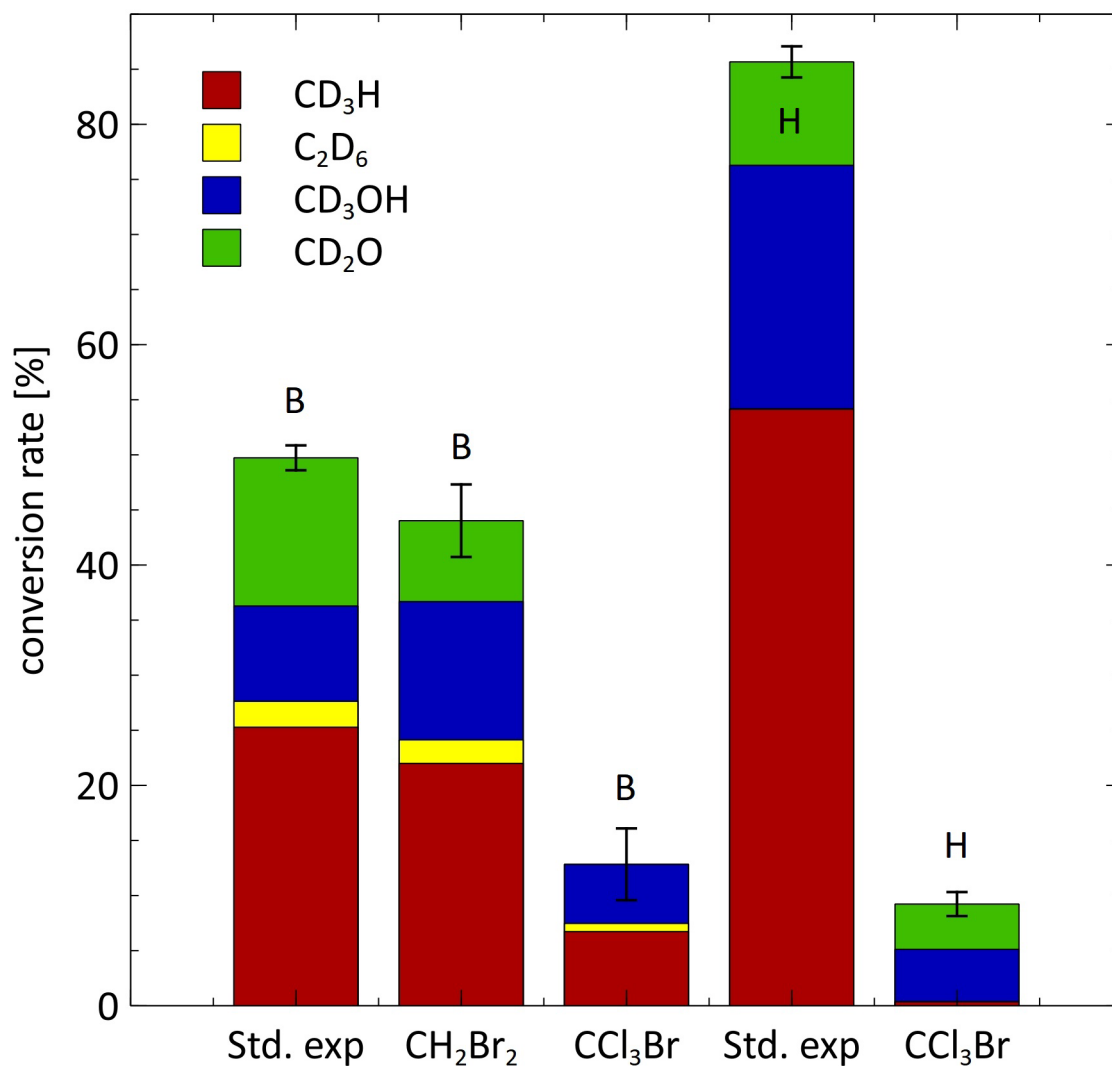


Figure 19: Formation of CD<sub>3</sub>H, C<sub>2</sub>D<sub>6</sub>, CD<sub>3</sub>OH and CD<sub>2</sub>O from d<sub>6</sub>-DMSO with the 10 μmol LFe<sup>II</sup>Cl<sub>2</sub> (bars B) or Fe<sub>2</sub>O<sub>3</sub> (bars H) 100 μmol Asc and 200 μmol H<sub>2</sub>O<sub>2</sub> in the presence of 1.25 mmol CH<sub>2</sub>Br<sub>2</sub> or CCl<sub>3</sub>Br, respectively, compared to the conversion rates observed in Chapter 3.1.2, without alkyl radical scavengers. Experiments were conducted under ambient atmospheric conditions with a reaction time of 48 h. Error bars refer to the SD of the total conversion of all major C1 and C2 compounds for n = 9, except for C<sub>2</sub>D<sub>6</sub>, n = 3. Taken from Hädeler et al. (2023).<sup>205</sup>

Figure 20a, b and c show the formation of deuterium labelled CD<sub>3</sub>Br in Nos. 2, 3, and 5 with CH<sub>2</sub>Br<sub>2</sub> or CCl<sub>3</sub>Br and 25 μmol d<sub>6</sub>-DMSO, 100 μmol Asc and 200 μmol H<sub>2</sub>O<sub>2</sub> and 10 μmol LFe<sup>II</sup>Cl<sub>2</sub>/Fe<sub>2</sub>O<sub>3</sub>. This shows that the CD<sub>3</sub> group from d<sub>6</sub>-DMSO becomes a radical, scavenged by CH<sub>2</sub>Br<sub>2</sub> or CCl<sub>3</sub>Br, and forms CD<sub>3</sub>Br.

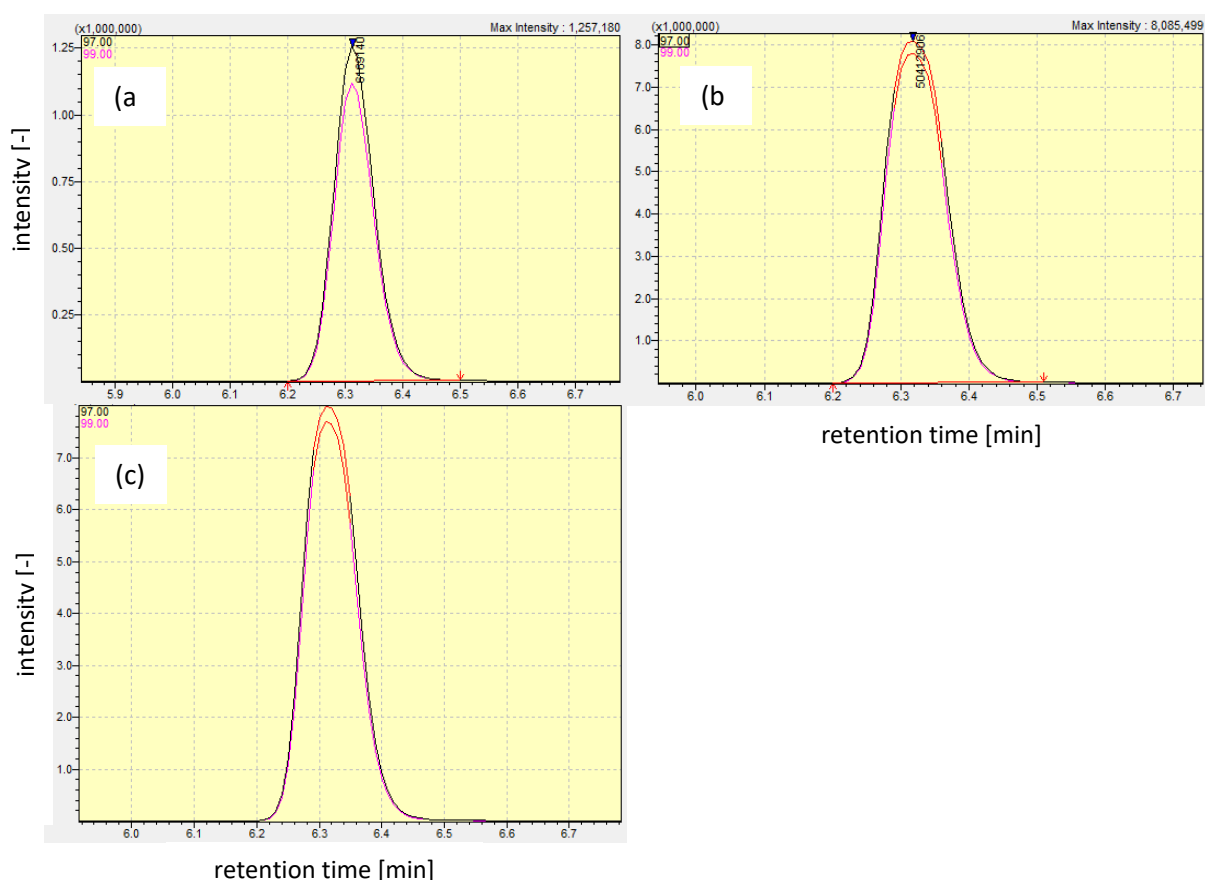


Figure 20: The chromatograms of isotopically labelled  $\text{CH}_3\text{Br}$  in the experiments with **a)**  $\text{LFe}^{\text{II}}\text{Cl}_2$  and  $\text{CH}_2\text{Br}_2$  (1.25 mmol), **b)**  $\text{LFe}^{\text{II}}\text{Cl}_2$  and 1.25 mmol of  $\text{CCl}_3\text{Br}$  and as well **c)**  $\text{Fe}_2\text{O}_3$  and 1.25 mmol of  $\text{CCl}_3\text{Br}$  and 25  $\mu\text{mol}$   $\text{d}_6\text{-DMSO}$ , 100  $\mu\text{mol}$  Asc and 200  $\mu\text{mol}$   $\text{H}_2\text{O}_2$  under ambient atmospheric conditions with a reaction time of 48 h. The presented chromatograms refer to the masses 97 (black) and 99 (pink), representing the  $\text{CD}_3\text{Br}$  with the stable isotopes of Br (79, 81). This represents a mass shift of 3 concerning  $\text{CH}_3\text{Br}$  (the mass of  $\text{CH}_3\text{Br}$  is 94 and 96). Taken from Hädeler et al. (2023).<sup>205</sup>

### 3.1.7 Discussion of DMSO as a case study to characterise the reaction to C1 and C2 compounds

The findings outlined in Chapters 3.1.1 to 3.1.6 reveal that DMSO can be converted to various C1 and C2 products using  $\text{LFe}^{\text{II}}\text{Cl}_2$  or  $\text{Fe}_2\text{O}_3$  and  $\text{H}_2\text{O}_2$  with Asc as a radical scavenger. Asc was originally added to facilitate the dissolution of  $\text{Fe}_2\text{O}_3$  and has the additional benefit of quenching OH radicals, thereby suppressing additional pathways and allowing the characterisation of  $\text{CH}_3$  radicals. The  $\text{LFe}^{\text{II}}\text{Cl}_2$  complex was used for the mechanistic studies and to have a well-characterized oxidant with added  $\text{H}_2\text{O}_2$  to form a  $[\text{Fe}^{\text{IV}}=\text{O}]^{2+}$  complex.<sup>14,238,250,251</sup>

High conversion rates of up to 86 % were observed for  $\text{CH}_4$ ,  $\text{C}_2\text{H}_6$ ,  $\text{CH}_3\text{OH}$  and  $\text{CH}_2\text{O}$ , and only slight differences between DMSO and  $\text{d}_6\text{-DMSO}$  as precursor compounds could be determined (Figure 8). An

isotopic effect during the reaction most likely causes this. Although the exact cause could not be clarified, it can be assumed that it could be due to the higher mass of the deuterium compared to the hydrogen and the different bonding energies of the C-H bond. The high total conversion rates demonstrate that the reaction of  $d_6$ -DMSO with Fe,  $H_2O_2$  and Asc is highly efficient and selective with regard to the C1 and C2 components.

The experiments with  $LFe^{II}Cl_2$  generally show lower total conversion rates compared to  $Fe_2O_3$ , probably due to the very fast (<0.5 h) conversion to the C1 and C2 compounds and the radicals ( $CH_3$ , OH, etc.) generated in a short time (Figure 9). It is assumed that Asc cannot immediately trap a large number of OH radicals produced by the Fenton reaction, so they react non-specifically with all the substances involved and disturb a reaction to C1 and C2 compounds. In contrast, experiments with  $Fe_2O_3$  and  $d_6$ -DMSO (Figure 8) showed an overall yield of 86 %. Therefore, a slower reaction involving  $Fe_2O_3$  can be considered more selective than the fast one with  $LFe^{II}Cl_2$ . The rapid reaction of  $d_6$ -DMSO with  $LFe^{II}Cl_2$  also results in higher concentrations of  $CH_3$  radicals due to the shorter reaction time compared to  $Fe_2O_3$ . This leads to an increasing probability of recombination of  $CH_3$  radicals and, therefore, to a higher  $C_2H_6$  concentration. Althoff et al. (2014) also observed high conversion rates to  $CH_4$  (83 %) with iron minerals with a comparable 48 h reaction time to finish the conversion.<sup>14</sup> Furthermore,  $HCOOH$  and  $CH_3COOH$  could not be quantified. Additionally, it cannot be excluded that other unidentified C1 and C2 components are formed, and all would have to be added to the total conversion rate.

In previous studies, Asc was added to bring the Fe minerals into solution<sup>14,37,238</sup>, but it also has the property of trapping OH radicals. This can be clearly demonstrated in the experiments with different concentrations of Asc. In the absence of Asc, when no OH radicals are trapped, only oxygenated compounds are formed. As the amount of Asc increases (10-100  $\mu\text{mol}$ ), the production of  $CH_4$  and  $C_2H_6$  also increases because some OH radicals are trapped, and non-oxygenated compounds could be formed (more on the mechanism below). At a high excess of Asc (1000  $\mu\text{mol}$ ), the total conversion of C1 and C2 compounds drops sharply, and  $CH_4$  and only 2.5–3 %  $CH_3OH$  and no  $CH_2O$  are produced. Due to the high Asc concentration, the low conversion rates to  $CH_3OH$  and no  $CH_2O$  can be explained by the high amounts of OH-radicals that are trapped. It is speculated that the high concentration of Asc deactivates the  $[Fe^{IV}=O]^{2+}$  species (i.e., the iron oxidant oxidises the antioxidant) and reduces the reactivity. At lower concentrations of Asc, the deactivation does not seem to be a very relevant process for C1 and C2 formation because high conversion rates are observed.

The presence or absence of  $O_2$  in the experiment has little effect on the conversion rates. Qualitatively, the same C1 and C2 components were detected in the experiments with or without Asc. Thus, it is assumed that  $O_2$  plays only a minor role in the reaction (more details below).

The isotopic detections of three deuterated atoms from  $d_6$ -DMSO in various products demonstrate, that the  $\text{CH}_3$  group is cleaved off homolytically and then rapidly reacts to the observed products as previously observed for  $\text{CH}_4$ .<sup>14,238</sup> The presence of three deuterated atoms per carbon atom in  $\text{CH}_4$ ,  $\text{C}_2\text{H}_6$ ,  $\text{CH}_3\text{OH}$  and  $\text{CH}_3\text{Cl}$  demonstrates that an OAT is occurring (Chapter 1.1.1) as a transfer of the oxygen in the  $[\text{Fe}^{\text{IV}}=\text{O}]^{2+}$  species to the substrate appears, and then the  $\text{CH}_3$  group splits. This mechanism has been demonstrated previously for methionine as a precursor.<sup>14</sup> It can be concluded that an abstraction of the hydrogen atom is impossible, given that one hydrogen atom must be detached from the  $\text{CH}_3$  group, resulting in only two deuterium being detected within the analysed C1 and C2 compounds.

In all investigations, the mass shift of 2 AMU in  $\text{CD}_2\text{O}$  indicates that the compound originates from  $d_6$ -DMSO. However, an experiment with  $\text{CD}_3\text{OH}$  shows that the  $\text{CD}_2\text{O}$  originates from the  $\text{CD}_3\text{OH}$  and is formed due to an overoxidation of  $\text{CD}_3\text{OH}$ . This is verified in experiments with and without DMSO, in which  $\text{CD}_3\text{OH}$  was used, and  $\text{CD}_2\text{O}$  could be detected (Figure 16).  $\text{HCOOH}$  is likely a secondary oxidation product of  $\text{CH}_2\text{O}$ , with  $\text{CH}_3\text{COOH}$  representing another secondary oxidation product of  $\text{HCOOH}$ , proofed due to detected deuterium labelling in all compounds and the highly oxidative milieu. However, these individual pathways have not been verified with isotopically labelled  $\text{CH}_2\text{O}$  and  $\text{HCOOH}$ . Nonetheless, the strongly oxidative environment and isotopic labelling support this hypothesis.

The  $\text{H}_2^{18}\text{O}_2$ - $d_6$ -DMSO experiments demonstrate that  $\text{CH}_3\text{OH}$  is formed directly by  $\text{CH}_3$  and  $\text{OH}$  radicals, despite the presence of Asc, which cannot fully scavenge the  $\text{OH}$  radicals, as evidenced by previous EPR spectroscopy studies.<sup>14,238</sup> Another indication is that in the absence of Asc, only oxygenated compounds are formed due to the high reactivity and excess of  $\text{OH}$  radicals. The use of  $^{18}\text{O}_2$  and  $d_6$ -DMSO also enabled the demonstration that  $\text{O}_2$  functions as a precursor to  $\text{CH}_3\text{OH}$ . Initially, the oxygen and the  $\text{CH}_3$  radical react to form a methyl peroxide, which then reacts following a Russel-type mechanism, undergoing equal parts of decay to form  $\text{CH}_2\text{O}$ ,  $\text{CH}_3\text{OH}$ , and  $\text{O}_2$ .<sup>252,253</sup> However, this process only accounts for a small proportion of products, as the turnover rates increase very little in the absence of  $\text{O}_2$ .

The  $\text{CH}_3$  group of  $\text{CD}_3\text{Cl}$  originated from the  $d_6$ -DMSO (Figure 15), and the chlorine originated from  $\text{LFe}^{\text{II}}\text{Cl}_2$  as it is the only chlorine present. Investigations with  $\text{Fe}_2\text{O}_3$ , where no  $\text{CD}_3\text{Cl}$  was measured, evidence this. This reaction presumably is a rebound reaction involving the  $\text{Cl}^\cdot$ , which occurs at the coordination center at the iron of  $\text{LFe}^{\text{II}}\text{Cl}_2$ .

The alkyl trapping experiments show that in the experiment with  $d_6$ -DMSO and  $\text{LFe}^{\text{II}}\text{Cl}_2$ , Asc and  $\text{H}_2\text{O}_2$ ,  $\text{CH}_3$  radicals are formed. This can be seen from the reduced conversion rates when  $\text{CH}_2\text{Br}_2$  and  $\text{CCl}_3\text{Br}$  are added to the experiment, trapping  $\text{CH}_3$ -radicals (Figure 20). It is evident that both alkyl scavengers demonstrate inadequate solubility in  $\text{H}_2\text{O}$ . Consequently, the conversion rate reduction depends on

the concentration of the alkyl scavengers present in the H<sub>2</sub>O. This renders a quantitative interpretation of the reduction unfeasible. Still, a definite proof is the measured mass shift of 3 AMU in the formed CD<sub>3</sub>Br that a CD<sub>3</sub> is present, which derives from the educt d<sub>6</sub>-DMSO (Figure 20). Due to this reaction, CH<sub>2</sub>Br-radicals and CCl<sub>3</sub>-radicals are also produced. These radicals abstract a hydrogen atom from (un)labelled compounds in solution, which is presumably Asc, d<sub>6</sub>-DMSO or other compounds in solution, and form either CH<sub>3</sub>Br (CH<sub>2</sub>DBr) or CCl<sub>3</sub>H (CCl<sub>3</sub>D).

Figure 21 summarises all investigated C1 and C2 components with their respective isotopic labels (<sup>2</sup>H, <sup>13</sup>C and <sup>18</sup>O). Almost all carbon oxidation states between -IV and +IV could be detected in the C1 and C2 compounds. Due to the isotopically labelled experiments, it is possible to clarify the origin of the different carbon species and identify the most likely pathways.

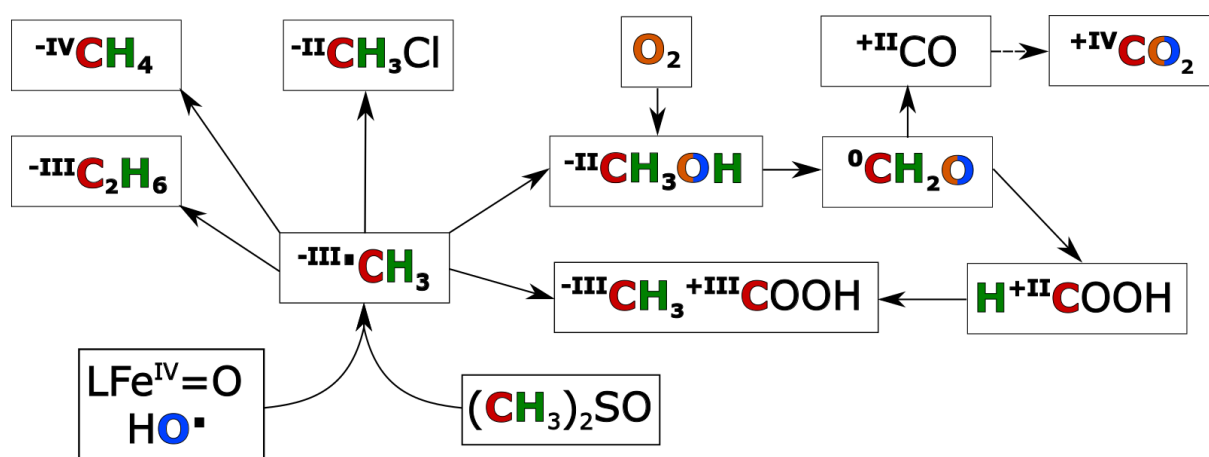


Figure 21: The portfolio of C1 and C2 components arises from the CH<sub>3</sub> radical, which is formed abiotically by the LFe<sup>IV</sup>Cl<sub>2</sub>/H<sub>2</sub>O<sub>2</sub> system from DMSO. Deuterated and <sup>13</sup>C-labelled DMSO and <sup>18</sup>O-labelled H<sub>2</sub>O<sub>2</sub> and O<sub>2</sub> were utilised to investigate the different pathways. The observed <sup>13</sup>C and <sup>2</sup>H labels are presented in bold red and green, respectively. Oxygenated C1 compounds with <sup>18</sup>O isotopes are highlighted in bold orange or blue, originating from <sup>18</sup>O-labelled H<sub>2</sub>O<sub>2</sub> or O<sub>2</sub>, respectively. Oxygen atoms in orange and blue indicate that the product derived oxygen from H<sub>2</sub>O<sub>2</sub> and O<sub>2</sub>. The oxidation states of carbon are shown in Roman numbers. Taken from Hädeler et al. (2023).<sup>205</sup>

Based on the previously described experimental research and the computational data, a reaction mechanism involving LFe<sup>IV</sup>Cl<sub>2</sub>/H<sub>2</sub>O<sub>2</sub> has been proposed (Figure 22).<sup>205</sup> This mechanism forms CH<sub>4</sub>, C<sub>2</sub>H<sub>6</sub>, CH<sub>3</sub>OH, CH<sub>2</sub>O, and traces of HCOOH, CH<sub>3</sub>COOH, CO<sub>2</sub>, and CH<sub>3</sub>Cl from DMSO. In this context, the following conclusions can be formulated:

1. The CH<sub>3</sub> group of the C1 and C2 components originates in DMSO and is cleaved off homolytically by the  $[\text{Fe}^{\text{IV}}=\text{O}]^{2+}$  species through an OAT (transition state).<sup>205</sup> The oxygen is transferred to the sulphur atom of DMSO, forming a CH<sub>3</sub> radical. This radical subsequently reacts to form the respective C1 and C2 components.

2. Most of the oxygen in  $\text{CH}_3\text{OH}$  originates in  $\text{H}_2\text{O}_2$  and minor parts from  $\text{O}_2$ . During the Fenton reaction, hydroxyl radicals are formed from  $\text{H}_2\text{O}_2$ , recombining with the  $\text{CH}_3$  radicals. Despite the presence of Asc, not all OH radicals are captured, resulting in the formation of  $\text{CH}_3\text{OH}$ . EPR studies support this.<sup>14,238</sup> The Russell-type mechanism may form a minor proportion of  $\text{CH}_3\text{OH}$  and  $\text{CH}_2\text{O}$ .

3. The majority of  $\text{CH}_2\text{O}$  is formed by the oxidation of  $\text{CH}_3\text{OH}$ ,  $\text{CH}_2\text{O}$  is then further oxidized to produce traces of  $\text{HCOOH}$ ,  $\text{CH}_3\text{COOH}$  and  $\text{CO}_2$ .

4. The chlorine in  $\text{CH}_3\text{Cl}$  is derived from  $\text{LFe}^{\text{II}}\text{Cl}_2$ . This reaction presumably is a rebound process involving the  $\text{Cl}^-$ , coordinated at the Fe centre of  $\text{LFe}^{\text{II}}\text{Cl}_2$ . It can be assumed that other halogens in solution would react similarly and form the corresponding halomethanes.

For a more comprehensive computational (DFT) analysis of the reaction mechanism, please refer to the study by Hädeler et al. (2023).<sup>205</sup>

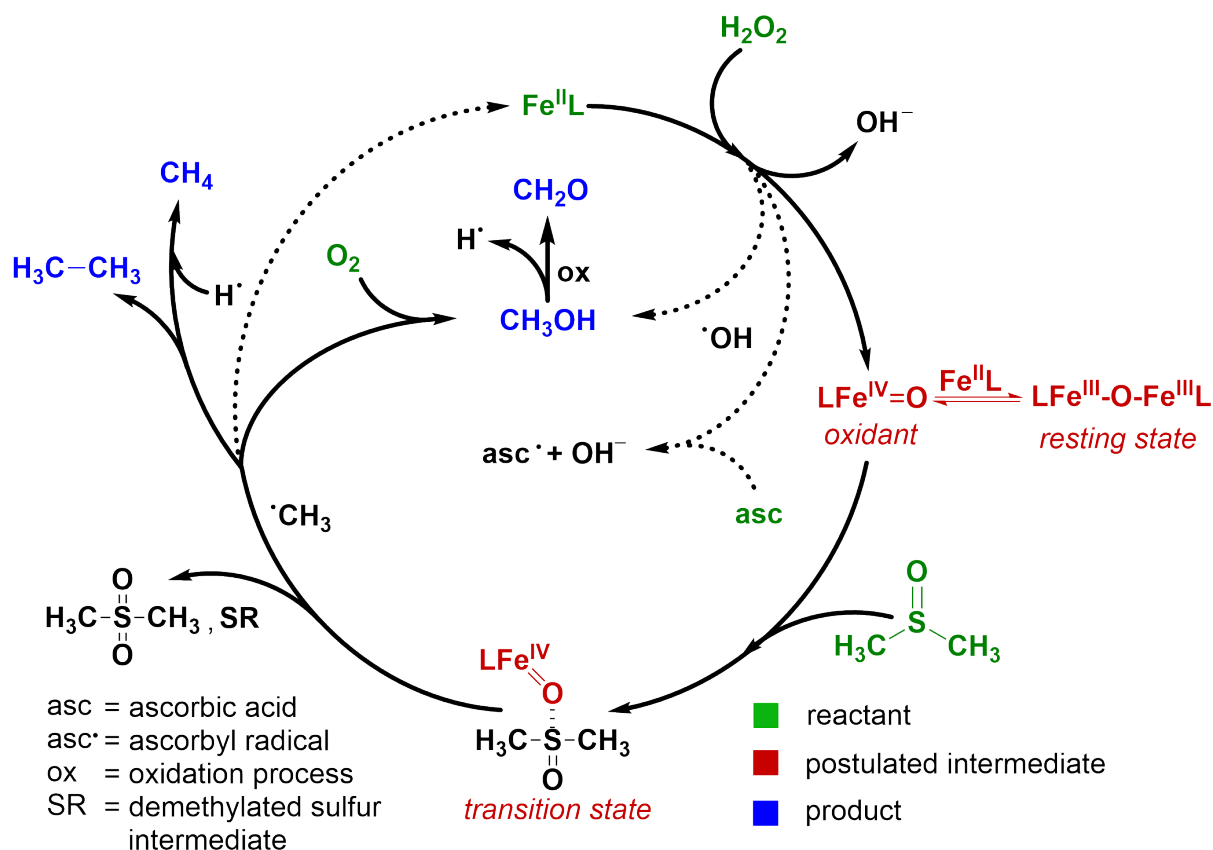


Figure 22: Postulated mechanism for forming  $\text{CH}_4$ ,  $\text{C}_2\text{H}_6$ ,  $\text{CH}_3\text{OH}$  and  $\text{CH}_2\text{O}$  by reaction of DMSO with a Fe species ( $\text{LFe}^{\text{II}}\text{Cl}_2$  or  $\text{Fe}_2\text{O}_3$ ),  $\text{H}_2\text{O}_2$  and Asc. (Postulated intermediates are highlighted in red; reactants are shown in green; products are shown in blue; for simplicity, the stoichiometry of some of the reactions has not been adjusted). Taken from Hädeler et al. (2023).<sup>205</sup>

Given the ubiquitous presence of DMSO and its related products (DMS and dimethylsulfoniopropionate) in the ocean (Chapter 1.3.1.1) and the ubiquitous presence of  $\text{Fe}^{254}$  and ROS in the ocean<sup>255</sup>, it can be postulated that the reaction also occurs in the ocean, contributing, for instance, to the  $\text{CH}_4$

paradox<sup>80,190</sup> (oversaturation of the ocean with CH<sub>4</sub>) and providing CH<sub>3</sub>OH as an energy source for microorganisms such as methylotrophic bacteria. Moreover, the volatile C1 and C2 components can be emitted into the atmosphere, where they exert a profound influence on the physical and chemical properties of the atmosphere as well as those of the ocean. As previously stated in Chapter 1.2, they serve various functions, including GHG, influencing the oxidation potential and ozone formation. Given that DMS is also present in sediments, soils and freshwater compartments<sup>159,160</sup> where all the requisite components for the reaction from DMS to DMSO are present, the previously described reaction could occur. Therefore, all investigated C1 and C2 components could be produced and would influence the physical and chemical properties of the atmosphere, the pedosphere and the hydrosphere (Chapter 1.2). Furthermore, these components serve as a source of energy for microorganisms living in these compartments, which transform them at the end to CO<sub>2</sub> with various carbon species as intermediates and contribute to the global carbon cycle.

### 3.2 Conversion of S-, N- and P- bonded CH<sub>3</sub> group containing compounds to C1 and C2 compounds

The compounds methionine, methylphosphonate, choline and trimethylamine were also investigated for their potential to produce C1 and C2 components. These were selected due to their environmental relevance, as described in Chapter 1.3.1. All compounds were fully deuterated at the CH<sub>3</sub> group except methylphosphonate because it was not commercially available. The experiments and measurements previously described for d<sub>6</sub>-DMSO were repeated for the above-mentioned precursor compounds (Table 9).

Table 9: Composition of the experiments with d<sub>3</sub>-methionine, methylphosphonate, d<sub>9</sub>-choline and d<sub>9</sub>-trimethylamine to determine the conversion rates and possible differences.

No.	Precursor compound	Fe species	Oxidant	acid
1 and 2	25 μmol d <sub>3</sub> -methionine	10 μmol LFe <sup>II</sup> Cl <sub>2</sub> /Fe <sub>2</sub> O <sub>3</sub>	200 μmol H <sub>2</sub> O <sub>2</sub>	100 μmol Asc
3 and 4	25 μmol methylphosphonate	10 μmol LFe <sup>II</sup> Cl <sub>2</sub> /Fe <sub>2</sub> O <sub>3</sub>	200 μmol H <sub>2</sub> O <sub>2</sub>	100 μmol Asc
5 and 6	25 μmol d <sub>9</sub> -choline	10 μmol LFe <sup>II</sup> Cl <sub>2</sub> /Fe <sub>2</sub> O <sub>3</sub>	200 μmol H <sub>2</sub> O <sub>2</sub>	100 μmol Asc
7 and 8	25 μmol d <sub>9</sub> -trimethylamine	10 μmol LFe <sup>II</sup> Cl <sub>2</sub> /Fe <sub>2</sub> O <sub>3</sub>	200 μmol H <sub>2</sub> O <sub>2</sub>	100 μmol Asc

### 3.2.1 Conversion rates of S-, N- and P- bonded CH<sub>3</sub> group containing compounds to CD<sub>3</sub>H, C<sub>2</sub>D<sub>6</sub>, CD<sub>3</sub>OH, and CD<sub>2</sub>O

In general, the use of d<sub>3</sub>-methionine, methylphosphonate, d<sub>9</sub>-choline and d<sub>9</sub>-trimethylamine resulted in lower conversion rates to CH<sub>4</sub>, C<sub>2</sub>H<sub>6</sub>, CH<sub>3</sub>OH and CH<sub>2</sub>O than for experiments with d<sub>6</sub>-DMSO (Figure 23). In experiments conducted with LFe<sup>II</sup>Cl<sub>2</sub>, d<sub>3</sub>-methionine was observed to produce CD<sub>3</sub>H (1.17 ± 0.06 %) and C<sub>2</sub>D<sub>6</sub> (0.012 ± 0.001 %), with no detection of CD<sub>3</sub>OH or CD<sub>2</sub>O. In contrast, the experiment with Fe<sub>2</sub>O<sub>3</sub> yielded the production of CD<sub>3</sub>H (5.70 ± 0.04 %), C<sub>2</sub>D<sub>6</sub> (0.69 ± 0.01 %), CD<sub>3</sub>OH (1.25 ± 0.13 %) and CD<sub>2</sub>O (3.46 ± 0.33 %). Methylphosphonate was observed to produce CH<sub>3</sub>OH (2.18 ± 0.22 %) solely with LFe<sup>II</sup>Cl<sub>2</sub> and only CH<sub>2</sub>O (0.92 ± 0.34 %) with Fe<sub>2</sub>O<sub>3</sub>. CD<sub>3</sub>OH (0.77 ± 0.25 %), CD<sub>2</sub>O (3.74 ± 0.86 %) and traces of CD<sub>3</sub>H (0.002 ± 0.000 %) could be detected in experiments with choline and LFe<sup>II</sup>Cl<sub>2</sub>. Furthermore, the presence of CD<sub>3</sub>OH (0.33 ± 0.06 %) and CD<sub>2</sub>O (2.41 ± 0.48 %) was also observed in the Fe<sub>2</sub>O<sub>3</sub> experiments, along with CD<sub>3</sub>H (0.16 ± 0.01 %). In experiments conducted with trimethylamine, only CD<sub>3</sub>OH (0.74 ± 0.51 %) and CD<sub>2</sub>O (0.29 ± 0.76 %) were detected in the presence of LFe<sup>II</sup>Cl<sub>2</sub>, while CD<sub>2</sub>O (1.18 ± 0.95 %) was also observed in the presence of Fe<sub>2</sub>O<sub>3</sub>.

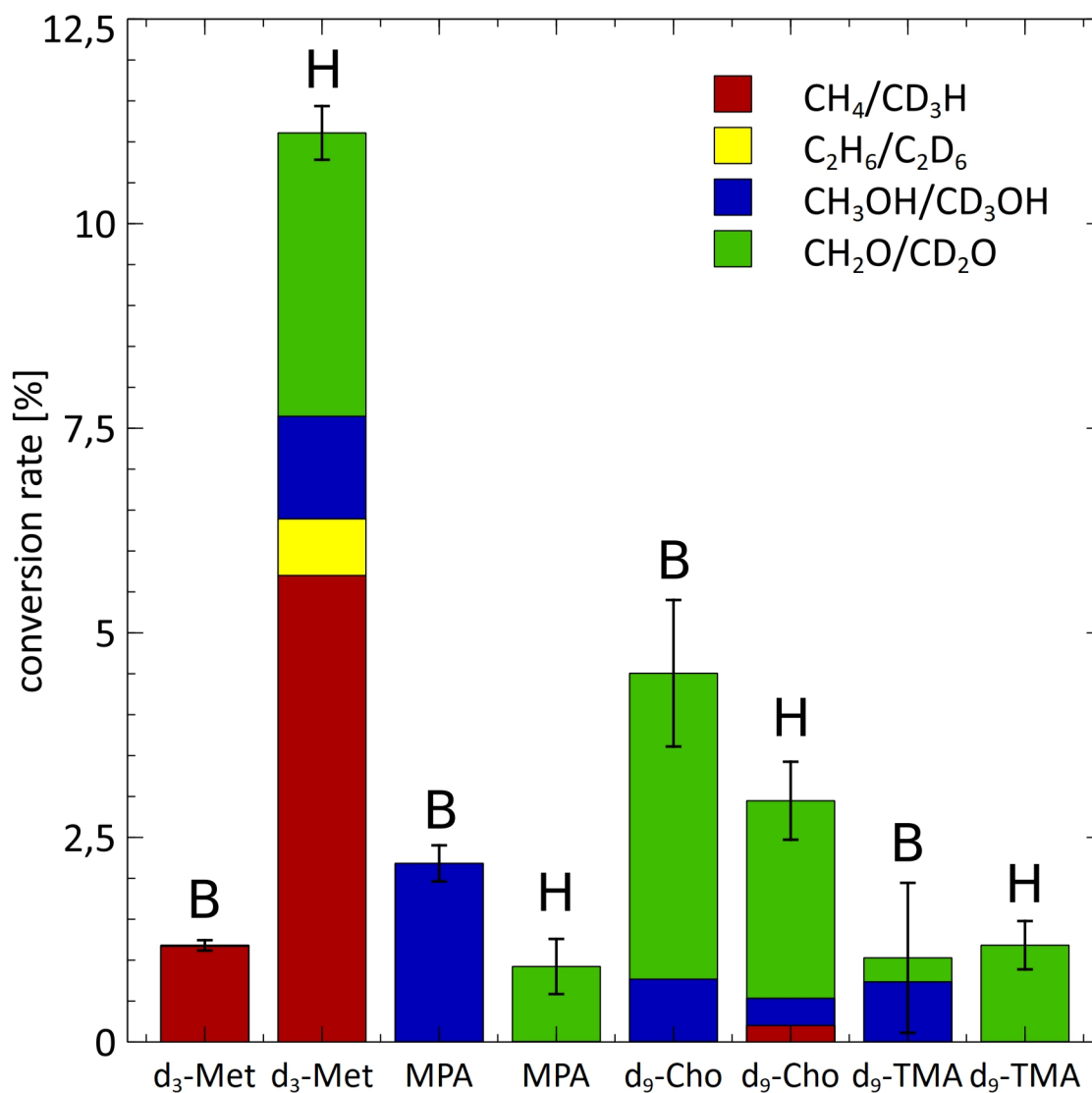


Figure 23: The formation of C1 and C2 compounds in experiments with 10  $\mu\text{mol}$   $\text{LFe}^{\text{II}}\text{Cl}_2$  (bar B) or  $\text{Fe}_2\text{O}_3$  (bar H), 200  $\mu\text{mol}$   $\text{H}_2\text{O}_2$  and 100  $\mu\text{mol}$  Asc with 25  $\mu\text{mol}$  d<sub>3</sub>-methionine (d<sub>3</sub>-Met), methylphosphonate (MPA; unlabelled C1 and C2 compounds), d<sub>9</sub>-choline (d<sub>9</sub>-Cho) or d<sub>9</sub>-trimethylamine (d<sub>9</sub>-TMA) as precursor compounds under ambient atmospheric conditions with a reaction time of 48 h. Error bars refer to the SD of the total conversion of all major C1 and C2 compounds for  $n = 9$ , except for  $\text{CH}_4$  and  $\text{C}_2\text{D}_6$ ,  $n = 3$ .

### 3.2.2 Investigation of the reaction mechanism with deuterium-labelled compounds

To determine whether the  $\text{CH}_3$  group of  $\text{CH}_3\text{OH}$  and  $\text{CH}_2\text{O}$  have the origin in the S- and N-labelled compounds,  $\text{CH}_3$ -deuterium-labelled methionine, choline, and trimethylamine was used to demonstrate the transfer of the deuterium label to  $\text{CD}_3\text{OH}$ . This is indicated by its isotopic signature by the mass increase of 3 AMU from 32 to 35 in  $\text{CD}_3\text{OH}$  (Figure 24). Furthermore, deuterium labelling was also identified in  $\text{CH}_2\text{O}$ . A shift of 2 AMU from 210 to 212 in the derivatised  $\text{CD}_2\text{O}$  is evident in the

experiments with methionine, and small percentages were also observed for trimethylamine and choline (Figure 25).

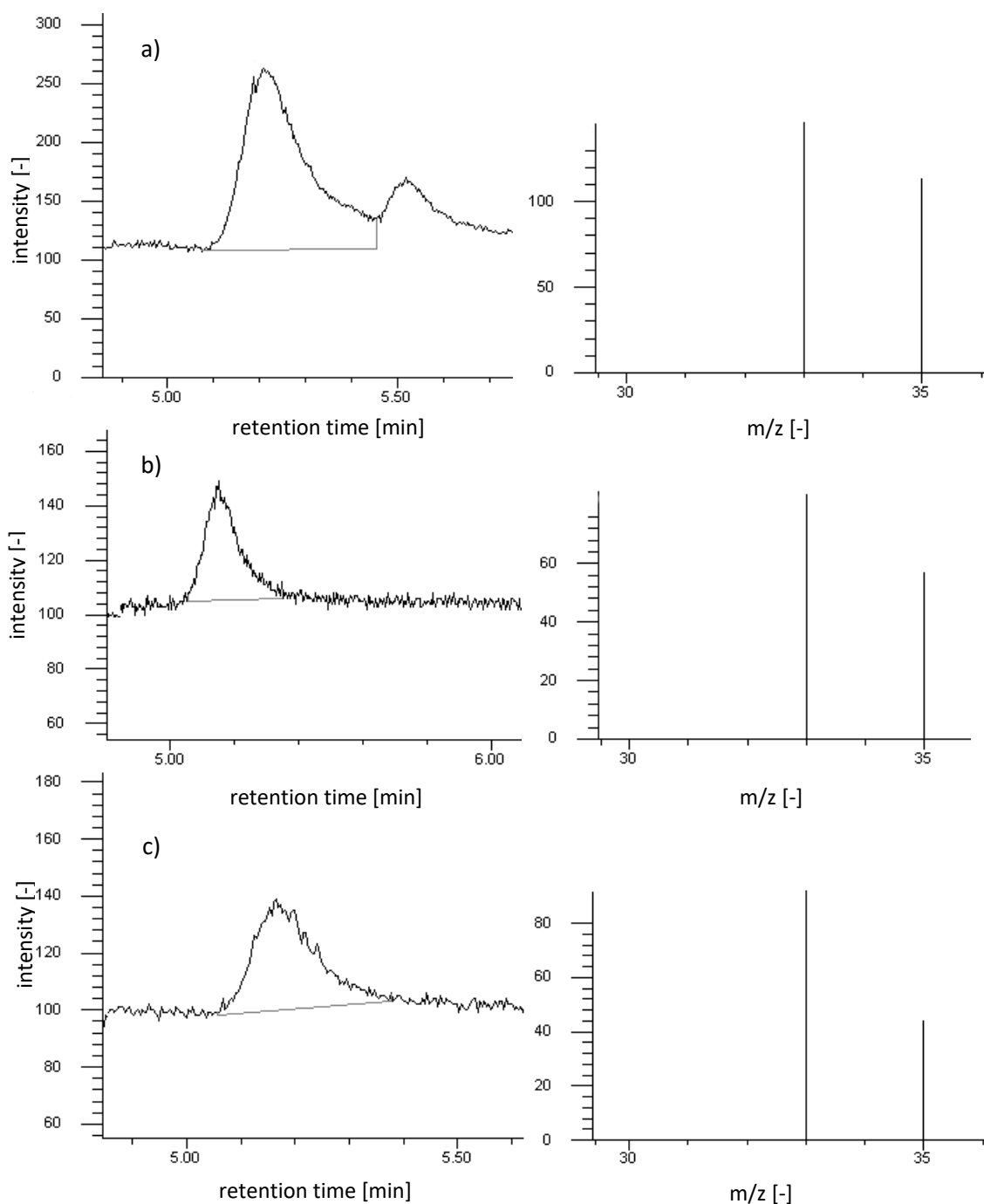


Figure 24: Chromatograms and mass tracks of  $\text{CD}_3\text{OH}$  with a shift to 35 in experiments with 25  $\mu\text{mol}$  **a)**  $\text{d}_3$ -methionine, **b)**  $\text{d}_9$ -choline and **c)**  $\text{d}_9$ -trimethylamine and 10  $\mu\text{mol}$   $\text{LFe}^{\text{II}}\text{Cl}_2$ , 100  $\mu\text{mol}$  Asc and 200  $\mu\text{mol}$   $\text{H}_2\text{O}_2$  as an oxidant under ambient atmospheric conditions with a reaction time of 48 h.

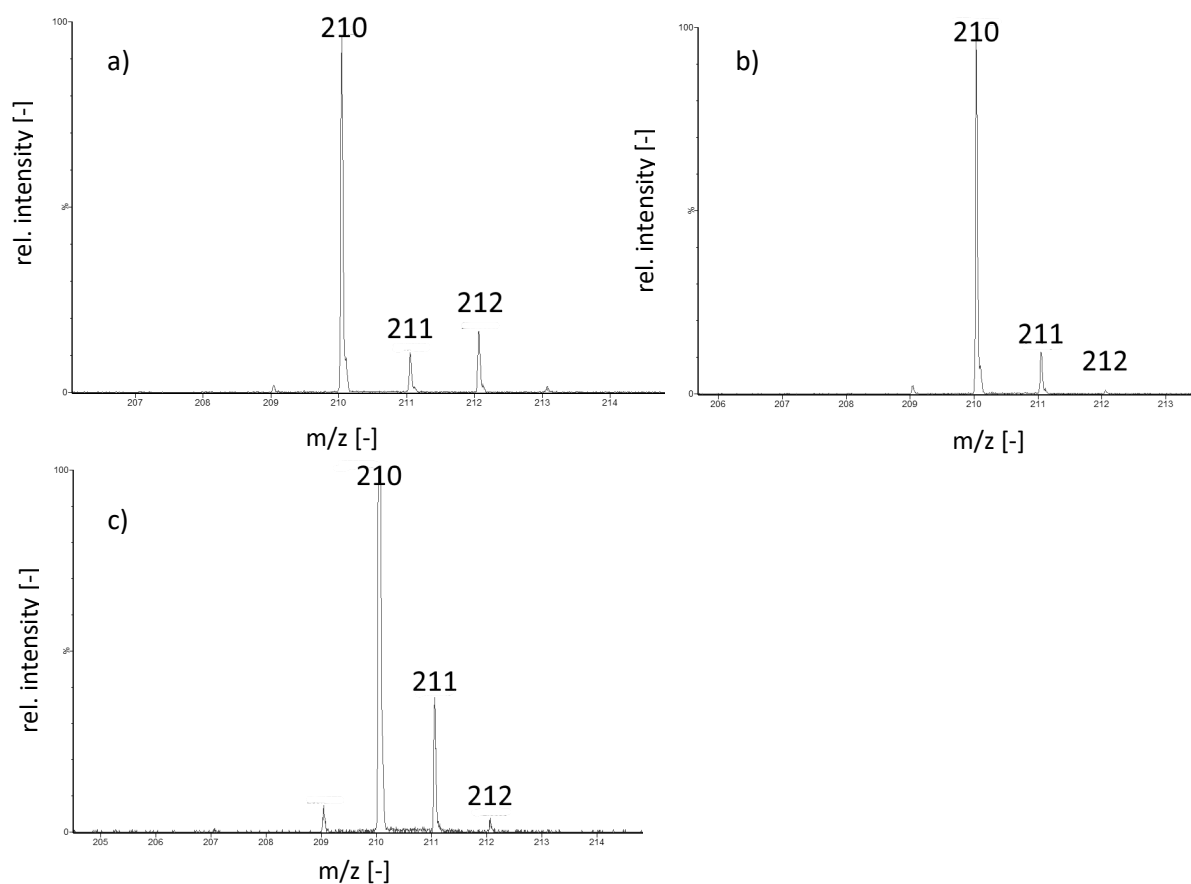


Figure 25: Mass tracks of CD<sub>2</sub>O with a shift of 2 AMU from 210 to 212 in experiments with 25 μmol **a)** d<sub>3</sub>-methionine, **b)** d<sub>9</sub>-choline and **c)** d<sub>9</sub>-trimethylamine and 10 μmol LFe<sup>II</sup>Cl<sub>2</sub>, 100 μmol Asc and 200 μmol H<sub>2</sub>O<sub>2</sub> as an oxidant under ambient atmospheric conditions with a reaction time of 48 h.

### 3.2.3 Discussion of the formation of C1 and C2 compounds originated in S-, N- and P-bonded CH<sub>3</sub> group containing compounds

The experiments with d<sub>3</sub>-methionine, methylphosphonate, d<sub>9</sub>-choline and d<sub>9</sub>-trimethylamine generally demonstrate lower conversion rates than those with DMSO and the OCH<sub>3</sub> compounds (Chapter 3.3.1). This is likely due to elevated energy barriers in the OAT reaction, as preliminary DFT modelling results suggested (unpublished). Nevertheless, in the case of methionine with the oxidant Fe<sub>2</sub>O<sub>3</sub>, for example, a conversion rate of exceeding 11 % was observed, with all C1 and C2 compounds analysed. In contrast, experiments conducted with LFe<sup>II</sup>Cl<sub>2</sub> detected only slightly more than 1 % CH<sub>4</sub> and traces of C<sub>2</sub>H<sub>6</sub>. This notable discrepancy contrasts the outcomes observed with DMSO. This finding suggests the potential for forming the same products, albeit to a lesser extent, attributable to the elevated energy barriers associated with the reaction.

The observed shift of the mass track by 3 or 2 in CH<sub>3</sub>OH and CH<sub>2</sub>O, respectively, in experiments with LFe<sup>II</sup>Cl<sub>2</sub> (Figure 24 and Figure 25) without blank subtraction indicates the formation of CH<sub>3</sub>OH and CH<sub>2</sub>O in this reaction. Given that the blank conversion rate is higher than that of the experiments, the

conversion rate is zero. The elevated blank value can be attributed, at least partially, to the inherent variability associated with the experimental procedures and the analytical measurements. It is also established that the  $\text{LFe}^{\text{II}}\text{Cl}_2$  complex is capable of reacting with  $\text{H}_2\text{O}_2$  to form  $\text{CH}_2\text{O}$ .<sup>256</sup> Since more  $\text{H}_2\text{O}_2$  is available in the blank due to the consumption of  $\text{H}_2\text{O}_2$  during the reaction in the experiment with the precursor compounds, more  $\text{CH}_2\text{O}$  can be formed from the  $\text{LFe}^{\text{II}}\text{Cl}_2$  in the blank and thus influences the concentration of  $\text{CH}_2\text{O}$  due to the subtraction of the blank.  $\text{CH}_3\text{OH}$  can then be converted to  $\text{CH}_2\text{O}$  through keto-enol tautomerism.<sup>257</sup> The acidic solution catalyses this process in the direction of the  $\text{CH}_2\text{O}$  and can, therefore, affect the respective conversion rates. This effect has a relatively minor impact on the high turnover rates of DMSO to  $\text{CH}_2\text{O}$ ; however, it becomes more significant at lower conversion rates.

The studies (Table 9) with methylphosphonate, choline and trimethylamine all produce  $\text{CH}_3\text{OH}$  and/or  $\text{CH}_2\text{O}$  in low conversion rates, and choline also produces traces of  $\text{CH}_4$ . These low conversion rates of all substrates may be attributed to steric hindering effects of the atom where the  $\text{CH}_3$  group is bonded. The phosphorus atom in methylphosphonate is surrounded by four neighbouring atoms (quaternary atom), analogous to the nitrogen atom in choline. The influence of steric effects was previously postulated by Althoff et al. (2012)<sup>258</sup> in the context of choline chloride. Trimethylamine has three atoms surrounding the nitrogen atom and two free electrons, which allows for better attack from the  $[\text{Fe}^{\text{IV}}=\text{O}]^{2+}$  species at the nitrogen atom. However, it still exhibits low reactivity compared to the DMSO (Figure 10). This may be attributed to the ability of trimethylamine to be readily oxidised by  $\text{H}_2\text{O}_2$  to trimethylamine-N-oxide<sup>259</sup>, which then sterically hinders the nitrogen atom by four neighbouring atoms. Also, preliminary DFT calculations suggest a higher activation energy for trimethylamine-N-oxide than for trimethylamine. This can explain the low conversion rate of trimethylamine. In living organisms, however, a high conversion of trimethylamine to  $\text{CH}_4$  was observed in a ROS-driven Fenton reaction, but likewise, there was no significant conversion of choline to  $\text{CH}_4$ .<sup>72</sup> This is in contrast to the low conversion rates shown here for trimethylamine. It is not considerably oxidised within the organism to trimethylamine-N-oxide due to the lack of high  $\text{H}_2\text{O}_2$  concentrations, making it readily available for Fenton reactions, whereas choline is, from the beginning, sterically hindered due to the four bonds. The lower conversion rates and lack of substantial amounts of  $\text{CH}_4$  and  $\text{C}_2\text{H}_6$  compared to methionine may be attributed to the different bonding of the  $\text{CH}_3$  to nitrogen or phosphorus. Also, due to lesser bonds to the sulphur atom in methionine and, therefore, more free electrons, reacting with the  $[\text{Fe}^{\text{IV}}=\text{O}]^{2+}$  species is easier and faster and, thus, the reaction can produce  $\text{C}_2\text{H}_6$  due to the higher  $\text{CH}_3$  radical concentration. The exact reason why hydrocarbons and oxygenated compounds are produced in higher amounts in experiments with sulphur-bonded compounds compared to nitrogen or phosphorus-bonded  $\text{CH}_3$  groups with the same Asc and  $\text{H}_2\text{O}_2$  concentrations has to be elucidated.

### 3.3 Conversion rates and mechanistic details of methoxy compounds to C1 and C2 compounds

Given OCH<sub>3</sub> groups' ubiquitous and pivotal role in natural systems due to their common occurrence in plants, a comprehensive series of experiments were conducted on a diverse range of aromatic compounds, each containing at least one OCH<sub>3</sub> group. Additionally, galacturonic acid methyl ester, a monomer of pectin, was subjected to investigation (Figure 26).

#### 3.3.1 Conversion rates of OCH<sub>3</sub> compounds to CD<sub>3</sub>H, C<sub>2</sub>D<sub>6</sub>, CD<sub>3</sub>OH, and CD<sub>2</sub>O

All compounds produced in the investigations are CH<sub>3</sub>OH and/or CH<sub>2</sub>O and no CH<sub>4</sub>, C<sub>2</sub>H<sub>6</sub> or CH<sub>3</sub>Cl (Figure 26). The conversion rates observed with Asc and sinapyl alcohol, or Game, are consistently lower than when Asc is substituted with triflic acid. Subsequently, the experiments with the remaining compounds were conducted without Asc to achieve higher conversion rates. This was presumably because Asc quenches OH radicals and reduces the amount of ROS in the experiments, which can react with the precursor compound to form CH<sub>3</sub>OH and CH<sub>2</sub>O. Experiments involving S-, N-, and P-bounded CH<sub>3</sub> groups result in the production of CH<sub>4</sub> and C<sub>2</sub>H<sub>6</sub> (Chapters 3.1 and 3.2). However, in the case of OCH<sub>3</sub> groups, no CH<sub>4</sub> and C<sub>2</sub>H<sub>6</sub> were detected in experiments with Asc or with triflic acid. This suggests that Asc is not a necessary component in these experiments, as no CH<sub>4</sub> and C<sub>2</sub>H<sub>6</sub> were produced in its presence. The Asc is replaced with triflic acid to have the same pH value as in all other investigations.

The experiments conducted with the LFe<sup>II</sup>Cl<sub>2</sub> complex consistently exhibited a higher total conversion rate than those utilising the Fe mineral Fe<sub>2</sub>O<sub>3</sub>. For the aromatic compound, the conversion rate ranged from 41.5 ± 4.3 % with anisole to 111 ± 8 % with sinapyl alcohol in the presence of the oxidant LFe<sup>II</sup>Cl<sub>2</sub>. The total conversion rates with Fe<sub>2</sub>O<sub>3</sub> as the oxidant ranged from anisole at 1.23 ± 2.95 % to 94.3 ± 4.0 % with sinapyl alcohol. The total conversion rate of Game as a non-aromatic compound and part of pectin ranged from 16.7 ± 1.1 % to 27.4 ± 4.0 % with LFe<sup>II</sup>Cl<sub>2</sub> and from 10.1 ± 1.6 % to 10.6 ± 0.6 % with Fe<sub>2</sub>O<sub>3</sub>.

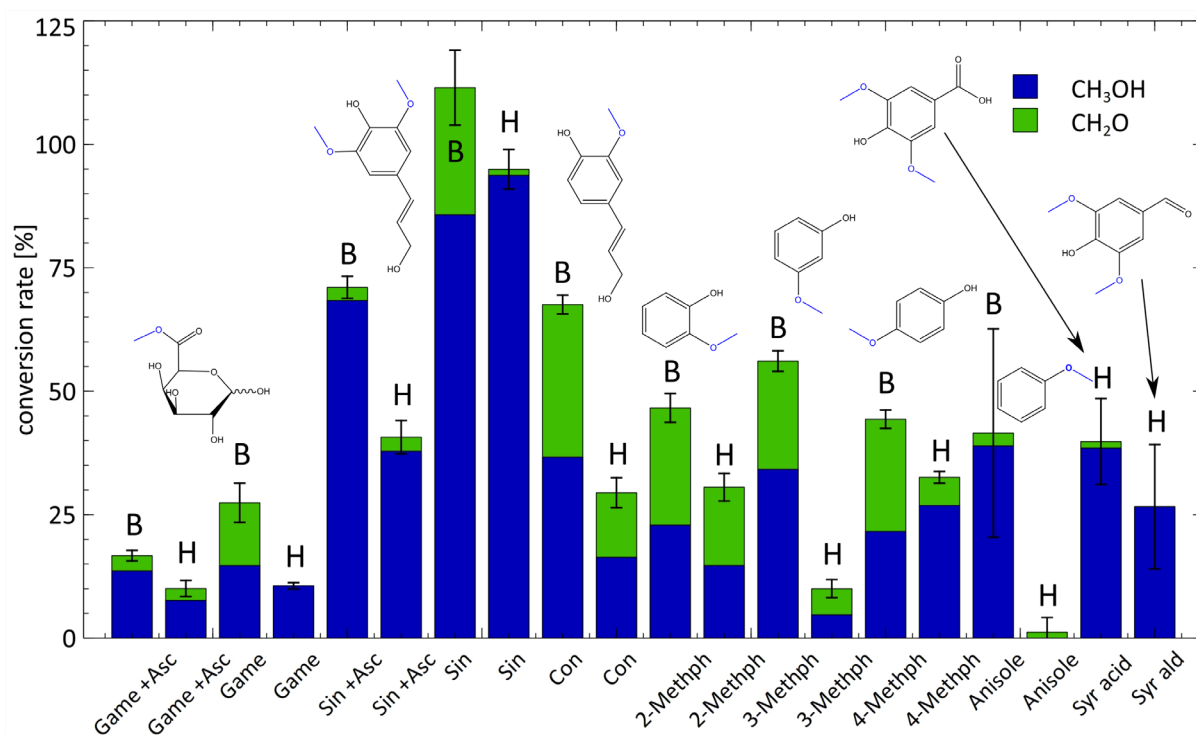


Figure 26: Investigations of OCH<sub>3</sub> group-containing compounds (25 μmol of Sinapyl alcohol (Sin); Galacturonic acid methyl ester (Game); 2-, 3- and 4-Methoxyphenol (2-, 3- and 4-Methph); Anisole; Syringic acid (Syr acid) and Syringaldehyde (Syr ald)), without Asc replaced by 0.05 μmol triflic acid (with 100 μmol Asc is marked as +Asc), 10 μmol LFe<sup>II</sup>Cl<sub>2</sub> (bar B) or Fe<sub>2</sub>O<sub>3</sub> (bar H) and 200 μmol H<sub>2</sub>O<sub>2</sub> as an oxidant under ambient atmospheric conditions with a reaction time of 48 h. Error bars refer to the SD of the total conversion of all major C1 and C2 compounds for n = 9.

### 3.3.2 Trapping CH<sub>3</sub> radicals with CH<sub>2</sub>Br<sub>2</sub> and CCl<sub>3</sub>Br

Similar to the experiments conducted with d<sub>6</sub>-DMSO (Chapter 3.1.6), alkyl trapping experiments (25 μmol substrate, 10 μmol LFe<sup>II</sup>Cl<sub>2</sub>, 100 μmol Asc, 200 μmol H<sub>2</sub>O<sub>2</sub>) were carried out with 1.25 mmol CCl<sub>3</sub>Br to determine whether CH<sub>3</sub> radicals are produced in this reaction. Figure 27 shows that the area of the produced CH<sub>3</sub>Br (mass 94 and 96, both bromine isotopes 79 and 81 plus 15 for the CH<sub>3</sub> group) due to the CH<sub>3</sub> radical trapping leads to the same areas in investigations with sinapyl alcohol, 2-methoxyphenol, or Game. The blank experiment (without substrate) shows the same areas as the measurements with the substrate.

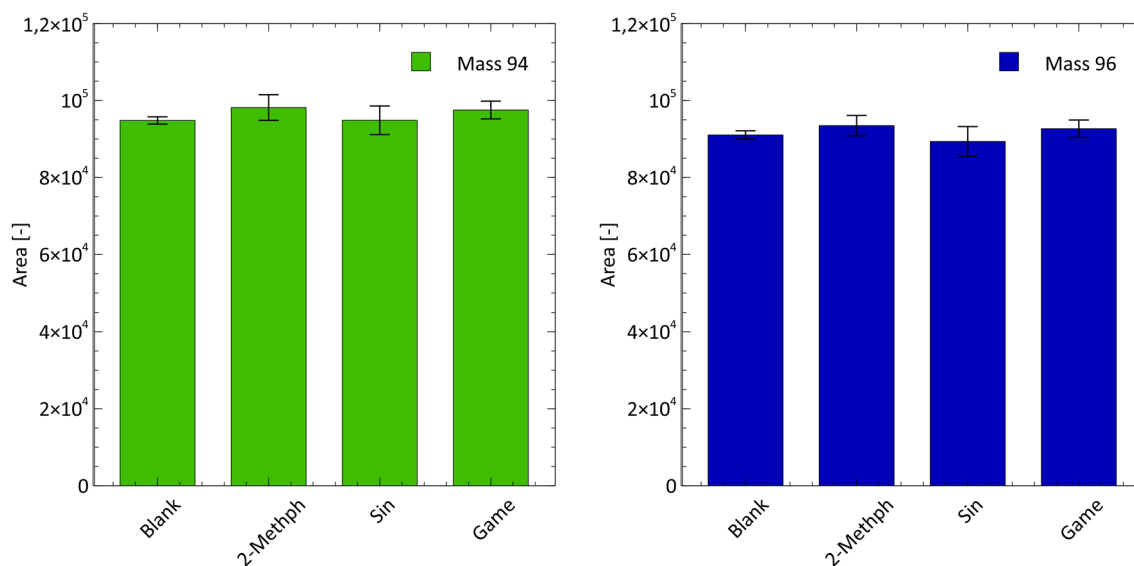


Figure 27: Comparison of CH<sub>3</sub>Br in experiments with 10 μmol LFe<sup>II</sup>Cl<sub>2</sub>, 100 μmol Asc and 200 μmol H<sub>2</sub>O<sub>2</sub>, 25 μmol sinapyl alcohol, 2-Methoxyphenol or Game and 1,25 mmol CCl<sub>3</sub>Br (alkyl radical trapping agent) compared to the blank experiment with the same setup but only without substrate (n = 3) under ambient atmospheric conditions with a reaction time of 48 h. **a)** Mass 94 (stable isotope 79 of bromine) and **b)** 96 (stable isotope 81 of bromine) of CH<sub>3</sub>Br.

### 3.3.3 Investigation of the reaction mechanism with deuterium and <sup>18</sup>O-labelled compounds

To gain insight into the reaction mechanism, experiments were conducted utilising <sup>18</sup>O-labelled H<sub>2</sub>O<sub>2</sub> and O<sub>2</sub> alongside sinapyl alcohol, coniferyl alcohol and 2-methoxyphenol. Additionally, the experiment depicted in Figure 26 was conducted with <sup>18</sup>O-labelled 2-methoxyphenol (<sup>18</sup>OCH<sub>3</sub>) and deuterated 2-methoxyphenol (OCD<sub>3</sub>) instead of regular 2-methoxyphenol. The investigation with 2-methoxyphenol and either H<sub>2</sub><sup>18</sup>O<sub>2</sub> or <sup>18</sup>O<sub>2</sub> showed no evidence of <sup>18</sup>O labelling in CH<sub>3</sub>OH. This is illustrated by the chromatograms of CH<sub>3</sub>OH in Figure 28a and b, which show a peak for masses 29, 30 and 31 (unlabelled CH<sub>3</sub>OH) but no peak for masses 33 and 34, which correspond to CH<sub>3</sub><sup>18</sup>OH. In contrast, the experiments with <sup>18</sup>OCH<sub>3</sub>-2-methoxyphenol yielded a prominent peak for masses 33 and 34, while no peaks were observed for masses 29, 30, and 31 (Figure 28c). In the setup from Figure 26 with OCD<sub>3</sub>-2-methoxyphenol, a mass shift of 3 AMU to mass 35 can be observed, representing the triple deuteration of CD<sub>3</sub>OH as observed for the S- and N-bonded CH<sub>3</sub> groups.

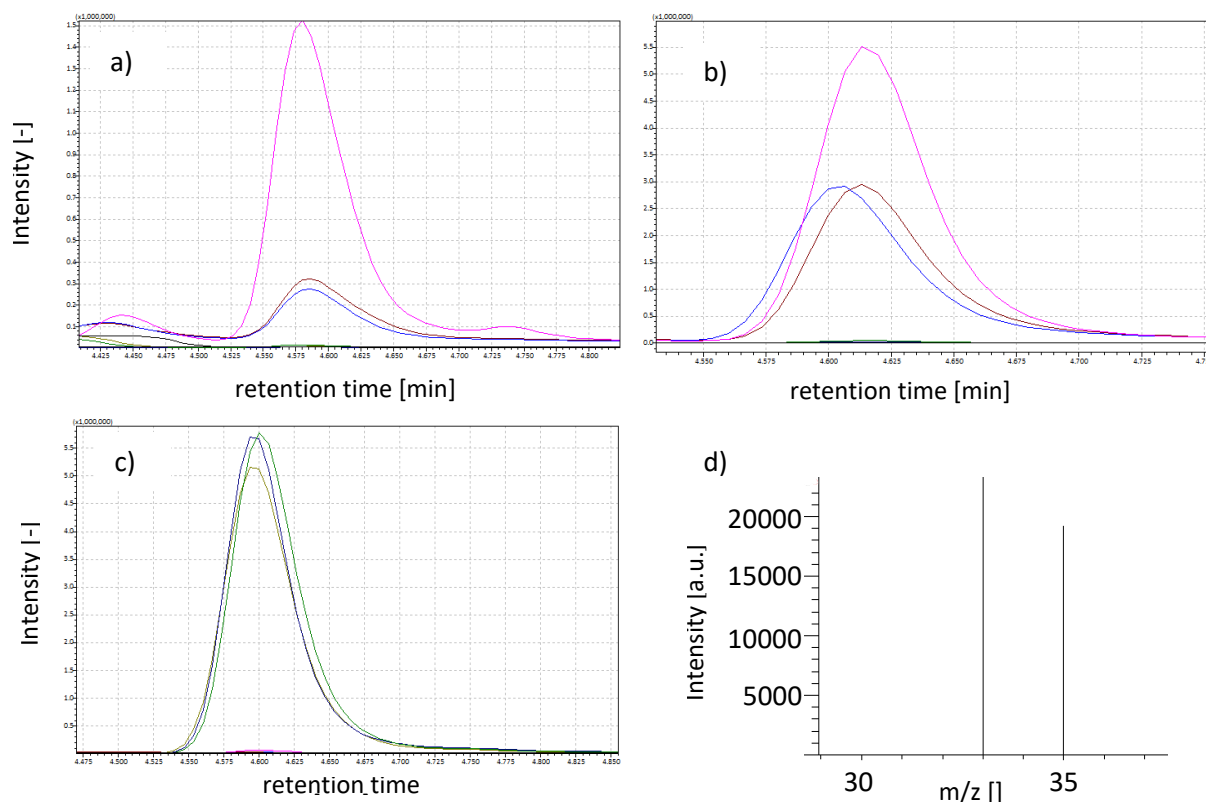


Figure 28: Chromatograms and mass track of  $\text{CH}_3\text{OH}$  from different isotopic labelling experiments with  $10 \mu\text{mol}$   $\text{LFe}^{\text{II}}\text{Cl}_2$ ,  $100 \mu\text{mol}$  Asc and  $200 \mu\text{mol}$   $\text{H}_2\text{O}_2$  and  $25 \mu\text{mol}$  sinapyl alcohol, coniferyl alcohol or 2-methoxyphenol under ambient atmospheric conditions with a reaction time of 48 h: **a)** with  $\text{H}_2^{18}\text{O}_2$  instead of  $\text{H}_2\text{O}_2$  ( $n = 3$ ) and **b)**  $\text{O}_2$  replaced in  $\text{H}_2\text{O}$  and headspace by  $^{18}\text{O}_2$  ( $n = 3$  measurement). **c)** Experiment with 1/10 of all compounds and with  $^{18}\text{OCH}_3$  2-methoxyphenol instead of unlabelled 2-methoxyphenol ( $n = 3$  measurement). Pink, blue and brown chromatograms are the measured mass of 29, 30 and 31 of the produced  $\text{CH}_3\text{OH}$ . The black line is the blank without substrate, and green, dark blue, and olive are the masses 33 and 34 of  $\text{CH}_3^{18}\text{OH}$  measured in the experiments. **d)** Mass track of  $\text{CH}_3\text{OH}$  in a standard experiment with d3-2-methoxyphenol with a mass shift of 3 AMU from 32 to 35 representing the  $\text{CD}_3\text{OH}$ .

### 3.3.4 Discussion and mechanistic details of the conversion of methoxy group containing compounds to $\text{CH}_3\text{OH}$ and $\text{CH}_2\text{O}$

The data presented for the  $\text{OCH}_3$  components demonstrate that only  $\text{CH}_3\text{OH}$  and  $\text{CH}_2\text{O}$  are produced; even in experiments conducted with Asc, no  $\text{CH}_4$ ,  $\text{C}_2\text{H}_6$ , or  $\text{CH}_3\text{Cl}$  could be quantified. This contrasts with the DMSO investigations, where hydrocarbons and other C1 and C2 compounds are produced with Asc (Chapter 3.1). All experiments with aromatic  $\text{OCH}_3$  compounds and the  $\text{LFe}^{\text{II}}\text{Cl}_2$  complex produce approximately 45 to 111 %  $\text{CH}_3\text{OH}$  and  $\text{CH}_2\text{O}$ , corresponding to a high conversion rate. More than 100 % conversion rate is possible due to the normalisation to one  $\text{OCH}_3$  group, and sinapyl alcohol has two. The lignin components sinapyl and coniferyl alcohol have the highest conversion rates, which

makes the reaction particularly relevant for natural environments. The isomers 2-, 3-, and 4-methoxyphenol exhibited conversion rates of approximately 50 % and comparable distributions of  $\text{CH}_3\text{OH}$  and  $\text{CH}_2\text{O}$ , suggesting that the position of the  $\text{OCH}_3$  group does not significantly influence the reaction. In contrast, experiments involving  $\text{Fe}_2\text{O}_3$  and the aromatic  $\text{OCH}_3$  compounds yielded lower conversion rates than those observed with  $\text{LFe}^{\text{II}}\text{Cl}_2$ . This disparity could be attributed to the distinct structural characteristics of the Fe species, resulting in divergent reaction behaviours, such as steric hindrance.  $\text{Fe}_2\text{O}_3$  exhibits 2-3 orders of magnitude lower solubility than other Fe species, potentially impeding the reaction rate.<sup>205</sup> However, the lower solubility of  $\text{Fe}_2\text{O}_3$  does not influence the conversion rate of the DMSO experiments due to the completion of the reaction observed in the kinetic study. This was not thoroughly examined in the study with the  $\text{OCH}_3$  compounds, necessitating further investigation due to the potential for alterations in kinetics resulting from disparities in reaction mechanisms. The experiments involving anisole and  $\text{Fe}_2\text{O}_3$  exhibited minimal conversion, which might be attributable to the absence of an OH group at the benzene ring and a potentially different reaction mechanism, as all other compounds comprise an OH group neighbouring the  $\text{OCH}_3$  group. For Game, the only non-aromatic compound with an  $\text{OCH}_3$  group, lower conversion rates have been measured than for the aromatic compounds. This phenomenon may be attributed to a divergent reaction mechanism, given that no aromatic system exists, as is the case with all other compounds. A possible reaction to form  $\text{CH}_3\text{OH}$  is the acidic ester cleavage and further oxidation to  $\text{CH}_2\text{O}$  as  $\text{H}_2\text{O}_2$  is present.

The only production of  $\text{CH}_3\text{OH}$  and  $\text{CH}_2\text{O}$  suggests that no  $\text{CH}_3$  radicals are formed, which would otherwise be indicated by the presence of  $\text{CH}_4$ ,  $\text{C}_2\text{H}_6$ ,  $\text{CH}_3\text{Cl}$  and other C1 and C2 compounds, as observed in the study with  $d_6$ -DMSO. To test this hypothesis, identical experiments with  $\text{CCl}_3\text{Br}$  as an alkyl radical scavenger were conducted using sinapyl alcohol, 2-methoxyphenol, and Game. Figure 27 illustrates no observable difference between the blank experiment and the experiments with substrates. This reveals that no  $\text{CH}_3$  radicals are formed and that an alternative reaction mechanism must be responsible for generating  $\text{CH}_3\text{OH}$  and, subsequently,  $\text{CH}_2\text{O}$ . To investigate this further, the isotopically labelled substances described above were employed. The experiments conducted with  $\text{H}_2^{18}\text{O}_2$  and  $^{18}\text{O}_2$  demonstrated that the oxygen present in  $\text{CH}_3\text{OH}$  does not originate from  $\text{H}_2\text{O}_2$  or  $\text{O}_2$ . This is demonstrated by the absence of  $\text{CH}_3^{18}\text{OH}$  in the experiments. In contrast to the results observed with DMSO, in which these compounds act as oxygen donors for  $\text{CH}_3\text{OH}$  and  $\text{CH}_2\text{O}$ , the present findings suggest another reaction mechanism. To ascertain which component of the  $\text{OCH}_3$  group is present in  $\text{CH}_3\text{OH}$ ,  $^2\text{H}$  or  $^{18}\text{O}$ -labelled 2-methoxyphenol was employed.

The results of experiments conducted with  $d_3$ -2-methoxyphenol indicate that the whole  $\text{CH}_3$  group of 2-methoxyphenol is present in  $\text{CH}_3\text{OH}$ , as evidenced by a shift of 3 AMU from mass 32 to 35. This also excludes the possibility of a hydrogen atom transfer as a reaction mechanism, which was similarly ruled

out in the experiments conducted with DMSO (Chapter 3.1.7). This is evident from the mass of 35 observed for  $\text{CH}_3\text{OH}$ , as during a hydrogen atom abstraction reaction, a deuterium atom is removed from the  $\text{CH}_3$  group and replaced by a hydrogen atom in the reaction, resulting in a final mass of 34 for  $\text{CH}_3\text{OH}$ . The  $^{18}\text{O}$ -labelled oxygen atom was successfully detected in the resulting  $\text{CH}_3\text{OH}$  using  $^{18}\text{OCH}_3$ -2-methoxyphenol (> 95 % labelling). Figure 28c illustrates the peaks for masses 33 and 34, which correspond to  $\text{CH}_3^{18}\text{OH}$ . In contrast, no peak is observed for masses 29, 30 and 31, which leads to the conclusion that the oxygen from  $\text{CH}_3\text{OH}$  originates exclusively from the  $\text{OCH}_3$  group of 2-methoxyphenol. These experiments demonstrate that the entire  $\text{OCH}_3$  group is cleaved off and reacts with a hydrogen atom to form  $\text{CH}_3\text{OH}$ . It can be postulated that the hydrogen originates from an excess of  $\text{H}^+$  ions present in the acidic solution. The resulting  $\text{CH}_3\text{OH}$  can undergo further oxidation to  $\text{CH}_2\text{O}$  by the oxidative environment, as previously described for DMSO. These observations provide a reaction mechanism for  $\text{CH}_3\text{OH}$  production from lignin monomers, where previous studies lack information.<sup>118,122,132</sup>

The reaction under consideration has not yet been the subject of scientific investigation in atmospheric conditions (1013 mbar and 22°C). However, it is of considerable environmental significance due to the ubiquitous distribution of aromatic  $\text{OCH}_3$  compounds alongside  $\text{H}_2\text{O}_2$  and other ROS and Fe species (Chapter 1.3.2 and 1.6). Chapters 3.6 and 3.7 provide a more detailed analysis of the impact on the global carbon cycle, particularly the pedosphere.

### 3.4 Results of the studies with different Mn, Fe, Co, Ni and Cu species instead of $\text{LFe}^{\text{II}}\text{Cl}_2$ and $\text{Fe}_2\text{O}_3$

To gain further insights into the reactions described previously, the Fe-containing species, i.e.,  $\text{LFe}^{\text{II}}\text{Cl}_2$  and  $\text{Fe}_2\text{O}_3$ , were replaced by various transition metals (Mn, Fe, Co, Ni and Cu) in the form of salts, oxides, sulphates and acetate. Investigations were carried out with  $\text{MnCl}_2$ ,  $\text{MnSO}_4$ ,  $\text{MnO}_2$ ,  $\text{FeCl}_2$ ,  $\text{FeSO}_4$ ,  $\text{CoCl}_2$ ,  $\text{NiCl}_2$ ,  $\text{NiSO}_4$ ,  $\text{CuCl}_2$ ,  $\text{CuO} + \text{CuO}_2$  and  $\text{Cu}(\text{OAc})_2$  using the precursor compounds  $d_6$ -DMSO,  $d_3$ -methionine and 2-methoxyphenol, respectively. This was done to see if other transition metals with different counterions react similarly due to the presence of all these transition metals in nature, particularly in the pedosphere.

#### 3.4.1 Conversion of $d_6$ -DMSO, $d_3$ -methionine and 2-methoxyphenol to $\text{CD}_3\text{H}$ , $\text{C}_2\text{D}_6$ , $\text{CD}_3\text{OH}$ , $\text{CD}_2\text{O}$ and $\text{CH}_3\text{Cl}$ mediated by transition metals

The above-listed transition metal species were utilised as substitutes for  $\text{LFe}^{\text{II}}\text{Cl}_2$  and  $\text{Fe}_2\text{O}_3$ . Consequently, a range of transition metals and counterions and different oxidation states of the transition

metals were examined. The experiments involved the analysis of CH<sub>4</sub>, C<sub>2</sub>H<sub>6</sub>, CH<sub>3</sub>OH and CH<sub>2</sub>O in the same setup as with d<sub>6</sub>-DMSO (10 μmol transition metal species, 25 μmol d<sub>6</sub>-DMSO, 100 μmol Asc and 200 μmol H<sub>2</sub>O<sub>2</sub>; (Table 10), with the addition of CH<sub>3</sub>Cl analysis in experiments involving chlorine counterions.

Table 10: Composition of the experiments on different transition metal species with d<sub>6</sub>-DMSO, d<sub>3</sub>-methionine and 2-methoxyphenol as precursor compounds to determine the conversion rates and possible differences.

No.	Precursor compound	Transition metal species	Oxidant	acid
1-11	25 μmol d <sub>6</sub> -DMSO	10 μmol MnCl <sub>2</sub> , MnSO <sub>4</sub> , MnO <sub>2</sub> , FeCl <sub>2</sub> , FeSO <sub>4</sub> , CoCl <sub>2</sub> , NiCl <sub>2</sub> , NiSO <sub>4</sub> , CuCl <sub>2</sub> , CuO + CuO <sub>2</sub> and Cu(OAc) <sub>2</sub>	200 μmol H <sub>2</sub> O <sub>2</sub>	100 μmol Asc
12-22	25 μmol d <sub>3</sub> -methio- nine	10 μmol MnCl <sub>2</sub> , MnSO <sub>4</sub> , MnO <sub>2</sub> , FeCl <sub>2</sub> , FeSO <sub>4</sub> , CoCl <sub>2</sub> , NiCl <sub>2</sub> , NiSO <sub>4</sub> , CuCl <sub>2</sub> , CuO + CuO <sub>2</sub> and Cu(OAc) <sub>2</sub>	200 μmol H <sub>2</sub> O <sub>2</sub>	100 μmol Asc
23-33	25 μmol 2-methoxy- phenol	10 μmol MnCl <sub>2</sub> , MnSO <sub>4</sub> , MnO <sub>2</sub> , FeCl <sub>2</sub> , FeSO <sub>4</sub> , CoCl <sub>2</sub> , NiCl <sub>2</sub> , NiSO <sub>4</sub> , CuCl <sub>2</sub> , CuO + CuO <sub>2</sub> and Cu(OAc) <sub>2</sub>	200 μmol H <sub>2</sub> O <sub>2</sub>	100 μmol Asc

#### 3.4.1.1 d<sub>6</sub>-DMSO

To facilitate a comparison with the process described in Chapter 2.1, d<sub>6</sub>-DMSO was again utilised in conjunction with the aforementioned transition metal species (No. 1-11; Table 10). Figure 29 illustrates the conversion of d<sub>6</sub>-DMSO to CH<sub>4</sub>, C<sub>2</sub>H<sub>6</sub>, CH<sub>3</sub>OH and CH<sub>2</sub>O. The predominant formation of CH<sub>4</sub> resulted in conversion rates ranging from 1.61 ± 0.10 % for CuCl<sub>2</sub> to 62.0 ± 2.0 % for FeSO<sub>4</sub>. The conversion rate for C<sub>2</sub>H<sub>6</sub> range from 0.00076 ± 0.00014 % for MnCl<sub>2</sub> to 3.28 ± 0.05 % for FeCl<sub>2</sub>, while the conversion rate for CH<sub>3</sub>OH range from 5.67 ± 0.35 % for Cu(OAc)<sub>2</sub> to 24.0 ± 0.8 % for MnO<sub>2</sub>. The conversion to CH<sub>2</sub>O demonstrates a moderate fluctuation between 2.29 ± 1.81 % and 7.45 ± 0.58 %.

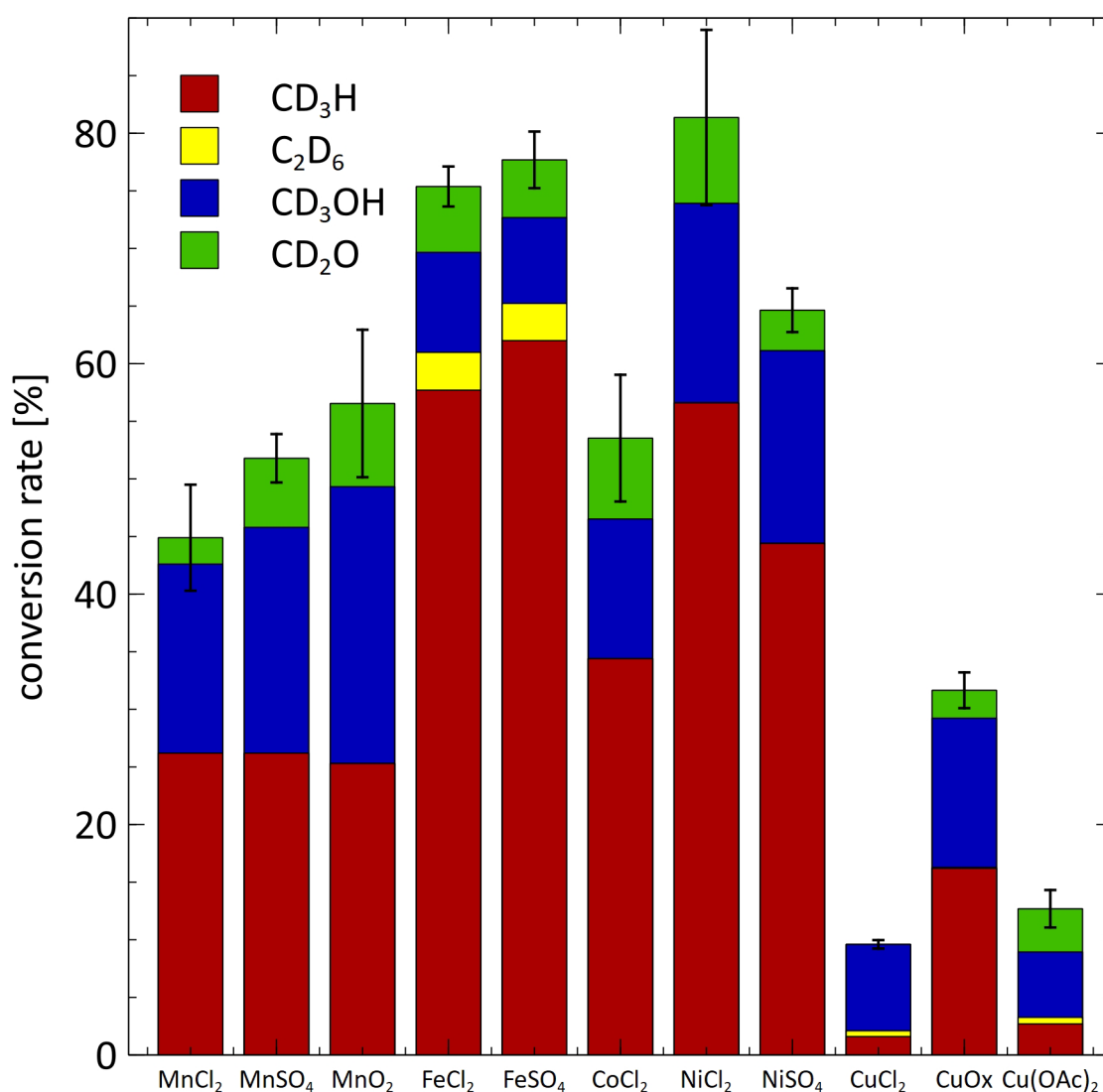


Figure 29: The experiments investigated the formation of C1 and C2 compounds from d<sub>6</sub>-DMSO using 10 μmol different transition metal species in conjunction with 200 μmol H<sub>2</sub>O<sub>2</sub> and 100 μmol Asc under ambient atmospheric conditions with a reaction time of 48 h. All C1 and C2 compounds could be measured for all transition metal species. Except for CuCl<sub>2</sub>, CH<sub>2</sub>O concentrations could not be determined; hence, no conversion rate was calculated. CuOx is a mixture of copper oxides (CuO and Cu<sub>2</sub>O), whereas Cu(OAc)<sub>2</sub> refers to copper(II) acetate. Error bars refer to the SD of the total conversion of all major C1 and C2 compounds for n = 9, except for C<sub>2</sub>D<sub>6</sub>, n = 3.

The total conversion rates of the Mn species range from  $44.9 \pm 4.6$  to  $56.5 \pm 6.4$  %, and the distributions of the Mn species' individual C1 and C2 components are similar. A comparison of the C1 and C2 components for the two Fe species reveals a similar distribution as for the Mn species, with a conversion rate of  $75.4 \pm 1.7$  % for FeCl<sub>2</sub> and  $77.7 \pm 2.5$  % for FeSO<sub>4</sub>, respectively. CoCl<sub>2</sub> exhibits a conversion rate of  $53.5 \pm 5.5$  %, falling within the range of Mn. NiCl<sub>2</sub> exhibit the highest conversion rate of  $81.4 \pm 7.6$  %, while NiSO<sub>4</sub> demonstrates a lower conversion rate of  $64.6 \pm 1.9$  %. In the context of the Cu species,

the conversion rates ranged from  $9.60 \pm 0.37$  % ( $\text{CH}_2\text{O}$  could not be measured due to analytical issues) to  $31.7 \pm 1.6$  %.

### 3.4.1.2 $\text{d}_3$ -Methionine

In experiments that involved 25  $\mu\text{mol}$   $\text{d}_3$ -methionine, 10  $\mu\text{mol}$  transition metal species, 100  $\mu\text{mol}$  Asc and 200  $\mu\text{mol}$   $\text{H}_2\text{O}_2$  (No. 12-22; Table 10), the observed conversion rates were consistently lower than those observed in experiments involving  $\text{d}_6$ -DMSO (Figure 30). The conversion rates ranged from 0 to  $4.07 \pm 1.52$  % for  $\text{CH}_4$  and from  $0.00043 \pm 0.00016$  % to  $0.45 \pm 0.01$  % for  $\text{C}_2\text{H}_6$ . Conversion rates ranging from 0.0 % to  $2.30 \pm 0.14$  % were observed for  $\text{CH}_3\text{OH}$  and between zero % and  $4.67 \pm 1.74$  % for  $\text{CH}_2\text{O}$ .

$\text{CH}_3\text{OH}$  was detected in considerable amounts ( $2.30 \pm 0.14$  %) only in experiments with  $\text{MnCl}_2$  compared to all other experiments. The total conversion rates for the Mn and Fe species range from  $4.52 \pm 1.07$  % to  $8.77 \pm 2.31$  %. Conversely, lower total conversion rates were observed for the Co, Ni, and Cu species compared to the Fe and Mn species. These range from  $1.18 \pm 0.12$  % to  $2.50 \pm 1.31$  %, except for  $\text{CuCl}_2$ , for which the rate was lower at  $0.064 \pm 0.038$  %. It should be noted that the  $\text{CH}_2\text{O}$  formation rate could not be determined due to technical issues in this instance.

$\text{CH}_4$  conversion rates are very similar in these experiments for Fe and Mn species, and  $\text{C}_2\text{H}_6$  conversion rates are more prominent for the Fe species than for the Mn species. Compared to  $\text{Fe}_2\text{O}_3$ , the total conversion rate is approximately 11 %, slightly higher, and the  $\text{LFe}^{\text{II}}\text{Cl}_2$  complex only exhibits approximately 1.2 % hydrocarbons. The Co and Ni species exhibit lower conversion rates than the Fe and Mn species, in contrast to the experiments with  $\text{d}_6$ -DMSO, where the conversion rates are similar.

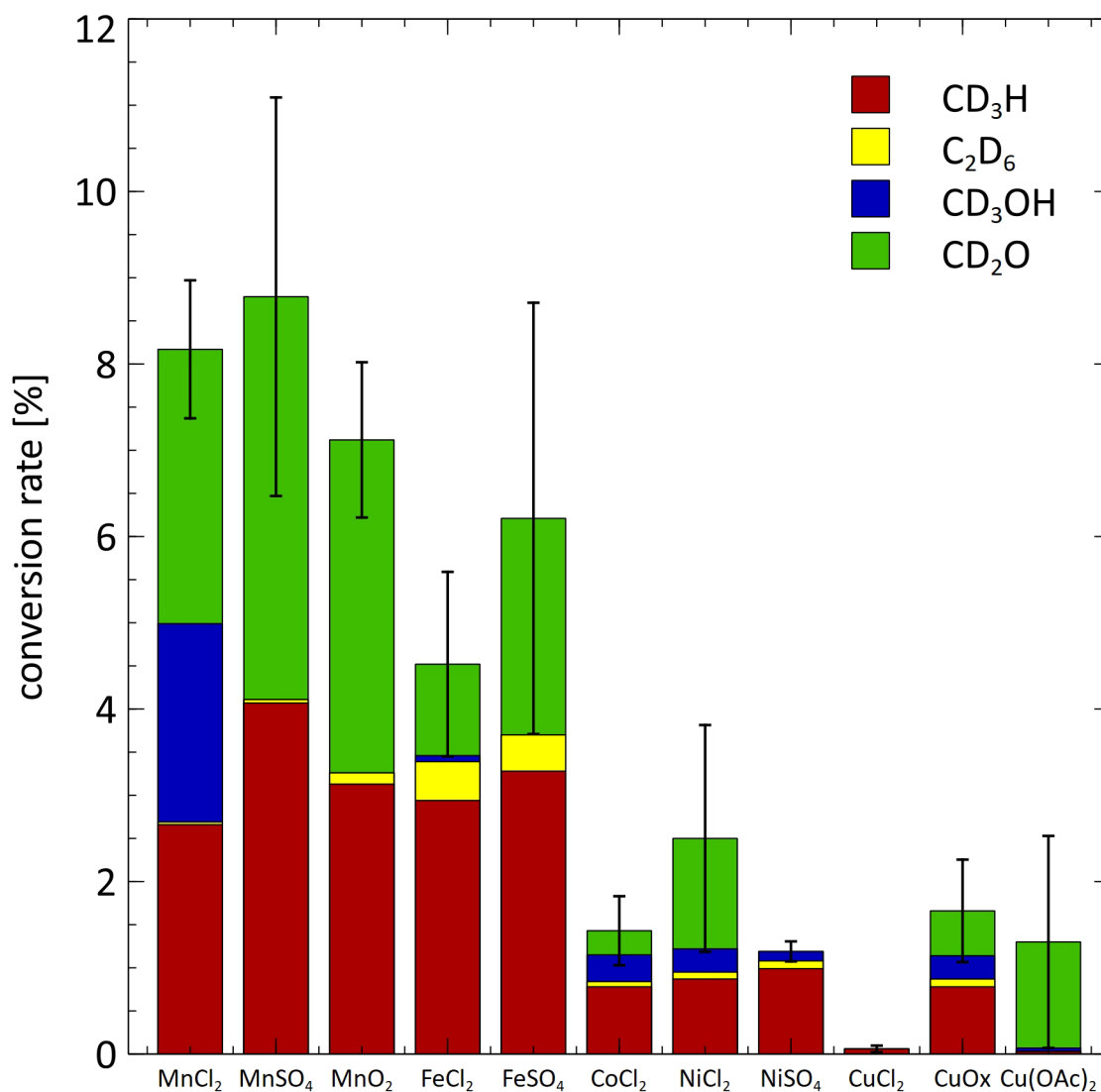


Figure 30: The experiments investigated the formation of C1 and C2 compounds from 25  $\mu\text{mol}$   $d_3$ -methionine using 10  $\mu\text{mol}$  of different transition metal species in conjunction with 200  $\mu\text{mol}$   $\text{H}_2\text{O}_2$  and 100  $\mu\text{mol}$  Asc under ambient atmospheric conditions with a reaction time of 48 h. For  $\text{CuCl}_2$ ,  $\text{CH}_2\text{O}$  concentrations could not be determined; hence, no conversion rate was calculated.  $\text{CuOx}$  is a mixture of copper oxides ( $\text{CuO}$  and  $\text{Cu}_2\text{O}$ ), whereas  $\text{Cu(OAc)}_2$  refers to copper(II) acetate. Error bars refer to the SD of the total conversion of all major C1 and C2 compounds for  $n = 9$ , except for  $\text{C}_2\text{D}_6$ ,  $n = 3$ .

### 3.4.1.3 2-Methoxyphenol

In experiments involving 2-methoxyphenol, a configuration analogous to  $d_6$ -DMSO and  $d_3$ -methionine was conducted (No. 23-33; Table 10). Asc was replaced with triflic acid, maintaining a pH value of 2.3. Asc is absent because the reaction mechanism described in Chapter 3.3 does not require a radical scavenger, as no OH and  $\text{CH}_3$  radicals are involved in forming  $\text{CH}_3\text{OH}$  and  $\text{CH}_2\text{O}$ . They are directly produced from the  $\text{OCH}_3$  group, and only the formation of  $\text{CH}_3\text{OH}$  and  $\text{CH}_2\text{O}$  was observed (Figure 31).

The conversion rates of CH<sub>3</sub>OH ranged from 0 to 23.6 ± 4.3 %, while those of CH<sub>2</sub>O fell within the range of 0 to 27.9 ± 2.0 %. Further analysis of the individual transition metals reveals that the total conversion rate for MnSO<sub>4</sub> (15.3 ± 2.1 %) is significantly higher than for MnCl<sub>2</sub> (1.36 ± 1.92 %) and MnO<sub>2</sub> (2.53 ± 0.65 %). For FeCl<sub>2</sub> and FeSO<sub>4</sub>, the total conversion rates are similar at 32.2 ± 1.7 % and 36.1 ± 2.0 %, respectively, and all experiments with both Mn and Fe species produced CH<sub>3</sub>OH and CH<sub>2</sub>O, except for MnCl<sub>2</sub>, where only CH<sub>2</sub>O was detected. In the case of Co, Ni and Cu, the only product observed was CH<sub>3</sub>OH, except NiCl<sub>2</sub>, which yielded CH<sub>2</sub>O at a conversion rate of 0.78 ± 1.32 %. It should be noted that the error margin for this measurement exceeds the conversion rate. The total conversion rates for these transition metal species range from 5.39 ± 3.62 % for CuCl<sub>2</sub> to 23.6 ± 4.3 % for NiSO<sub>4</sub>. A divergence in the observed patterns is apparent compared to the d<sub>6</sub>-DMSO and d<sub>3</sub>-methionine experiments. The absence of hydrocarbons is a general observation, and with 2-methoxyphenol, the conversion rates of the Mn species are comparatively low compared to other transition metal species. This contrasts the d<sub>6</sub>-DMSO and d<sub>3</sub>-methionine experiments, wherein the Mn species demonstrate higher conversion rates than the other transition metal species. The Fe species demonstrate the highest conversion rates, analogous to the d<sub>6</sub>-DMSO experiments. Conversely, the Co, Ni and Cu species exhibit lower conversion rates than the Fe species. This phenomenon has also been observed in experiments involving d<sub>6</sub>-DMSO except for Ni species and d<sub>3</sub>-methionine. The conversion rates are intermediate between those documented in the d<sub>6</sub>-DMSO and d<sub>3</sub>-methionine experiments.

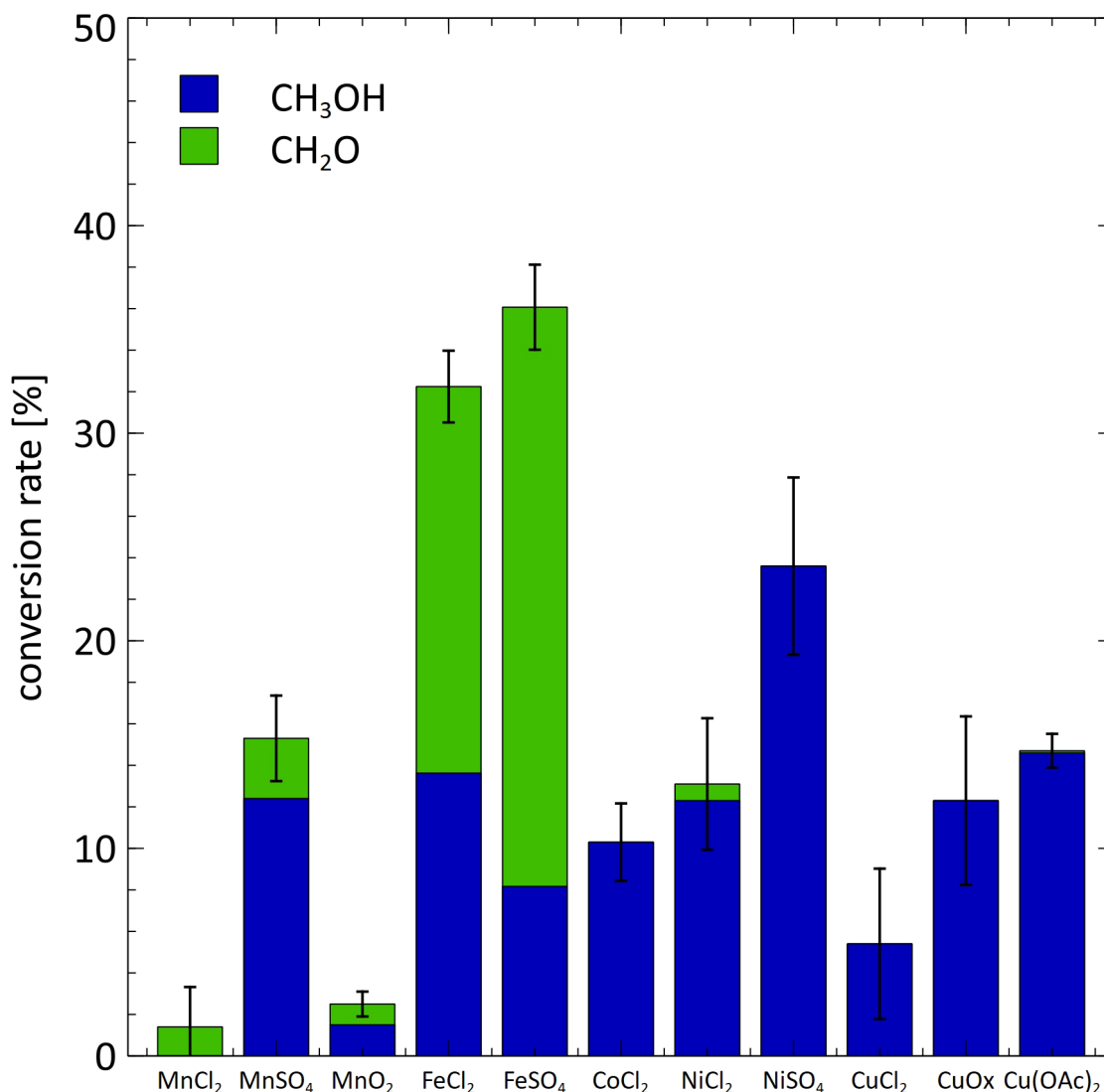


Figure 31: The formation of CH<sub>3</sub>OH and CH<sub>2</sub>O compounds from 25  $\mu$ mol 2-methoxyphenol was investigated using 10  $\mu$ mol of different transition metal species, 200  $\mu$ mol H<sub>2</sub>O<sub>2</sub> and 0.05  $\mu$ mol triflic acid under ambient atmospheric conditions with a reaction time of 48 h. No CH<sub>4</sub> and C<sub>2</sub>H<sub>6</sub> formation was observed. For CuCl<sub>2</sub>, CH<sub>2</sub>O concentrations could not be determined due to analytical issues. Hence, no conversion rate was calculated. CuOx is a mixture of copper oxides (CuO and Cu<sub>2</sub>O), whereas Cu(OAc)<sub>2</sub> refers to copper(II) acetate. Error bars refer to the SD of the total conversion of all major C1 and C2 compounds for n = 9.

#### 3.4.1.4 CH<sub>3</sub>Cl

For all transition metal species that possess chlorine as a counter ion, the experiments with d<sub>6</sub>-DMSO, d<sub>3</sub>-methionine and 2-methoxyphenol were further analysed for CH<sub>3</sub>Cl formation (Figure 32). In the studies with d<sub>6</sub> DMSO, CH<sub>3</sub>Cl was observed for all transition metal species with a range of conversion rates from 0.00006 to 0.00097 %. CuCl<sub>2</sub>, however, exhibited a conversion rate of  $0.69 \pm 0.13$  %, approximately three orders of magnitude higher than in the rest of the study. With d<sub>3</sub>-methionine, a conversion rate of  $0.00017 \pm 0.00002$  % and  $0.0026 \pm 0.0025$  % were detected exclusively for FeCl<sub>2</sub> and

$\text{CuCl}_2$ , respectively. In experiments with 2-methoxyphenol, only experiments with  $\text{FeCl}_2$  show a low production of  $0.000044 \pm 0.000025$  %  $\text{CH}_3\text{Cl}$ .

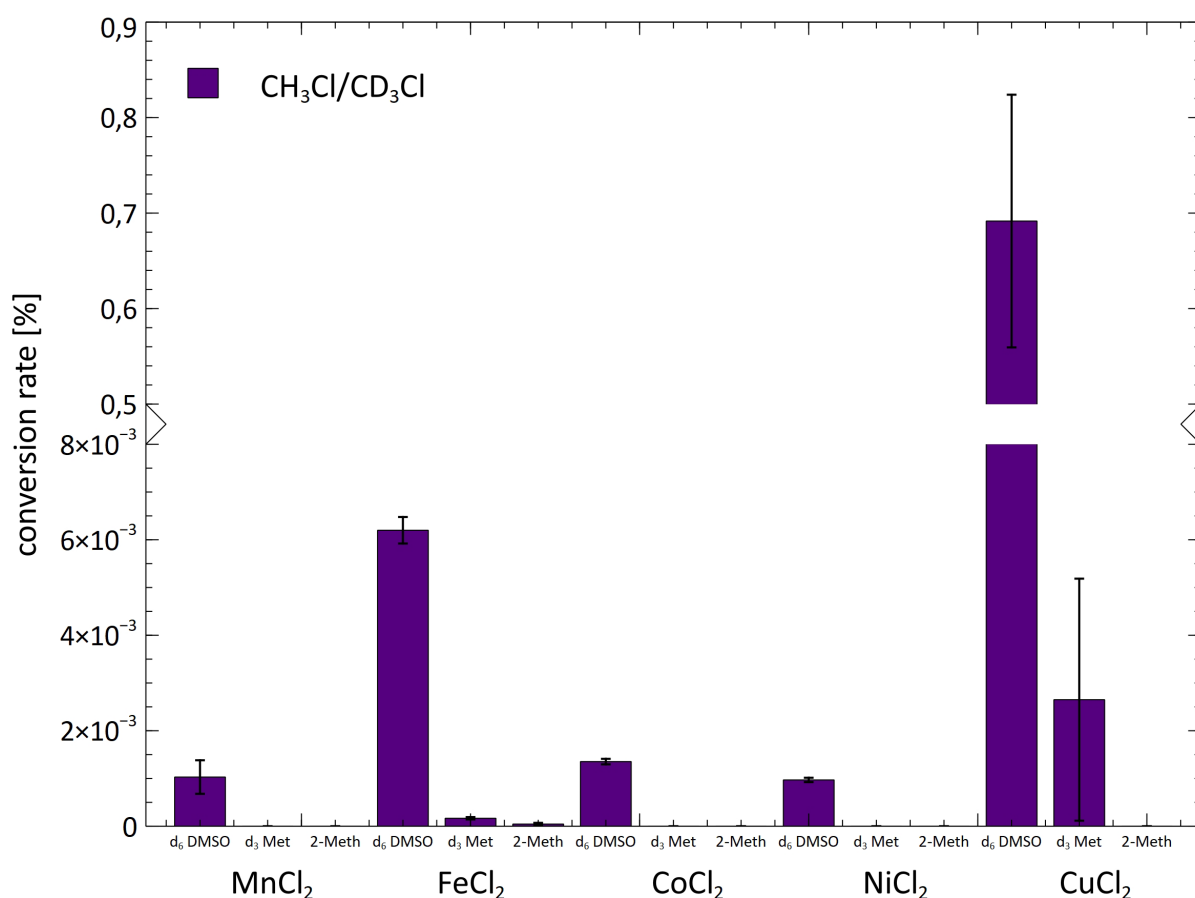


Figure 32: The formation of  $\text{CH}_3\text{Cl}$  from 25  $\mu\text{mol}$   $\text{d}_6$ -DMSO,  $\text{d}_3$ -methionine, or 2-methylphenol with 100  $\mu\text{mol}$  Asc or 0.05  $\mu\text{mol}$  triflic acid in case of 2-methoxyphenol and 200  $\mu\text{mol}$   $\text{H}_2\text{O}_2$  was investigated using 10  $\mu\text{mol}$  different transition metal species with chlorine counter ions in the experiments described above. Error bars refer to the SD of the conversion of  $\text{CH}_3\text{Cl}$  for  $n = 3$ .

### 3.4.2 Discussion and implications of the different transition metal species in reaction with $\text{d}_6$ -DMSO, $\text{d}_3$ -methionine and 2-methoxyphenol and the formation of $\text{CH}_4$ , $\text{C}_2\text{H}_6$ , $\text{CH}_3\text{OH}$ , $\text{CH}_2\text{O}$ and $\text{CH}_3\text{Cl}$

#### 3.4.2.1 $\text{d}_6$ -DMSO

A comparative analysis of the conversion rates for  $\text{FeCl}_2$  and  $\text{FeSO}_4$  with  $\text{d}_6$ -DMSO shows that the identical products  $\text{CH}_4$ ,  $\text{C}_2\text{H}_6$ ,  $\text{CH}_3\text{OH}$ , and  $\text{CH}_2\text{O}$  were formed in a consistent pattern. The highest conversion rates were observed for  $\text{CH}_4$  (up to 62 %), followed by moderate yields for  $\text{CH}_3\text{OH}$  and  $\text{CH}_2\text{O}$  (up to 24.2 and 7.45 %, respectively). High conversion rates for  $\text{C}_2\text{H}_6$  (up to 3.28 %) are also observed for Fe species compared to the other transition metal species, and they are within the range of the experiments with

the  $\text{LFe}^{\text{II}}\text{Cl}_2$  complex (Chapter 3.1.2). The conversion rates to  $\text{CH}_4$  are similar for the naturally occurring  $\text{Fe}_2\text{O}_3$ ,  $\text{FeCl}_2$  and  $\text{FeSO}_4$ . The production of  $\text{CH}_3\text{OH}$  from  $\text{FeCl}_2$  and  $\text{FeSO}_4$  is more closely related to that of the  $\text{LFe}^{\text{II}}\text{Cl}_2$  complex than that of  $\text{Fe}_2\text{O}_3$ . This may be attributable to the complete solubility of the iron species compared to the very low solubility of  $\text{Fe}_2\text{O}_3$ .<sup>205</sup> Conversely, for  $\text{CH}_2\text{O}$  production,  $\text{FeCl}_2$  and  $\text{FeSO}_4$  show a behaviour more similar to  $\text{Fe}_2\text{O}_3$  than to the  $\text{LFe}^{\text{II}}\text{Cl}_2$  complex. However, Althoff et al. (2010)<sup>31</sup> reported that the type of Fe oxide or hydroxide significantly affects the yield of  $\text{CH}_4$  in experiments with Asc as a precursor compound, with ferrihydrite having the highest yield and  $\text{Fe}_2\text{O}_3$  the lowest. Nevertheless, a direct comparison is not feasible due to their experiments' absence of a sulfur-bound  $\text{CH}_3$  group. Compared to the data from Althoff et al. 2014<sup>14</sup>, the  $\text{CH}_4$  conversion rates are generally lower. The high ratio of Asc to precursor compound (100:1) in the study conducted by Althoff compared to the 4 to 1 ratio in this study influences the  $\text{CH}_4$  production considerably since more OH radicals are trapped and less oxygenated compounds are generated. The  $\text{CH}_3$  radicals can react to  $\text{CH}_4$  instead of the OH radicals. It is essential to consider methodological differences, particularly in the amounts of substances used and the incubation duration. In addition, Althoff's study focused exclusively on  $\text{CH}_4$  conversion rates without considering other C1 and C2 compounds.

The results indicate that  $d_6$ -DMSO can be converted to various C1-C2 compounds using different Fe species as catalysts. Differences in the C1 and C2 conversion rates may be attributed to differences in the solubility and crystal structure of the Fe species. While the mechanism underlying the formation of the high-valent iron-oxo complex from the  $\text{LFe}^{\text{II}}\text{Cl}_2$  complex is well established, similar mechanisms for  $\text{Fe}_2\text{O}_3$  and Fe salts, sulfates, and acetates remain poorly understood and require further investigation.

Within each transition metal, the conversion rates for all C1-C2 compounds investigated are similar, indicating that the oxidation state and counterions have a lesser impact than the choice of the transition metal itself. Interestingly, C1 and C2 emissions from Cu compounds differ significantly from the other transition metal species, with substantially lower conversion rates. The underlying causes of these discrepancies remain to be elucidated, particularly given the reported evidence for the formation of  $\text{CH}_3$  radicals from DMSO mediated by Cu(II) salts.<sup>260-262</sup> One potential explanation for these variations may be found in the redox potential exhibited by the transition metal compounds; however, this potential is influenced by a complex network of interacting factors. For instance, factors such as pH and ionic strength significantly influence redox behaviour. Furthermore, the transition metal ion's electronic configuration and spin state, particularly in transition metals with multiple oxidation states, can impact its redox potential, as these factors affect the transition metal ion's ability to interact with surrounding ligands and solvent molecules.<sup>263,264</sup> Consequently, further experimental and theoretical studies are required to elucidate the underlying mechanisms fully.

The present study extends transition metal complex-based Fenton chemistry beyond Fe as a redox catalyst. The formation of oxidised species in Fenton-like reactions at circumneutral pH has been shown to generally follow the order  $\text{Cu}^{\text{II}} < \text{Ni}^{\text{II}} < \text{Mn}^{\text{II}} < \text{Fe}^{\text{III}} < \text{Co}^{\text{II}}$ .<sup>265</sup> However, this is not the case in the present study because the conversion rates do not follow this trend. These differences are likely attributed to variations in reaction conditions, particularly to the lower pH values of 2.3 in this study. The redox properties of each transition metal- $\text{H}_2\text{O}_2$  system are unique and significantly influenced by the transition metal's oxidation state and the solution pH.<sup>266</sup> For instance,  $\text{Mn}^{2+}$ -chelates have been shown to enhance  $\text{O}_2^-$  generation by reacting with  $\text{H}_2\text{O}_2$ .<sup>267</sup> Transition metals with multiple redox states, such as Fe, Cu, Co, and Mn, can directly decompose  $\text{H}_2\text{O}_2$  into HO via conventional Fenton-like pathways. Although such Fenton systems demonstrate efficiency even at neutral pH, the mechanism of  $\text{H}_2\text{O}_2$  activation is distinguished by its high specificity to the nature and composition of the catalyst.<sup>268</sup> Consequently, the mechanisms by which non-iron catalysts facilitate the decomposition of organic matter remain ambiguous, and thus, extensive further research is necessary.

The proposed mechanism for  $\text{CH}_3$  radical formation from  $d_6$ -DMSO via S-demethylation (Chapter 3.1.7) is supported by the deuterium incorporation into  $\text{CH}_2\text{O}$  and  $\text{CH}_3\text{Cl}$  as indicated by a change in mass of 2 or 3 AMU in all transition metal catalysts examined. This was determined using GC-MS, analogous to Chapter 3.1.5, but not shown here. This finding indicates that a demethylation process may occur analogous to  $d_6$ -DMSO with  $\text{LFe}^{\text{II}}\text{Cl}_2$ . Also, the production of  $\text{C}_2\text{H}_6$ , likely formed through recombining two  $\text{CH}_3$  radicals, is observed and supports this mechanism. Consequently, it is reasonable to hypothesise that the remaining C1 and C2 compounds will also demonstrate isotopic labelling, as  $\text{CH}_3$  radicals should be the predominant precursors in this process.

Notably, Fe and Cu species appear to be the only transition metals capable of mediating substantial  $\text{C}_2\text{H}_6$  formation, while transition metals such as Mn, Co, and Ni exhibit minor  $\text{C}_2\text{H}_6$  production. This observation might suggest differing or slower C1 and C2 formation mechanisms in the latter transition metals than in Fe and Cu. However, further mechanistic studies and theoretical calculations are necessary to elucidate the underlying processes fully. The findings reported here are consistent with those observed in experimental studies involving various Fe species, which have documented high conversion rates to  $\text{CH}_4$  compounds.<sup>14</sup> In addition to Fe compounds, Mn, Co, and Ni catalysts have been shown to exhibit similarly high yields, suggesting that these transition metal species are effective in C1 and C2 formation. Chapter 3.7 will discuss potential implications for the global production of C1 and C2 compounds in detail.

### 3.4.2.2 d<sub>3</sub>-methionine

In a setup conducted analogous to d<sub>6</sub>-DMSO, d<sub>3</sub>-methionine was employed as a substrate to investigate abiotic C1 and C2 production. A comparison of conversion rates in experiments involving d<sub>3</sub>-methionine across various Fe and Mn species (Fe<sub>2</sub>O<sub>3</sub>, FeCl<sub>2</sub>, FeSO<sub>4</sub>, MnCl<sub>2</sub> and MnO<sub>2</sub>) reveals a consistent pattern of C1 and C2 formation observed among these species and lower rates for the Co, Ni and Cu species. In contrast, the LFe<sup>II</sup>Cl<sub>2</sub> complex produced no CH<sub>2</sub>O or CH<sub>3</sub>OH (Chapter 3.2.1). The conversion rates to C<sub>2</sub>H<sub>6</sub> from Fe salts are in a similar range to those of Fe<sub>2</sub>O<sub>3</sub>, as compared to LFe<sup>II</sup>Cl<sub>2</sub>, and generally higher than with the other transition metal species. CH<sub>4</sub> conversion rates for Fe and Mn species are approximately 3%, in contrast to previous studies where conversion rates are 10%.<sup>14</sup> This discrepancy may be attributed to a different setup and using another Fe species (ferrihydrite). However, the conversion rates from d<sub>3</sub>-methionine are lower than those documented for d<sub>6</sub>-DMSO. The observed discrepancy between d<sub>3</sub>-methionine and d<sub>6</sub>-DMSO may be attributed to the different chemical structures resulting in different chemical properties which influence the reaction mechanism. According to preliminary DFT calculations, this reaction with methionine requires a higher activation energy than the calculated activation energy for DMSO.<sup>205</sup>

The data show that d<sub>3</sub>-methionine can be converted to different C1-C2 compounds using various transition metal species as catalysts. Solubility and lattice structure variations may contribute to the observed differences in C1 and C2 conversion rates from distinct transition metal species. The oxidation state and choice of counterion have less influence on C1 and C2 formation than the choice of transition metal, as observed for DMSO. In particular, Cu compounds' C1 and C2 emissions, especially CuCl<sub>2</sub>, differ from those of other transition metal species by exhibiting lower conversion rates. While the high-valent iron-oxo complex formation from LFe<sup>II</sup>Cl<sub>2</sub> is well established<sup>206,211,250</sup>, mechanistic studies for all other transition metal species have yet to be carried out. The demonstration of deuterium incorporation into CD<sub>2</sub>O and CD<sub>3</sub>Cl, evidenced by a mass shift of 2 or 3 AMU in all transition metal catalysts, suggests that a demethylation mechanism analogous to d<sub>6</sub>-DMSO is most likely the reaction mechanism. Thus, isotopic labelling can also be expected for the other C1 and C2 compounds, as CH<sub>3</sub> radicals will likely serve as the primary precursors.

### 3.4.2.3 2-Methoxyphenol

The conversion patterns to C1 and C2 compounds in experiments with 2-methoxyphenol exhibited notable deviations from those observed with S-methylated substrates. Only CH<sub>3</sub>OH and CH<sub>2</sub>O were produced, and no CH<sub>4</sub> or C<sub>2</sub>H<sub>6</sub> was detected. Their absence suggests a lack of CH<sub>3</sub> radicals, as described earlier for Fe<sub>2</sub>O<sub>3</sub> and LFe<sup>II</sup>Cl<sub>2</sub> (Chapter 3.3.3). FeCl<sub>2</sub> and FeSO<sub>4</sub> exhibited CH<sub>3</sub>OH and CH<sub>2</sub>O formation patterns consistent with those observed for the previously described experiments with Fe<sub>2</sub>O<sub>3</sub> and

$\text{LFe}^{\text{II}}\text{Cl}_2$ , suggesting a similar reaction mechanism (Chapter 3.1). In contrast, Mn species exhibited minimal conversion to oxygenated C1 compounds except  $\text{MnSO}_4$  with medium conversion rates, indicating a low catalytic efficiency. Furthermore, the experiments involving Co, Ni, or Cu resulted in the exclusive production of  $\text{CH}_3\text{OH}$ , with a minimal yield of  $\text{CH}_2\text{O}$  in experiments with  $\text{NiSO}_4$ , suggesting a reduced oxidative capacity compared to the Fe species. Notably, the overoxidation from  $\text{CH}_3\text{OH}$  to  $\text{CH}_2\text{O}$  appears unlikely for these transition metal species, in contrast to the Fe and Mn species. Nevertheless, these findings underscore the significant catalytic influence of transition metal species on the degradation of methoxylated substrates under ambient conditions (1013 mbar, 22°C). Potential contributions to the global production of C1 compounds will be discussed in detail in Chapter 3.7.

#### 3.4.2.4 Methyl chloride

$\text{CD}_3\text{Cl}$  has been observed in all experiments involving  $d_6$ -DMSO, with conversion rates of less than  $0.0062 \pm 0.0002$  %, indicative of low production levels compared to the other C1 and C2 compounds. Conversely,  $\text{CuCl}_2$  exhibits a significantly higher abundance of  $\text{CD}_3\text{Cl}$ , with a conversion rate approximately three orders of magnitude higher than the other compounds. However, its concentrations remain relatively low relative to other C<sub>1</sub> and C<sub>2</sub> compounds. The findings on  $\text{CH}_3\text{Cl}$  production are consistent with previous observations on  $d_6$ -DMSO.

The  $\text{CD}_3\text{Cl}$  concentration is quantified with masses 53 and 55 via GC-MS, thereby confirming the  $\text{CD}_3$  group origin from  $d_6$ -DMSO, as the masses are shifted by 3 AMU relative to non-deuterated  $\text{CD}_3\text{Cl}$ . A similar outcome was observed in the case of  $d_3$ -methionine, where  $\text{CD}_3\text{Cl}$  formation was observed to occur at low conversion rates with  $\text{FeCl}_2$  and  $\text{CuCl}_2$ . However, no  $\text{CH}_3\text{Cl}$  was detected in experiments involving 2-methoxyphenol, which may be attributed to the alternative mechanism of  $\text{OCH}_3$  group cleavage, where no  $\text{CH}_3$  radical is formed (Chapter 3.3.2).

Given the similarities in chemical properties exhibited by these chlorine counterions, it can be hypothesised that analogous processes occur in the presence of other halogenated counterions, forming methyl halides. In addition, Keppler et al. (2000) have documented the formation of  $\text{CH}_3\text{Cl}$ ,  $\text{CH}_3\text{Br}$ , and  $\text{CH}_3\text{I}$  in soils, a process catalysed by Fe.<sup>35</sup> This observation, supported by a comparable reaction mechanism involving Fe, provides a compelling argument for the potential formation of other methyl halides. Despite the low conversion rates, the potential impact of this process on the environment cannot be discounted, as the precursor compounds, transition metal species, and ROS are present in substantial quantities in the environment. Consequently, low conversion rates can still result in substantial amounts of halogenated compounds being released, which, in turn, can considerably affect the atmosphere's chemistry.

### 3.5 Lignin and pectin as precursors of CH<sub>4</sub>, C<sub>2</sub>H<sub>6</sub>, CH<sub>3</sub>OH and CH<sub>2</sub>O

Lignin and pectin were investigated the same way as the previous compounds, including sinapyl alcohol, coniferyl alcohol, and Gai (Chapter 3.3), which are monomers of lignin and pectin. Plant matter, particularly cell walls, comprises a significant portion of lignin and pectin, which are important organic components of the soil. It was previously shown that lignin and pectin can emit CH<sub>3</sub>OH and CH<sub>3</sub>Cl under elevated temperatures (> 150°C)<sup>17</sup> and that polygalacturonic acid can emit CH<sub>4</sub> at elevated temperatures (> 40°C) and irradiated with UV light.<sup>269</sup> All these properties of lignin and pectin are of interest for this study and make them possible precursor compounds for various other C1 and C2 compounds.

#### 3.5.1 Formation of CH<sub>4</sub>, C<sub>2</sub>H<sub>6</sub>, CH<sub>3</sub>OH and CH<sub>2</sub>O from lignin and pectin under abiotic and oxic conditions

To investigate the environmental implications of these reactions, pure lignin and pectin (50 mg dry weight) were studied for their potential to produce CH<sub>3</sub>OH, CH<sub>2</sub>O, CH<sub>4</sub> and C<sub>2</sub>H<sub>6</sub> (Figure 33) using 10 μmol Fe<sub>2</sub>O<sub>3</sub>, 100 μmol Asc and 200 μmol H<sub>2</sub>O<sub>2</sub> in different setups (Table 11) following the procedure described in Chapter 2.1.1. The C1 and C2 compounds were shown in concentrations instead of conversion rates for comparison with other studies and the fact that lignin and pectin are weighed in grams.

Table 11: Composition of the experiments with lignin or pectin and with or without Fe<sub>2</sub>O<sub>3</sub> and Asc to determine the conversion rates and possible differences.

No.	Precursor compound	Fe species	Oxidant	acid
1	Lignin	10 μmol Fe <sub>2</sub> O <sub>3</sub>	200 μmol H <sub>2</sub> O <sub>2</sub>	100 μmol Asc
2	Lignin	10 μmol Fe <sub>2</sub> O <sub>3</sub>	200 μmol H <sub>2</sub> O <sub>2</sub>	0.05 μmol Triflic acid
3	Lignin	-	200 μmol H <sub>2</sub> O <sub>2</sub>	0.05 μmol Triflic acid
4	Pectin	10 μmol Fe <sub>2</sub> O <sub>3</sub>	200 μmol H <sub>2</sub> O <sub>2</sub>	100 μmol Asc
5	Pectin	10 μmol Fe <sub>2</sub> O <sub>3</sub>	200 μmol H <sub>2</sub> O <sub>2</sub>	0.05 μmol Triflic acid
6	Pectin	-	200 μmol H <sub>2</sub> O <sub>2</sub>	0.05 μmol Triflic acid

The highest concentrations of CH<sub>3</sub>OH and CH<sub>2</sub>O (Figure 33a) were observed in experiments with Fe<sub>2</sub>O<sub>3</sub> and Asc for both lignin (399 ± 28 μg/g, No. 1) or pectin (422 ± 52 μg/g, No. 4). In experiments without Asc and Fe<sub>2</sub>O<sub>3</sub>, the concentrations are lower at 251 ± 31 μg/g<sub>d</sub> for lignin (No. 2) and 311 ± 76 μg/g for pectin (No. 5). Moreover, experiments without Fe<sub>2</sub>O<sub>3</sub> and Asc resulted in concentrations of 307 ± 24 μg/g for lignin (No. 3) and 106 ± 8 μg/g for pectin (No. 6). Additionally, the production of CH<sub>4</sub> and C<sub>2</sub>H<sub>6</sub>

was observed (Figure 33b). Notably, hydrocarbons were only detected in the presence of Asc (lignin:  $2.76 \pm 0.04 \mu\text{g/g}$  and pectin:  $1.44 \pm 0.04 \mu\text{g/g}$ ), with concentrations two orders of magnitude lower than those of the oxygenated compounds. Experiments conducted without Asc did not yield any hydrocarbon production.

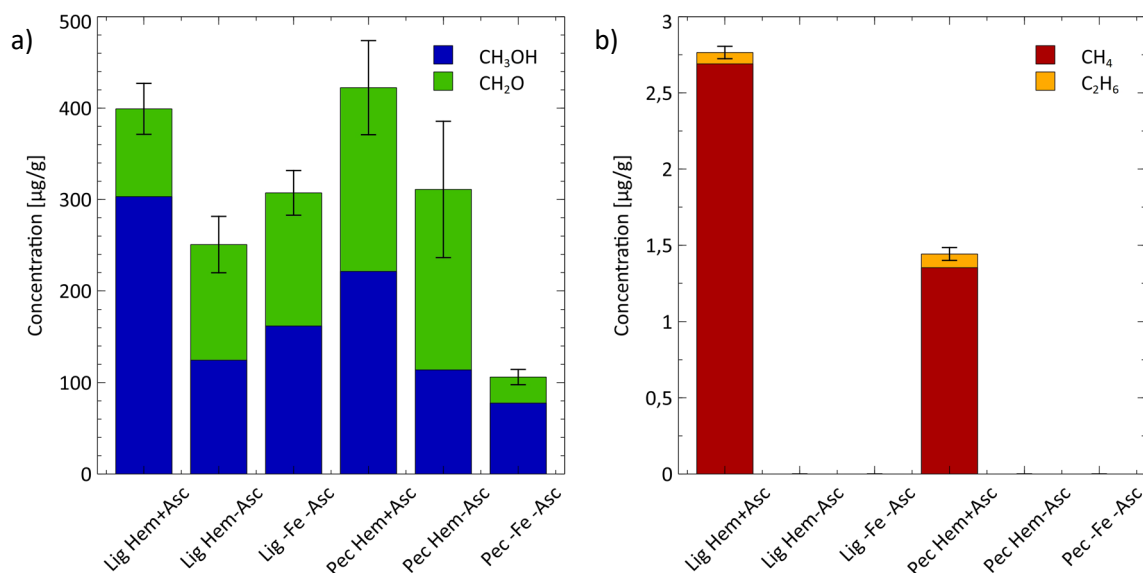


Figure 33: Formation of **a)** CH<sub>3</sub>OH and CH<sub>2</sub>O and **b)** CH<sub>4</sub> and C<sub>2</sub>H<sub>6</sub> were detected in experiments involving 50 mg (dry weight) of either lignin or pectin. These experiments were carried out with either 10 μmol Fe<sub>2</sub>O<sub>3</sub> and 100 μmol Asc or without Asc and 10 μmol Fe<sub>2</sub>O<sub>3</sub>, and the third experiment with 0.05 μmol triflic acid and no Fe<sub>2</sub>O<sub>3</sub> and with 200 μmol H<sub>2</sub>O<sub>2</sub> in each experiment under ambient atmospheric conditions with a reaction time of 48 h. Error bars refer to the SD of the total conversion of all major C1 and C2 compounds for n = 9, except for CH<sub>4</sub> and C<sub>2</sub>D<sub>6</sub>, n = 3.

### 3.5.2 Discussion of the production CH<sub>4</sub>, C<sub>2</sub>H<sub>6</sub>, CH<sub>3</sub>OH and CH<sub>2</sub>O and the influence of Fe<sub>2</sub>O<sub>3</sub>, H<sub>2</sub>O<sub>2</sub> and Asc

Lignin and pectin exhibit elevated concentrations of CH<sub>3</sub>OH and CH<sub>2</sub>O, analogous to those observed in OCH<sub>3</sub>-containing substrates with Fe<sub>2</sub>O<sub>3</sub>, H<sub>2</sub>O<sub>2</sub> and Asc. A contrasting picture emerges when the experiments with and without Asc but with triflic acid are compared in the context of sinapyl alcohol and lignin. While sinapyl alcohol yields are lower in the presence of Asc, lignin experiments exhibit higher concentrations of CH<sub>3</sub>OH and CH<sub>2</sub>O (Chapter 3.3.1). These discrepancies can be attributed to the complex three-dimensional structure of lignin, which allows for a multitude of side reactions. In the case of Game and pectin, analogous trends can be observed. Here, structural differences are confined to the cross-links between the Game monomeric units in pectin, and the potential for additional side reactions is limited. Nevertheless, a comparable reaction could be feasible.

In the case of experiments conducted solely with H<sub>2</sub>O<sub>2</sub> and lignin or pectin, respectively, a contrasting pattern emerges. In lignin experiments, the absence of Asc and Fe<sub>2</sub>O<sub>3</sub> results in CH<sub>3</sub>OH and CH<sub>2</sub>O concentrations comparable to those observed in their presence. In contrast, pectin experiments show a notable decline in CH<sub>3</sub>OH and CH<sub>2</sub>O concentrations in the absence of Asc and Fe<sub>2</sub>O<sub>3</sub>. This discrepancy may be attributed to differing reaction mechanisms observed in the experiments with the absence of Fe<sub>2</sub>O<sub>3</sub> compared to those conducted with Fe<sub>2</sub>O<sub>3</sub>. In the latter, an iron-oxo species ([Fe<sup>IV</sup>=O]<sup>2+</sup>) is responsible for initiating the reaction, whereas, in the former, H<sub>2</sub>O<sub>2</sub> and possibly other radicals like O<sub>2</sub><sup>-</sup> or OH may directly interact with the substrate. Also, differences in the general structure of these molecules are evident, with an aromatic system in lignin and a non-aromatic system in pectin. This may also account for variations in the product concentrations.

The observed release of CH<sub>3</sub>OH from methoxybenzenes and lignin is a well-described process in the literature, but always at high temperatures and pressures and regularly under an H<sub>2</sub> atmosphere; therefore, a comparison is not feasible. It is well known that wood (lignin) releases low amounts of CH<sub>2</sub>O<sup>133</sup>; a lignin-mediated Fenton generation of CH<sub>2</sub>O is postulated with the OH radical attacking the OCH<sub>3</sub> group and releasing CH<sub>2</sub>O. That is enhanced with rising H<sub>2</sub>O<sub>2</sub> and Fe concentrations.<sup>132</sup> This mechanism is similar to the investigated here, but the mechanism remains unclear, and no direct evidence has been provided for the origin of the CH<sub>2</sub>O.

Adding Asc to experiments with lignin or pectin resulted in a significant increase in CH<sub>4</sub> and C<sub>2</sub>H<sub>6</sub> production. Conversely, no hydrocarbon production was observed in the absence of Asc. These findings indicate that an OH radical scavenger, such as Asc, is essential for facilitating hydrocarbon production. These findings are analogous to the reactions described earlier with DMSO (Chapter 3.1). Still, the ratio of CH<sub>3</sub>OH + CH<sub>2</sub>O to CH<sub>4</sub> + C<sub>2</sub>H<sub>6</sub> is two orders of magnitude higher than in the experiments with DMSO (approximately 1:1). This discrepancy may also be attributed to different reaction mechanisms. In the case of the DMSO, all C1 and C2 compounds are produced from a CH<sub>3</sub> radical, whereas CH<sub>3</sub>OH and CH<sub>2</sub>O are produced from the whole OCH<sub>3</sub> group of methoxyphenols and presumably from the OCH<sub>3</sub> group of lignin and pectin. A multitude of side chains from lignin and pectin could act as precursors of the hydrocarbons. A decay of lignin or pectin itself due to the highly oxidative milieu and subsequent reactions could also lead to the production of hydrocarbons. A release of CH<sub>4</sub> from OCH<sub>3</sub> groups of pectin is reported at elevated temperatures with greater than 40°C and isotically confirmed.<sup>269</sup> The origin of CH<sub>4</sub> and C<sub>2</sub>H<sub>6</sub> is unclear and requires further investigation. With isotopically labelled precursor substances, as described in Keppler et al. (2008)<sup>269</sup>, more knowledge could be gained concerning the origin of CH<sub>4</sub> and C<sub>2</sub>H<sub>6</sub>.

### 3.6 Abiotic and oxic production of CH<sub>3</sub>OH, CH<sub>2</sub>O, CH<sub>4</sub> and C<sub>2</sub>H<sub>6</sub> from sterile soils and their controlling factors<sup>2</sup>

Experiments were conducted using 24 soil samples (5 g) that were sterilised at 105°C and homogenised and incubated with 10 ml ultra-pure H<sub>2</sub>O and subsequently analysed for CH<sub>3</sub>OH, CH<sub>2</sub>O, CH<sub>4</sub> and C<sub>2</sub>H<sub>6</sub>. Establishing a direct link between the studies with precursor compounds and natural processes, especially soils where high concentrations of lignin and pectin are found, provides a perfect objective for studying the formation of C1 and C2 compounds. All relevant reactants and additives employed in the previous investigations, including transition metal precursors (e.g., Fe<sub>2</sub>O<sub>3</sub>), organic substrates possessing CH<sub>3</sub> groups, H<sub>2</sub>O<sub>2</sub>, and OH radical scavengers such as ascorbic acid, naturally occur in soils. Consequently, experiments were conducted on various soil types, including modifications to the OCH<sub>3</sub> content, wet-dry cycles (WDC), pH adjustments, and temperature variations. The degradation of CH<sub>3</sub>OH in untreated soils was also investigated. Additionally, the OCH<sub>3</sub> content and TOC of the soils were determined to enable preliminary estimation of the global impact of the abiotic processes described herein.

#### 3.6.1 Production of CH<sub>3</sub>OH, CH<sub>2</sub>O, CH<sub>4</sub> and C<sub>2</sub>H<sub>6</sub> from sterile soils under abiotic and atmospheric conditions

Following the protocols described in Chapter 2.1.4, 24 sterilised and homogenised soils (5 g each) were incubated with ultra-pure H<sub>2</sub>O (10 ml) for 48 h. Following incubation, the samples were analysed for the presence of CH<sub>3</sub>OH and CH<sub>2</sub>O in the H<sub>2</sub>O phase and CH<sub>4</sub> and C<sub>2</sub>H<sub>6</sub> in the headspace. All 24 soils from the different locations and sampling depths (Chapter 2.1.4.2) emitted oxygenated compounds and hydrocarbons. The concentrations of CH<sub>3</sub>OH ranged from  $0.76 \pm 0.03 \mu\text{g}/\text{g}_{\text{soil,dw}}$  to  $18.0 \pm 0.6 \mu\text{g}/\text{g}_{\text{soil,dw}}$ , except for WA2 10-40, where no CH<sub>3</sub>OH could be measured. The concentrations of CH<sub>2</sub>O ranged from  $0.41 \pm 0.53 \mu\text{g}/\text{g}_{\text{soil,dw}}$  to  $21.4 \pm 1.0 \mu\text{g}/\text{g}_{\text{soil,dw}}$  (Figure 34a). For CH<sub>4</sub> concentrations between 0 and  $6.50 \pm 0.30 \text{ ng}/\text{g}_{\text{soil,dw}}$  could be determined; furthermore, for C<sub>2</sub>H<sub>6</sub>  $0.02 \pm 0.02 \text{ ng}/\text{g}_{\text{soil,dw}}$  to  $2.65 \pm 0.20 \text{ ng}/\text{g}_{\text{soil,dw}}$  concentrations were observed (Figure 34b).

---

<sup>2</sup> Please note that parts of this section are taken from Hädel et al (2023)<sup>205</sup>.

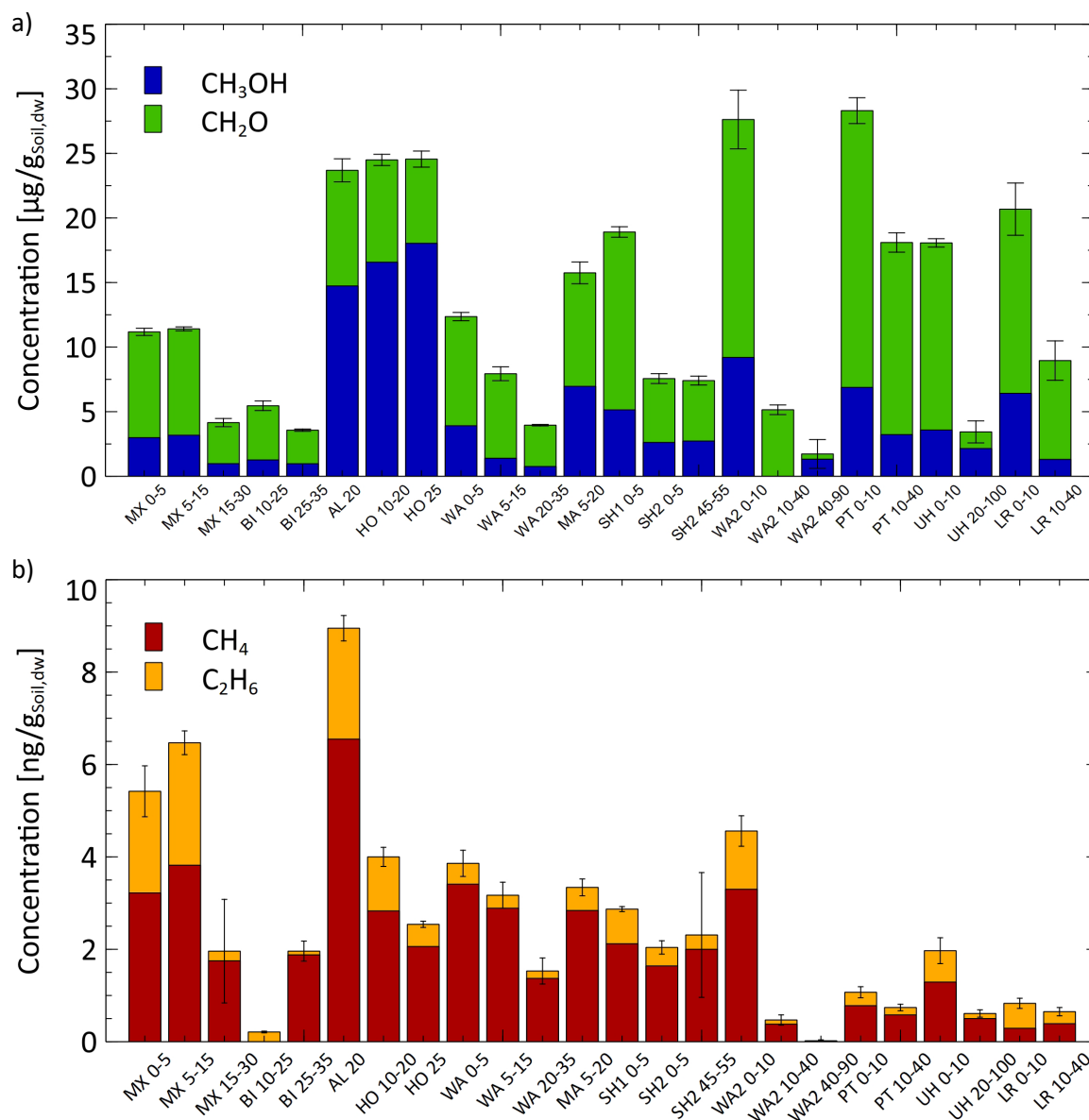


Figure 34: abiotic formation of  $\text{CH}_3\text{OH}$ ,  $\text{CH}_2\text{O}$ ,  $\text{CH}_4$ , and  $\text{C}_2\text{H}_6$  from 24 sterilised soils at  $105^\circ\text{C}$  (5 g each, with indicated depths in cm) using ultra-pure  $\text{H}_2\text{O}$  (10 ml), incubated for 48 h under ambient conditions ( $22^\circ\text{C}$  and 1013 mbar). **a)**  $\text{CH}_3\text{OH}$  and  $\text{CH}_2\text{O}$  were displayed in  $\mu\text{g}/\text{g}_{\text{soil,dw}}$ , with three orders of magnitude lower concentrations for **b)**  $\text{CH}_4$  and  $\text{C}_2\text{H}_6$  displayed in  $\text{ng}/\text{g}_{\text{soil,dw}}$ . Error bars refer to the SD of the total conversion of all major C1 and C2 compounds for  $n = 9$ , except for  $\text{CH}_4$  and  $\text{C}_2\text{H}_6$ ,  $n = 3$ . Parts of the data are taken from Hädel et al. (2023).<sup>205</sup>

### 3.6.2 Methoxy groups in soils as a precursor of $\text{CH}_3\text{OH}$ , $\text{CH}_2\text{O}$ , $\text{CH}_4$ and $\text{C}_2\text{H}_6$

To determine whether  $\text{OCH}_3$  groups in soils serve as precursors to  $\text{CH}_3\text{OH}$ ,  $\text{CH}_2\text{O}$ ,  $\text{CH}_4$  and  $\text{C}_2\text{H}_6$ , they were removed using the Zeisel method (Chapter 2.2.2.4) in three different soils that produced high amounts of  $\text{CH}_3\text{OH}$ ,  $\text{CH}_2\text{O}$ ,  $\text{CH}_4$  and  $\text{C}_2\text{H}_6$ . Figure 35a illustrates  $\text{OCH}_3$  content in three different soil samples before and after HI treatment, which causes the removal of the  $\text{OCH}_3$  group and the reduction ranging from 81.1 % to 93.6 %. The soil samples with high organic content, in which the  $\text{OCH}_3$  group

were removed, were then incubated as described in Chapter 2.1.4 and the concentrations of  $\text{CH}_3\text{OH}$  and  $\text{CH}_2\text{O}$  were analysed. The results demonstrated an absence of  $\text{CH}_3\text{OH}$  and a reduction in  $\text{CH}_2\text{O}$  concentrations by 28.8 % to 83.5 % in HI-treated soils (Figure 35b). Furthermore, the removal of  $\text{OCH}_3$  groups resulted in a decrease in  $\text{CH}_4$  concentration by 81.4 % to 96 %. A reduction in the concentrations of  $\text{C}_2\text{H}_6$  by 40 % and 96 % was also noted in the PT and WA2 soils, respectively. Conversely, a substantial increase of 590 % was recorded for soil AL 20 (Figure 35c).

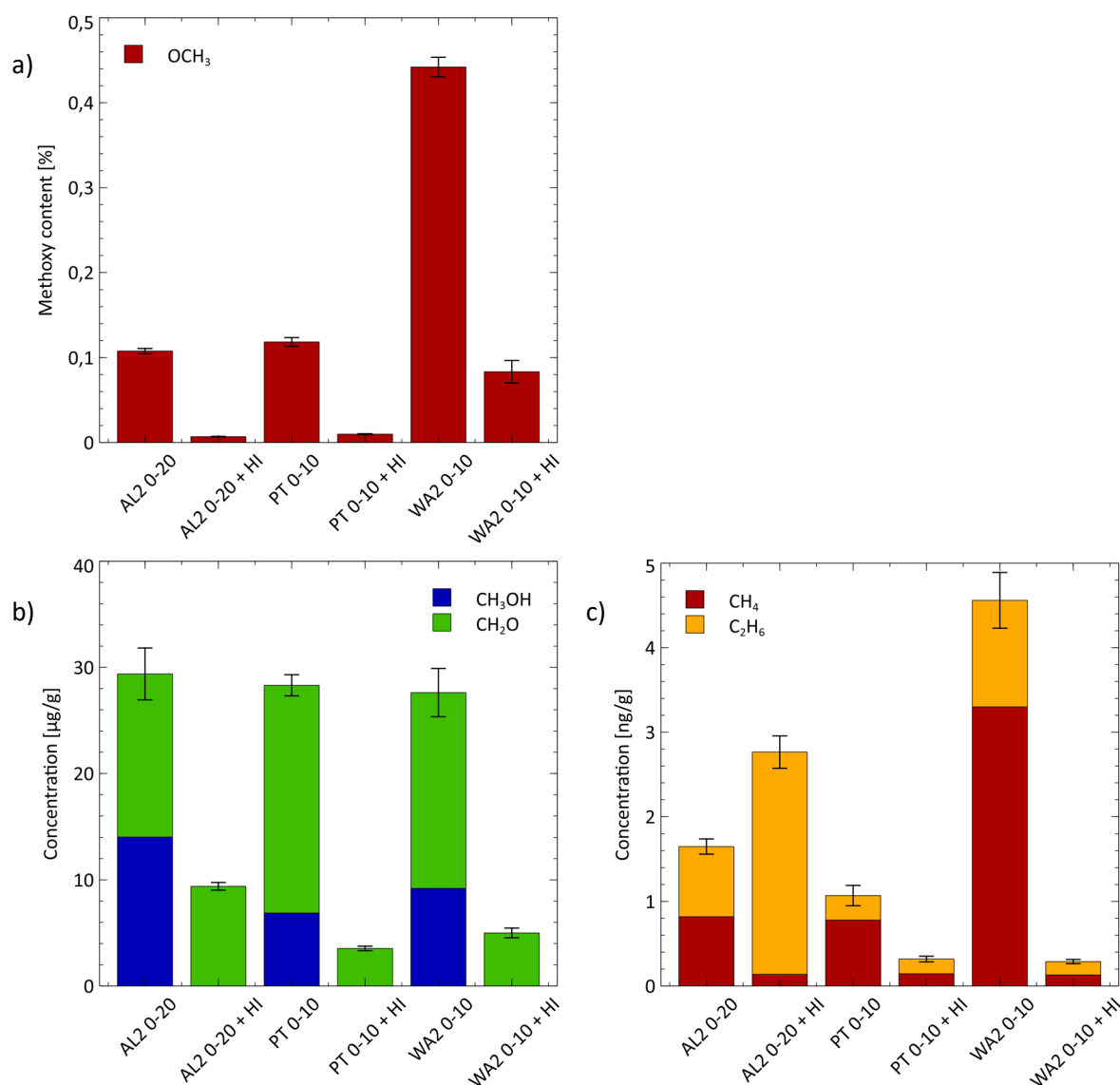


Figure 35: **a)**  $\text{OCH}_3$  content in soil samples AL 20, PT 0-10 and WA2 0-10 before and after  $\text{OCH}_3$  removal due to HI treatment. **b)** Comparison of the concentrations of  $\text{CH}_3\text{OH}$  and  $\text{CH}_2\text{O}$  and **c)**  $\text{CH}_4$  and  $\text{C}_2\text{H}_6$  from soil experiments with and without  $\text{OCH}_3$  group removal. Error bars refer to the SD of the total conversion of all major C1 and C2 compounds for  $n = 9$ , except for  $\text{CH}_4$  and  $\text{C}_2\text{D}_6$ ,  $n = 3$ .

### 3.6.3 Identification of the origin of CH<sub>3</sub>OH in soils with deuterated or <sup>18</sup>O-OCH<sub>3</sub> labelled 2-methoxyphenol

The three soils from which the OCH<sub>3</sub> group was removed were used. 1 g soil each was mixed with 2 ml H<sub>2</sub>O, and then 5 μmol deuterated or <sup>18</sup>O-OCH<sub>3</sub> labelled 2-methoxyphenol was added to the incubation to show that the soil splits off the whole OCH<sub>3</sub> group. By measuring CH<sub>3</sub>OH and the masses 33, 34 and 35, Figure 36 clearly shows the production of the deuterated CH<sub>3</sub>OH in these soils. This is evident due to the pronounced peaks observed in experiments utilising deuterated 2-methoxyphenol and measuring the mass shift from 32 to 33-35 (Figure 36a). Also, measuring the mass 33 and 34 from CH<sub>3</sub>OH in experiments with <sup>18</sup>O-labelled 2-methoxyphenol (Figure 36b) and the resulting peaks for these experiments demonstrate the origin of CH<sub>3</sub>OH from the OCH<sub>3</sub> group of 2-methoxyphenol. The unlabelled soils and ultra-pure H<sub>2</sub>O as controls exhibit minimal to no peaks. These experiments demonstrate that the OCH<sub>3</sub> group is cleaved off in soils and forms CH<sub>3</sub>OH only by adding H<sub>2</sub>O.

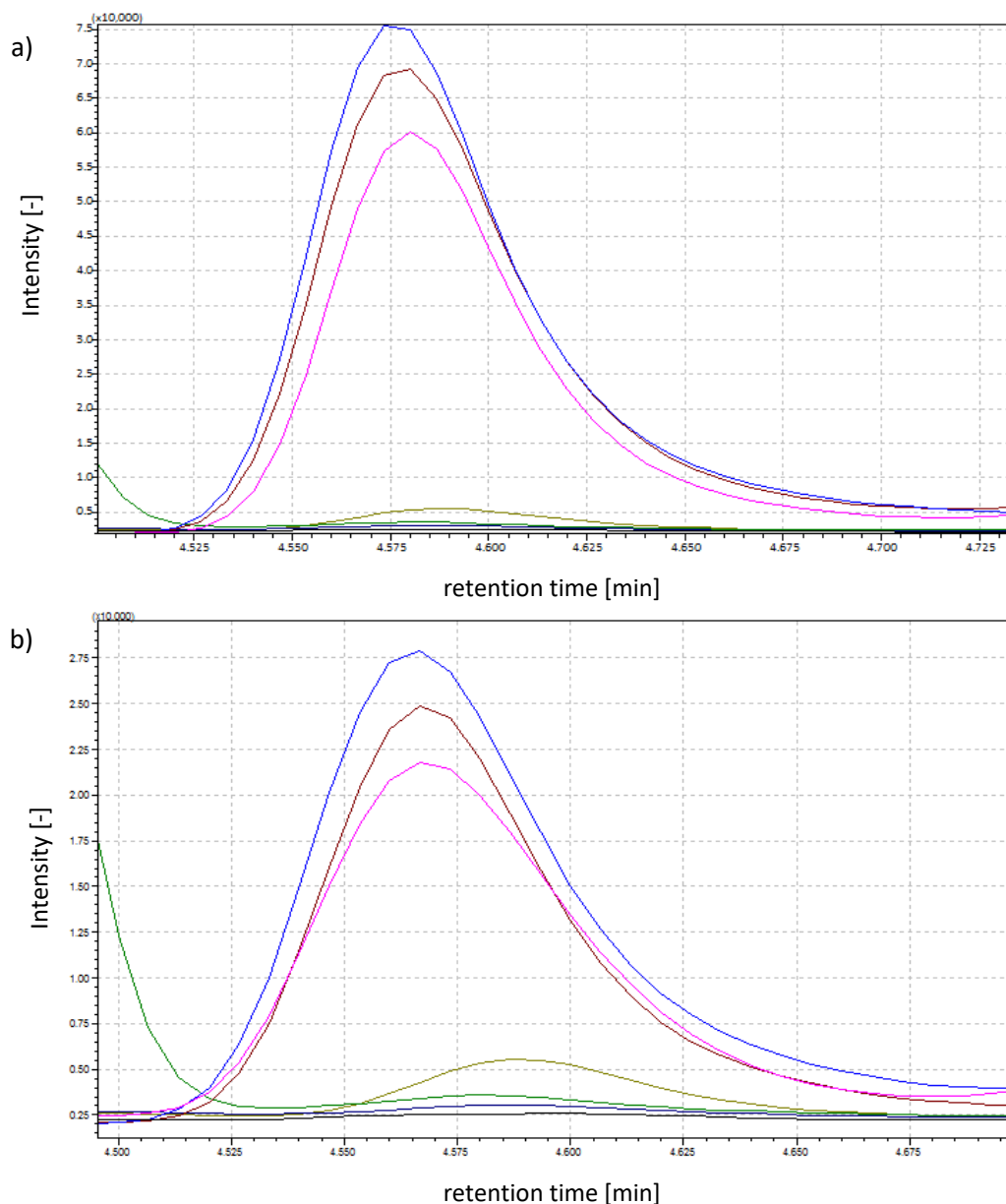


Figure 36: Chromatogram of labelled  $CH_3OH$  in soil experiments with added deuterated or  $^{18}O$ - $OCH_3$  labelled 2-Methoxyphenol. The m/z 33, 34 and 35 of  $CD_3OH$  **a)** or m/z 33 and 34 of  $CH_3^{18}OH$  **b)** in experiments where the  $OCH_3$  groups were removed from the soil samples GL1, PO and GL2 using the Zeisel method. 1 g soil and 2 ml ultra-pure  $H_2O$  with added 5  $\mu mol$  **a)** deuterated  $OCH_3$ -2-Methoxyphenol and **b)** 5  $\mu mol$   $^{18}O$ - $OCH_3$ -2-Methoxyphenol. Blue, brown and pink are the experiments with labelled 2-methoxyphenol; light green, dark green and purple are the non-spiked soils, and black is pure  $H_2O$ .

### 3.6.4 Determination of the ability of soils to degrade $d_6$ -DMSO

To investigate whether soils have the capacity to convert substrates with S-bonded  $CH_3$  groups to  $CH_3OH$  and  $CH_2O$ , 25  $\mu mol$   $d_6$ -DMSO was added to soils WF, MX, BI, AL1, HO WA1, MA, SH1 and SH2.

The formation of  $\text{CD}_3\text{OH}$  and  $\text{CD}_2\text{O}$  was observed in these soil samples, as illustrated by one example in Figure 37 and Figure 38. Deuterium labelling of  $\text{CH}_3\text{OH}$  and  $\text{CH}_2\text{O}$  is evidenced by a mass shift of 3 or 2 AMU, respectively, as previously described (Chapter 3.1.5.1). It can be hypothesised that  $\text{CH}_4$  and  $\text{C}_2\text{H}_6$  can also be formed from  $\text{d}_6\text{-DMSO}$ , as described in Chapter 3.1.5.1. As demonstrated in Chapter 3.2, N- or P-bonded  $\text{CH}_3$  groups can also produce  $\text{CH}_3\text{OH}$ ,  $\text{CH}_2\text{O}$ ,  $\text{CH}_4$  and  $\text{C}_2\text{H}_6$ , which lends evidence to support the hypothesis that these can also be converted within the soil.

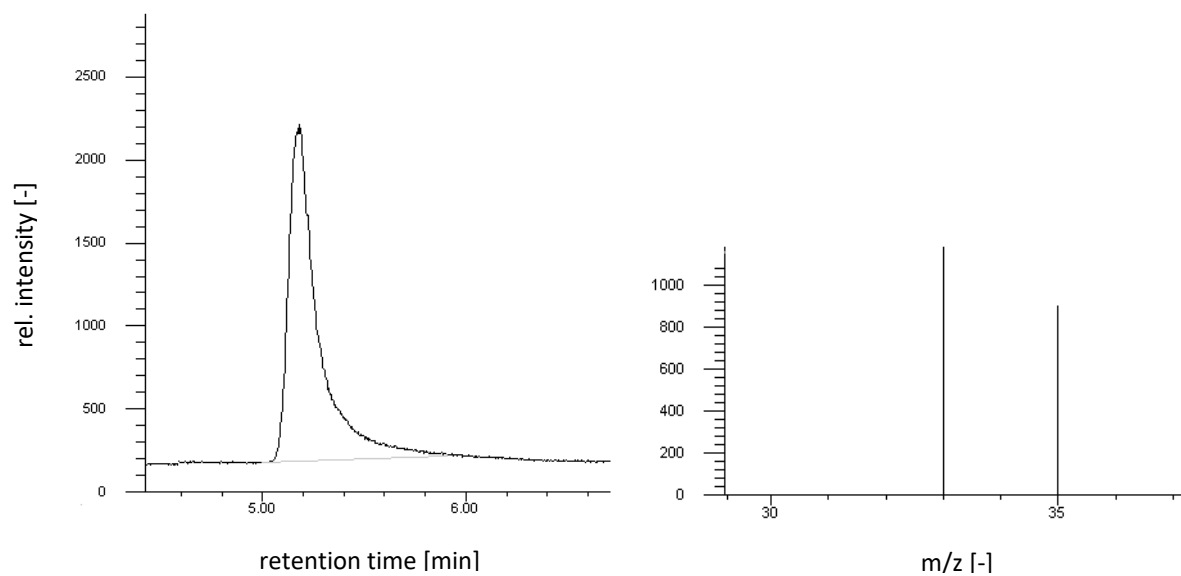


Figure 37: Chromatogram and mass track 33 and 35 of deuterated  $\text{CH}_3\text{OH}$  in an experiment with 5 g sterile soil (WF 0-5) in 10 ml ultra-pure  $\text{H}_2\text{O}$  and 25  $\mu\text{mol}$   $\text{d}_6\text{-DMSO}$ . Taken from Hädeler et al. (2023).<sup>205</sup>

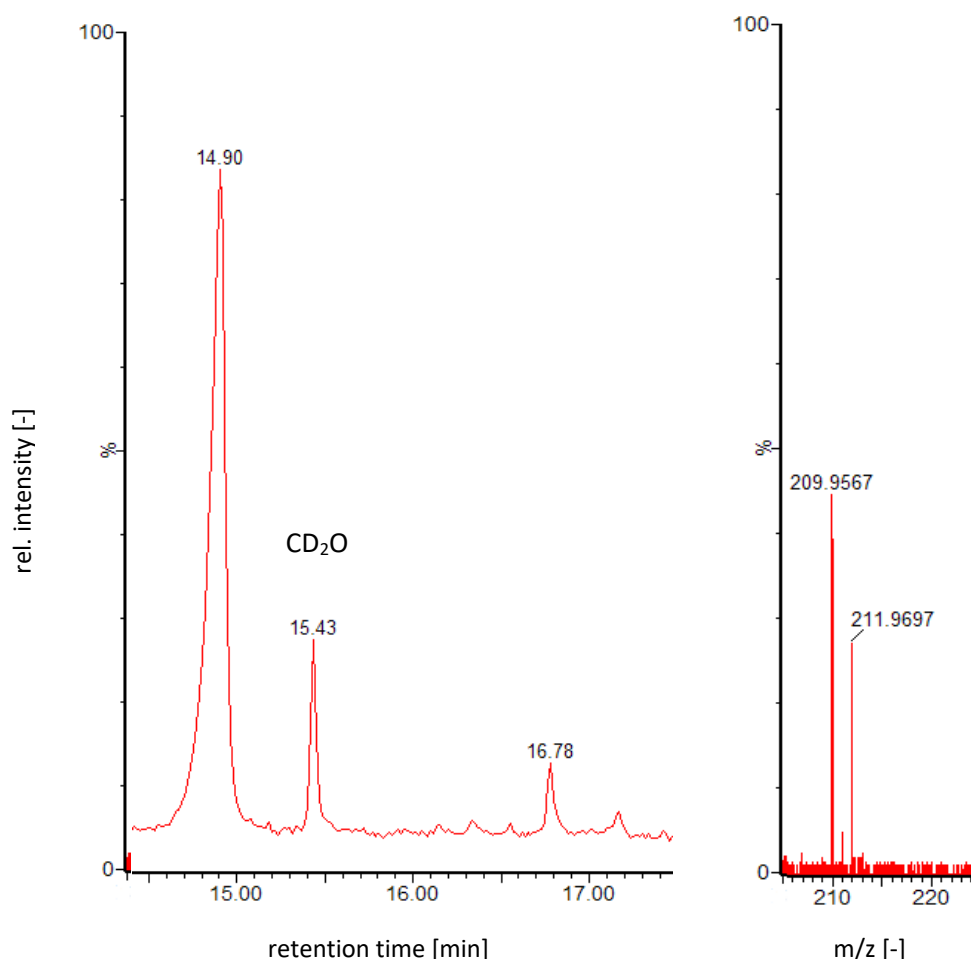


Figure 38: Chromatogram and mass track 210 and 212 of deuterated and derivatised CH<sub>2</sub>O in an experiment with 5 g sterile soil (WF 0-5) in 10 ml ultra-pure H<sub>2</sub>O and d<sub>6</sub>-DMSO. Taken from Hädeler et al. (2023).<sup>205</sup>

### 3.6.5 Wet-dry cycles with soils and their effect on CH<sub>3</sub>OH and CH<sub>2</sub>O formation

The objective of the 10 wet-dry cycles was to observe the soils' behaviour when subjected to a drying and subsequent rewetting process. Soil samples UH 0-10 and AL 20 were chosen because of their high organic content and different genesis (Chapter 2.1.4.2), and a third experiment was conducted with AL 20, where 200 μmol H<sub>2</sub>O<sub>2</sub> was added (Figure 39). This was done to see whether higher concentrations of oxidant impact the concentrations of the products. The investigation was focused on CH<sub>3</sub>OH and CH<sub>2</sub>O formation, as these are the C1 compounds with the highest concentrations in the soil investigations and have a high impact on carbon cycling and the chemical composition of the soil.

The concentration of CH<sub>3</sub>OH in all soil samples in all WDCs was within the range of  $4.44 \pm 0.21 \mu\text{g}/\text{g}_{\text{soil,dw}}$  to  $6.18 \pm 0.35 \mu\text{g}/\text{g}_{\text{soil,dw}}$ , with a general downward trend with continuing cycles (Figure 39a). However, there were exceptions with higher concentrations, particularly in the second and third cycles. Following ten cycles of wetting and drying, the concentration is observed to range between  $0.98 \pm 0.25 \mu\text{g}/\text{g}_{\text{soil,dw}}$  and  $1.55 \pm 0.30 \mu\text{g}/\text{g}_{\text{soil,dw}}$ . The total concentration after 10 cycles of CH<sub>3</sub>OH is  $17.6 \pm 1.1$

$\mu\text{g}/\text{g}_{\text{soil,dw}}$ ,  $30.2 \pm 1.6 \mu\text{g}/\text{g}_{\text{soil,dw}}$  and  $49.5 \pm 2.7 \mu\text{g}/\text{g}_{\text{soil,dw}}$  for soil UH 0-10, AL 20 and AL 20 with  $\text{H}_2\text{O}_2$ , respectively.

A differentiated pattern is evident for  $\text{CH}_2\text{O}$  compared with  $\text{CH}_3\text{OH}$ , with overall higher concentrations (Figure 39b). The starting concentrations in the samples were  $7.49 \pm 0.39 \mu\text{g}/\text{g}_{\text{soil,dw}}$ ,  $6.55 \pm 0.75 \mu\text{g}/\text{g}_{\text{soil,dw}}$  and  $14.5 \pm 0.8 \mu\text{g}/\text{g}_{\text{soil,dw}}$   $\text{CH}_2\text{O}$  for soil UH 0-10, AL 20 and AL 20 with  $\text{H}_2\text{O}_2$ , respectively. The final concentrations of  $\text{CH}_2\text{O}$  are  $8.40 \pm 0.33 \mu\text{g}/\text{g}_{\text{soil,dw}}$ ,  $6.80 \pm 0.25 \mu\text{g}/\text{g}_{\text{soil,dw}}$  and  $4.92 \pm 0.59 \mu\text{g}/\text{g}_{\text{soil,dw}}$  for soils UH 0-10, AL 20 and AL 20 with  $\text{H}_2\text{O}_2$ , respectively. Furthermore, the measurement of AL 20 with  $\text{H}_2\text{O}_2$  failed at the 9th WDC and AL 20 in the 10th WDC due to technical issues. No discernible trends are evident for UH 0-10 and AL 20, with a slight decline observed for AL 20 with  $\text{H}_2\text{O}_2$ . The sum of all concentrations observed is  $51.8 \pm 1.35 \mu\text{g}/\text{g}_{\text{soil,dw}}$  for UH 0-10,  $85.7 \pm 2.3 \mu\text{g}/\text{g}_{\text{soil,dw}}$  for AL 20, and  $86.7 \pm 2.4 \mu\text{g}/\text{g}_{\text{soil,dw}}$   $\text{CH}_2\text{O}$  for AL 20 with  $\text{H}_2\text{O}_2$ .

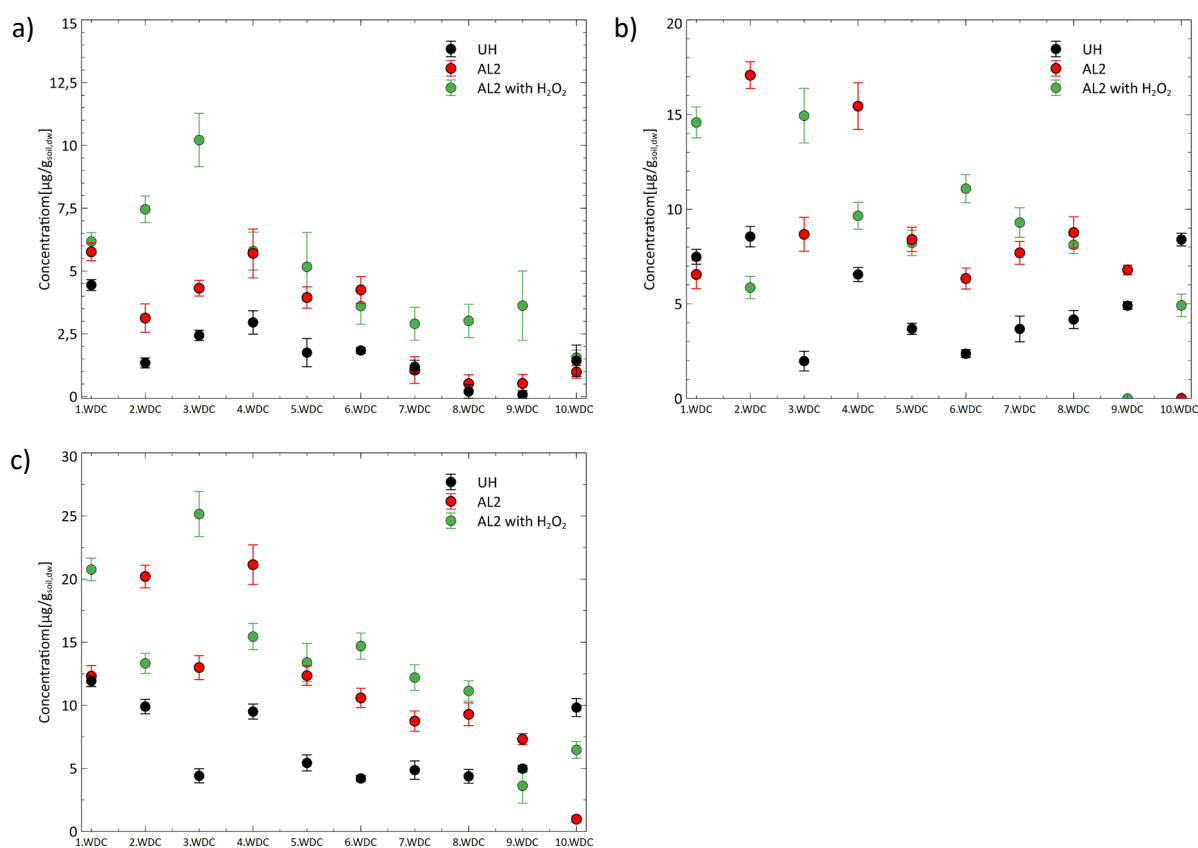


Figure 39:  $\text{CH}_3\text{OH}$  **a)** and  $\text{CH}_2\text{O}$  **b)** concentrations in 10 wet-dry-cycle experiments (5 g soil with 10 ml  $\text{H}_2\text{O}$ ; 2-day wetting phase and then sterilisation at  $105^\circ\text{C}$ ) of soil UH 0-10 and AL 20 (also with added  $\text{H}_2\text{O}_2$ ) and the sum of  $\text{CH}_3\text{OH}$  and  $\text{CH}_2\text{O}$  concentrations **c)**. Error bars refer to the SD of the total conversion of  $\text{CH}_3\text{OH}$  and  $\text{CH}_2\text{O}$  for  $n = 9$ .

The sum of  $\text{CH}_3\text{OH}$  and  $\text{CH}_2\text{O}$  results in a discernible decline in the values of all three WDCs (Figure 39c). The starting concentrations range from  $11.9 \pm 0.5 \mu\text{g}/\text{g}_{\text{soil,dw}}$  to  $20.7 \pm 0.9 \mu\text{g}/\text{g}_{\text{soil,dw}}$ , with values between  $6.47 \pm 0.67 \mu\text{g}/\text{g}_{\text{soil,dw}}$  and  $9.82 \pm 0.71 \mu\text{g}/\text{g}_{\text{soil,dw}}$  observed in the ninth and tenth WDCs. The

summed concentrations are  $69.4 \pm 1.8 \mu\text{g}/\text{g}_{\text{soil,dw}}$  for UH 0-10,  $115 \pm 3 \mu\text{g}/\text{g}_{\text{soil,dw}}$  for AL 20 and  $136 \pm 4 \mu\text{g}/\text{g}_{\text{soil,dw}}$  for AL 20 with  $\text{H}_2\text{O}_2$ .

### 3.6.6 Influence of pH variations on soil and the impact on $\text{CH}_3\text{OH}$ , $\text{CH}_2\text{O}$ , $\text{CH}_4$ and $\text{C}_2\text{H}_6$ production

To gain insights into the impact of pH change on the formation of  $\text{CH}_3\text{OH}$ ,  $\text{CH}_2\text{O}$ ,  $\text{CH}_4$  and  $\text{C}_2\text{H}_6$ , NaOH was added to the soil sample PT 0-10, which has the lowest pH of all soil samples (pH 3.2), and the soil sample was then incubated at pH values of 3.9, 5.2, 6.2 and 6.9 (Figure 40). The concentration of  $\text{CH}_3\text{OH}$  exhibited gradually increased from  $6.88 \pm 0.06$  to  $26.0 \pm 4.8 \mu\text{g}/\text{g}_{\text{soil,dw}}$  with rising pH levels. Conversely, the concentration of  $\text{CH}_2\text{O}$  demonstrated a consistent decline from  $21.4 \pm 1.0$  to  $6.49 \pm 0.33 \mu\text{g}/\text{g}_{\text{soil,dw}}$ , except for the pH 6.9.

The total concentration of  $\text{CH}_3\text{OH} + \text{CH}_2\text{O}$  remains constant at approximately  $25 \mu\text{g}/\text{g}_{\text{soil,dw}}$  within the error margins except for pH 6.9, where total concentrations of  $41.2 \pm 6.1 \mu\text{g}/\text{g}_{\text{soil,dw}}$  were observed. No major changes were observed in the concentrations of  $\text{CH}_4$  and  $\text{C}_2\text{H}_6$ , except at pH 3.9, where a slight increase in the concentration of  $\text{CH}_4$  was noted. The attempt to modify the pH value from a high to a low pH in various soil samples was unsuccessful due to the decomposition of the soil matrix, the inability to take  $\text{H}_2\text{O}$  samples, and the consequence of obtaining reliable measurements.

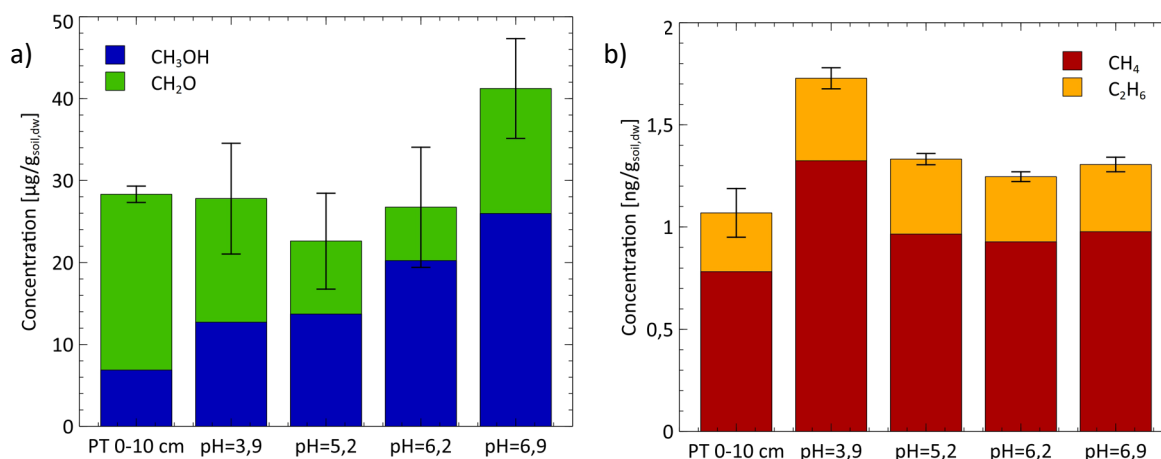


Figure 40: Measurement of  $\text{CH}_3\text{OH}$ ,  $\text{CH}_2\text{O}$  a) and  $\text{CH}_4$  and  $\text{C}_2\text{H}_6$  b) in soil sample PT 0-10 (5 g and 10 ml  $\text{H}_2\text{O}$ ) with the adjustment of the pH-value with NaOH. Error bars refer to the SD of the total conversion of all major C1 and C2 compounds for  $n = 9$ , except for  $\text{CH}_4$  and  $\text{C}_2\text{D}_6$ ,  $n = 3$ .

### 3.6.7 Variation of incubation temperature in soil and the influence on $\text{CH}_3\text{OH}$ , $\text{CH}_2\text{O}$ , $\text{CH}_4$ and $\text{C}_2\text{H}_6$ production

The impact of temperature (-26, 6, 12, 22, 30, 40 and  $50^\circ\text{C}$ ) on the soil experiments was investigated using soil WA2 0-10 as a case study (Figure 41). It was selected because of the previously observed

high production of  $\text{CH}_3\text{OH}$ ,  $\text{CH}_2\text{O}$ ,  $\text{CH}_4$ , and  $\text{C}_2\text{H}_6$ , which were again analysed. The concentration of  $\text{CH}_3\text{OH}$  exhibited a gradual increase with increasing temperature, from  $2.14 \pm 0.33 \mu\text{g}/\text{g}_{\text{soil,dw}}$  to  $30.1 \pm 1.2 \mu\text{g}/\text{g}_{\text{soil,dw}}$ . In contrast, there is no considerable variation in the concentration of  $\text{CH}_2\text{O}$ , which ranges between  $21.6 \pm 0.6 \mu\text{g}/\text{g}_{\text{soil,dw}}$  and  $26.8 \pm 2.2 \mu\text{g}/\text{g}_{\text{soil,dw}}$ , except for  $-26^\circ\text{C}$ , where it is observed to be lower at  $14.0 \pm 3.9 \mu\text{g}/\text{g}_{\text{soil,dw}}$ . The concentration of  $\text{CH}_4$  increases with temperature, rising from  $0.97 \pm 0.03 \text{ ng}/\text{g}_{\text{soil,dw}}$  to  $5.54 \pm 0.41 \text{ ng}/\text{g}_{\text{soil,dw}}$ . A similar trend is observed for  $\text{C}_2\text{H}_6$ , with the concentration increasing from  $0.30 \pm \text{zero} \text{ ng}/\text{g}_{\text{soil,dw}}$  to  $1.36 \pm 0.07 \text{ ng}/\text{g}_{\text{soil,dw}}$ . An exponential growth for  $\text{CH}_3\text{OH}$ ,  $\text{CH}_4$  and  $\text{C}_2\text{H}_6$  is observed between  $R^2 = 0.86$  and  $0.97$ , while the exponential  $R^2$  for  $\text{CH}_2\text{O}$  is lower at  $0.36$ .

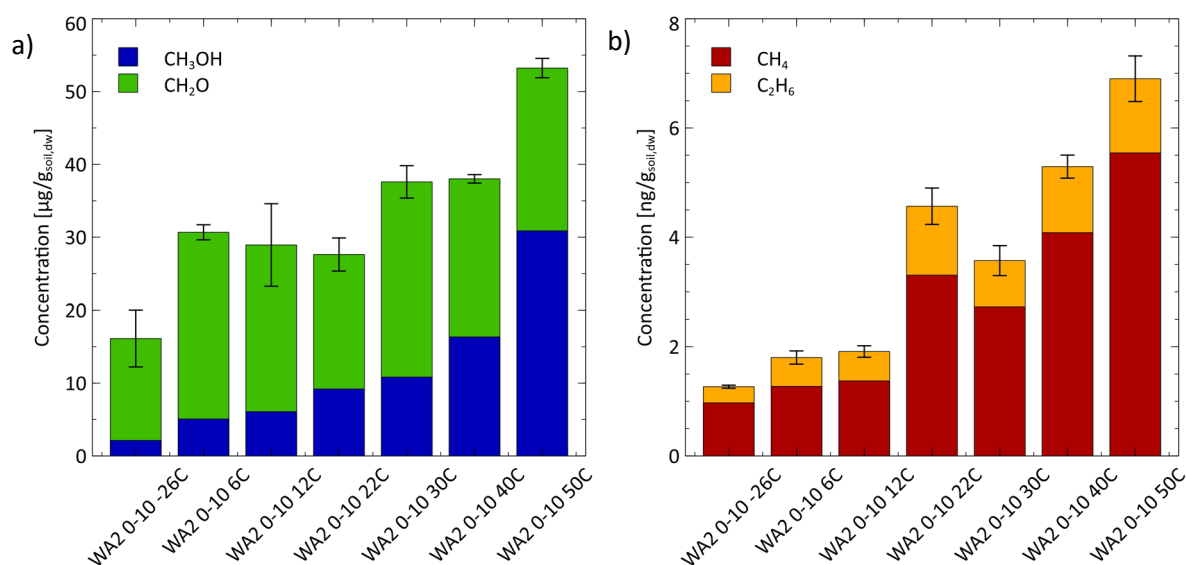


Figure 41: Measurement of  $\text{CH}_3\text{OH}$ ,  $\text{CH}_2\text{O}$  a) and  $\text{CH}_4$  and  $\text{C}_2\text{H}_6$  b) in soil WA2 0-10 at different incubation temperatures ( $-26$ ,  $6$ ,  $12$ ,  $22$ ,  $30$ ,  $40$  and  $50^\circ\text{C}$ ). Error bars refer to the SD of the total conversion of all major C1 and C2 compounds for  $n = 9$ , except for  $\text{CH}_4$  and  $\text{C}_2\text{H}_6$ ,  $n = 3$ .

### 3.6.8 Addition of $\text{CH}_3\text{OH}$ to non-sterile soils for demonstration of soil degradation potential

Experiments were conducted with untreated and non-sterile soil samples AL 20, WA2 0-10, and UH 0-10 to investigate if they could directly degrade abiotically produced  $\text{CH}_3\text{OH}$ , considering the presence of microorganisms within them. The initial addition of  $\text{CH}_3\text{OH}$  to wetted soils resulted in a degradation of  $\text{CH}_3\text{OH}$  over 21 days. The initial concentrations of  $\text{CH}_3\text{OH}$  were  $230 \mu\text{g}/\text{g}_{\text{soil,dw}}$ ,  $249 \mu\text{g}/\text{g}_{\text{soil,dw}}$  and  $214 \mu\text{g}/\text{g}_{\text{soil,dw}}$  for the soil samples AL 20, WA2 0-10 and UH 0-10, respectively. A gradual degradation was observed until day 10, after which it accelerated significantly. Complete degradation of the  $\text{CH}_3\text{OH}$  was achieved within 15-21 days and demonstrates the degradation potential of the soils (Figure 42a).

In addition, 5 g soil sample (AL 20) was incubated with 10 ml ultra-pure  $\text{H}_2\text{O}$  and in two additional experiments, methylotrophic bacteria (*Methylobacterium extorquens*) was added before the incubation

started and after the incubation and the latter measured again two days later (Figure 42b). The  $\text{CH}_3\text{OH}$  concentration within the error bars is zero, indicating a degradation due to *Methylorubrum extorquens*. A negative value is observed due to the subtraction of the blank concentration. The  $\text{CH}_2\text{O}$  concentration is unchanged in all three experiments, suggesting that the *Methylorubrum extorquens* did not consume  $\text{CH}_2\text{O}$ .

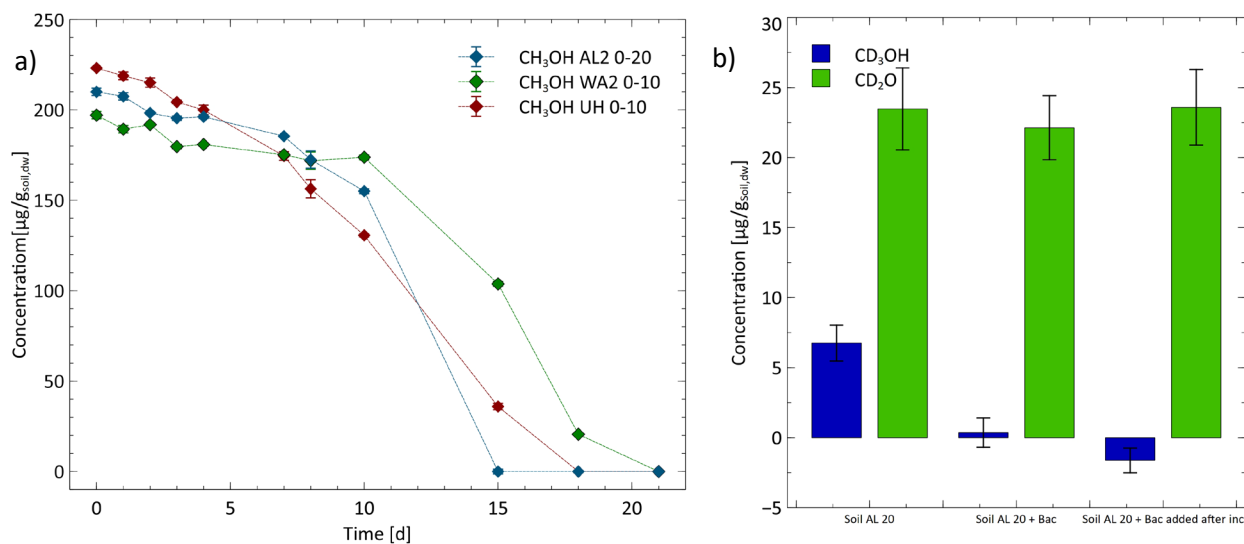


Figure 42: **a)** Degradation of added  $\text{CH}_3\text{OH}$  in untreated soil samples AL 20 0-20, WA2 0-10, and UH 0-10 ( $n = 3$ ). **b)** Measurement of  $\text{CH}_3\text{OH}$  and  $\text{CH}_2\text{O}$  in soil AL 20 with added methylotrophic bacteria (*Methylorubrum extorquens*) before and after the incubation compared with the experiment of AL 20 from Figure 34. Error bars refer to the SD of the total conversion of  $\text{CH}_3\text{OH}$  and  $\text{CH}_2\text{O}$  for  $n = 9$ .

### 3.6.9 Correlation of TOC and methoxy content as a basis for a first extrapolation of the production of $\text{CH}_3\text{OH}$ and $\text{CH}_2\text{O}$ from soils on a global scale

The TOC and  $\text{OCH}_3$  content were analysed for all 24 investigated soil samples using the methods described in Chapters 2.2.2.4 and 2.2.5. The concentrations of TOC range from 0 to 16.2 w%, and the  $\text{OCH}_3$  content ranges from  $0.0043 \pm 0.0026$  w% to  $0.42 \pm 0.00$  w%. The TOC and  $\text{OCH}_3$  content show a high correlation of  $R^2 = 0.88$  (Figure 43).

The degrees regression equation was used to calculate the  $\text{OCH}_3$  content as a percentage of the TOC with the following equation:

$$y = 0.0218x + 0.0102 \quad (10)$$

Filling in 100 % TOC as  $x$  in equation 10 yields an  $\text{OCH}_3$  content of 2.19 % per 100 % TOC. This was done to extrapolate the  $\text{OCH}_3$  content to a global scale and was undertaken to calculate initial projections using the scientific data available.

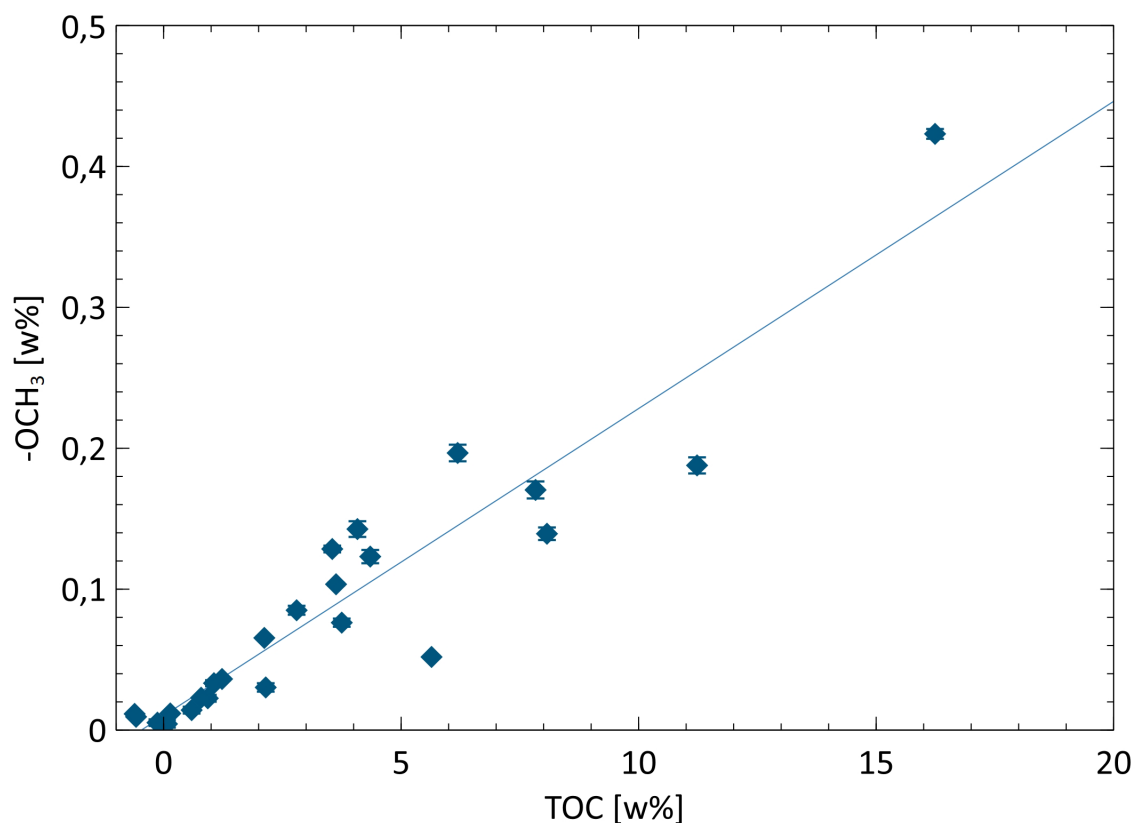


Figure 43: Correlation of the TOC ( $n = 1$ ) with  $\text{OCH}_3$  content ( $n = 3$ ) of the 24 investigated soil samples with an  $R^2 = 0.88$ .

### 3.6.10 TOC and $\text{CH}_3\text{OH} + \text{CH}_2\text{O}$ correlation for initial global predictions of $\text{CH}_3\text{OH}$ and $\text{CH}_2\text{O}$ production

Figure 44 illustrates the relationship between TOC and the measured concentrations of  $\text{CH}_3\text{OH}$  and  $\text{CH}_2\text{O}$  from all 24 soil experiments (Figure 34). A linear regression equation with an  $R^2$  value of 0.67 was obtained (Equation 11).

$$y = 1.71x + 7.03 \quad (11)$$

This shows a high correlation of the TOC with the produced  $\text{CH}_3\text{OH}$  and  $\text{CH}_2\text{O}$ , indicating that the TOC measurement gives a good prediction for the  $\text{CH}_3\text{OH}$  and  $\text{CH}_2\text{O}$  production of the soil. When 100 % TOC is entered into the equation, it predicts a production of  $178 \mu\text{g}/\text{g}_{\text{TOC}}$   $\text{CH}_3\text{OH}$  and  $\text{CH}_2\text{O}$  from a two-day incubation time. This value can then be extrapolated globally for the two-day incubation period for the soils, resulting in a value of 0.41 Gt  $\text{CH}_3\text{OH}$  and  $\text{CH}_2\text{O}$  production from the 2350 Gt TOC.

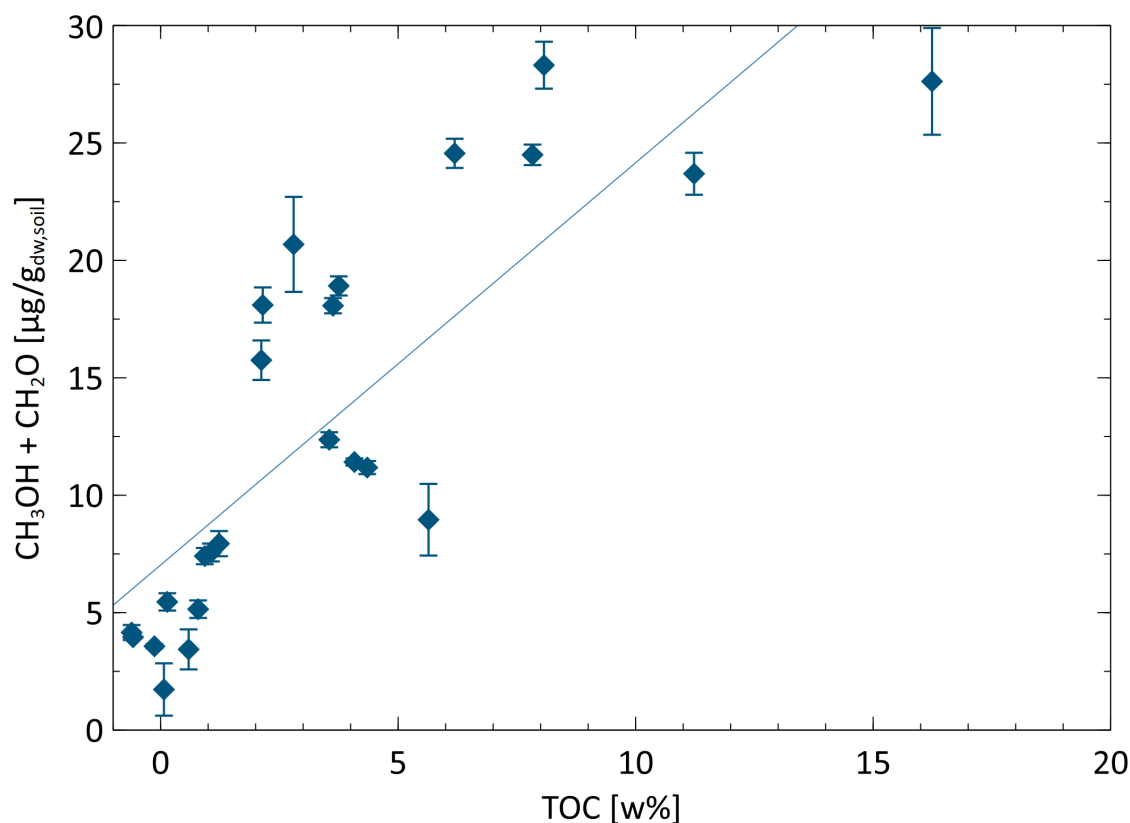


Figure 44: The TOC was correlated with the sum of CH<sub>3</sub>OH and CH<sub>2</sub>O concentrations of all 24 soils investigated. The experiments involved a two-day incubation period, during which 5 g of soil was incubated in 10 ml ultra-pure H<sub>2</sub>O.

### 3.6.11 Discussion and implications of the abiotic production of CH<sub>3</sub>OH, CH<sub>2</sub>O, CH<sub>4</sub> and C<sub>2</sub>H<sub>6</sub> in natural environments, especially the pedosphere

The results from various experiments with sterile soil samples provide evidence that they possess the potential for the abiotic formation of CH<sub>3</sub>OH, CH<sub>2</sub>O, CH<sub>4</sub> and C<sub>2</sub>H<sub>6</sub>, which represent environmentally important C1 and C2 compounds. High production of 2-28 µg/g<sub>soil,dw</sub> CH<sub>3</sub>OH and CH<sub>2</sub>O in soils was observed. These results correspond to the high CH<sub>3</sub>OH and CH<sub>2</sub>O production already obtained for aromatic OCH<sub>3</sub> compounds, as well as for lignin and pectin in aqueous solution in the presence of H<sub>2</sub>O<sub>2</sub>, an acid and a transition metal species. To further confirm these similarities, OCH<sub>3</sub> groups were removed from the soil samples, and experiments with isotopically labelled substrates were carried out.

The almost complete removal of OCH<sub>3</sub> groups from the soil samples resulted in a complete absence of CH<sub>3</sub>OH and a substantial decrease in CH<sub>2</sub>O concentration. This suggests that the OCH<sub>3</sub> groups may serve as precursors for CH<sub>3</sub>OH and CH<sub>2</sub>O in soil samples. To investigate this further, deuterated or <sup>18</sup>O-OCH<sub>3</sub> labelled 2-methoxyphenol was added to three soil experiments with removed OCH<sub>3</sub> groups. Subsequent measurements of the deuterated and <sup>18</sup>O-labelled CH<sub>3</sub>OH formed in the reaction provided direct evidence for the production of CH<sub>3</sub>OH from the OCH<sub>3</sub> group of 2-methoxyphenol. This is

presumably further oxidised to  $\text{CH}_2\text{O}$ , as described in Chapter 3.1.5.1, as ROS are generated in the soil, initiating various oxidation reactions (Chapter 1.6). As discussed in Chapters 1.6, 1.4 and 1.3, ROS, transition metal species and various precursor compounds, particularly lignin, are ubiquitous in soils. This suggests that the prerequisites for the reactions are given, and it can be hypothesised that this reaction occurs in soils, as observed for the aromatic  $\text{OCH}_3$  compounds. Given the capacity of C1 and C2 formation by other compounds with S-, N- and P-bound  $\text{CH}_3$  groups (chapters 3.1.2 and 3.2.1), which are also abundant in soils, it is proposed that these compounds should also be considered as precursor compounds. Furthermore, adding  $d_6$ -DMSO to the soils resulted in deuterium-labelling in  $\text{CH}_3\text{OH}$  and  $\text{CH}_2\text{O}$ , thereby supporting the hypothesis (Chapter 3.6.4).

The production of  $\text{CH}_4$  and  $\text{C}_2\text{H}_6$  can be observed in all experiments with soils; however, the concentrations are 3-4 orders of magnitude lower than for  $\text{CH}_3\text{OH}$  and  $\text{CH}_2\text{O}$ . Concentrations up to  $6,55 \pm 0,27 \text{ ng/g}_{\text{soil,dw}}$  ( $0,14 \text{ ng g}^{-1}_{\text{soil,dw}} \text{ dw h}^{-1}$ ) in a two-day incubation time were measured at  $22^\circ\text{C}$ . These are comparable to those observed in other studies with  $0.20 \pm 0.05^{34}$  or  $0.24 \pm 0.06 \text{ ng g}^{-1} \text{ dw h}^{-1}$ <sup>133</sup> at  $40^\circ\text{C}$ . Furthermore, the production of  $\text{CH}_4$  and  $\text{C}_2\text{H}_6$  is also 2-3 orders of magnitude lower in lignin and pectin, but only in the presence of Asc (chapter 3.5.1). In contrast, no production of  $\text{CH}_4$  and  $\text{C}_2\text{H}_6$  is observed for the analysed monomers of lignin and pectin in the absence of Asc. This suggests that an OH radical scavenger such as Asc and lignin or pectin must be present as a macromolecule in the soil to produce  $\text{CH}_4$  and  $\text{C}_2\text{H}_6$ . This behaviour of Asc was also observed in experiments with  $d_6$ -DMSO, which can also be transferred to other S- and N-hetero-bonded compounds due to a similar reaction mechanism.<sup>14</sup> Based on this observation, many other precursor compounds with a  $\text{CH}_3$  group should also be considered sources of  $\text{CH}_4$  and  $\text{C}_2\text{H}_6$ , as well as  $\text{CH}_3\text{OH}$  and  $\text{CH}_2\text{O}$ . This is particularly relevant given the considerable variation in soil composition, which can harbour a vast reservoir of potential precursor compounds. Other pathways of  $\text{CH}_4$  production in soils are also possible, such as photolysis, electrocatalysis, and others.<sup>270</sup>

A decrease in  $\text{CH}_4$  and  $\text{C}_2\text{H}_6$  concentration has been observed upon removal of the  $\text{OCH}_3$  groups in soil samples, in contrast to the experiments with the aromatic  $\text{OCH}_3$  compounds, which do not produce  $\text{CH}_4$  and  $\text{C}_2\text{H}_6$  (Chapter 3.3.1). Therefore, removing the  $\text{OCH}_3$  group should not influence  $\text{CH}_4$  and  $\text{C}_2\text{H}_6$  production. Since the production of  $\text{CH}_4$  and  $\text{C}_2\text{H}_6$  has been observed in lignin and pectin in the presence of Asc, it is reasonable to conclude that other functional groups of Lignin or pectin could be responsible for  $\text{CH}_4$  and  $\text{C}_2\text{H}_6$  production. However, these groups are possibly altered by the HI treatment of the soil samples, thereby reducing the production of  $\text{CH}_4$  and  $\text{C}_2\text{H}_6$ . Another possibility is that the Asc produces  $\text{CH}_4$  and  $\text{C}_2\text{H}_6$ , as previously observed for  $\text{CH}_4$ .<sup>31</sup> Furthermore, HI has been shown to cleave  $\text{CH}_3$  groups from other compounds, such as DMSO (experiments with DMSO demonstrate this). Consequently, the production of  $\text{CH}_4$  and  $\text{C}_2\text{H}_6$  from other compounds is reduced, influencing the total

production rate. The source of  $\text{CH}_4$  and  $\text{C}_2\text{H}_6$  remains to be elucidated; thus, the precise factors influencing their production remain to be determined.

Additional experimental setups were conducted using various configurations to enhance the understanding of the dominant processes. Initially, two soils were subjected to 10 wet-dry cycles to examine the behaviour of  $\text{CH}_3\text{OH}$  and  $\text{CH}_2\text{O}$  formation from the soil following several reaction cycles. Furthermore,  $\text{H}_2\text{O}_2$  was added to soil sample AL 20 to investigate whether the availability of an additional oxidising agent would affect the conversion rates. It was observed that there was a continuous decrease in the concentration of  $\text{CH}_3\text{OH}$  over the 10 cycles for all soil samples. A similar trend was observed for  $\text{CH}_2\text{O}$ , although its concentration remained consistently higher than that of  $\text{CH}_3\text{OH}$ . Adding  $\text{H}_2\text{O}_2$  to soil sample AL 20 resulted in an increase of approximately 18 % in the total concentration of  $\text{CH}_3\text{OH}$  and  $\text{CH}_2\text{O}$ . Given that the total addition of 2 mmol  $\text{H}_2\text{O}_2$  corresponds to a 3-orders of magnitude higher conversion if every  $\text{H}_2\text{O}_2$  molecule produces a  $\text{CH}_3\text{OH}$  molecule, this does not appear to be the limiting factor for the reaction. It is also noteworthy that  $\text{H}_2\text{O}_2$  can be utilised by other reactions within the soil, which can limit its availability. This is supported by the observation that not all  $\text{CH}_3\text{OH}$  is oxidised to  $\text{CH}_2\text{O}$ , which would be feasible due to an excess of  $\text{H}_2\text{O}_2$ . This finding indicates that  $\text{H}_2\text{O}_2$  is rapidly consumed in other reactions, limiting availability. This phenomenon can be attributed to the high reactivity of  $\text{H}_2\text{O}_2$ . Consequently, the extent to which the additional  $\text{H}_2\text{O}_2$  contributes to the overall reaction is challenging to determine.

Other limiting factors can be the presence of ROS in the soil and other factors that may impose limitations, including the accessibility of  $\text{OCH}_3$  groups. Notably, most of these groups are incorporated within the complex 3D structure of lignin and may not be available for the reaction with the iron-oxo species. Furthermore, the availability of free Fe to form reactive Fe species may also be a limiting factor due to the incorporation of complex molecular structures.<sup>271</sup> In general, the experiments demonstrate that, over a more extended period of time, the soil retains its capacity to produce  $\text{CH}_3\text{OH}$  and  $\text{CH}_2\text{O}$ , albeit with a decline in turnover rates. However, following the completion of 10 wet-dry cycles, a conversion of 6.19 % to 7.25 % of the  $\text{OCH}_3$  group to  $\text{CH}_3\text{OH}$  and  $\text{CH}_2\text{O}$  was observed, indicating a substantial conversion to C1 components when extrapolated on a global scale (as discussed in detail in Chapter 3.7).

In addition, the pH value in soil sample PT was increased from 3.2 to 6.9 in 5 steps with NaOH, and the concentrations of  $\text{CH}_3\text{OH}$ ,  $\text{CH}_2\text{O}$ ,  $\text{CH}_4$  and  $\text{C}_2\text{H}_6$  were analysed. However, the reduction of the pH value with HCl from around 7 to around 3 could not be carried out in the experiments due to the decomposition of the soil. No discernible change in the concentration of the sum of  $\text{CH}_3\text{OH}$  and  $\text{CH}_2\text{O}$  was observed, except for a slight increase at pH 6.9. The observed increase in  $\text{CH}_3\text{OH}$  with increasing pH may be attributable to a deficiency in oxidation capacity. This capacity is essential for the oxidation of Fe,

which is present in increasing amounts in  $\text{Fe}^{\text{II}}$  at higher pH values.<sup>272</sup> Consequently, an enhanced oxidation capacity is required to oxidise  $\text{Fe}^{\text{II}}$  to  $\text{Fe}^{\text{III}}$  and subsequently to  $\text{Fe}^{\text{IV}}$  for the generation of the iron-oxo species and, subsequently, for the production of  $\text{CH}_3\text{OH}$ . Consequently, a shortage of oxidation capacity to oxidise  $\text{CH}_3\text{OH}$  to  $\text{CH}_2\text{O}$  arises due to the need for enhanced iron oxidation that increases the percentage of  $\text{CH}_3\text{OH}$ . The observation of a constant concentration of both  $\text{CH}_3\text{OH}$  and  $\text{CH}_2\text{O}$  further indicates that the reaction from  $\text{CH}_3\text{OH}$  has a lower energy barrier than the oxidation of  $\text{CH}_3\text{OH}$  to  $\text{CH}_2\text{O}$  because  $\text{CH}_3\text{OH}$  has to be produced first, and only the  $\text{CH}_2\text{O}$  could be produced. This suggests that the conversion of  $\text{CH}_3\text{OH}$  to  $\text{CH}_2\text{O}$  occurs faster. In that case,  $\text{CH}_3\text{OH}$  and the total concentration rate will decrease due to this reaction's consumption of oxidation capacity, which is missing for the  $\text{CH}_3\text{OH}$  formation. It is also assumed that the oxidation capacity remains constant because the concentration of  $\text{CH}_4$  and  $\text{C}_2\text{H}_6$  remains approximately constant over the entire pH range, indicating that the production of  $\text{CH}_4$  and  $\text{C}_2\text{H}_6$  is independent of the pH value.

Temperature-dependent experiments (ranging from  $-26$ - $50^\circ\text{C}$ ) were conducted using soil sample WA2 0-10, and the concentrations of  $\text{CH}_3\text{OH}$ ,  $\text{CH}_2\text{O}$ ,  $\text{CH}_4$  and  $\text{C}_2\text{H}_6$  were analysed. The results demonstrated an exponential growth trend for all components with increasing temperature, exhibiting high  $R^2$  values ranging from 0.86 to 0.97. However, the exponential regression for  $\text{CH}_2\text{O}$  has an  $R^2$  of 0.36, indicating a different growth pattern. A substantial increase in  $\text{CH}_3\text{OH}$  concentration by over 1340 % was observed with rising temperatures, in contrast to the increase of only 60 % in  $\text{CH}_2\text{O}$ . As temperature rises, production increases, but oxidation capacity may not keep pace, resulting in more  $\text{CH}_3\text{OH}$  formation at higher temperatures that are not converted to  $\text{CH}_2\text{O}$ . For  $\text{CH}_4$  and  $\text{C}_2\text{H}_6$ , a consistent increase in concentration was observed across the temperature range, with concentrations rising by approximately 500 %, attributable to the enhanced energy in the system and a faster reaction in general.

To investigate the degradation of  $\text{CH}_3\text{OH}$  in soils,  $\text{CH}_3\text{OH}$  concentrations were artificially elevated in untreated (non-sterile) soil samples. The results demonstrate that the degradation of  $\text{CH}_3\text{OH}$  occurs in soils in approximately 15-21 days. Additionally, methylotrophic bacteria (*Methylobacterium extorquens*) were added before and after the soil experiments. In both cases, no  $\text{CH}_3\text{OH}$  was observed after the incubation. These experiments demonstrate that soils and added methylotrophic bacteria possess the capacity to degrade internally produced  $\text{CH}_3\text{OH}$ .

All soil samples' TOC and  $\text{OCH}_3$  content were determined to provide initial estimates of the effects on global production rates of C1 and C2 components in soils. The TOC and  $\text{OCH}_3$  content concentrations lie within the range of natural fluctuations at 0-16.2 w%<sup>273</sup> and  $0.0043 \pm 0.0026$  w% to  $0.42 \pm 0.003$  w%, respectively.<sup>274,275</sup> These values can then be related to the resulting C1 and C2 components, allowing for the initial estimation of these processes' global potential. Given the high correlation between  $\text{OCH}_3$  content and TOC, as well as the significant correlation of TOC with the production of  $\text{CH}_3\text{OH}$  +

CH<sub>2</sub>O, one can make accurate predictions for CH<sub>3</sub>OH + CH<sub>2</sub>O production based solely on the measurement of either the TOC or the OCH<sub>3</sub> content in the soils.

### 3.7 Global implications of the abiotic and oxic formation of CH<sub>3</sub>OH, CH<sub>2</sub>O, CH<sub>4</sub> and C<sub>2</sub>H<sub>6</sub> in soils

The effects of lignin-derived demethoxylation and the resulting C1 and C2 components are discussed in this section. As lignin constitutes a significant proportion of soil organic matter, its transformation is a pivotal process in the global carbon cycle and, thus, the environment. Utilising the mean content of 2.19 % of OCH<sub>3</sub> groups in the TOC of the soil samples determined in this study (Chapter 3.6.9), an average content of approximately 50 Gt OCH<sub>3</sub> group can be calculated from the approximately 2350 Gt TOC in the soil globally.<sup>276</sup> This corresponds to approximately 50 Gt CH<sub>3</sub>OH that can be produced maximally from the OCH<sub>3</sub> groups. Utilising the 10 wet-dry cycles as the basis for the CH<sub>3</sub>OH and CH<sub>2</sub>O produced (6.71, 6.17 or 7.25 % conversion of the OCH<sub>3</sub> content), the quantity obtained is 3.46, 3.19 and 3.74 Gt CH<sub>3</sub>OH + CH<sub>2</sub>O, respectively. When the individual experiments with the soil samples are used as a basis for calculations, 0.41 Gt CH<sub>3</sub>OH + CH<sub>2</sub>O conversion is obtained with an incubation time of 2 days, as described in Chapter 3.6.1. If the annual emissions of CH<sub>3</sub>OH into the atmosphere (0.075-0.490 Gt yr<sup>-1</sup>)<sup>109-111</sup> compared with this, the production rate is in the same range for the two-day incubation time and is approximately one order of magnitude lower than the 10 wet-dry cycles. A lower emission rate from dead leaf matter was calculated to be 0.018 to 0.040 Gt yr<sup>-1</sup> CH<sub>3</sub>OH as an additional abiotic source.

These calculations, however, are subject to significant uncertainties, including competitive reactions of microorganisms that degrade lignin and can produce CH<sub>3</sub>OH.<sup>197</sup> In turn, other microorganisms like methylotrophic bacteria can utilise CH<sub>3</sub>OH as an energy source; therefore, only net emission rates are observed, leading to low emission rates in the atmosphere. Additionally, the laboratory conditions do not accurately reflect natural conditions, and measurement inaccuracies and the analysis of soil samples from only temperate latitudes introduce further uncertainties concerning global turnover rates. Also, the sterilisation of the soil samples could change the structure of the organic molecules and, therefore, potentially influence the conversion rates. Nonetheless, it can be suggested that the recently identified processes play a substantial role in the global carbon cycle. However, further investigations are required to evaluate the precise environmental implications. Moreover, experiments on CH<sub>3</sub>OH degradation have demonstrated that soil microorganisms can degrade CH<sub>3</sub>OH, thereby indicating that CH<sub>3</sub>OH can be effectively degraded directly in the soil and is, therefore, not emitted in high quantities into the atmosphere.<sup>110,111</sup> The demethoxylation process provides many easily accessible

carbon molecules, such as  $\text{CH}_3\text{OH}$  and  $\text{CH}_2\text{O}$ , as an energy source for the microbial community.<sup>54</sup> This phenomenon elucidates the discrepancy between the substantial production capacity and the low atmospheric emissions mentioned earlier. Also,  $\text{CH}_4$  and  $\text{C}_2\text{H}_6$  generated in soils are food for microorganisms like methylotrophic bacteria.<sup>277</sup> All these generated C1 and C2 compounds influence the carbon cycle and have to be considered by calculating the fluxes in the carbon cycle (Figure 45).

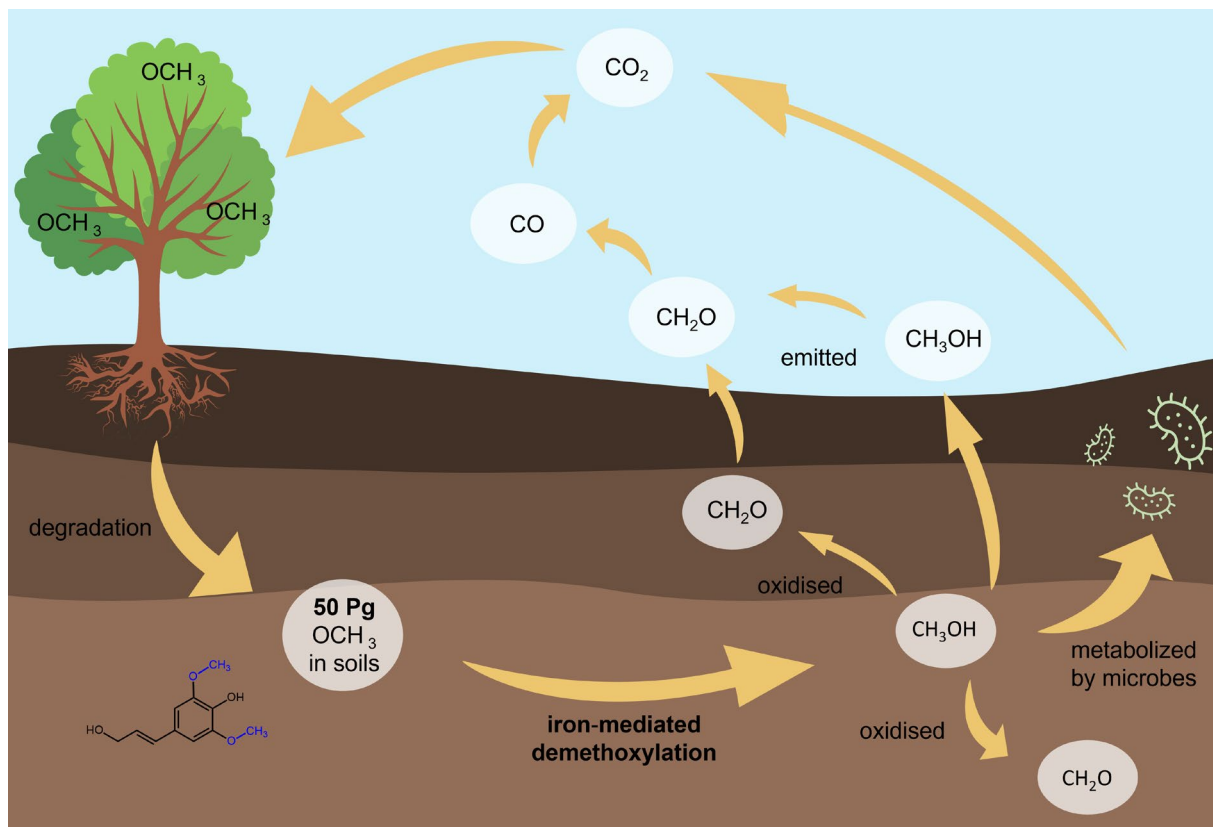


Figure 45: Overview of the cycle of iron-mediated demethylation from lignin-derived substrates and the production of  $\text{CH}_3\text{OH}$  and  $\text{CH}_2\text{O}$ . Subsequently, the degradation by microbes or emission into the atmosphere and, finally, the mineralisation to  $\text{CO}_2$ , which is taken up by plants.

## 4 Summary and Outlook

The present study investigates environmentally relevant substances like DMSO, 2-methoxyphenol, sinapyl alcohol and others with hetero-bonded CH<sub>3</sub> groups and the release of C1 and C2 components from them in the presence of transition metals like Fe, H<sub>2</sub>O<sub>2</sub> and an acid. This was done with laboratory incubation experiments and isotopically labelled substrates, especially to elucidate the underlying reaction mechanism. This system produces, among others, a [Fe<sup>IV</sup>=O]<sup>2+</sup> species, which initiates the reaction. With lignin or pectin and soil samples that were incubated, the reactions are transferred close to natural environments.

A conversion to C1 and C2 compounds was observed for all substrates with heteroatom-bonded CH<sub>3</sub> groups in a chemical model system under abiotic and oxic conditions. This contrasts with metabolic and combustion processes, typically considered the primary sources of these C1 and C2 compounds. Using DMSO as a model substance, the following C1 and C2 components were identified with conversion rates up to 86 %: CH<sub>4</sub>, C<sub>2</sub>H<sub>6</sub>, CH<sub>3</sub>OH, CH<sub>2</sub>O, CH<sub>3</sub>Cl, CO, CO<sub>2</sub>, HCOOH and CH<sub>3</sub>COOH. The CH<sub>3</sub> group was identified as a precursor for all components using deuterated or <sup>13</sup>C-labelled DMSO. Furthermore, in alkyl trapping experiments, it was observed that a CH<sub>3</sub> radical is generated from DMSO. The origin of the oxygen in CH<sub>3</sub>OH, CH<sub>2</sub>O and CO<sub>2</sub> was identified using <sup>18</sup>O-labelled H<sub>2</sub>O, H<sub>2</sub>O<sub>2</sub> and O<sub>2</sub>, with the origin in H<sub>2</sub>O<sub>2</sub> and O<sub>2</sub>. Applying deuterated CH<sub>3</sub>OH, it was demonstrated that CH<sub>2</sub>O is an oxidation product of CH<sub>3</sub>OH. The presence of chlorine in LFe<sup>II</sup>Cl<sub>2</sub> results in the formation of CH<sub>3</sub>Cl, which has shown a reaction of chlorine with the CH<sub>3</sub> radical.

The conversion rates of CH<sub>4</sub>, C<sub>2</sub>H<sub>6</sub>, CH<sub>3</sub>OH, and CH<sub>2</sub>O depend on the choice of substrates, the iron species, and the presence or absence of Asc. Replacing LFe<sup>II</sup>Cl<sub>2</sub> with Fe<sub>2</sub>O<sub>3</sub> results in enhanced yields, particularly with CH<sub>4</sub> at 100 μmol Asc concentrations. Asc concentrations influence the species distribution of the reaction products, with elevated levels of CH<sub>3</sub>OH and CH<sub>2</sub>O observed at lower Asc concentrations. The absence of Asc results in the exclusive formation of CH<sub>3</sub>OH and CH<sub>2</sub>O. Notably, a pronounced shift in the ratio towards CH<sub>4</sub> and a near absence of all other C1 and C2 compounds are observed. In addition, lower conversion rates are generally observed in response to changes in Asc concentration compared to the initial setup (100 μmol Asc). The influence of oxygen on the reaction was investigated by replacing it with nitrogen; however, no discernible influence was found on conversion rates to C1 and C2 compounds.

Based on these observations, an extended reaction mechanism was developed. Utilising iron species, Asc and H<sub>2</sub>O<sub>2</sub>, the formation of [Fe<sup>IV</sup>=O]<sup>2+</sup> species and OH radicals was observed, as previously documented.<sup>14,16</sup> The [Fe<sup>IV</sup>=O]<sup>2+</sup> species then reacts with DMSO, resulting in the cleavage of a CH<sub>3</sub> radical. This radical subsequently reacts with the OH radical, forming CH<sub>3</sub>OH, and can undergo further

oxidation to CH<sub>2</sub>O and up to CO<sub>2</sub>. The reaction that leads to CH<sub>4</sub> occurs by recombining the CH<sub>3</sub> radical with a hydrogen atom. The formation of C<sub>2</sub>H<sub>6</sub> results from the recombination of two CH<sub>3</sub> radicals.

The substitution of DMSO with methionine (S-bonded) or compounds featuring N- and P-bonded CH<sub>3</sub> groups (choline, trimethylamine or methylphosphonate) in identical experiments has been shown to yield reduced conversion rates. With methionine, the presence of CH<sub>4</sub>, C<sub>2</sub>H<sub>6</sub>, CH<sub>3</sub>OH, and CH<sub>2</sub>O was confirmed, whereas, in the case of the N- and P-bonded compounds, only smaller quantities of primarily CH<sub>3</sub>OH and CH<sub>2</sub>O were observed possibly due to structural differences in molecules. In instances involving methionine, choline, and trimethylamine, the CH<sub>3</sub> group could likewise be identified as a precursor of CH<sub>3</sub>OH and CH<sub>2</sub>O due to its deuteration, suggesting that it may also function as a precursor for CH<sub>4</sub> and C<sub>2</sub>H<sub>6</sub>. The production of C1 and C2 compounds in these reactions has a considerable impact on natural environments due to the ubiquitous distribution of all involved compounds.

In contrast, substrates with O-bonded CH<sub>3</sub> groups attached to an aromatic system exhibit different behaviour under the same experimental conditions, characterised by the formation of CH<sub>3</sub>OH and CH<sub>2</sub>O and the absence of CH<sub>4</sub> and C<sub>2</sub>H<sub>6</sub>. The investigation of the monomers sinapyl alcohol and coniferyl alcohol, which are parts of the lignin structure, reveals high conversion rates (up to 111 %) of CH<sub>3</sub>OH and CH<sub>2</sub>O compared to one CH<sub>3</sub> group. Furthermore, 2-methoxyphenol was selected as a representative substance for aromatically bound OCH<sub>3</sub> groups owing to its simple structure and the availability of isotopically labelled variants. The behaviour of other aromatic compounds with an OCH<sub>3</sub> group was examined, and it was found that they exhibit comparable behaviour in producing CH<sub>3</sub>OH and CH<sub>2</sub>O, which also represent the sole reaction products. The iron species was also found to influence the conversion rate, with consistently higher conversion rates for LFe<sup>II</sup>Cl<sub>2</sub> than Fe<sub>2</sub>O<sub>3</sub>, in contrast to the DMSO studies. Using Asc led to generally lower conversion rates and exclusively to CH<sub>3</sub>OH and CH<sub>2</sub>O. Hence, it was replaced with triflic acid in follow-up experiments. This is in contrast to the other hetero-bonded CH<sub>3</sub> groups where, in the presence of Asc, CH<sub>4</sub> and C<sub>2</sub>H<sub>6</sub> are produced. The monomer galacturonic acid methyl ester, which is part of the pectin structure and lacks an aromatic system, was also analysed, revealing lower conversion rates for CH<sub>3</sub>OH and CH<sub>2</sub>O only.

A detailed investigation of the reaction mechanism associated with methoxylated substrates was carried out due to the observed differences in the C1 and C2 compounds produced compared to DMSO. Contrary to DMSO, alkyl trapping experiments indicated no formation of CH<sub>3</sub> radicals. Furthermore, <sup>18</sup>O-labelled H<sub>2</sub>O<sub>2</sub> and O<sub>2</sub> were used to identify the origin of the oxygen, demonstrating that the oxygen in CH<sub>3</sub>OH and CH<sub>2</sub>O does not originate from H<sub>2</sub>O<sub>2</sub> or O<sub>2</sub>. Consequently, deuterated and <sup>18</sup>O-labelled OCH<sub>3</sub>-2-methoxyphenol was employed, confirming that the entire OCH<sub>3</sub> group is the source of CH<sub>3</sub>OH. This led to the proposal of a novel mechanism for forming CH<sub>3</sub>OH from aromatically bound OCH<sub>3</sub> groups, where the whole OCH<sub>3</sub> group is split off due to the [Fe<sup>IV</sup>=O]<sup>2+</sup> species and reacts to CH<sub>3</sub>OH. This

mechanism has not been previously documented under atmospheric conditions and could occur in natural environments with significant impact on them.

The investigation of transition metal species ( $\text{MnCl}_2$ ,  $\text{MnSO}_4$ ,  $\text{MnO}_2$ ,  $\text{FeCl}_2$ ,  $\text{FeSO}_4$ ,  $\text{CoCl}_2$ ,  $\text{NiCl}_2$ ,  $\text{NiSO}_4$ ,  $\text{CuCl}_2$ ,  $\text{CuO} + \text{CuO}_2$  and  $\text{Cu}(\text{OAc})_2$ ) other than  $\text{LFe}^{\text{IV}}\text{Cl}_2$  and  $\text{Fe}_2\text{O}_3$  in combination with DMSO, methionine and 2-methoxyphenol, and the otherwise identical setup, demonstrated that the identical C1 and C2 components were formed as with  $\text{LFe}^{\text{IV}}\text{Cl}_2$  and  $\text{Fe}_2\text{O}_3$ . With DMSO as a substrate, all transition metal species apart from the Cu species exhibited a comparably high conversion rate. In the case of methionine, the Mn and Fe species exhibited similar turnover rates, while the remaining transition metal species demonstrated smaller rates.  $\text{FeCl}_2$  and  $\text{FeSO}_4$  exhibited conversion rates analogous to those of  $\text{LFe}^{\text{IV}}\text{Cl}_2$  and  $\text{Fe}_2\text{O}_3$  in the presence of 2-methoxyphenol. All other transition metal species exhibited lower conversion rates, particularly  $\text{MnCl}_2$  and  $\text{MnO}_2$ , which exhibited almost no formation to the respective products. Using chlorinated transition metal species,  $\text{CH}_3\text{Cl}$  was detected for DMSO and, to a lesser extent, for methionine, but none was detected for 2-methoxyphenol. Altogether, various transition metal species have been shown to act as effective mediators in the process of C1 and C2 formation from hetero-bonded  $\text{CH}_3$  groups.

To get closer to natural conditions, lignin and pectin were initially incubated under the previously established experimental conditions. The presence of Asc led to the formation of  $\text{CH}_4$ ,  $\text{C}_2\text{H}_6$ , and approximately 2-3 orders of magnitude more  $\text{CH}_3\text{OH}$  and  $\text{CH}_2\text{O}$ . In contrast, the absence of Asc resulted in the formation of only  $\text{CH}_3\text{OH}$  and  $\text{CH}_2\text{O}$  in comparable concentrations. This shows that these biomolecules can also be converted to C1 and C2 compounds.

Subsequently, various soils with different organic content were sterilised at  $105^\circ\text{C}$  to eliminate all microbial activity. These were incubated with solely ultra-pure  $\text{H}_2\text{O}$ , and the formation of  $\text{CH}_4$  and  $\text{C}_2\text{H}_6$  was observed alongside a three- to fourfold higher production of  $\text{CH}_3\text{OH}$  and  $\text{CH}_2\text{O}$  across all soil types with concentrations between  $2\text{--}28 \mu\text{g}/\text{g}_{\text{soil,dw}}$ . The  $\text{OCH}_3$  group was identified as the source of both  $\text{CH}_3\text{OH}$  and  $\text{CH}_2\text{O}$ , a conclusion supported by the addition of isotopically labelled 2-methoxyphenol and the subsequent removal of the  $\text{OCH}_3$  groups from the soil, which results in the lack of  $\text{CH}_3\text{OH}$  formation and a substantial decrease in  $\text{CH}_2\text{O}$  formation. The precise origins of  $\text{CH}_4$  and  $\text{C}_2\text{H}_6$  remain unclear; however, lignin and pectin produce them in the presence of Asc. Also, other hetero-bonded  $\text{CH}_3$  groups can produce  $\text{CH}_4$  and  $\text{C}_2\text{H}_6$ , as evidenced by adding  $\text{d}_6$ -DMSO. Therefore, many sources are possible for the generation of  $\text{CH}_4$  and  $\text{C}_2\text{H}_6$ . Through the implementation of 10 wet-dry cycles, it has been shown that soil demonstrates a gradual decline in its capacity to produce  $\text{CH}_3\text{OH}$  and  $\text{CH}_2\text{O}$  while retaining the ability to generate these components over an extended period.

The demethylation process has been identified as a previously unobserved source of many different C1 and C2 components in the environment where  $\text{CH}_4$  was described earlier. A novel process is the

special case of O-methyl groups and the demethoxylation of the whole  $\text{OCH}_3$  group under atmospheric and abiotic conditions. It has a presumably high impact on natural environments, especially the pedosphere, due to the widespread and essential biomolecules like lignin and the ubiquitous distribution of all components involved in the reaction.

Figure 46 provides a comprehensive summary of the processes described in this study. The formation of C1 and C2 components from DMSO is particularly relevant in the marine environment due to the high abundance of DMSO and related compounds like DMS. Meanwhile, other S-, N, and P-bonded  $\text{CH}_3$  groups are ubiquitous and generally influence the Earth's system. Methionine is an essential amino acid, and choline functions as a precursor to other biomolecules in animals therefore, they are widespread in the biosphere. The formation of  $\text{CH}_3\text{OH}$  and  $\text{CH}_2\text{O}$  from  $\text{OCH}_3$  groups is important in the pedosphere, as evidenced in this work, contributing to a more comprehensive understanding of the carbon cycle within this environment and on a global scale.

The present study provides an initial understanding of the abiotic and oxic formation of C1 and C2 compounds in the environment. However, several aspects require further investigation to refine the comprehension of these processes and their broader implications. The interaction between abiotic and microbial pathways in soil remains a critical open question. While this study identifies abiotic  $\text{CH}_3\text{OH}$  and  $\text{CH}_2\text{O}$  production, the extent to which microbial degradation counteracts its production requires more detailed studies. Scaling up the experimental results to quantify the contribution of these processes to global biogeochemical cycles requires additional field-based studies across different soil types and climatic regions. Incorporating isotopic tracing methods in environmental monitoring could validate the proposed reaction mechanisms and improve global flux estimations. The role of environmental stress factors such as pH, temperature variations, and redox fluctuations should be further explored to assess their impact on the reaction and the turnover rates. Understanding these factors will enhance predictive models of carbon turnover in ecosystems and refine climate models incorporating trace gas emissions.

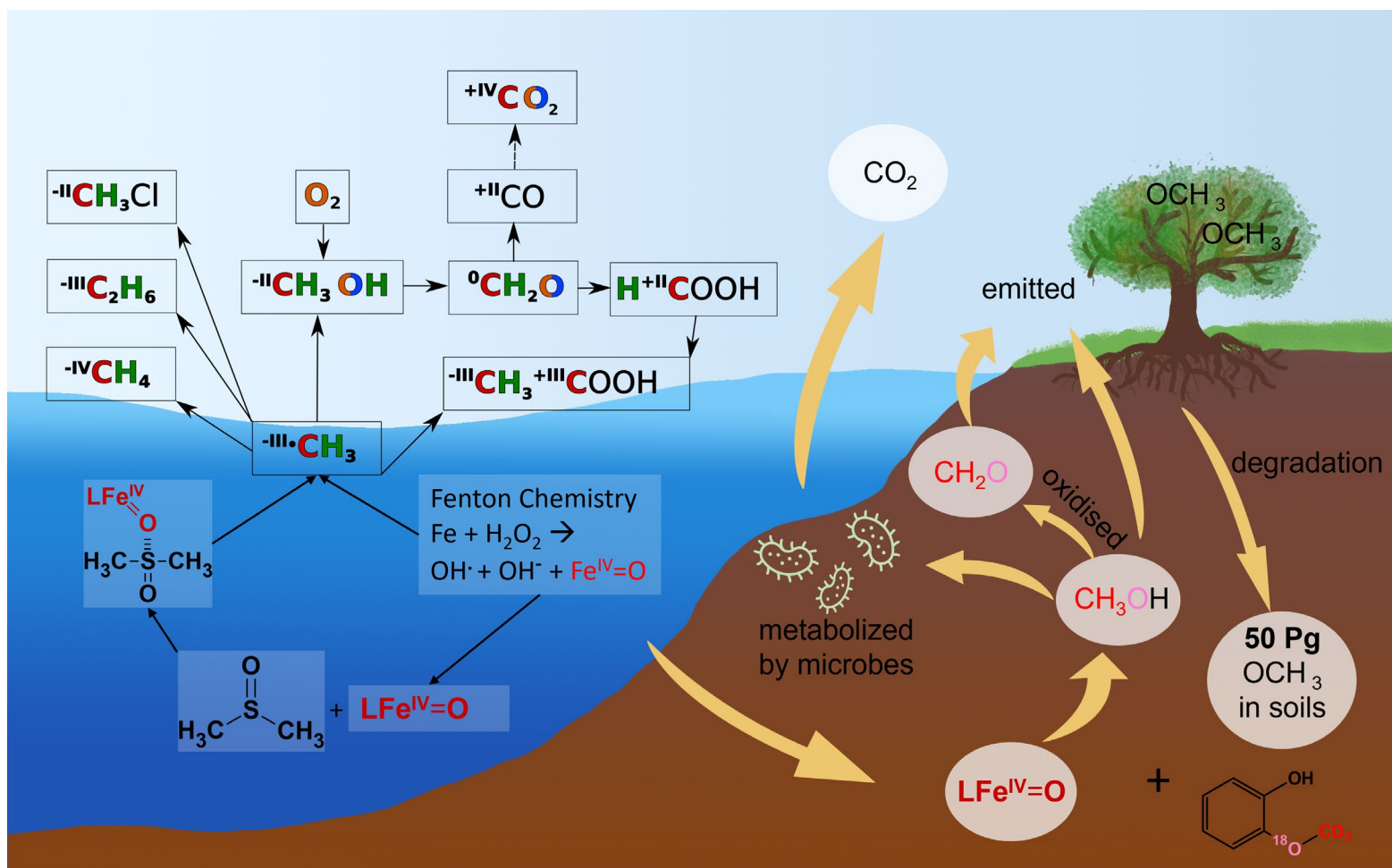


Figure 46: Summary of the CH<sub>3</sub> radical-based (left) and OCH<sub>3</sub>-based cycles (right) that form C1 and C2 compounds. Fenton Chemistry generates the [Fe<sup>IV</sup>=O]<sup>2+</sup> species that initiates the demethylation (left) or the demethoxylation (right) of the substrates with hetero-bonded CH<sub>3</sub> groups. The observed <sup>13</sup>C and <sup>2</sup>H labels in the CH<sub>3</sub> radical-based mechanism are presented in bold red and green, respectively. Oxygenated C1 compounds with <sup>18</sup>O isotopes are highlighted in bold orange or blue, originating from <sup>18</sup>O-labeled H<sub>2</sub>O<sub>2</sub> or O<sub>2</sub>, respectively. The deuterated and <sup>18</sup>O labels from the OCH<sub>3</sub> group of 2-methoxyphenol are shown in red and pink, respectively.

Overall, this study extended an overlooked abiotic pathway for C1 and C2 formation from CH<sub>3</sub> radicals that takes place in many compartments in the earth's system. This system comprises transition metals, H<sub>2</sub>O<sub>2</sub> and Asc, in conjunction with compounds containing hetero-bonded CH<sub>3</sub> groups. The novel discovered demethoxylation process is especially important in the pedosphere and contributes significantly to the carbon cycle within the soil. By addressing the identified knowledge gaps, future research can incorporate these findings into a more comprehensive framework that considers both biotic and abiotic contributions to the global carbon budget.

## 5 Related scientific work

### Peer-reviewed journal articles

**Hädeler, J. et al.** Natural Abiotic Iron-Oxido-Mediated Formation of C1 and C2 Compounds from Environmentally Important Methyl-Substituted Substrates. *Journal of the American Chemical Society* **145**, 24590–24602; 10.1021/jacs.3c06709 (2023).

### Additional contributions (not directly related to this thesis):

Ernst, L. et al. Methane formation driven by light and heat prior to the origin of life and beyond. *Nat Commun* **14**, 4364; 10.1038/s41467-023-39917-0 (2023).

### Conference Proceedings

**Hädeler, J.**, Velmurugan, G., Lauer, R., Comba, P., Keppler, F.:  $^{18}\text{O}$  labelling experiments reveal new abiotic pathway of methanol and formaldehyde formation in soil orally presented at: Jahrestagung der Arbeitsgemeinschaft Stabile Isotope e.V. (ASI), online conference, 30 September – 02 October 2024.

**Hädeler, J.**, Velmurugan, G., Lauer, R., Comba, P., Keppler, F.: Natural abiotic iron-oxido-mediated formation of C1 and C2 compounds from environmentally important methyl-substituted substrates Jahrestagung der Arbeitsgemeinschaft Stabile Isotope e.V. (ASI), online conference, 27-29 September 2023.

## 6 Appendix

All individual measurements displayed in the figures are listed in a separate Excel sheet.

It is accessible online from heiDATA, an institutional repository for data from Heidelberg University.

(<https://doi.org/10.11588/DATA/M2GCOQ>)

## 7 References

1. Atkinson, R. & Arey, J. Atmospheric degradation of volatile organic compounds. *Chemical reviews* **103**, 4605–4638; 10.1021/cr0206420 (2003).
2. Guenther, A. Natural emissions of non-methane volatile organic compounds, carbon monoxide, and oxides of nitrogen from North America. *Atmospheric Environment* **34**, 2205–2230; 10.1016/S1352-2310(99)00465-3 (2000).
3. Shen, X., Zhao, Y., Chen, Z. & Huang, D. Heterogeneous reactions of volatile organic compounds in the atmosphere. *Atmospheric Environment* **68**, 297–314; 10.1016/j.atmosenv.2012.11.027 (2013).
4. Montzka, S. A., Dlugokencky, E. J. & Butler, J. H. Non-CO<sub>2</sub> greenhouse gases and climate change. *Nature* **476**, 43–50; 10.1038/nature10322 (2011).
5. Insam, H. & Seewald, M. S. A. Volatile organic compounds (VOCs) in soils. *Biol Fertil Soils* **46**, 199–213; 10.1007/s00374-010-0442-3 (2010).
6. Tang, J., Schurgers, G. & Rinnan, R. Process Understanding of Soil BVOC Fluxes in Natural Ecosystems: A Review. *Reviews of Geophysics* **57**, 966–986; 10.1029/2018RG000634 (2019).
7. Conrad, R. The global methane cycle: recent advances in understanding the microbial processes involved. *Environmental Microbiology Reports* **1**, 285–292; 10.1111/j.1758-2229.2009.00038.x (2009).
8. Saunio, M. *et al.* The Global Methane Budget 2000–2017. *Earth System Science Data* **12**, 1561–1623; 10.5194/essd-12-1561-2020 (2020).
9. Montero-Montoya, R., López-Vargas, R. & Arellano-Aguilar, O. Volatile Organic Compounds in Air: Sources, Distribution, Exposure and Associated Illnesses in Children. *Annals of Global Health* **84**, 225–238; 10.29024/aogh.910 (2018).
10. Chaturvedi, S. *et al.* Recent Advancement in Organic Aerosol Understanding: a Review of Their Sources, Formation, and Health Impacts. *Water Air Soil Pollut* **234**, 1–21; 10.1007/s11270-023-06772-0 (2023).
11. Fall, R. & Benson, A. A. Leaf methanol — the simplest natural product from plants. *Trends in Plant Science* **1**, 296–301; 10.1016/S1360-1385(96)88175-0 (1996).

12. McBride, S. G., Osburn, E. D., Barrett, J. E. & Strickland, M. S. Volatile methanol and acetone additions increase labile soil carbon and inhibit nitrification. *Biogeochemistry* **145**, 127–140; 10.1007/s10533-019-00595-0 (2019).
13. Dixon, J. L., Beale, R. & Nightingale, P. D. Rapid biological oxidation of methanol in the tropical Atlantic: significance as a microbial carbon source. *Biogeosciences* **8**, 2707–2716; 10.5194/bg-8-2707-2011 (2011).
14. Althoff, F. *et al.* Abiotic methanogenesis from organosulphur compounds under ambient conditions. *Nat Commun* **5**, 4205; 10.1038/ncomms5205 (2014).
15. Comba, P., Kerscher, M., Krause, T. & Schöler, H. F. Iron-catalysed oxidation and halogenation of organic matter in nature. *Environ. Chem.* **12**, 381; 10.1071/EN14240 (2015).
16. Benzing, K., Comba, P., Martin, B., Pokrandt, B. & Keppler, F. Nonheme Iron-Oxo-Catalyzed Methane Formation from Methyl Thioethers: Scope, Mechanism, and Relevance for Natural Systems. *Chemistry – A European Journal* **23**, 10465–10472; 10.1002/chem.201701986 (2017).
17. Keppler, F., Hamilton, J. T. G., Brass, M. & Röckmann, T. Methane emissions from terrestrial plants under aerobic conditions. *Nature* **439**, 187–191; 10.1038/nature04420 (2006).
18. Keppler, F. *et al.* Methane formation in aerobic environments. *Environ. Chem.* **6**, 459; 10.1071/EN09137 (2009).
19. Lenhart, K. *et al.* Evidence for methane production by saprotrophic fungi. *Nat Commun* **3**, 1046; 10.1038/ncomms2049 (2012).
20. Schroll, M. *et al.* Fungal Methane Production Controlled by Oxygen Levels and Temperature. *Methane* **3**, 257–275; 10.3390/methane3020015 (2024).
21. Ghyczy, M. *et al.* Hypoxia-induced generation of methane in mitochondria and eukaryotic cells: an alternative approach to methanogenesis. *Cellular Physiology and Biochemistry* **21**, 251–258; 10.1159/000113766 (2008).
22. Bautz, J. *et al.* Formation of an aqueous oxoiron(IV) complex at pH 2–6 from a nonheme iron(II) complex and H<sub>2</sub>O<sub>2</sub>. *Angewandte Chemie (International ed. in English)* **45**, 5681–5684; 10.1002/anie.200601134 (2006).
23. Tuboly, E. *et al.* Methane biogenesis during sodium azide-induced chemical hypoxia in rats. *American journal of physiology. Cell physiology* **304**, C207–14; 10.1152/ajpcell.00300.2012 (2013).

24. Dueck, T. A. *et al.* No evidence for substantial aerobic methane emission by terrestrial plants: a <sup>13</sup>C-labelling approach. *The New phytologist* **175**, 29–35; 10.1111/j.1469-8137.2007.02103.x (2007).
25. Evans, J. R. Resolving methane fluxes. *The New phytologist* **175**, 1–4; 10.1111/j.1469-8137.2007.02114.x (2007).
26. Kirschbaum, M. U. F. *et al.* A comment on the quantitative significance of aerobic methane release by plants. *Functional Plant Biol.* **33**, 521–530; 10.1071/FP06051 (2006).
27. Keppler, F. *et al.* Methoxyl groups of plant pectin as a precursor of atmospheric methane: evidence from deuterium labelling studies. *New Phytologist* **178**, 808–814; 10.1111/j.1469-8137.2008.02411.x (2008).
28. Lenhart, K., Althoff, F., Greule, M. & Keppler, F. Technical Note: Methionine, a precursor of methane in living plants. *Biogeosciences* **12**, 1907–1914; 10.5194/bg-12-1907-2015 (2015).
29. Ghyczy, M., Torday, C. & Boros, M. Simultaneous generation of methane, carbon dioxide, and carbon monoxide from choline and ascorbic acid: a defensive mechanism against reductive stress? *The FASEB Journal* **17**, 1124–1126; 10.1096/fj.02-0918fje (2003).
30. Bruhn, D., Mikkelsen, T. N., Rolsted, M. M. M., Egsgaard, H. & Ambus, P. Leaf surface wax is a source of plant methane formation under UV radiation and in the presence of oxygen. *Plant Biology* **16**, 512–516; 10.1111/plb.12137 (2014).
31. Althoff, F., Jugold, A. & Keppler, F. Methane formation by oxidation of ascorbic acid using iron minerals and hydrogen peroxide. *Chemosphere* **80**, 286–292; 10.1016/j.chemosphere.2010.04.004 (2010).
32. Ernst, L. *et al.* Methane formation driven by light and heat prior to the origin of life and beyond. *Nat Commun* **14**, 4364; 10.1038/s41467-023-39917-0 (2023).
33. Jugold, A. *et al.* Non-microbial methane formation in oxic soils. *Biogeosciences* **9**, 5291–5301; 10.5194/bg-9-5291-2012 (2012).
34. Hurkuck, M., Althoff, F., Jungkunst, H. F., Jugold, A. & Keppler, F. Release of methane from aerobic soil: an indication of a novel chemical natural process? *Chemosphere* **86**, 684–689; 10.1016/j.chemosphere.2011.11.024 (2012).
35. Keppler, F., Eiden, R., Niedan, V., Pracht, J. & Schöler, H. F. Halocarbons produced by natural oxidation processes during degradation of organic matter. *Nature* **403**, 298–301; 10.1038/35002055 (2000).

36. Pracht, J., Boenigk, J., Isenbeck-Schröter, M., Keppler, F. & Schöler, H. F. Abiotic Fe(III) induced mineralization of phenolic substances. *Chemosphere* **44**, 613–619; 10.1016/s0045-6535(00)00490-2 (2001).
37. Comba, P. *et al.* Iron catalyzed demethylation of acetic acid\*. *Journal of Coordination Chemistry* **71**, 1704–1714; 10.1080/00958972.2018.1490414 (2018).
38. Lenhart, K. *et al.* Evidence for methane production by the marine algae *Emiliana huxleyi*. *Biogeosciences* **13**, 3163–3174; 10.5194/bg-13-3163-2016 (2016).
39. Keppler, F. *et al.* Stable isotope and high precision concentration measurements confirm that all humans produce and exhale methane. *J. Breath Res.* **10**, 16003; 10.1088/1752-7155/10/1/016003 (2016).
40. *Radical-Driven Methane Formation in Humans Evidenced by Exogenous Isotope-Labeled DMSO and Methionine. Antioxidants* **2023**, *12*, 1381 (2023).
41. Bruhn, D., Mikkelsen, T. N., Rolsted, M. M. M., Egsgaard, H. & Ambus, P. Leaf surface wax is a source of plant methane formation under UV radiation and in the presence of oxygen. *Plant Biology* **16**, 512–516; 10.1111/plb.12137 (2014).
42. John T. G. Hamilton, Mcroberts, W. C., Keppler, F., Kalin, R. M. & Harper, D. B. Chloride Methylation by Plant Pectin: An Efficient Environmentally Significant Process. *American Association for the Advancement of Science* (2003).
43. Yang, H., Yin, W., Zhu, X., Deuss, P. J. & Heeres, H. J. Selective Demethoxylation of Guaiacols to Phenols using Supported MoO<sub>3</sub> Catalysts. *ChemCatChem* **14**, e202200297; 10.1002/cctc.202200297 (2022).
44. Ishikawa, M., Tamura, M., Nakagawa, Y. & Tomishige, K. Demethoxylation of guaiacol and methoxybenzenes over carbon-supported Ru–Mn catalyst. *Applied Catalysis B: Environmental* **182**, 193–203; 10.1016/j.apcatb.2015.09.021 (2016).
45. Zhang, X., Yan, P., Zhao, B. & Zhang, Z. C. Identification of electron-rich mononuclear Ni atoms on TiO<sub>2</sub>-A distinguished from Ni particles on TiO<sub>2</sub>-R in guaiacol hydrodeoxygenation pathways. *Catal. Sci. Technol.* **11**, 297–311; 10.1039/D0CY01720E (2021).
46. Fu, Y., Zhu, Y., Shi, S. Q. & Goodell, B. Formaldehyde emission from wood promoted by lignin in the presence of iron residues. *Green Chem.* **24**, 6631–6638; 10.1039/D2GC02632E (2022).

47. Hildén, L. *et al.* Do the extracellular enzymes cellobiose dehydrogenase and manganese peroxidase form a pathway in lignin biodegradation? *FEBS Letters* **477**, 79–83; 10.1016/S0014-5793(00)01757-9 (2000).
48. Henriksson, G. *et al.* Is cellobiose dehydrogenase from *Phanerochaete chrysosporium* a lignin degrading enzyme? *Biochimica et biophysica acta* **1480**, 83–91; 10.1016/S0167-4838(00)00096-0 (2000).
49. Global Monitoring Laboratory - Carbon Cycle Greenhouse Gases. Available at [https://gml.noaa.gov/ccgg/trends\\_ch4/](https://gml.noaa.gov/ccgg/trends_ch4/) (2025).
50. Atkinson, R. & Arey, J. Gas-phase tropospheric chemistry of biogenic volatile organic compounds: a review. *Atmospheric Environment* **37**, 197–219; 10.1016/S1352-2310(03)00391-1 (2003).
51. Claeys, M. *et al.* Formation of Secondary Organic Aerosols Through Photooxidation of Isoprene. *American Association for the Advancement of Science* (2004).
52. Volkamer, R. *et al.* Secondary organic aerosol formation from anthropogenic air pollution: Rapid and higher than expected. *Geophysical Research Letters* **33**; 10.1029/2006GL026899 (2006).
53. Laothawornkitkul, J., Taylor, J. E., Paul, N. D. & Hewitt, C. N. Biogenic volatile organic compounds in the Earth system. *New Phytologist* **183**, 27–51; 10.1111/j.1469-8137.2009.02859.x (2009).
54. Kesselmeier, J. & Staudt, M. Biogenic Volatile Organic Compounds (VOC): An Overview on Emission, Physiology and Ecology. *J Atmos Chem* **33**, 23–88; 10.1023/A:1006127516791 (1999).
55. Halsey, K. H., Padaki, V. G. & Giovannoni, S. Chapter 12 - The volatile organic carbon component of dissolved organic matter in the ocean. In *Biogeochemistry of marine dissolved organic matter*, edited by D. A. Hansell & C. A. Carlson (Academic Press, an imprint of Elsevier, London, San Diego, CA, 2024), pp. 587–612.
56. Peñuelas, J. & Staudt, M. BVOCs and global change. *Trends in Plant Science* **15**, 133–144; 10.1016/j.tplants.2009.12.005 (2010).
57. Etminan, M., Myhre, G., Highwood, E. J. & Shine, K. P. Radiative forcing of carbon dioxide, methane, and nitrous oxide: A significant revision of the methane radiative forcing. *Geophysical Research Letters* **43**, 12,614–12,623; 10.1002/2016GL071930 (2016).
58. Marielle, S. *et al.* The global methane budget 2000–2012. *Earth System Science Data* **8**, 697–751; 10.5194/essd-8-697-2016 (2016).

59. Rosentreter, J. A. *et al.* Half of global methane emissions come from highly variable aquatic ecosystem sources. *Nat. Geosci.* **14**, 225–230; 10.1038/s41561-021-00715-2 (2021).
60. Kirschke, S. *et al.* Three decades of global methane sources and sinks. *Nature Geosci* **6**, 813–823; 10.1038/ngeo1955 (2013).
61. Charles L. Curry. Modeling the soil consumption of atmospheric methane at the global scale. *Global Biogeochemical Cycles* **21**; 10.1029/2006GB002818 (2007).
62. Q. Zhuang *et al.* Methane fluxes between terrestrial ecosystems and the atmosphere at northern high latitudes during the past century: A retrospective analysis with a process-based biogeochemistry model. *Global Biogeochemical Cycles* **18**; 10.1029/2004GB002239 (2004).
63. R. J. Cicerone & R. S. Oremland. Biogeochemical aspects of atmospheric methane. *Global Biogeochemical Cycles* **2**, 299–327; 10.1029/GB002i004p00299 (1988).
64. W. Allan, H. Struthers & D. C. Lowe. Methane carbon isotope effects caused by atomic chlorine in the marine boundary layer: Global model results compared with Southern Hemisphere measurements. *Journal of Geophysical Research: Atmospheres* **112**; 10.1029/2006JD007369 (2007).
65. Whiticar, M. J. Carbon and hydrogen isotope systematics of bacterial formation and oxidation of methane. *Chemical Geology* **161**, 291–314; 10.1016/S0009-2541(99)00092-3 (1999).
66. Lenhart, K. *et al.* Evidence for methane production by saprotrophic fungi. *Nat Commun* **3**, 1046; 10.1038/ncomms2049 (2012).
67. Tuboly, E. *et al.* Determination of endogenous methane formation by photoacoustic spectroscopy. *Journal of breath research* **7**, 46004; 10.1088/1752-7155/7/4/046004 (2013).
68. Keppler, F. *et al.* Stable isotope and high precision concentration measurements confirm that all humans produce and exhale methane. *J. Breath Res.* **10**, 16003; 10.1088/1752-7155/10/1/016003 (2016).
69. Klintzsch, T. *et al.* Methane production by three widespread marine phytoplankton species: release rates, precursor compounds, and potential relevance for the environment. *Biogeosciences* **16**, 4129–4144; 10.5194/bg-16-4129-2019 (2019).
70. Hartmann, J. F. *et al.* High Spatiotemporal Dynamics of Methane Production and Emission in Oxic Surface Water. *Environmental science & technology* **54**, 1451–1463; 10.1021/acs.est.9b03182 (2020).
71. Bižić, M. *et al.* Aquatic and terrestrial cyanobacteria produce methane. *Science Advances* **6**, eaax5343; 10.1126/sciadv.aax5343 (2020).

72. Ernst, L. *et al.* Methane formation driven by reactive oxygen species across all living organisms. *Nature* **603**, 482–487; 10.1038/s41586-022-04511-9 (2022).
73. Ordóñez, C. *et al.* Evaluation of the methane paradox in four adjacent pre-alpine lakes across a trophic gradient. *Nat Commun* **14**, 2165; 10.1038/s41467-023-37861-7 (2023).
74. Encinas Fernández, J., Peeters, F. & Hofmann, H. On the methane paradox: Transport from shallow water zones rather than in situ methanogenesis is the major source of CH<sub>4</sub> in the open surface water of lakes. *JGR Biogeosciences* **121**, 2717–2726; 10.1002/2016JG003586 (2016).
75. Peeters, F., Encinas Fernandez, J. & Hofmann, H. Sediment fluxes rather than oxic methanogenesis explain diffusive CH<sub>4</sub> emissions from lakes and reservoirs. *Sci Rep* **9**, 243; 10.1038/s41598-018-36530-w (2019).
76. Morana, C. *et al.* Methane paradox in tropical lakes? Sedimentary fluxes rather than pelagic production in oxic conditions sustain methanotrophy and emissions to the atmosphere. *Biogeosciences* **17**, 5209–5221; 10.5194/bg-17-5209-2020 (2020).
77. *Evidence for methane production by marine algae (Emiliana huxleyi) and its implication for the methane paradox in oxic waters* (2015).
78. Klintzsch, T. *et al.* Stable Carbon Isotope Signature of Methane Released From Phytoplankton. *Geophysical Research Letters* **50**, e2023GL103317; 10.1029/2023GL103317 (2023).
79. Mao, Y. *et al.* Aerobic methane production by phytoplankton as an important methane source of aquatic ecosystems: Reconsidering the global methane budget. *The Science of the total environment* **907**, 167864; 10.1016/j.scitotenv.2023.167864 (2024).
80. Repeta, D. J. *et al.* Marine methane paradox explained by bacterial degradation of dissolved organic matter. *Nature Geosci* **9**, 884–887; 10.1038/ngeo2837 (2016).
81. Zindler, C. *et al.* Sulphur compounds, methane, and phytoplankton: interactions along a north–south transit in the western Pacific Ocean. *Biogeosciences* **10**, 3297–3311; 10.5194/bg-10-3297-2013 (2013).
82. Zhang, Y., Tan, D.-D., He, Z., Yu, J. & Yang, G.-P. Dimethylated Sulfur, Methane and Aerobic Methane Production in the Yellow Sea and Bohai Sea. *Journal of Geophysical Research: Oceans* **128**, e2023JC019736; 10.1029/2023JC019736 (2023).
83. Defratyka, S. M. *et al.* Ethane measurement by Picarro CRDS G2201-i in laboratory and field conditions: potential and limitations. *Atmospheric Measurement Techniques* **14**, 5049–5069; 10.5194/amt-14-5049-2021 (2021).

84. Simpson, I. J. *et al.* Long-term decline of global atmospheric ethane concentrations and implications for methane. *Nature* **488**, 490–494; 10.1038/nature11342 (2012).
85. Pozzer, A. *et al.* Observed and simulated global distribution and budget of atmospheric C2-C5 alkanes. *Atmospheric Chemistry and Physics* **10**, 4403–4422; 10.5194/acp-10-4403-2010 (2010).
86. Kesselmeier, J. & Staudt, M. Biogenic Volatile Organic Compounds (VOC): An Overview on Emission, Physiology and Ecology. *Journal of Atmospheric Chemistry* **33**, 23–88; 10.1023/A:1006127516791 (1999).
87. Etiopie, G. & Ciccioli, P. Earth's Degassing: A Missing Ethane and Propane Source. *American Association for the Advancement of Science* (2009).
88. González Abad, G. *et al.* Ethane, ethyne and carbon monoxide concentrations in the upper troposphere and lower stratosphere from ACE and GEOS-Chem: a comparison study. *Atmos. Chem. Phys.* **11**, 9927–9941; 10.5194/acp-11-9927-2011 (2011).
89. Rudolph, J. The tropospheric distribution and budget of ethane. *J. Geophys. Res.* **100**, 11369–11381; 10.1029/95JD00693 (1995).
90. Kumar, A., Kumar, S. & Kumari, A. Carbon Monoxide Concentration in Atmosphere—A Review. In *IRC-SET 2022. Proceedings of the 8th IRC Conference on Science, Engineering and Technology, August 2022, Singapore*, edited by H. Guo, *et al.* (Springer Nature, Singapore, 2023), pp. 97–109.
91. Hoesly, R. M. *et al.* Historical (1750–2014) anthropogenic emissions of reactive gases and aerosols from the Community Emissions Data System (CEDS). *Geosci. Model Dev.* **11**, 369–408; 10.5194/gmd-11-369-2018 (2018).
92. van der Werf, G. R. *et al.* Global fire emissions estimates during 1997–2016. *Earth Syst. Sci. Data* **9**, 697–720; 10.5194/essd-9-697-2017 (2017).
93. Bruhn, D., Albert, K. R., Mikkelsen, T. N. & Ambus, P. UV-induced carbon monoxide emission from living vegetation. *Biogeosciences* **10**, 7877–7882; 10.5194/bg-10-7877-2013 (2013).
94. Conte, L., Szopa, S., Séférian, R. & Bopp, L. The oceanic cycle of carbon monoxide and its emissions to the atmosphere. *Biogeosciences* **16**, 881–902; 10.5194/bg-16-881-2019 (2019).
95. Atkinson, R. Atmospheric chemistry of VOCs and NO<sub>x</sub>. *Atmospheric Environment* **34**, 2063–2101; 10.1016/S1352-2310(99)00460-4 (2000).
96. Lelieveld, J., Gromov, S., Pozzer, A. & Taraborrelli, D. Global tropospheric hydroxyl distribution, budget and reactivity. *Atmos. Chem. Phys.* **16**, 12477–12493; 10.5194/acp-16-12477-2016 (2016).

97. Anthropogenic and Natural Radiative Forcing. In *Climate Change 2013. The physical science basis*, edited by T. Stocker (Cambridge University Press, New York, 2014), pp. 659–740.
98. Liu, L. *et al.* Global soil consumption of atmospheric carbon monoxide: an analysis using a process-based biogeochemistry model. *Atmos. Chem. Phys.* **18**, 7913–7931; 10.5194/acp-18-7913-2018 (2018).
99. Stein, O. *et al.* On the wintertime low bias of Northern Hemisphere carbon monoxide found in global model simulations. *Atmos. Chem. Phys.* **14**, 9295–9316; 10.5194/acp-14-9295-2014 (2014).
100. Fisher, J. A. *et al.* Seasonal changes in the tropospheric carbon monoxide profile over the remote Southern Hemisphere evaluated using multi-model simulations and aircraft observations. *Atmos. Chem. Phys.* **15**, 3217–3239; 10.5194/acp-15-3217-2015 (2015).
101. Zeng, G. *et al.* Multi-model simulation of CO and HCHO in the Southern Hemisphere: comparison with observations and impact of biogenic emissions. *Atmos. Chem. Phys.* **15**, 7217–7245; 10.5194/acp-15-7217-2015 (2015).
102. Michel Ramonet *et al.* CO<sub>2</sub> in the Atmosphere: Growth and Trends Since 1850. In *Oxford Research Encyclopedia of Climate Science* (2023).
103. Raupach, M. R., Canadell, J. G. & Le Quéré, C. Anthropogenic and biophysical contributions to increasing atmospheric CO<sub>2</sub> growth rate and airborne fraction. *Biogeosciences* **5**, 1601–1613; 10.5194/bg-5-1601-2008 (2008).
104. Guinotte, J. M. & Fabry, V. J. Ocean acidification and its potential effects on marine ecosystems. *Annals of the New York Academy of Sciences* **1134**, 320–342; 10.1196/annals.1439.013 (2008).
105. Le Quéré, C. *et al.* Trends in the sources and sinks of carbon dioxide. *Nat. Geosci.* **2**, 831–836; 10.1038/ngeo689 (2009).
106. Sarmiento, J. L. *et al.* Trends and regional distributions of land and ocean carbon sinks. *Biogeosciences* **7**, 2351–2367; 10.5194/bg-7-2351-2010 (2010).
107. Taylor, J. A. & Lloyd, J. Sources and Sinks of Atmospheric CO<sub>2</sub>. *Aust. J. Bot.* **40**, 407; 10.1071/bt9920407 (1992).
108. Seco, R., Peñuelas, J. & Filella, I. Short-chain oxygenated VOCs: Emission and uptake by plants and atmospheric sources, sinks, and concentrations. *Atmospheric Environment* **41**, 2477–2499; 10.1016/j.atmosenv.2006.11.029 (2007).

109. Singh, H. *et al.* Distribution and fate of selected oxygenated organic species in the troposphere and lower stratosphere over the Atlantic. *J. Geophys. Res.* **105**, 3795–3805; 10.1029/1999JD900779 (2000).
110. Heikes, B. G. *et al.* Atmospheric methanol budget and ocean implication. *Global Biogeochemical Cycles* **16**, 80-1-80-13; 10.1029/2002GB001895 (2002).
111. Jacob, D. J. *et al.* Global budget of methanol: Constraints from atmospheric observations. *J. Geophys. Res.* **110**; 10.1029/2004JD005172 (2005).
112. Dennis, P. G., Miller, A. J. & Hirsch, P. R. Are root exudates more important than other sources of rhizodeposits in structuring rhizosphere bacterial communities? *FEMS Microbiol Ecol* **72**, 313–327; 10.1111/j.1574-6941.2010.00860.x (2010).
113. Schade, G. W. & Custer, T. G. OVOC emissions from agricultural soil in northern Germany during the 2003 European heat wave. *Atmospheric Environment* **38**, 6105–6114; 10.1016/j.atmosenv.2004.08.017 (2004).
114. Kolb, S. Aerobic methanol-oxidizing bacteria in soil. *FEMS microbiology letters* **300**, 1–10; 10.1111/j.1574-6968.2009.01681.x (2009).
115. Peñuelas, J. *et al.* Biogenic volatile emissions from the soil. *Plant, Cell & Environment* **37**, 1866–1891; 10.1111/pce.12340 (2014).
116. Asensio, D. *et al.* Interannual and seasonal changes in the soil exchange rates of monoterpenes and other VOCs in a Mediterranean shrubland. *European Journal of Soil Science* **59**, 878–891; 10.1111/j.1365-2389.2008.01057.x (2008).
117. Bourtsoukidis, E. *et al.* Strong sesquiterpene emissions from Amazonian soils. *Nat Commun* **9**, 2226; 10.1038/s41467-018-04658-y (2018).
118. Warneke, C. *et al.* Acetone, methanol, and other partially oxidized volatile organic emissions from dead plant matter by abiological processes: Significance for atmospheric HO<sub>x</sub> chemistry. *Global Biogeochemical Cycles* **13**, 9–17; 10.1029/98GB02428 (1999).
119. Gray, C. M., Monson, R. K. & Fierer, N. Emissions of volatile organic compounds during the decomposition of plant litter. *J. Geophys. Res.* **115**; 10.1029/2010JG001291 (2010).
120. Dorokhov, Y. L., Shindyapina, A. V., Sheshukova, E. V. & Komarova, T. V. Metabolic methanol: molecular pathways and physiological roles. *Physiological Reviews* **95**, 603–644; 10.1152/physrev.00034.2014 (2015).

121. Yurimoto, H., Shiraishi, K. & Sakai, Y. Physiology of Methyloprotophytes Living in the Phyllosphere. *Microorganisms* **9**, 809; 10.3390/microorganisms9040809 (2021).
122. Schade, G. W. & Goldstein, A. H. Fluxes of oxygenated volatile organic compounds from a ponderosa pine plantation. *J. Geophys. Res.* **106**, 3111–3123; 10.1029/2000JD900592 (2001).
123. Luecken, D. J., Hutzell, W. T., Strum, M. L. & Pouliot, G. A. Regional sources of atmospheric formaldehyde and acetaldehyde, and implications for atmospheric modeling. *Atmospheric Environment* **47**, 477–490; 10.1016/j.atmosenv.2011.10.005 (2012).
124. Granby, K., Christensen, C. S. & Lohse, C. Urban and semi-rural observations of carboxylic acids and carbonyls. *Atmospheric Environment* **31**, 1403–1415; 10.1016/s1352-2310(96)00347-0 (1997).
125. Possanzini, M., Di Palo, V. & Cecinato, A. Sources and photodecomposition of formaldehyde and acetaldehyde in Rome ambient air. *Atmospheric Environment* **36**, 3195–3201; 10.1016/s1352-2310(02)00192-9 (2002).
126. Bakeas, E. B., Argyris, D. I. & Siskos, P. A. Carbonyl compounds in the urban environment of Athens, Greece. *Chemosphere* **52**, 805–813; 10.1016/S0045-6535(03)00257-1 (2003).
127. Holzinger, R. *et al.* Biomass burning as a source of formaldehyde, acetaldehyde, methanol, acetone, acetonitrile, and hydrogen cyanide. *Geophysical Research Letters* **26**, 1161–1164; 10.1029/1999GL900156 (1999).
128. Fortems-Cheiney, A. *et al.* The formaldehyde budget as seen by a global-scale multi-constraint and multi-species inversion system. *Atmos. Chem. Phys.* **12**, 6699–6721; 10.5194/acp-12-6699-2012 (2012).
129. Palmer, P. I. *et al.* Mapping isoprene emissions over North America using formaldehyde column observations from space. *J. Geophys. Res.* **108**; 10.1029/2002JD002153 (2003).
130. SCHMITZ, H., HILGERS, U. T. & WEIDNER, M. Assimilation and metabolism of formaldehyde by leaves appear unlikely to be of value for indoor air purification. *New Phytologist* **147**, 307–315; 10.1046/j.1469-8137.2000.00701.x (2000).
131. Liang, H., Zhao, S., Liu, K. & Su, Y. Roles of reactive oxygen species and antioxidant enzymes on formaldehyde removal from air by plants. *Journal of environmental science and health. Part A, Toxic/hazardous substances & environmental engineering* **54**, 193–201; 10.1080/10934529.2018.1544477 (2019).

132. Fu, Y., Zhu, Y., Shi, S. Q. & Goodell, B. Formaldehyde emission from wood promoted by lignin in the presence of iron residues. *Green Chem.* **24**, 6631–6638; 10.1039/D2GC02632E (2022).
133. Schäfer, M. & Roffael, E. On the formaldehyde release of wood. *Eur. J. Wood Prod.* **58**, 259–264; 10.1007/s001070050422 (2000).
134. Wan, G. & Frazier, C. E. Lignin Acidolysis Predicts Formaldehyde Generation in Pine Wood. *ACS Sustainable Chem. Eng.* **5**, 4830–4836; 10.1021/acssuschemeng.7b00264 (2017).
135. Millet, D. B. *et al.* A large and ubiquitous source of atmospheric formic acid. *Atmos. Chem. Phys.* **15**, 6283–6304; 10.5194/acp-15-6283-2015 (2015).
136. Paulot, F. *et al.* Importance of secondary sources in the atmospheric budgets of formic and acetic acids. *Atmos. Chem. Phys.* **11**, 1989–2013; 10.5194/acp-11-1989-2011 (2011).
137. Enders, G. *et al.* Biosphere/Atmosphere interactions: Integrated research in a European coniferous forest ecosystem. *Atmospheric Environment. Part A. General Topics* **26**, 171–189; 10.1016/0960-1686(92)90269-q (1992).
138. Yokelson, R. J. *et al.* Emissions from biomass burning in the Yucatan. *Atmos. Chem. Phys.* **9**, 5785–5812; 10.5194/acp-9-5785-2009 (2009).
139. Chebbi, A. & Carlier, P. Carboxylic acids in the troposphere, occurrence, sources, and sinks: A review. *Atmospheric Environment* **30**, 4233–4249; 10.1016/1352-2310(96)00102-1 (1996).
140. Peña, R. M. *et al.* Organic acids and aldehydes in rainwater in a northwest region of Spain. *Atmospheric Environment* **36**, 5277–5288; 10.1016/S1352-2310(02)00648-9 (2002).
141. Falkovich, A. H., Schkolnik, G., Ganor, E. & Rudich, Y. Adsorption of organic compounds pertinent to urban environments onto mineral dust particles. *J. Geophys. Res.* **109**; 10.1029/2003JD003919 (2004).
142. Yokouchi, Y., Saito, T., Ishigaki, C. & Aramoto, M. Identification of methyl chloride-emitting plants and atmospheric measurements on a subtropical island. *Chemosphere* **69**, 549–553; 10.1016/j.chemosphere.2007.03.028 (2007).
143. Carpenter, L. J. *et al.* *Scientific assessment of ozone depletion. 2014* (World Meteorological Organisation, Geneva, Switzerland, 2014).
144. Bahlmann, E. *et al.* Evidence for a major missing source in the global chloromethane budget from stable carbon isotopes. *Atmos. Chem. Phys.* **19**, 1703–1719; 10.5194/acp-19-1703-2019 (2019).

145. John T. G. Hamilton, Mcroberts, W. C., Keppler, F., Kalin, R. M. & Harper, D. B. Chloride Methylation by Plant Pectin: An Efficient Environmentally Significant Process. *American Association for the Advancement of Science* (2003).
146. Hu, L., Yvon-Lewis, S. A., Butler, J. H., Lobert, J. M. & King, D. B. An improved oceanic budget for methyl chloride. *JGR Oceans* **118**, 715–725; 10.1029/2012JC008196 (2013).
147. Rhew, R. C. & Abel, T. Measuring simultaneous production and consumption fluxes of methyl chloride and methyl bromide in annual temperate grasslands. *Environmental science & technology* **41**, 7837–7843; 10.1021/es0711011 (2007).
148. Keppler, F., Eiden, R., Niedan, V., Pracht, J. & Schöler, H. F. Halocarbons produced by natural oxidation processes during degradation of organic matter. *Nature* **403**, 298–301; 10.1038/35002055 (2000).
149. Rhew, R. C., Miller, B. R. & Weiss, R. F. Natural methyl bromide and methyl chloride emissions from coastal salt marshes. *Nature* **403**, 292–295; 10.1038/35002043 (2000).
150. Varner, R. K., Crill, P. M. & Talbot, R. W. Wetlands: A potentially significant source of atmospheric methyl bromide and methyl chloride. *Geophysical Research Letters* **26**, 2433–2435; 10.1029/1999GL900587 (1999).
151. Yevich, R. & Logan, J. A. An assessment of biofuel use and burning of agricultural waste in the developing world. *Global Biogeochemical Cycles* **17**; 10.1029/2002GB001952 (2003).
152. Watling, R. & Harper, D. B. Chloromethane production by wood-rotting fungi and an estimate of the global flux to the atmosphere. *Mycological Research* **102**, 769–787; 10.1017/S0953756298006157 (1998).
153. Khalil, M. & RASMUSSEN, R. A. Atmospheric methyl chloride. *Atmospheric Environment* **33**, 1305–1321; 10.1016/S1352-2310(98)00234-9 (1999).
154. Lee-Taylor, J. M., Brasseur, G. P. & Yokouchi, Y. A preliminary three-dimensional global model study of atmospheric methyl chloride distributions. *J. Geophys. Res.* **106**, 34221–34233; 10.1029/2001JD900209 (2001).
155. LOVELOCK, J. E., MAGGS, R. J. & RASMUSSEN, R. A. Atmospheric Dimethyl Sulphide and the Natural Sulphur Cycle. *Nature* **237**, 452–453; 10.1038/237452a0 (1972).
156. Glasow, R. von & Crutzen, P. J. Model study of multiphase DMS oxidation with a focus on halogens. *Atmos. Chem. Phys.* **4**, 589–608; 10.5194/acp-4-589-2004 (2004).

157. Bates, T. S., Lamb, B. K., Guenther, A., Dignon, J. & Stoiber, R. E. Sulfur emissions to the atmosphere from natural sources. *J Atmos Chem* **14**, 315–337; 10.1007/BF00115242 (1992).
158. Chen, Q., Sherwen, T., Evans, M. & Alexander, B. DMS oxidation and sulfur aerosol formation in the marine troposphere: a focus on reactive halogen and multiphase chemistry. *Atmos. Chem. Phys.* **18**, 13617–13637; 10.5194/acp-18-13617-2018 (2018).
159. Lomans, B. P. *et al.* Formation of dimethyl sulfide and methanethiol in anoxic freshwater sediments. *Applied and environmental microbiology* **63**, 4741–4747; 10.1128/aem.63.12.4741-4747.1997 (1997).
160. Kiene, R. P. & Hines, M. E. Microbial formation of dimethyl sulfide in anoxic sphagnum peat. *Applied and environmental microbiology* **61**, 2720–2726; 10.1128/aem.61.7.2720-2726.1995 (1995).
161. Gibson, R. N., Atkinson, R. J. A. & Gordon, J. D. M. *Oceanography and Marine Biology: Volume 42. An annual review. Volume 42* (CRC Press, London, 2004).
162. Keppler, F., Boros, M. & Polag, D. Radical-Driven Methane Formation in Humans Evidenced by Exogenous Isotope-Labeled DMSO and Methionine. *Antioxidants* **12**, 1381; 10.3390/antiox12071381 (2023).
163. Brosnan, J. T., Brosnan, M. E., Bertolo, R. F. & Brunton, J. A. Methionine: A metabolically unique amino acid. *Livestock Science* **112**, 2–7; 10.1016/j.livsci.2007.07.005 (2007).
164. Martínez, Y. *et al.* The role of methionine on metabolism, oxidative stress, and diseases. *Amino Acids* **49**, 2091–2098; 10.1007/s00726-017-2494-2 (2017).
165. Blachier, F., Wu, G. & Yin, Y. (eds.). *Nutritional and physiological functions of amino acids in pigs* (Springer, Vienna, New York, 2013).
166. Roje, S. S-Adenosyl-L-methionine: beyond the universal methyl group donor. *Phytochemistry* **67**, 1686–1698; 10.1016/j.phytochem.2006.04.019 (2006).
167. Bain, M. A., Fornasini, G. & Evans, A. M. Trimethylamine: metabolic, pharmacokinetic and safety aspects. *Current Drug Metabolism* **6**, 227–240; 10.2174/1389200054021807 (2005).
168. Koeth, R. A. *et al.* Intestinal microbiota metabolism of L-carnitine, a nutrient in red meat, promotes atherosclerosis. *Nat Med* **19**, 576–585; 10.1038/nm.3145 (2013).
169. Wang, Z. *et al.* Gut flora metabolism of phosphatidylcholine promotes cardiovascular disease. *Nature* **472**, 57–63; 10.1038/nature09922 (2011).

170. Lambert, D. M. *et al.* In vivo variability of TMA oxidation is partially mediated by polymorphisms of the FMO3 gene. *Molecular Genetics and Metabolism* **73**, 224–229; 10.1006/mgme.2001.3189 (2001).
171. Velasquez, M. T., Ramezani, A., Manal, A. & Raj, D. S. Trimethylamine N-Oxide: The Good, the Bad and the Unknown. *Toxins* **8**, 326; 10.3390/toxins8110326 (2016).
172. Yancey, P. H. Organic osmolytes as compatible, metabolic and counteracting cytoprotectants in high osmolarity and other stresses. *J Exp Biol* **208**, 2819–2830; 10.1242/jeb.01730 (2005).
173. Colby, J. & Zatman, L. J. Trimethylamine metabolism in obligate and facultative methylotrophs. *Biochem J* **132**, 101–112; 10.1042/bj1320101 (1973).
174. Catalá, R., López-Cobollo, R., Berbís, M. Á., Jiménez-Barbero, J. & Salinas, J. Trimethylamine N-oxide is a new plant molecule that promotes abiotic stress tolerance. *Science Advances* **7**; 10.1126/sciadv.abd9296 (2021).
175. Ho, K.-L., Chung, Y.-C. & Tseng, C.-P. Continuous deodorization and bacterial community analysis of a biofilter treating nitrogen-containing gases from swine waste storage pits. *Bioresource Technology* **99**, 2757–2765; 10.1016/j.biortech.2007.06.041 (2008).
176. Rappert, S. & Müller, R. Odor compounds in waste gas emissions from agricultural operations and food industries. *Waste Management* **25**, 887–907; 10.1016/j.wasman.2005.07.008 (2005).
177. Rehbein, P. J. G. *et al.* Cloud and fog processing enhanced gas-to-particle partitioning of trimethylamine. *Environmental science & technology* **45**, 4346–4352; 10.1021/es1042113 (2011).
178. Di, Y., Liu, J., Liu, J., Liui, S. & Yan, L. Characteristic analysis for odor gas emitted from food waste anaerobic fermentation in the pretreatment workshop. *Journal of the Air & Waste Management Association (1995)* **63**, 1173–1181; 10.1080/10962247.2013.807318 (2013).
179. Murphy, S. M. *et al.* Secondary aerosol formation from atmospheric reactions of aliphatic amines. *Atmos. Chem. Phys.* **7**, 2313–2337; 10.5194/acp-7-2313-2007 (2007).
180. Zeisel, S. H. & Niculescu, M. D. Perinatal choline influences brain structure and function. *Nutr Rev* **64**, 197–203; 10.1111/j.1753-4887.2006.tb00202.x (2006).
181. Blusztajn, J. K. Choline, a Vital Amine. *American Association for the Advancement of Science* (1998).
182. Medicine, Institute of, Board, F. a. N., Nutrients, Subcommittee on Upper Reference Levels of & Standing Committee on the Scientific Evaluation of Dietary Reference Intakes and its Panel on Folate, Other B Vitamins, and Choline. *Dietary reference intakes for thiamin, riboflavin, niacin,*

- vitamin B<sub>6</sub>, folate, vitamin B<sub>12</sub>, pantothenic acid, biotin, and choline* (National Academy Press, Washington, D.C., 1998).
183. Hollenbeck, C. B. An introduction to the nutrition and metabolism of choline. *Central nervous system agents in medicinal chemistry* **12**, 100–113; 10.2174/187152412800792689 (2012).
184. Fernández-Murray, J. P. & McMaster, C. R. Glycerophosphocholine catabolism as a new route for choline formation for phosphatidylcholine synthesis by the Kennedy pathway. *The Journal of biological chemistry* **280**, 38290–38296; 10.1074/jbc.M507700200 (2005).
185. Rhodes, D. Quaternary Ammonium and Tertiary Sulfonium Compounds in Higher Plants. *Annual Review of Plant Physiology and Plant Molecular Biology* **44**, 357–384; 10.1146/annurev.arplant.44.1.357 (1993).
186. Kolowitz, L. C., Ingall, E. D. & Benner, R. Composition and cycling of marine organic phosphorus. *Limnology & Oceanography* **46**, 309–320; 10.4319/lo.2001.46.2.0309 (2001).
187. Sosa, O. A., Repeta, D. J., DeLong, E. F., Ashkezari, M. D. & Karl, D. M. Phosphate-limited ocean regions select for bacterial populations enriched in the carbon-phosphorus lyase pathway for phosphonate degradation. *Environmental Microbiology* **21**, 2402–2414; 10.1111/1462-2920.14628 (2019).
188. White, A. K. & Metcalf, W. W. Microbial metabolism of reduced phosphorus compounds. *Annual Review of Microbiology* **61**, 379–400; 10.1146/annurev.micro.61.080706.093357 (2007).
189. Born, D. A. *et al.* Structural basis for methylphosphonate biosynthesis. *American Association for the Advancement of Science* (2017).
190. Karl, D. M. *et al.* Aerobic production of methane in the sea. *Nature Geosci* **1**, 473–478; 10.1038/ngeo234 (2008).
191. Ali Shah, T., Zhihe, L., Zhiyu, L. & Andong, Z. Composition and Role of Lignin in Biochemicals. In *Lignin. Chemistry, structure, and application*, edited by A. Sand & J. Tuteja (IntechOpen, London, 2023).
192. Boerjan, W., Ralph, J. & Baucher, M. Lignin biosynthesis. *Annual Review of Plant Biology* **54**, 519–546; 10.1146/annurev.arplant.54.031902.134938 (2003).
193. Dorrestijn, E., Laarhoven, L. J., Arends, I. W. & Mulder, P. The occurrence and reactivity of phenoxyl linkages in lignin and low rank coal. *Journal of Analytical and Applied Pyrolysis* **54**, 153–192; 10.1016/S0165-2370(99)00082-0 (2000).

194. Ralph, J., Lapierre, C. & Boerjan, W. Lignin structure and its engineering. *Current Opinion in Biotechnology* **56**, 240–249; 10.1016/j.copbio.2019.02.019 (2019).
195. Hatfield, R. & Vermerris, W. Lignin formation in plants. The dilemma of linkage specificity. *Plant Physiol* **126**, 1351–1357; 10.1104/pp.126.4.1351 (2001).
196. *Modification of Kraft lignin by biological demethylation* (2012).
197. Datta, R. *et al.* Enzymatic Degradation of Lignin in Soil: A Review. *Sustainability* **9**, 1163; 10.3390/su9071163 (2017).
198. Venkatesagowda, B. & Dekker, R. F. H. Microbial demethylation of lignin: Evidence of enzymes participating in the removal of methyl/methoxyl groups. *Enzyme and Microbial Technology* **147**, 109780; 10.1016/j.enzmictec.2021.109780 (2021).
199. Yang, B. *et al.* Experimental and theoretical studies on gas-phase reactions of NO<sub>3</sub> radicals with three methoxyphenols: Guaiacol, creosol, and syringol. *Atmospheric Environment* **125**, 243–251; 10.1016/j.atmosenv.2015.11.028 (2016).
200. Mohnen, D. Pectin structure and biosynthesis. *Current Opinion in Plant Biology* **11**, 266–277; 10.1016/j.pbi.2008.03.006 (2008).
201. Voragen, A. G. J., Coenen, G.-J., Verhoef, R. P. & Schols, H. A. Pectin, a versatile polysaccharide present in plant cell walls. *Struct Chem* **20**, 263–275; 10.1007/s11224-009-9442-z (2009).
202. Bonnin, E., Garnier, C. & Ralet, M.-C. Pectin-modifying enzymes and pectin-derived materials: applications and impacts. *Appl Microbiol Biotechnol* **98**, 519–532; 10.1007/s00253-013-5388-6 (2014).
203. Caffall, K. H. & Mohnen, D. The structure, function, and biosynthesis of plant cell wall pectic polysaccharides. *Carbohydrate Research* **344**, 1879–1900; 10.1016/j.carres.2009.05.021 (2009).
204. Haller, R. Metallchelat pyridyl-(2)-substituierter 3,7-Diaza-bicyclo-(3,3,1)-nonanone. *Archiv der Pharmazie und Berichte der Deutschen Pharmazeutischen Gesellschaft* **302**, 113–118; 10.1002/ardp.19693020206 (1969).
205. Hädeler, J. *et al.* Natural Abiotic Iron-Oxide-Mediated Formation of C<sub>1</sub> and C<sub>2</sub> Compounds from Environmentally Important Methyl-Substituted Substrates. *Journal of the American Chemical Society* **145**, 24590–24602; 10.1021/jacs.3c06709 (2023).
206. Comba, P., Rudolf, H. & Wadepohl, H. Synthesis and transition metal coordination chemistry of a novel hexadentate bispidine ligand. *Dalton transactions (Cambridge, England : 2003)* **44**, 2724–2736; 10.1039/C4DT03262D (2015).

207. Bukowski, M. R. *et al.* Bispidin-Ligandeneffekte in der Eisen-Wasserstoffperoxid-Chemie. *Angewandte Chemie* **116**, 1303–1307; 10.1002/ange.200352523 (2004).
208. Bautz, J., Comba, P., Lopez de Laorden, C., Menzel, M. & Rajaraman, G. Biomimetic high-valent non-heme iron oxidants for the cis-dihydroxylation and epoxidation of olefins. *Angewandte Chemie (International ed. in English)* **46**, 8067–8070; 10.1002/anie.200701681 (2007).
209. Benet-Buchholz, J. *et al.* Iron vs. ruthenium--a comparison of the stereoselectivity in catalytic olefin epoxidation. *Dalton Trans.*, 5910–5923; 10.1039/B902037C (2009).
210. Benet-Buchholz, J. *et al.* The Ru(IV)=O-catalyzed sulfoxidation: a gated mechanism where O to S linkage isomerization switches between different efficiencies. *Dalton Trans.* **39**, 3315–3320; 10.1039/B924614B (2010).
211. Comba, P., Fukuzumi, S., Kotani, H. & Wunderlich, S. Electron-transfer properties of an efficient nonheme iron oxidation catalyst with a tetradentate bispidine ligand. *Angewandte Chemie International Edition* **49**, 2622–2625; 10.1002/anie.200904427 (2010).
212. U. Schwertmann & R.M. Taylor. Iron Oxides. In *Minerals in Soil Environments* (John Wiley & Sons, Ltd2018), pp. 379–438.
213. Colombo, C., Di Iorio, E., Liu, Q., Jiang, Z. & Barrón, V. Iron Oxide Nanoparticles in Soils: Environmental and Agronomic Importance. *Journal of nanoscience and nanotechnology* **18**, 761; 10.1166/jnn.2018.15294 (2018).
214. Jiang, Z. *et al.* The Magnetic and Color Reflectance Properties of Hematite: From Earth to Mars. *Reviews of Geophysics* **60**, e2020RG000698; 10.1029/2020RG000698 (2022).
215. Colombo, C. & Torrent, J. Relationships between aggregation and iron oxides in Terra Rossa soils from southern Italy. *CATENA* **18**, 51–59; 10.1016/0341-8162(91)90006-J (1991).
216. Colombo, C., Palumbo, G., He, J.-Z., Pinton, R. & Cesco, S. Review on iron availability in soil: interaction of Fe minerals, plants, and microbes. *J Soils Sediments* **14**, 538–548; 10.1007/s11368-013-0814-z (2014).
217. *Manganese in Soils and Plants* (Springer, Dordrecht, 1988).
218. Marshall, K. C. Chapter 5 Biogeochemistry of Manganese Minerals. In *Studies in Environmental Science : Biogeochemical Cycling of Mineral-Forming Elements*, edited by P. A. Trudinger & D. J. Swaine (Elsevier1979), Vol. 3, pp. 253–292.
219. Young, R. S. The geochemistry of cobalt. *Geochimica et Cosmochimica Acta* **13**, 28–41; 10.1016/0016-7037(57)90056-X (1957).

220. Poznanović Spahić, M. M. *et al.* Natural and anthropogenic sources of chromium, nickel and cobalt in soils impacted by agricultural and industrial activity (Vojvodina, Serbia). *Journal of environmental science and health. Part A, Toxic/hazardous substances & environmental engineering* **54**, 219–230; 10.1080/10934529.2018.1544802 (2019).
221. Banerjee, R. & Ragsdale, S. W. The many faces of vitamin B12: catalysis by cobalamin-dependent enzymes. *Annual Review of Biochemistry* **72**, 209–247; 10.1146/annurev.biochem.72.121801.161828 (2003).
222. James W. Morris, Kirk G. Scheckel & David H. McNear. Biogeochemistry of Nickel in Soils, Plants, and the Rhizosphere. In *Nickel in Soils and Plants* (CRC Press 2018), pp. 51–86.
223. Morrison, J. M. *et al.* Weathering and transport of chromium and nickel from serpentinite in the Coast Range ophiolite to the Sacramento Valley, California, USA. *Applied Geochemistry* **61**, 72–86; 10.1016/j.apgeochem.2015.05.018 (2015).
224. Stern, B. R. *et al.* Copper and human health: biochemistry, genetics, and strategies for modeling dose-response relationships. *Journal of toxicology and environmental health. Part B, Critical reviews* **10**, 157–222; 10.1080/10937400600755911 (2007).
225. Ballabio, C. *et al.* Copper distribution in European topsoils: An assessment based on LUCAS soil survey. *The Science of the total environment* **636**, 282–298; 10.1016/j.scitotenv.2018.04.268 (2018).
226. Navel, A. & Martins, J. M. F. Effect of long term organic amendments and vegetation of vineyard soils on the microscale distribution and biogeochemistry of copper. *The Science of the total environment* **466–467**, 681–689; 10.1016/j.scitotenv.2013.07.064 (2014).
227. Arrigoni, O. & Tullio, M. C. de. Ascorbic acid: much more than just an antioxidant. *Biochimica et biophysica acta* **1569**, 1–9; 10.1016/S0304-4165(01)00235-5 (2002).
228. ALSCHER, R. G. *ANTIOXIDANTS IN HIGHER PLANTS* (CRC Press, [Place of publication not identified], 2017).
229. Yu, G.-H. & Kuzyakov, Y. Fenton chemistry and reactive oxygen species in soil: Abiotic mechanisms of biotic processes, controls and consequences for carbon and nutrient cycling. *Earth-Science Reviews* **214**, 103525; 10.1016/j.earscirev.2021.103525 (2021).
230. Wang, B., Lerdau, M. & He, Y. Widespread production of nonmicrobial greenhouse gases in soils. *Global Change Biology* **23**, 4472–4482; 10.1111/gcb.13753 (2017).

231. Zent, A. P., Ichimura, A. S., Quinn, R. C. & Harding, H. K. The formation and stability of the superoxide radical ( $O_2^-$ ) on rock-forming minerals: Band gaps, hydroxylation state, and implications for Mars oxidant chemistry. *J. Geophys. Res.* **113**; 10.1029/2007JE003001 (2008).
232. Yen, A. S., Kim, S. S., Hecht, M. H., Frant, M. S. & Murray, B. Evidence that the reactivity of the martian soil is due to superoxide ions. *Science* **289**, 1909–1912; 10.1126/science.289.5486.1909 (2000).
233. Gonçalves, C., Santos, M. A. d., Fornaro, A. & Pedrotti, J. J. Hydrogen peroxide in the rainwater of Sao Paulo megacity: measurements and controlling factors. *J. Braz. Chem. Soc.* **21**, 331–339; 10.1590/s0103-50532010000200020 (2010).
234. Arantes, V., Jellison, J. & Goodell, B. Peculiarities of brown-rot fungi and biochemical Fenton reaction with regard to their potential as a model for bioprocessing biomass. *Appl Microbiol Biotechnol* **94**, 323–338; 10.1007/s00253-012-3954-y (2012).
235. Hall, S. J., Silver, W. L., Timokhin, V. I. & Hammel, K. E. Lignin decomposition is sustained under fluctuating redox conditions in humid tropical forest soils. *Global Change Biology* **21**, 2818–2828; 10.1111/gcb.12908 (2015).
236. Krumina, L., Lyngsie, G., Tunlid, A. & Persson, P. Oxidation of a Dimethoxyhydroquinone by Ferrihydrite and Goethite Nanoparticles: Iron Reduction versus Surface Catalysis. *Environmental science & technology* **51**, 9053–9061; 10.1021/acs.est.7b02292 (2017).
237. Nurmi, J. T. & Tratnyek, P. G. Electrochemical properties of natural organic matter (NOM), fractions of NOM, and model biogeochemical electron shuttles. *Environmental science & technology* **36**, 617–624; 10.1021/es0110731 (2002).
238. Benzing, K., Comba, P., Martin, B., Pokrandt, B. & Keppler, F. Nonheme Iron-Oxo-Catalyzed Methane Formation from Methyl Thioethers: Scope, Mechanism, and Relevance for Natural Systems. *Chemistry – A European Journal* **23**, 10465–10472; 10.1002/chem.201701986 (2017).
239. GPS Geoplaner - GeoConverter | Routenplaner online. Available at <https://www.geoplaner.de/> (2024).
240. *Moore und Anmoore in der Oberrheinebene* (1997).
241. Littlewood, A. B. *Gas Chromatography. Principles, Techniques, and Applications*. 2nd ed. (Elsevier Science, Saint Louis, 2014).
242. John V. Hinshaw. *The Flame Ionization Detector* (MJH Life Sciences, 2005).

243. Robards, K. & Ryan, D. *Principles and practice of modern chromatographic methods* (Academic Press, an imprint of Elsevier, London, United Kingdom, San Diego, CA, 2022).
244. BID | Research & Development | SHIMADZU CORPORATION. Available at [https://www.shimadzu.com/research\\_and\\_development/technology\\_branding/nexis\\_technologies/bid.html](https://www.shimadzu.com/research_and_development/technology_branding/nexis_technologies/bid.html) (2021).
245. Greule, M. *et al.* Three wood isotopic reference materials for  $\delta^2\text{H}$  and  $\delta^{13}\text{C}$  measurements of plant methoxy groups. *Chemical Geology* **533**, 119428; 10.1016/j.chemgeo.2019.119428 (2020).
246. Zeisel, S. ber ein Verfahren zum quantitativen Nachweise von Methoxyl. *Monatshefte fr Chemie* **6**, 989–997; 10.1007/bf01554683 (1885).
247. *Simultaneous measurement of plasma concentrations and  $^{13}\text{C}$ -enrichment of short-chain fatty acids, lactic acid and ketone bodies by gas chromatography ...* (2003).
248. Zhang, H. *et al.* MTBSTFA derivatization-LC-MS/MS approach for the quantitative analysis of endogenous nucleotides in human colorectal carcinoma cells. *Journal of Pharmaceutical Analysis* **12**, 77–86; 10.1016/j.jpha.2021.01.001 (2022).
249. Andreae, M. O. Dimethylsulfoxide in marine and freshwaters. *Limnology and Oceanography* **25**, 1054–1063; 10.4319/lo.1980.25.6.1054 (1980).
250. Comba, P., Faltermeier, D., Krieg, S., Martin, B. & Rajaraman, G. Spin state and reactivity of iron(IV)oxido complexes with tetradentate bispidine ligands. *Dalton Trans.* **49**, 2888–2894; 10.1039/C9DT04578C (2020).
251. Comba, P., Nunn, G., Scherz, F. & Walton, P. H. Intermediate-spin iron(IV)-oxido species with record reactivity. *Faraday Discussions* **234**, 232–244; 10.1039/D1FD00073J (2022).
252. Russell, G. A. Deuterium-isotope Effects in the Autoxidation of Aralkyl Hydrocarbons. Mechanism of the Interaction of PEroxy Radicals 1. *Journal of the American Chemical Society* **79**, 3871–3877; 10.1021/ja01571a068 (1957).
253. Comba, P., Maurer, M. & Vadivelu, P. Oxidation of cyclohexane by high-valent iron bispidine complexes: tetradentate versus pentadentate ligands. *Inorganic chemistry* **48**, 10389–10396; 10.1021/ic901702s (2009).
254. Boyd, P. W. & Ellwood, M. J. The biogeochemical cycle of iron in the ocean. *Nat. Geosci.* **3**, 675–682; 10.1038/ngeo964 (2010).
255. Morris, J. J., Rose, A. L. & Lu, Z. Reactive oxygen species in the world ocean and their impacts on marine ecosystems. *Redox Biology* **52**, 102285; 10.1016/j.redox.2022.102285 (2022).

256. Abu-Odeh, M. *et al.* Pathways of the Extremely Reactive Iron(IV)-oxido complexes with Tetradentate Bispidine Ligands. *Chemistry – A European Journal* **27**, 11377–11390; 10.1002/chem.202101045 (2021).
257. Bouchoux, G. Keto-enol tautomers and distonic ions: The chemistry of [C n H 2 n O] radical cations. Part I. *Mass Spectrometry Reviews* **7**, 1–39; 10.1002/mas.1280070102 (1988).
258. Althoff, F. Sources and pathways of methane formed in oxidative environments. Johannes Gutenberg-Universität Mainz, 2012.
259. Pearson, A. J. & Yamamoto, Y. Trimethylamine N -Oxide. In *Encyclopedia of reagents for organic synthesis*, edited by L. A. Paquette (J. Wiley & Sons, New York, 1995).
260. Huang, J., Chen, Z. & Wu, J. Recent Progress in Methyl-Radical-Mediated Methylation or Demethylation Reactions. *ACS Catal.* **11**, 10713–10732; 10.1021/acscatal.1c02010 (2021).
261. Cao, H. *et al.* Cu-Catalyzed selective C3-formylation of imidazo1,2-apyridine C-H bonds with DMSO using molecular oxygen. *Chemical communications (Cambridge, England)* **51**, 1823–1825; 10.1039/C4CC09134E (2015).
262. Jia, J. *et al.* Copper-Catalyzed O-Methylation of Carboxylic Acids Using DMSO as a Methyl Source. *Synthesis* **48**, 421–428; 10.1055/s-0035-1560967 (2016).
263. Konezny, S. J. *et al.* Reduction of Systematic Uncertainty in DFT Redox Potentials of Transition-Metal Complexes. *J. Phys. Chem. C* **116**, 6349–6356; 10.1021/jp300485t (2012).
264. van Gaal, H. & van der Linden, J. Trends in redox potentials of transition metal complexes. *Coordination Chemistry Reviews* **47**, 41–54; 10.1016/0010-8545(82)85009-1 (1982).
265. *A comparative study of several transition metals in Fenton-like reaction systems at circum-neutral pH* (2003).
266. Hussain, S., Aneggi, E. & Goi, D. Catalytic activity of metals in heterogeneous Fenton-like oxidation of wastewater contaminants: a review. *Environ Chem Lett* **19**, 2405–2424; 10.1007/s10311-021-01185-z (2021).
267. Li, Y., Sun, J. & Sun, S.-P. Mn(2+)-mediated homogeneous Fenton-like reaction of Fe(III)-NTA complex for efficient degradation of organic contaminants under neutral conditions. *Journal of Hazardous Materials* **313**, 193–200; 10.1016/j.jhazmat.2016.04.003 (2016).
268. Bokare, A. D. & Choi, W. Review of iron-free Fenton-like systems for activating H<sub>2</sub>O<sub>2</sub> in advanced oxidation processes. *Journal of Hazardous Materials* **275**, 121–135; 10.1016/j.jhazmat.2014.04.054 (2014).

269. Keppler, F. *et al.* Methoxyl groups of plant pectin as a precursor of atmospheric methane: evidence from deuterium labelling studies. *New Phytologist* **178**, 808–814; 10.1111/j.1469-8137.2008.02411.x (2008).
270. Ye, J. *et al.* Abiotic Methane Production Driven by Ubiquitous Non-Fenton-Type Reactive Oxygen Species. *Angewandte Chemie* **136**; 10.1002/ange.202403884 (2024).
271. Lucena, J. J., Gárate, A. & Villén, M. Stability in solution and reactivity with soils and soil components of iron and zinc complexes. *Z. Pflanzenernähr. Bodenk.* **173**, 900–906; 10.1002/jpln.200900154 (2010).
272. Pehkonen, S. Determination of the oxidation states of iron in natural waters. A review. *Analyst* **120**, 2655; 10.1039/an9952002655 (1995).
273. Benbi, D. K. Evaluation of a rapid microwave digestion method for determination of total organic carbon in soil. *Communications in Soil Science and Plant Analysis* **49**, 2103–2112; 10.1080/00103624.2018.1495732 (2018).
274. Lloyd, M. K. *et al.* Methoxyl stable isotopic constraints on the origins and limits of coal-bed methane. *Science* **374**, 894–897; 10.1126/science.abg0241 (2021).
275. Cox, T. *et al.* Isotopic analysis ( $\delta^{13}\text{C}$  and  $\delta^2\text{H}$ ) of lignin methoxy groups in forest soils to identify and quantify lignin sources. *The Science of the total environment* **949**, 175025; 10.1016/j.scitotenv.2024.175025 (2024).
276. Stockmann, U. *et al.* The knowns, known unknowns and unknowns of sequestration of soil organic carbon. *Agriculture, Ecosystems & Environment* **164**, 80–99; 10.1016/j.agee.2012.10.001 (2013).
277. Hanson, R. S. & Hanson, T. E. Methanotrophic bacteria. *Microbiological Reviews* **60**, 439–471; 10.1128/mr.60.2.439-471.1996 (1996).



**Eidesstattliche Versicherung gemäß § 8 der Promotionsordnung für die Gesamtfakultät für Mathematik, Ingenieur- und Naturwissenschaften der Universität Heidelberg / Sworn Affidavit according to § 8 of the doctoral degree regulations of the Combined Faculty of Mathematics, Engineering and Natural Sciences at the Heidelberg University**

1. Bei der eingereichten Dissertation zu dem Thema / The thesis I have submitted entitled

.....

handelt es sich um meine eigenständig erbrachte Leistung / is my own work.

2. Ich habe nur die angegebenen Quellen und Hilfsmittel benutzt und mich keiner unzulässigen Hilfe Dritter bedient. Insbesondere habe ich wörtlich oder sinngemäß aus anderen Werken übernommene Inhalte als solche kenntlich gemacht. / I have only used the sources indicated and have not made unauthorised use of services of a third party. Where the work of others has been quoted or reproduced, the source is always given.

3. Die Arbeit oder Teile davon habe ich wie folgt/bislang nicht<sup>1)</sup> an einer Hochschule des In- oder Auslands als Bestandteil einer Prüfungs- oder Qualifikationsleistung vorgelegt. / I have not yet/have already<sup>1)</sup> presented this thesis or parts thereof to a university as part of an examination or degree.

Titel der Arbeit / Title of the thesis:.....

Hochschule und Jahr / University and year:.....

Art der Prüfungs- oder Qualifikationsleistung / Type of examination or degree:.....

4. Die Richtigkeit der vorstehenden Erklärungen bestätige ich. / I confirm that the declarations made above are correct.

5. Die Bedeutung der eidesstattlichen Versicherung und die strafrechtlichen Folgen einer unrichtigen oder unvollständigen eidesstattlichen Versicherung sind mir bekannt. / I am aware of the importance of a sworn affidavit and the criminal prosecution in case of a false or incomplete affidavit

Ich versichere an Eides statt, dass ich nach bestem Wissen die reine Wahrheit erklärt und nichts verschwiegen habe. / I affirm that the above is the absolute truth to the best of my knowledge and that I have not concealed anything.

.....  
Ort und Datum / Place and date

.....  
Unterschrift / Signature

<sup>1)</sup> Nicht Zutreffendes streichen. Bei Bejahung sind anzugeben: der Titel der andernorts vorgelegten Arbeit, die Hochschule, das Jahr der Vorlage und die Art der Prüfungs- oder Qualifikationsleistung. / Please cross out what is not applicable. If applicable, please provide: the title of the thesis that was presented elsewhere, the name of the university, the year of presentation and the type of examination or degree.